

Diss. ETH N° 18922

Novel Dendritic Macromolecules with Water-Soluble,
Thermoresponsive and Amphiphilic Properties

DISSERTATION

Submitted to

ETH-ZURICH

for the degree of

DOCTOR OF SCIENCES

by

Wen LI

M.Sc., A Joint Master Program of Freie Universität Berlin, Technische Universität
Berlin, Humboldt Universität zu Berlin and Universität Potsdam

born: December 16th, 1981

citizen of P. R. China

accepted on the recommendation of

Prof. Dr. A. Dieter Schlüter, examiner

Prof. Dr. Nicholas D. Spencer, co-examiner

Prof. Dr. Peter Walde, co-examiner

Prof. Dr. Ludwig Gauckler, chairman

Zürich 2010

Acknowledgements

I would like to express my sincere thanks to many people who gave me various forms of help, advice, support and encouragement during the three-year-work here. This doctoral dissertation could never be finished without their involvement.

First of all, I would like to thank Prof. A. D. Schlüter for providing me the opportunity to pursue my PhD study in his group and giving me great support and help during my work here. He is also thanked for writing the Zusammenfassung of this thesis. At the same time, many thanks to Prof. Afang Zhang who supervised me patiently and gave me continuous help during the whole thesis work. I learned from him not only the experience on doing experiment but also the delicate attitude on doing researches. He is further thanked for careful correction of this thesis.

I would like to send special thanks to Prof. Peter Walde who helped me a lot in many AFM measurements and spent time on correcting this thesis. Prof. Ludwig Gauckler is thanked in particular for the valuable discussions and suggestions on my project. Prof. Ludwig Gauckler, Prof. Nicholas D. Spencer, Prof. Paul Smith and Prof. Andrea Vasella, Prof. Massimo Morbidelli are all thanked for kindly providing access to their instruments.

Besides, Prof. Matthias Balauff (University of Bayreuth, Bayreuth, Germany), Prof. Gerhard Wegner and Prof. Hans W. Spiess as well as Dr. Dariush Hinderberger (Max Plank Institute for Polymer Research, Mainz, Germany) are all thanked for their interesting on my project and for their efforts on the fruitful collaborations.

Further more, I appreciate that the technical support from many people. Mr. Martin Colussi and Mr. Thomas Schweizer always supported on the GPC and DSC measurements. Junji Sakamoto gave the detail introduction of the HPLC. Dr. Kirill Feldman (Prof. Smith's group) and Dr. Hua Wu (Prof. Morbidelli's group) were quite helpful with the OM and DLS measurements, respectively. Lorenz Herdeis (Prof. Vasella's group) helped with UV/Vis measurements. Ilke Akartuna and Ben Seeber (Prof. Gauckler's group) gave me the patient introduction of the surface tension and SEM measurements, respectively. Matthias J. N. Junk (Prof. Spiess' group) kindly

assisted with the EPR spectroscopy. Yong Chen (Prof. Detmar's group) offered the supports of the cytotoxicity studies. Dr. Heinz Rüegger and Ms. Doris Sutter provided many help with the NMR measurements. Rolf Häfliger, Louis Bertschi and Dr. Xiangyang Zhang provided continuous support on the Mass spectrometric measurements.

Additionally, I would like to send my great appreciation to Daniela Zehnder for her kind help during my staying in Zürich. I am happy to have Jingyi Rao and Xiuqiang Zhang as the lab members. They not only created a nice lab environment but also helped me a lot both in the research work and daily life.

I am also grateful for all of the colleagues and former group members for their warmful friendship: Jeroen van Heijst, Malte Standera, Zengwei Guo, Liangfei Tian, Tobias Hoheisel, Jialong Yuan, Patrick Kissel and many others.

Finally, I am deeply indebted to my parents and younger sister who give me the love and provide mental supports.

Table of Contents

Abstract	III
Zusammenfassung	VII
1. Introduction	1
1.1 Dendrons, Dendrimers and Dendronized Polymers	2
1.1.1 Dendrons and Dendrimers Background	2
1.1.2 Dendronized Polymer Background	3
1.1.3 Synthesis Methodology to Various Dendronized Polymers	4
1.1.4 Applications of Dendronized Polymers	7
1.2 Thermoresponsive Polymers	10
1.2.1 Thermoresponsive Polymers with Linear Architecture	11
1.2.2 Thermoresponsive Polymers with Non-linear Architecture	12
1.2.3 Phase Transition Mechanism of Thermoresponsive Polymers	17
1.3 Amphiphilic Polymers	19
1.3.1 Amphiphilic Dendronized Block Copolymers	19
1.3.2 Amphiphilic Homopolymers	21
1.4 Fabrication of Porous Polymer Films <i>via</i> the “Breath Figure” Technique	24
2. Objectives and Considerations of the Thesis	29
3. OEG-Based Water-Soluble Dendronized Polymers	33
3.1 Synthesis of the Macromonomers	33
3.2 Polymerization and Characterization	36
3.3 Polymerization Kinetics Study	38
4. OEG-Based Thermoresponsive Dendritic Macromolecules	41
4.1 Methoxy-Terminated Thermoresponsive Dendronized Polymers	41
4.1.1 Synthesis and Characterization	42
4.1.2 Thermoresponsive Behavior	46
4.2 Thermoresponsive Dendronized Polymers with Tunable LCSTs	54
4.2.1 Synthesis and Characterization	55
4.2.2 Thermoresponsive Behavior	63
4.2.3 <i>In Vitro</i> Cytotoxicity Study	69

4.3 Thermoresponsive Dendrimers	71
4.3.1 Synthesis and Characterization	72
4.3.2 Thermoresponsive Behavior	73
4.3.3 <i>In Vitro</i> Cytotoxicity Study	77
4.4 Collapse Mechanism of Thermoresponsive Dendronized Polymers	79
4.4.1 Doubly Dendronized Polymer with Interior Hydrophobic and Peripheral Hydrophilic Dendrons.....	80
4.4.2 Thermoresponsive Behavior	82
4.4.3. Study of the Collpase Mechanism via EPR Spectroscopy	83
5. Amphiphilic Dendronized Homopolymers	89
5.1 Synthesis and Characterization.....	89
5.2 Thermoresponsive Behavior	92
5.3 Secondary Structure Analysis	92
5.4 Fabrication of Porous Films with the “Breath Figure” Technique.....	93
6. Conclusions and Outlook	97
7. List of All the Dendritic Macromolecules Synthesized in This Thesis Work	101
8. Experimental Part	103
8.1 Materials.....	103
8.2 Instrumentation and Measurements	103
8.3 Synthesis.....	107
8.3.1 Compounds of Chapter 3.1	109
8.3.2 Compounds of Chapter 4.1	115
8.3.4 Compounds of Chapter 4.3	132
8.3.5 Compounds of Chapter 4.4	136
8.3.6 Compounds of Chapter 5.1	140
9. Reference	149
10. Appendix	159
List of Publications	163
Poster Presentations.....	164

Abstract

A series of novel OEG-based water-soluble, thermoresponsive or amphiphilic dendritic macromolecules were efficiently synthesized and characterized in this thesis work. All dendrons were prepared in multi-gram scales with good over-all yields and high purity. Macromonomer route *via* conventional free radical polymerization was utilized for the synthesis of dendronized polymers to ensure the well-defined structures and easy protocol.

In the first part, the first and second generation neutral and water-soluble dendronized polymethacrylates **PG1(HT)** and **PG2(HT)** carrying hydroxyl terminal groups were synthesized (Figure A1). They are constructed by three-fold branched dendrons with short oligoethylene glycol (OEG) units as the linker and gallic acid as the branching point. Due to the liquid and water-soluble characteristics of the macromonomers, their free radical polymerization can be carried out in versatile mediums (DMF, aqueous solution, or in bulk). Dendronized polymers of high molar masses were obtained both in aqueous solutions and in bulk. Remarkably, the polymerization of hydroxyl terminated G1 macromonomers in aqueous solutions proceeded with an unprecedented fast rate and afforded polymers of extremely high molar masses (more than two million). The different polymerization kinetics in DMF and aqueous solutions were then investigated by using ^1H NMR spectroscopy.

In the following part, slight structure modifications of the previous polymers at the periphery afforded the dendronized polymers thermoresponsiveness and tunable lower critical solution temperatures (LCSTs) from 33 °C to 64°C [Figure A1, **PG1(MT)**, **PG2(MT)**, **PG1(MD)**, **PG2(MD)**, **PG1(ET)** and **PG2(ET)**]. Ethoxy-terminated third generation polymer **PG3(ET)** was further synthesized *via* an improved synthetic strategy. These polymers are hydrated at room temperature and start to dehydrate when the temperature increased to their LCSTs (Figure A2). The thermally induced phase transitions were followed by ^1H NMR spectroscopy and turbidimetry. The influence of the molar mass, polymer concentration, dendron generation and salt addition on their thermal transitions were all addressed and compared with other synthetic thermoresponsive systems. The thermally induced aggregation processes were monitored by dynamic light scattering and optical

microscopy. The morphologies of the aggregates were determined via static and dynamic light scattering, optical microscopy as well as cryo-TEM. Besides, the biocompatibilities of these polymers were also tested through an in vitro cytotoxicity study. Furthermore, thermoresponsive dendrimers constructed by the same dendrons as for the polymers were synthesized, and their thermal sensitive behavior were compared to that of the corresponding polymers. The specific architecture of these polymers, especially the sizeable thickness, gives rise to them interesting collapse mechanisms: the peripheral groups dominated over the interior parts on the phase transitions. To further prove this point, a doubly dendronized polymer **[PG2(ETalkyl)]** with interior totally constructed by hydrophobic alkyl units was prepared. It was found that **PG2(ETalkyl)** shows similar LCST to **PG1(ET)**, **PG2(ET)** and **PG3(ET)**. EPR spectroscopy was then applied to investigate the phase transition mechanism of these polymers on molecular level.

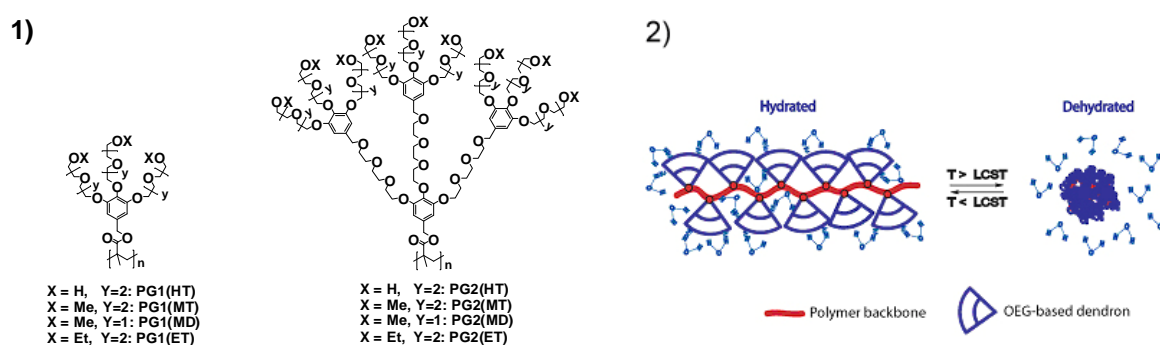


Figure A. 1) Chemical structures of the OEG-based water-soluble and thermoresponsive dendronized polymers; 2) Cartoon illustration of the hydration and dehydration processes of thermoresponsive dendronized polymers.

Finally, amphiphilic dendronized homopolymers **PG2(0)**, **PG2(1)** and **PG2(2)** were prepared by combination of OEG-based (hydrophilic) and proline-based (hydrophobic) dendrons into each repeat unit (Figure B1). Their hydrophilicity (water-solubility) can be tuned by the proline dendron generation (from zero to second). **PG2(0)** and **PG2(1)** are water-soluble and also show thermoresponsiveness, which were studied by turbidimetry. Their secondary ordered structures were investigated with both optical rotation and circular dichroism spectroscopies. Additionally, these polymers were employed for fabrication of porous films via the “breath figure” technique and found that only the highest hydrophobic **PG2(2)** could form ordered patterns (Figure B2).

Zusammenfassung

Es wurde eine Serie neuartiger Oligoethylenglykol (OEG)-basierter wasserlöslicher, thermoresponsiver bzw. amphiphiler dendritischer Makromoleküle synthetisiert und charakterisiert. Alle Dendrone wurden im Massstab von mehreren Gramm in guten Gesamtausbeuten und hohen Reinheiten erhalten. Für die Synthese der entsprechenden dendronisierten Polymere wurde die Makromonomerroute unter Ausnutzung konventioneller freier radikalischer Polymerisation verwendet, um einerseits zu wohldefinierten Strukturen gelangen zu können und andererseits einen einfachen Prozess zu haben.

Im ersten Teil der vorliegenden Arbeit wurden die neutralen und wasserlöslichen dendronisierten Polymere erster und zweiter Generation, **PG1(HT)** und **PG2(HT)**, synthetisiert, die terminale Hydroxylgruppen tragen (Abb. A1). Sie besitzen dreifach verzweigte Dendrone mit kurzen OEG-Einheiten als Linkern und Gallensäure als Verzweigungseinheit. Aufgrund der flüssigen Natur der entsprechenden Makromonomere und ihrer Wasserlöslichkeit, konnte die Polymerisation in verschiedenen Medien durchgeführt werden (DMF, Wasser, Reinsubstanz). Höhere Molmassen liessen sich sowohl in DMF Lösung als auch bei Polymerisation in Reinsubstanz realisieren. Die Polymerisation des G1 Makromonomers verlief in wässriger Lösung mit einer ungewöhnlich hohen Geschwindigkeit und lieferte extrem hochmolekulares Produkt (> 2 Mio Da). Die unterschiedlichen Reaktionsgeschwindigkeiten in DMF und in Wasser wurden mittels ^1H NMR Spektroskopie untersucht.

Im darauf folgenden Teil führte eine leichte Modifikation in der Peripherie dieser Polymere zu den thermoresponsiven dendronisierten Polymeren **PG1(MT)**, **PG2(MT)**, **PG1(MD)**, **PG2(MD)**, **PG1(ET)** und **PG2(ET)**, deren untere kritische Lösungstemperatur (LCST) von 33°C bis 64°C reichte (Abb. A1). Zusätzlich wurde das Polymer **PG3(ET)** durch eine verbesserte Synthesestrategie gewonnen. Alle diese Polymere liegen bei Raumtemperatur in wässrigem Medium in hydratisierter Form vor und beginnen zu dehydratisieren, sobald die Temperatur der Lösung die LCST erreicht (Abb. A2). Die thermisch induzierten Phasenübergänge wurden mittels ^1H NMR Spektroskopie und Trübungsmessung verfolgt. Dabei wurden die Einflüsse

der Molmasse, der Polymerkonzentration, der Dendron-Generation und des Salzhintergrundes auf die LCST für alle Polymere miteinander verglichen. Die der Dehydratisierung nachgeschaltete Aggregation wurde mit Lichtstreuung und optischer Mikroskopie verfolgt. Die Morphologie der Aggregate wurde mit statischer und dynamischer Lichtstreuung, optischer Mikroskopie und *cryo*-Transmissionselektronen-mikroskopie (TEM) bestimmt. Zusätzlich wurde die Bioverträglichkeit einiger dieser Polymere durch *in vitro* Zytotoxizitätsuntersuchungen festgestellt.

Zu Vergleichszwecken wurden neben den dendronisierten Polymeren auch sphärische Dendrimere hergestellt, wobei dieselben Dendrone Einsatz fanden. Ihr thermisches Verhalten war demjenigen der Polymere sehr ähnlich. Die spezielle Architektur der dendronisierten Polymere, und dabei besonders ihre beträchtliche Dicke, bewirkten einen interessanten Kollapsmechanismus. Dieser involviert zunächst besonders die peripheralen Einheiten und dann erst die inneren. Dieser neuartige Gesichtspunkt wurde durch das eigens zu diesem Zweck synthetisierte, doppelt-dendronisierte Polymer **PG2(ETalkyl)** bestätigt. Dieses trägt in seinem Inneren hydrophobe Gruppen und zeigt trotzdem den Phasenübergang bei praktisch identischer Temperatur wie **PG1(ET)**, **PG2(ET)** und **PG3(ET)**. In Kollaboration mit Prof. Spiess und Dr. Hinderberger, MPI Polymerforschung, Mainz, wurde der Kollaps unter Zuhilfenahme von Spinsonden und der Elektronenspinresonanz (EPR) Spektroskopie auf molekularem Niveau untersucht.

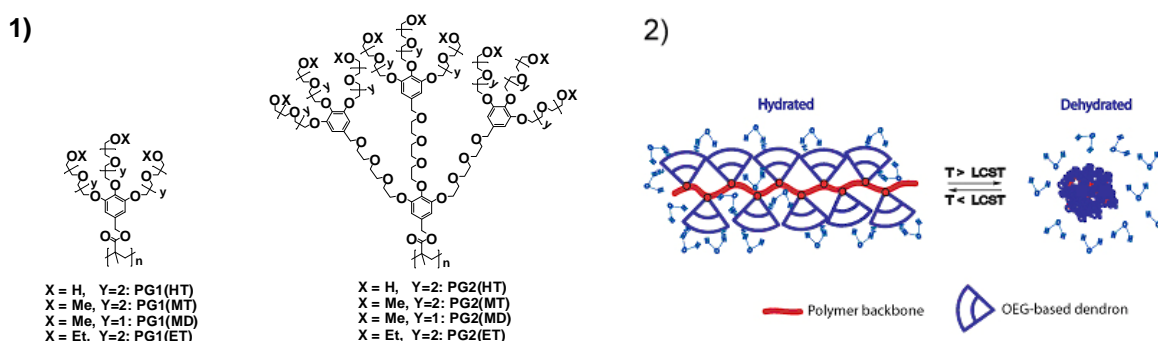


Abb. A. 1) Chemische Strukturen der OEG-basierten, wasserlöslichen und thermoresponsiven dendronisierten Polymere. 2) Graphische Darstellung des Hydrations- und Dehydratationsprozesses bei dendronisierten Polymeren.

Schliesslich wurden noch die amphiphilen dendronisierten Polymere **PG2(0)**, **PG2(1)** und **PG2(2)** synthetisiert. Hierzu wurden OEG-basierte Dendrone (hydrophil) mit solchen aufgebaut aus Prolinen (hydrophob) in einer Wiederholungseinheit zusammengefügt. Die Hydrophile der entsprechenden Polymere kann durch die Generation des Prolinteils eingestellt werden. **PG2(0)** und **PG2(1)** sind wasserlöslich und zeigen ebenfalls Thermoresponsivität, die mittels Trübungsmessungen untersucht wurde. Die Sekundärstruktur wurde sowohl durch Bestimmung der optischen Rotation als auch durch Circular dichroismusspektroskopie untersucht. Zusätzlich wurden diese Polymere für die Herstellung poröser Filme mittels der "Breath Figure" Technik eingesetzt, wobei nur mit dem hydrophobsten Vertreter geordnete Strukturen erhalten werden konnten (Abb. B2).

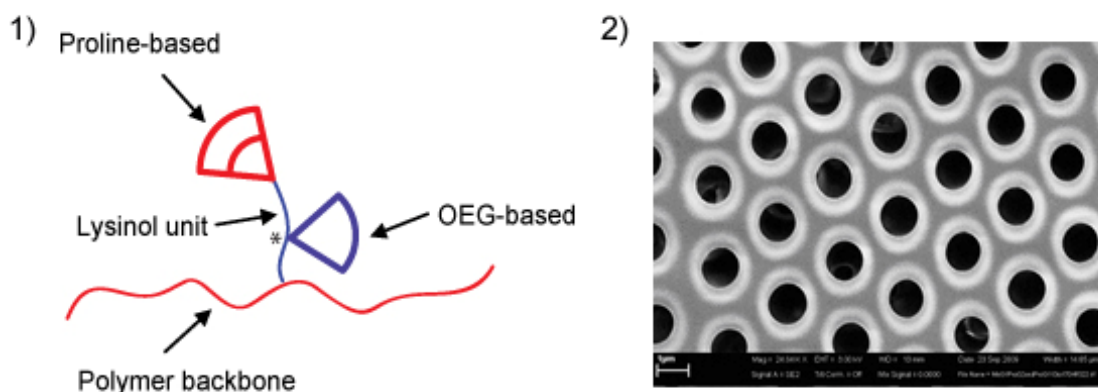


Abb. B. 1) Darstellung des Konstruktionsprinzips der amphiphilen dendronisierten Polymere bestehend aus einer OEG- und einer Prolin-Einheit. 2) Beispiel für geordnete, poröse Strukturen, die mittels der "Breath Figure" Technik aus PG2(2) erhalten wurden.

1. Introduction

The fast development of synthetic chemistry gives rise to novel polymers with various architectures. This includes linear homopolymers, block copolymers, cross-linked, comb-like or star-shaped polymers. Due to the versatile structures of polymers, their chemical and physical properties are different which attract lots of research interests. Learnt from Nature, a new type of branched polymers with dendritic (“tree-like”) architecture has recently been developed and gathered lots of attention. They can be further classified into dendron, dendrimer, dendritic-linear, hyperbranched and dendronized polymers. In contrast to conventional polymers, their individual molecular sizes can be tuned by branching (i.e. dendron) generations, and furthermore, they provide more chances for structure variation in both interior and exterior parts (for high generations). The special architectures provide these macromolecules with even more attractive properties.¹ Besides, many efforts have also been undertaken to develop synthetic macromolecules with various properties in order to broaden their applications. Most of the motivations still come from nature. It is known that biological molecules have the ability to respond to small environment alternations, which results in dramatic conformational changes. To mimic this, macromolecules with stimuli-responsive properties were developed to build “smart” synthetic systems. These macromolecules (especially, polymers) can easily undergo physical changes with the presence of external stimuli, such as pH value, temperature, light, ionic strength, etc. Among them, temperature sensitive macromolecules have been widely studied because temperature is a convenient stimulus, and many non-ionic polymers can exhibit a lower critical solution temperature (LCST) in aqueous solutions. Furthermore, learnt from natural amphiphiles, polymers with amphiphilic properties have also been developed. In a word, creating of synthetic polymers with novel architectures and properties to mimic nature is essential for the further development of polymer science.

Based on above concerns, this PhD thesis is focused on developing novel dendritic macromolecules with water-soluble, thermoresponsive and amphiphilic characteristics. In the introduction part, the concept, structure variations, synthesis approaches, applications, as well as the limitation of the present researches on dendritic macromolecules will be described. Following this, thermoresponsive

macromolecules of different structures are discussed in detail, including their applications, phase transition behavior, as well as methodology for investigation of the phase transition mechanism. Finally, amphiphilic polymers, especially amphiphilic homopolymers, are discussed. A technique named “breath figure” is introduced for the fabrication of polymer porous films with ordered pattern.

1.1 Dendrons, Dendrimers and Dendronized Polymers

1.1.1 Dendrons and Dendrimers Background

Dendrons and dendrimers are all dendritic macromolecules with “tree-like” architecture. Normally, dendrons can be considered as an individual branch unit, while dendrimers have a core unit surrounded by a number of dendrons (Figure 1). The first successful synthesis of dendritic molecules, which were named as “casade molecules”, was reported by Vögtle and co-workers in 1978.² In the years 1984 and 1985, Tomalia and co-works developed a series of amide-based, well-defined dendritic macromolecules, which were named for the first time “dendrimers”.^{3,4} With improved synthetic methods, these poly(amidoamine) (PAMAM) dendrimers could be produced on commercial scales. Afterwards, this kind of macromolecule attracted more and more attention, and various other dendrimer systems were developed.^{5–7} The typical structural properties of dendrimers include well-defined highly branched structures, three-dimensional spherical geometry, nanometer size of individual molecule, as well as large number of functional surface groups. These make them attractive for diverse applications, such as, as “dendritic box” for drug delivery and molecular imaging,^{8–10} organic light emitting diodes,^{11,12} molecular electronics,¹³ catalysis¹⁴ and so on.

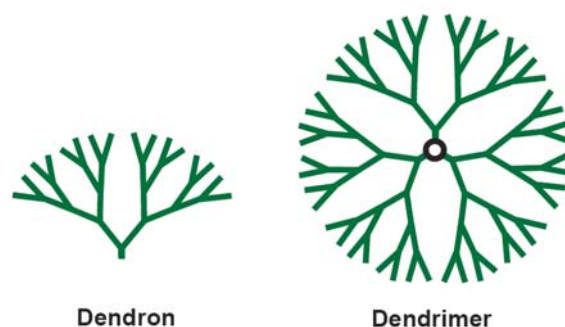


Figure 1. Cartoon of dendron and dendrimer.

1.1.2 Dendronized Polymer Background

The main drawback of dendrimers is the requirement of a sophisticated synthesis, which limits achievability of higher generations, while the molecular size is mainly dependent on dendron generation. As an alternative, dendronized polymers were first reported as “rod-shaped dendrimers” by Tomalia at Dow,^{15–17} and further developed by Percec,¹⁸ Schlüter¹⁹ and Fréchet,²⁰ *et al.* These polymers are constructed by a linear polymer backbone together with densely grafted dendrons at each repeat unit.^{21–25} As shown in Figure 2, the linear, random-coil polymer has been stretched due to the densely packed dendrons, and the molecules adopt rod-like nanocylindrical shape. In contrast to both linear polymers and dendrimers, this kind of architecture affords dendronized polymers with several new characteristics, including a large molecule size (3–12 nm in diameter and several hundred to thousand nanometers in length), variable thickness (dependent on dendron generations), as well as increased rigidity and more chance for further functionalization either on the periphery or in the interior parts. It provides the possibility to directly visualize or manipulate individual polymer chains. A typical example from a recent work of our group is shown in Figure 3. A homologous series of first to fourth generation (G1 to G4) amide-based dendronized polymers were synthesized via attach-to route.²⁶ They were mixed together and spin coated onto the mica surface. From their AFM images, individual chains of these four different generation polymers can be identified directly due to their different thickness.

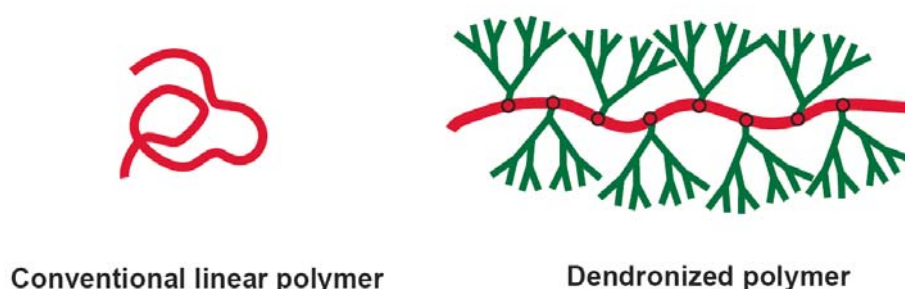


Figure 2. Cartoon of conventional linear and dendronized polymers.

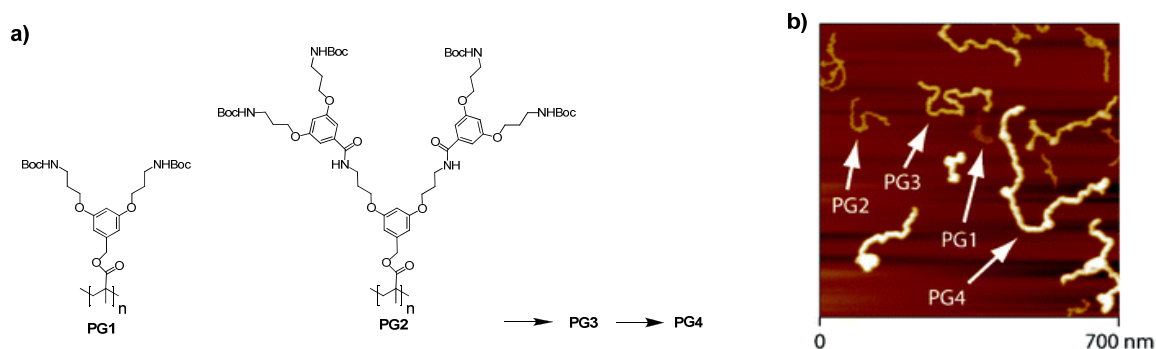


Figure 3. a) Chemical structures of the amide-based, first to fourth generation dendronized polymers; b) AFM height image of a mixture of PG1-PG4 polymers spin-coated from chloroform onto mica, showing mainly individual entities. Representative chains of each generation are marked. The picture was taken from the reference.²⁶

1.1.3 Synthesis Methodology to Various Dendronized Polymers

Several strategies have been developed for the synthesis of dendronized polymers, which have been detailed in review papers.^{22,24} The two mostly used methods are “macromonomer” and “attach to” routes (Figure 4). In the former route, the macromonomers carrying dendron of desired generation are polymerized and directly lead to the corresponding polymers with well-defined structures. This method normally works well for the synthesis of low generation polymers with high molar masses, but is difficult for the high generation polymers to reach high molar masses. While for the later route, low generation polymers are synthesized first, and then, the desired high generation ones are obtained by attaching low generation dendrons onto the periphery of low generation polymers through the peripheral functional groups. By this method, high generation polymers with high molar masses can be achieved, but their structure will be more or less ill-defined due to the difficulties in achieving 100% coverage for each reaction step. Normally the higher the generation, the lower the coverage will be.

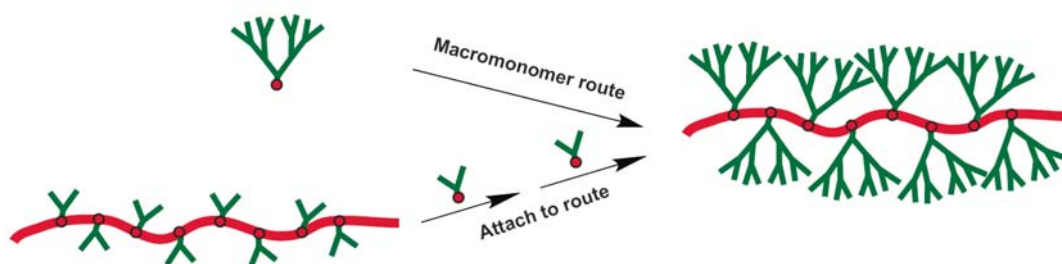


Figure 4. Schematic illustration of the two synthetic strategies toward dendronized polymers: macromonomer and attach to routes.

The specific architecture of dendronized polymers has inspired many research groups involved in this field. Up to now, dendronized polymers with various dendrons and polymer backbones were reported. Typical examples are shown in Figure 5. Polymers 1 to 7 were synthesized *via* the macromonomer route. The acrylamide (1),^{27,28} thiophene (2)²⁹ and proline (3)³⁰ -based dendronized polymers with polymethacrylate backbone were developed in our group. The Y at the surface of polymer 1 can be either neutral (Boc, Cbz and azide-protected amines) or charged ammonium functional groups for further modification. Polymer 2 constructed by thiophene dendrons was designed as cylindrical organic semiconductor. The use of proline as the branching units affords polymer 3 with extremely high rigidity and chirality, which forces the polymer adopting a stable helical conformation. Dendronized poly(fluorene) 4 with charged amino groups at the periphery was synthesized by Bo and co-workers.³¹ It is water-soluble and exhibits remarkably high photoluminescence quantum efficiency in water. The dendronized polystyrene 5 with long alkyl chains and poly(phenylacetylene) 6 were reported by the Percec group.^{32,33} The bulkiness of the dendrons, the crystallinity of the alkyl chains and the tacticity of the polymer backbone led to the formation of ordered secondary structures in the solid state. Besides these homopolymers, alternating copolymer 7, was also synthesized and their self-assembly behavior investigated.³⁴ For more examples about dendronized block copolymers, please refer to Figure 13. Concerning the common drawback of the macromonomer route for achieving high generation polymers with high molar masses, several other dendronized polymers were prepared *via* the attach-to route. The homologous series of G1 to G4 amide-based polymers (Figure 3) mentioned before is a typical example. Besides, another two famous analogs were developed by the Fréchet group: the dendronized polymethacrylate 8 carrying benzyl ether dendrons^{35,36} and the poly(L-lysine) 9 bearing polyester dendrons.³⁷ Due to the easy synthesis of the benzyl ether dendron, it has been widely used for constructing more interesting dendritic macromolecular systems. Polymer 9 is water-soluble and biodegradable, which is believed to be a good candidate for bio-related applications.

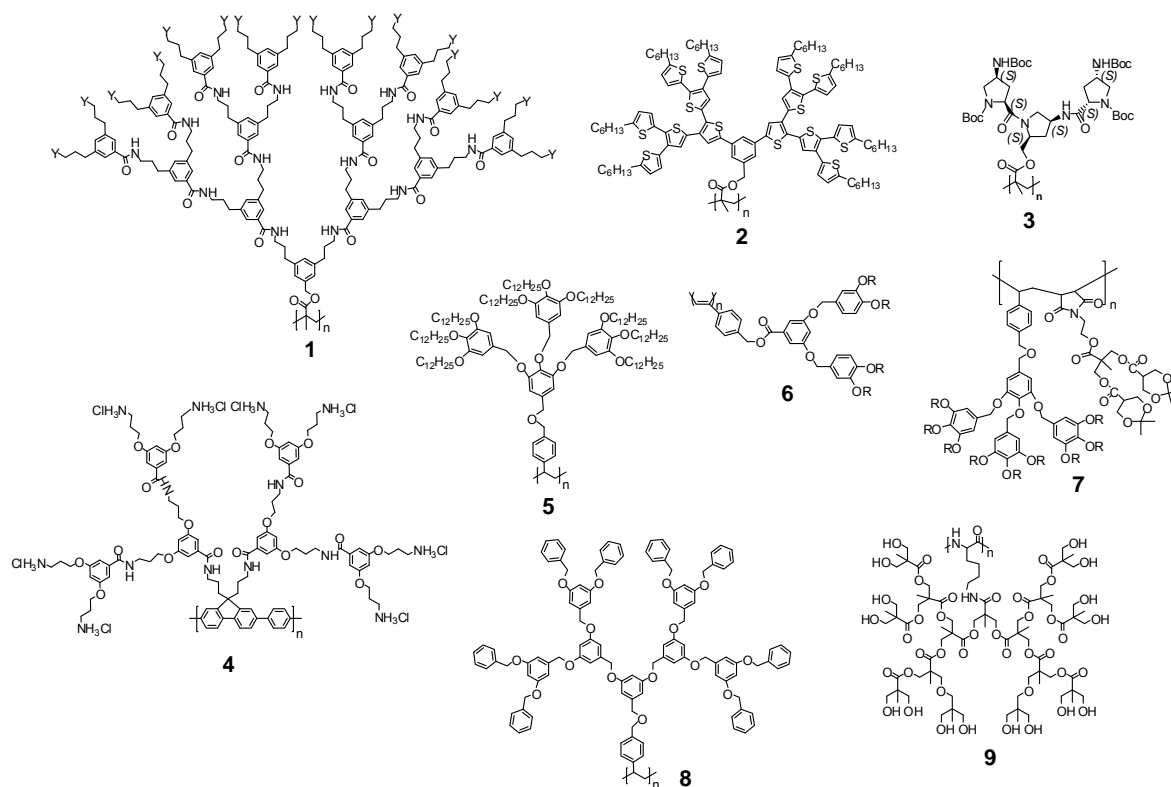


Figure 5. Dendronized polymers with various chemical structures: **1–3**, amide,^{27,28} thiophene²⁹ and proline³⁰-based dendronized polymethacrylates prepared by Schlüter *et al.*; **4**, dendronized poly(fluorene)³¹ prepared by Bo *et al.*; **5** and **6**, dendronized polystyrene with long alkyl chains³² and poly(phenylacetylene)³³ prepared by Percec *et al.*; **7**, Dendronized copolymer³⁴ prepared by Wang *et al.*; **8** and **9**, benzyl ether^{35,36} and polyester³⁷-based dendronized polymers prepared by Fréchet *et al.*

The polymer systems described above are all constructed *via* covalent linkages. Recently, supramolecular dendronized polymers constructed through non-covalent interactions (hydrogen bonding or host-guest interaction) have drawn much attention and some examples are shown in Figure 6. Interactions of chiral dendrons with optically inactive polyacetylene led to the formation of supramolecular helical polymers.³⁸ Supramolecular dendronized polyacetylenes from G1 to G3 were reported by Stoddart and co-workers (Figure 6b).³⁹ These polymers were constructed by multiple self-assembly between Fréchet-type dendritic dialkylammonium salts (“hooks”) and side-chain functionalized crown ether (“eyes”) polymers. The formed systems are acid-base switchable to either an ON (rigid dendronized polymers) or an OFF (flexible polymers) state. Jiang and co-workers reported hydrogen-bonded dendronized polymers (Figure 6c),⁴⁰ which were formed by the attachment of

Fréchet-type benzyl ether dendrons (G2 and G3) with a carboxyl group at the apex site to the linear poly(4-vinylpyridine) via hydrogen bonding in chloroform. It was found that these polymers could self-assemble into stable nanosized vesicles in common solvents. Based on a similar mechanism, Tong and co-workers recently reported the formation of dendronized polymers through the ionic binding of amphiphilic dendrons (tri-substituted benzoic acid) on linear polymers [poly(ethylenimine) (PEI) or poly(allylamine hydrochloride) (PAH)] (Figure 6d).⁴¹ The mesomorphous structures of these polymers were determined by the binding sites. The complexation of PEI and PAH with the dendrons resulted lamellar smectic and hexagonal columnar phases, respectively.

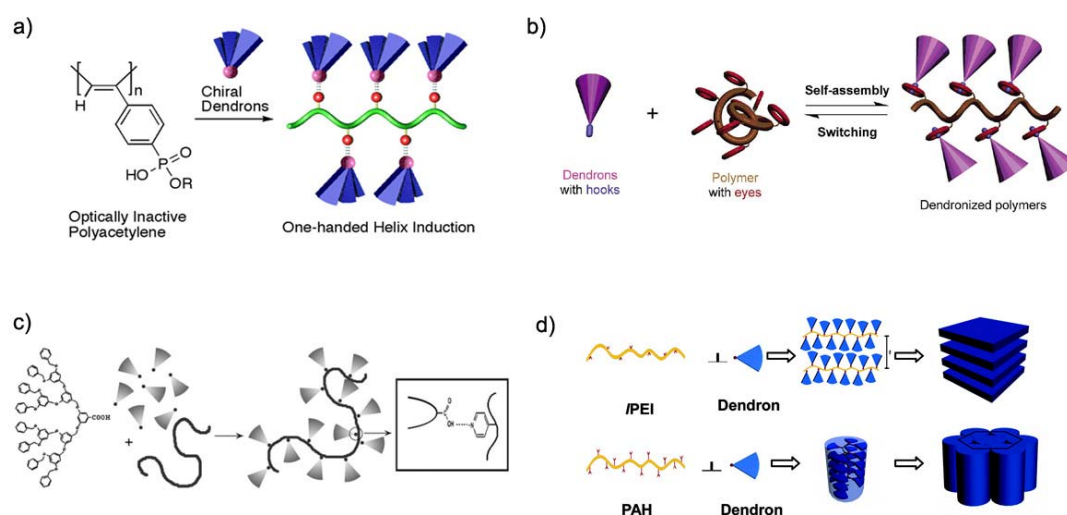


Figure 6. Schematic representation of dendronized polymers formed *via* supramolecular construction based on either donor-acceptor interaction (b),³⁹ or hydrogen bonding (a,³⁸ c,⁴⁰ and d⁴¹).

1.1.4 Applications of Dendronized Polymers

To date, dendronized polymers have already been explored for various fundamental applications due to their versatile chemical structures and the unique architecture. Some typical examples are shown in Figure 7. The polycationic, amide-based dendronized polymers reported by our group have been used for different purposes. The positively charged ammonium groups at the periphery led to interactions of these polymers with negatively charged DNA, forming supra-helices (Figure 7a).⁴² Besides, the charged periphery and the un-charged interior made these polymers amphiphilic, which led the high generation (G3 and G4) analogs to form double-stranded fibers in water at relatively high concentrations.⁴³ The structure varies along the fibers

including the formation of a double helix with a pitch of about 7.0 nm for PG3 and 9.0 nm for PG4 (Figure 7b). Furthermore, by ionic complexation of the amide dendronized polymers with anionic sulfonated lipid surfactants, supramolecular comb-like liquid-crystalline polymers were obtained.⁴⁴ It was found that by variation of the polymer generation and chain length of lipids, various ordered microphases were observed, including amorphous isotropic fluid, columnar rectangular, columnar hexagonal, columnar tetragonal and lamellar morphologies (Figure 7c). Due to their nanoscopic sizes, dendronized polymers can also be applied as a target for single molecular reaction. For this purpose, alkylamide-based dendronized polymers (G3) with peripheral photo-sensitive azide groups were synthesized.⁴⁵ As shown in the AFM image of Figure 7d, the individual molecule chains could be moved across the surface, and then cross-linked together by irradiation with UV light. The successful formation of covalent bonds between two polymer molecules was further proved by mechanically challenging the linkage with the AFM tip until the chain ruptured beside the linkage. Dendronized polymers can also be used in catalysis. As shown in Figure 7e, a hybrid dendronized cyclo-copolymer containing catalytic sites along the polymer backbone was reported by Fréchet and co-workers.⁴⁶ In this work, the polymer bearing supernucleophilic catalytic pyrrolidinopyridine pendent groups was dendronized with Fréchet type polyester dendrons terminated with long alkyl chains. The catalytic sites were buried within the “rod-like” polymer chains and encapsulated by surrounding dendrons, forming a polarity field along the cross-section of the individual molecule. By this way, a nano-environment was created which led to an enhanced catalysis activity of the esterification of a tertiary alcohol with pivalic anhydride. Dendronized polymers were also used as stabilizers and templates for the formation of cadmium sulfide (CdS) nanoparticle necklaces (Figure 7f).⁴⁷ The pyridine-functionalized polymers with Fréchet-type benzyl ether dendrons as the pendent groups were first prepared. The Cadmium ions were coordinated with the pyridine and carboxyl groups along the polymer backbone and transformed to Cds particles by H₂S gas. It was found that only polymer bearing G2 dendrons could lead to the arrangement of nanoparticles into a necklace. Recently, amphiphilic dendronized copolymers were designed to form superstructures *via* self-assembly. One example is shown in Figure 7g. An amphiphilic rod-coil-rod type triblock copolymer composed of a hydrophilic linear PEG in the middle and two hydrophobic dendronized polymethacrylates at the ends was prepared.⁴⁸ Its self-assembly

behavior in a mixed solvent (THF/water) was investigated. Interestingly, different morphologies, including spherical and cylindrical micelles, super-helices and super-rings were realized by changing the water content of the solvent. Last but not the least, dendronized polymers have also been utilized as new scaffolds for drug delivery. The multiple functional groups in the periphery and cavities in the interior of these polymers provide good environment for drug loading and encapsulation. Their relative large molecular size can lead to long circulation time inside the body, which is an advantage for targeted drug delivery due to the enhanced permeation and retention (EPR) effect.⁴⁹

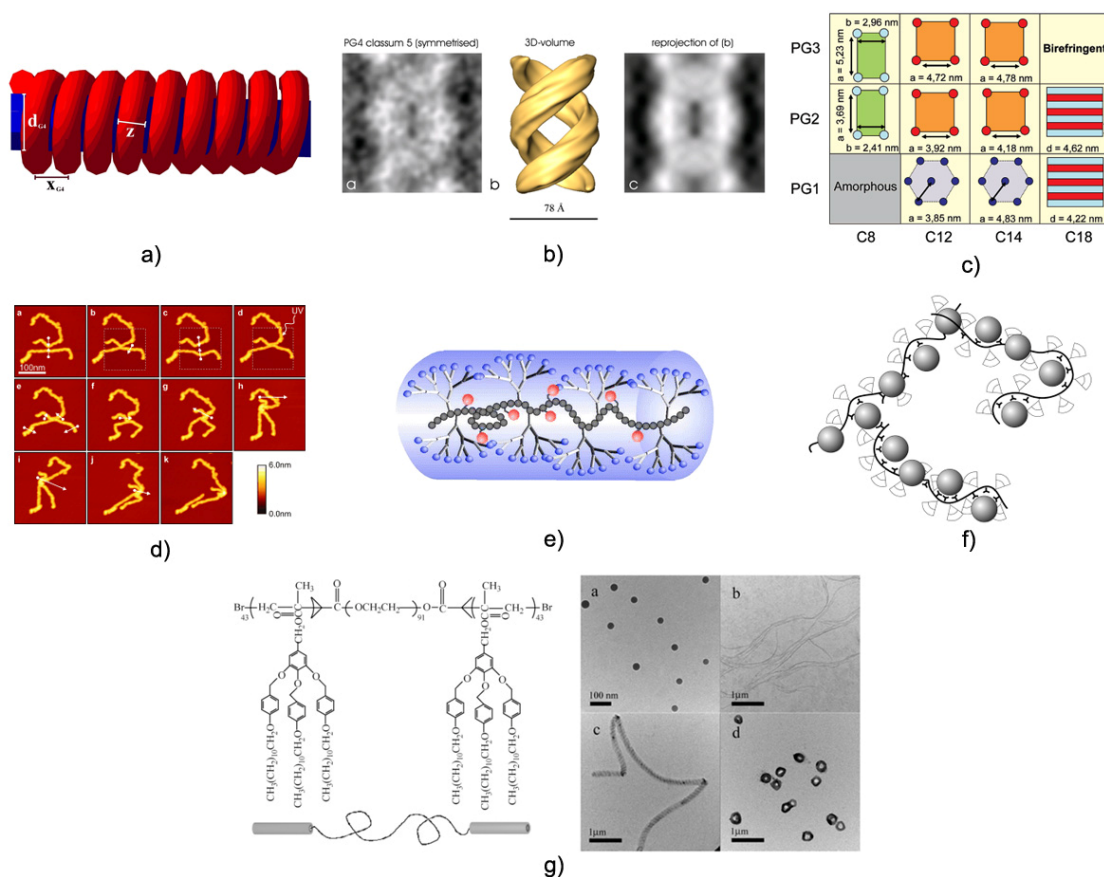


Figure 7. Various applications of dendronized polymers: a) DNA wrapping;⁴² b) Double helix formation;⁴³ c) Bulk structures;⁴⁴ d) Single molecular reaction;⁴⁵ e) Catalysis;⁴⁶ f) Nano-templates;⁴⁷ g) Self-assembly.⁴⁸

Though dendronized polymers have already been used for some fundamental researches, only few of them with functional groups were reported,⁵⁰ and most of the cases still lack of functionality or property for real material applications. Except some charged homopolymers⁴³ or copolymers (Figure 5, polymer 1 with $Y = \text{NH}_3^+$)⁵¹ as well as Fréchet-type polyester dendron-based systems (Figure 5, polymer 9),^{37,52} most of

the reported dendronized polymers can only be dissolved in organic solvents. Less water-soluble analogs were reported, and some polymers even contain toxic groups. All these hamper their further applications in bio-related areas. Besides, synthesis of dendronized polymers normally suffers from expensive materials, multiple synthetic steps and tedious purification. These hinder their large scale synthesis, not mentioning for industry production. When high generation polymers are targeted, the obtained polymers are either with low molar mass (even oligomers) from macromonomer route or with ill-defined structures from attach to route. Although well-defined polymers could be achieved from the macromonomer route and it is easy to achieve high molar mass polymers in high concentration media, most of the reported macromonomers are, unfortunately, solid. They can not be polymerized in bulk or even can not form highly concentrated solutions due to their low solubility. Therefore, it is highly necessary to design new dendritic macromolecules with the characteristics of cheap and easy synthesis, more functionality, as well as water-solubility and biocompatibility.

1.2 Thermoresponsive Polymers

As discussed before, thermoresponsive polymers are one of the most interesting molecules among the “smart” polymers. Normally, this kind of polymers has a LCST. They are water-soluble at low temperature, but start to collapse from water due to dehydration, and subsequently form aggregates when the temperature is increased to their LCST (Figure 8). This leads to a change of the solution from homogeneous to heterogeneous. The LCST of these polymers normally depends on the hydrophobic and hydrophilic balance within the polymers, whereas the phase transition rate is influenced either by the polymers themselves or their architectures.^{53,54}

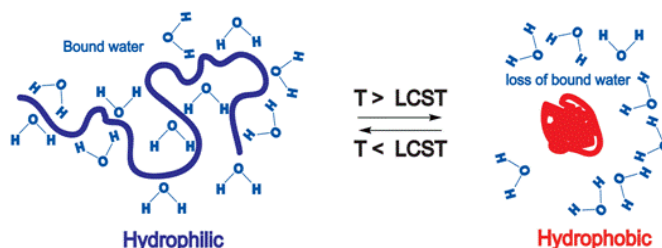


Figure 8. Schematic representation of the collapse of thermoresponsive polymers from a hydrophilic conformation (left) to a hydrophobic conformation (right) when the temperature passes through the LCST. This collapse is associated with liberation of water molecules.

Because of their special properties, thermoresponsive polymers have been intensively explored for many applications in areas ranging from material science to biology. They are considered to be good vehicles for controlled drug delivery as the encapsulation and release of the drug molecules can be controlled simply by temperature.^{55–58} For this purpose, the polymers need to be biocompatible and show a LCST around body temperature. They have also been widely used to create bio-relevant switchable surfaces for bioseparation, biosensors and cell adhesion.^{59–62} There are also a lot of reports on gold nanoparticle surface decorations with thermoresponsive polymers.^{63–66} Furthermore, this kind of polymers have been applied as actuator,^{67–69} as artificial muscles,⁷⁰ for catalysis,⁷¹ and so on.

Until now, various thermoresponsive polymers with either linear or non-linear structures have been investigated. The linear polymers include homo- and block (co)polymers. The non-linear ones include comb-like and star-shaped polymers, as well as dendritic macromolecules.

1.2.1 Thermoresponsive Polymers with Linear Architecture

Conventional linear thermoresponsive polymers include poly(N-isopropylacrylamide) (PNiPAM), poly (ethylene glycol) (PEG), poly (methyl vinyl ether), poly(vinylmethyloxazolidinone), poly(N-vinylcaprolactam), elastin-like polypeptides. Among them, PNiPAM is the most famous one (Figure 9a). It has been widely studied and applied for various applications due to several reasons: 1) The commercial availability of the monomer and the easy synthesis of the polymer; 2) Its LCST is about 32°C, which is close to body temperature; 3) Its LCST is less sensitive to slight change of environment conditions (pH value and concentration); 4) It shows fast and sharp coil-globule phase transition above the LCST.⁷² However, as shown in the turbidity curves in Figure 9b, one obvious disadvantage of PNiPAM is that its phase transition shows large hysteresis between the heating (dehydration) and cooling (rehydration) processes. This phenomenon was examined by both thermal kinetic measurements *via* modulated temperature differential scanning calorimetry (MTDSC)⁷³ and by hydrogen-bonding analysis *via* Fourier-transform infrared (FTIR) spectroscopy.⁷⁴ It is believed that this hysteresis is attributed to the formation of some additional intra- and interchain hydrogen bonds between the >C=O and H-N< groups of PNiPAM in the collapsed state. The interchain hydrogen bonds, which act

as “cross-linking” points among different chains, can not break immediately when the temperature decreased to or below the LCST, so that the chain dissociation is delayed when comparing to the heating process. Though it has such a drawback, PNIPAM is nevertheless a popular polymer due to its other unique properties. Considering different application purposes, PNIPAM has been combined into (co)polymers with different architectures, including block,⁷⁵ star-shaped,^{76,77} cross-linked^{78,79} or dendritic ones.⁸⁰

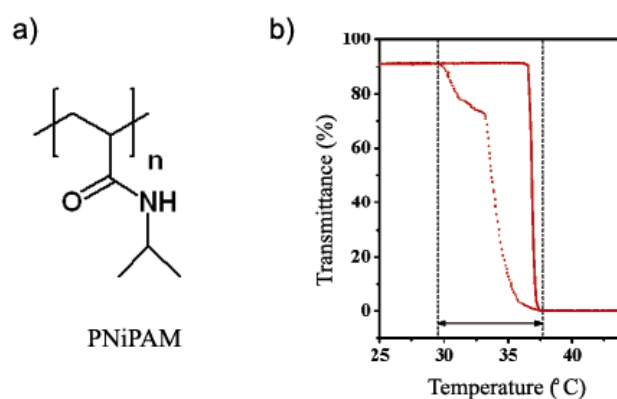


Figure 9. Chemical structure (a) and turbidity curves (b) of PNIPAM.⁸¹ Solid line: heating cycle; Dotted line: cooling cycle.

1.2.2 Thermoresponsive Polymers with Non-linear Architecture

Polymers with non-linear architecture have more structure variable possibilities, thus, they are more interesting than their linear counterparts. Different from linear PEG which exhibits a LCST above 85 $^{\circ}\text{C}$,⁸² polymers carrying short oligo(ethylene glycol) (OEG) side chains are able to show much lower LCSTs, forming another kind of interesting thermoresponsive polymers. The same as linear PEG, they are normally biocompatible. Compared to PNIPAM, they show much smaller or negligible hysteresis between heating and cooling processes. Allcock and coworkers reported the first example of OEG-based thermoresponsive polymers with comb-like and dendritic architectures.⁸³ They contain polyphosphazenes as backbone and linear or dendritic OEG chains of different length, density and terminal groups as the pendants (Figure 10). The LCSTs of these polymers cover a broad temperature range from 30 to 80 $^{\circ}\text{C}$, which are independent on the polymer concentrations. But, unfortunately, these LCSTs were determined only by visual observations during heating, and therefore, their thermoresponsiveness was not investigated in detail.

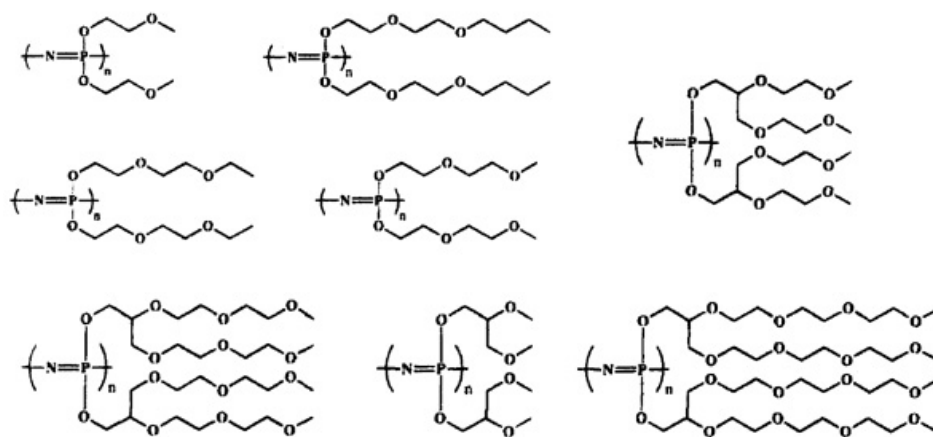


Figure 10. OEG-based comb-like and dendritic polyphosphazenes.⁸³

Recent years, comb-like polymers with short OEG chains have received increasing interest, and some examples are summarized in Figure 11. A series of poly[oligo(ethylene glycol) alkyl ether methacrylate]s were prepared *via* anionic polymerization by Ishizone and co-workers (Figure 11a).^{84,85} The LCSTs of these polymers can be tuned from 4 °C to 68 °C by changing length (di-, tri- and tetra-) or terminal groups (methyl or ethyl) of the OEG side chains. They found that the molar masses of the polymers exhibited pronounced influence on the LCSTs. The turbidity curves in Figure 9c show that the LCST changed about 4 degrees with a change of molar mass from 16000 to 37000. Although the hysteresis is not obvious (normally within 3 °C), the phase transitions of these polymers tend to be broad ($\Delta T \sim 2\text{--}6$ °C). Zhao and coworkers reported the synthesis of thermoresponsive polyacrylates and polystyrenics with short OEG pendent groups by the nitroxide mediate radical polymerization (NMRP) method (Figure 11b).^{86,87} They noticed that in the molar mass range investigated, the LCSTs of the polymers were affected greatly by the hydrophobic end-groups, the molar masses and concentrations of the polymers. As show in Figure 11b, for each of the four polymers, the LCST decreased dramatically about 10 to 15 °C with the increase of polymer concentrations from 0.1% to 2%. A novel class of copolymers based on 2-(2-methoxyethoxy)ethyl methacrylate and oligo(ethylene glycol) methacrylate P(MEO₂MA-co-OEGMA) were synthesized *via* the atom transfer radical polymerization (ATRP) technique by Lutz *et al.*^{81,88} These polymers show improved thermoresponsive properties and their LCSTs can be tuned in the range of 26 ~ 90 °C, by adjusting the copolymer composition (Figure 11c). As

shown in the turbidity curves, though the hysteresis between heating and cooling processes is negligible, most of the polymers show relatively broad phase transitions. Besides, all these comb-like polymers were prepared *via* living controlled radical polymerization, which required restrict experimental conditions.

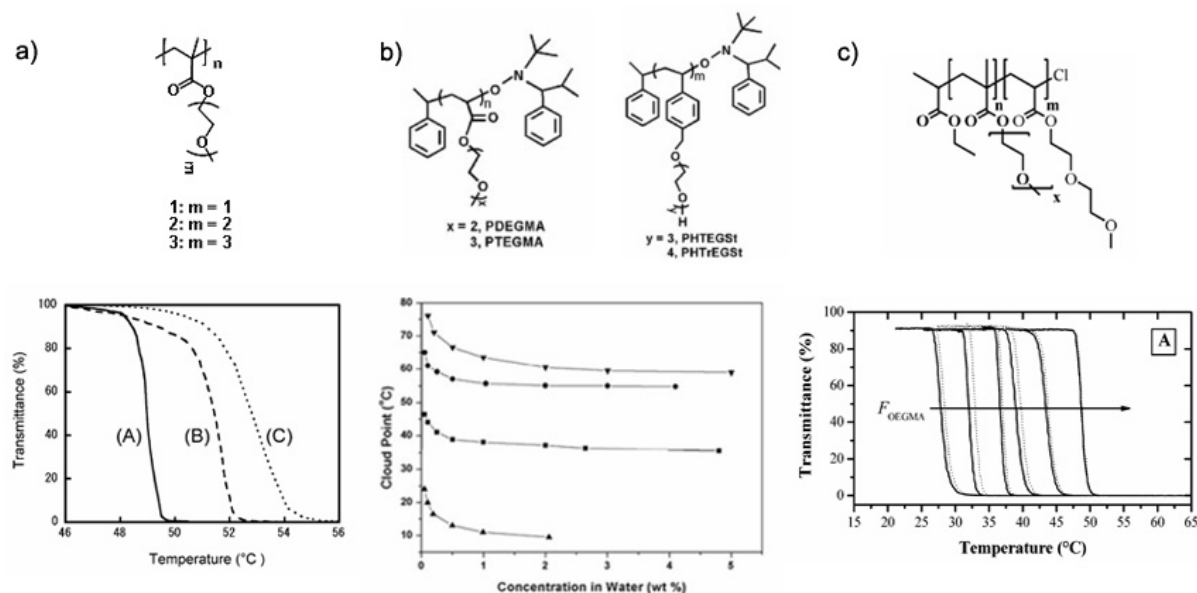


Figure 11. Chemical structures of short OEG chains based thermoresponsive polymers and typical results from turbidity measurement: a) Polymethacrylates with different length of OEG side chains and turbidity curves obtained from 0.2 wt % aqueous solution of poly(3)s (curve A, $M_n = 37\,000$; curve B, $M_n = 16\,000$; curve C, $M_n = 6700$);⁸⁴ b) polyacrylates and polystyrenics with short OEG side chains and concentration effect on the cloud point of (■) PDEGMA, (●) PTEGMA, (▲) PHTEGSt, and (▼) PHTrEGSt in water;⁸⁶ c) P(MEO₂MA-co-OEGMA) copolymers with different m, n ratio and turbidity curves measured from their aqueous solutions (3 mg/mL).⁸⁸ Solid lines: heating cycles; Dotted lines: cooling cycles.

Thermoresponsive polymers with dendritic architectures have also been developed and some examples are outlined in Figure 12. Their thermoresponsiveness can normally be achieved either by introduction of thermoresponsive units onto the surface of the dendritic macromolecules^{89–92} or by incorporation of both hydrophobic and hydrophilic moieties properly into the dendritic structures.^{93,94} Kono and coworkers reported that alkylamide groups covered poly(amidoamine) (PAMAM) or poly(propylenimine)(PPI) dendrimers show thermoresponsiveness.^{90,95,96} As shown in Figure 12a, except G2, all other PAMAM dendrimers show thermally induced phase

transitions (LCSTs) below 80 °C, which are dependent on dendrimer generations. G5 dendrimer with the most densely packed terminal thermoresponsive moieties shows the lowest LCST. But unfortunately, these dendrimers exhibit slightly broad phase transitions. Their thermally induced aggregation is unstable, as de-aggregation started when further increased the temperature. It was also found that the LCSTs of these dendrimers are dependent on their concentrations. Besides, *in vitro* cytotoxicity study proved that the PAMAM dendrimers possess certain toxicity.^{97,98} Therefore, further structure modification is necessary for their bio-applications. You and coworkers prepared a novel dendrimer via RAFT polymerization with a thermoresponsive PNiPAM chain as the shell and a non-thermoresponsive polyester-based dendrimer as the core (Figure 12b).⁸⁰ Unlike free PNiPAM, this dendritic macromolecule shows much broader phase transition ($\Delta T = 5$ °C). By using pentaethylene glycol as the hydrophilic functionality and decyl chain as the hydrophobic functionality, amphiphilic dendrons of up to the third generation were reported by Aathimanikandan *et al.* (Figure 12c).⁹³ These dendrons are thermoresponsive and their LCSTs are also generation dependent. Interestingly, they can self-assemble into micelles in polar solvents and reverse micelles in apolar solvents. But these dendrons also show broad phase transition as indicated from their turbidity curves. Different from the above examples whose thermoresponsiveness stem from the incorporation of thermoresponsive moieties, hyperbranched polyethers with a thermoresponsive backbone were developed by Yan and coworkers (Figure 12d).⁹⁹ These hyperbranched polymers were synthesized by proton-transfer polymerization of 1,4-butanediol diglycidyl ether (BDE) and various triols. Their LCSTs can be adjusted by changing either the ratio of different triols [TMP (trimethylolpropane) to TME (trimethylolethane)] or the ratio of BDE to TME. But some of them show slightly broad phase transitions. Besides, hyperbranched polymers are well-known for their ill-defined structures.

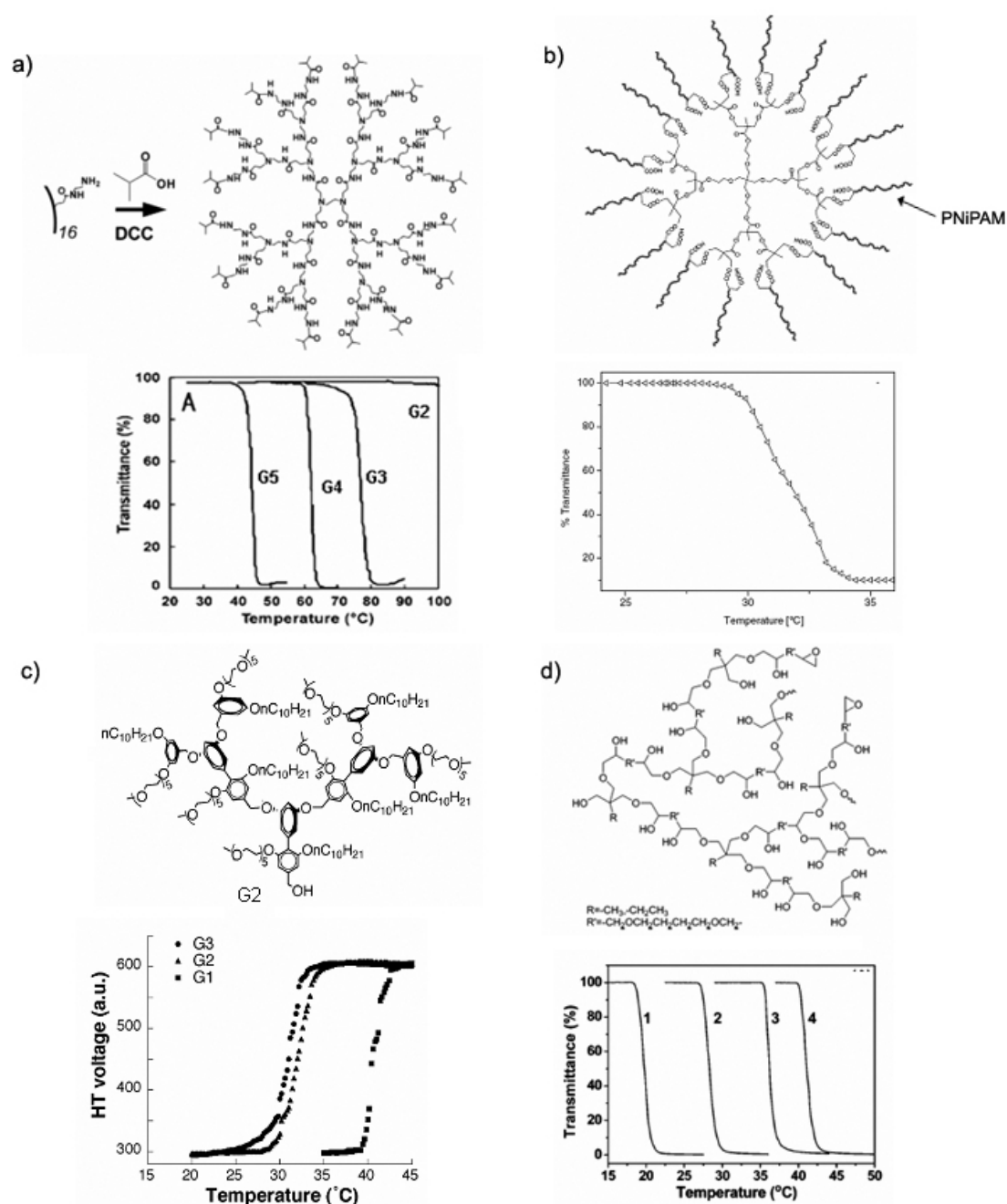


Figure 12. Chemical structures of dendritic thermoresponsive polymers and their turbidity curves: a) PAMAM dendrimer (G3) with IBAM terminal groups and turbidity curves (1°C/min) of different generation PAMAM dendrimers in 10 mM phosphate-buffered solutions (10 mg/mL, pH 9.0);⁹⁰ b) Dendrimer with PNIPAM at the surface and the turbidity curve from its aqueous solution;⁸⁰ c) Amphiphilic dendron (G2) and turbidity curves (2 °C/min) from the aqueous solutions of different generation dendrons;⁹³ d) Hyperbranched polymer (G2) and turbidity curves (0.5 °C/min) from the aqueous solutions (1 wt%) of hyperbranched polymers constructed by different mol ratios of BDE to triols (1: BDE/TMP = 1/1, 2: BDE/TMP/TME = 1/0.5/0.5, 3: BDE/TMP/TME = 1/0.1/0.9, 4: BDE/TME = 1/1).⁹⁹

1.2.3 Phase Transition Mechanism of Thermoresponsive Polymers

The thermally induced phase transitions of thermoresponsive polymers have gained a lot of attention and various analysis methods have been applied for understanding these processes on both macro- and microscopic levels. The dehydration or rehydration, chain collapse, aggregation or de-aggregation, the phase transition kinetics and reversibility, as well as the aggregate morphologies were all addressed.

Turbidimetry is an easy and commonly used methodology for determination of the LCST of a polymer, as well as the sharpness and the reversibility of the phase transition. All these information can be obtained from the turbidity curves as shown in Figure 11 and 12. The thermally induced aggregation of the polymer chains can be followed by dynamic light scattering (DLS) from which the hydrodynamic size of the aggregates can be determined. Combination of both dynamic and static light scattering, the morphologies of either the single collapsed polymer chain or the aggregates formed from multiple polymer chains can be estimated. By this way, Wu and coworkers successfully proved that the single PNIPAM chains in an extremely dilute aqueous solution followed a coil to globule transition at its LCST.^{100–103} Besides, the dehydration process of the polymer chains can be monitored via ^1H NMR spectroscopy, as once the dehydration starts, the proton signals of the polymer will become broad.^{86,104} As mentioned before, FTIR spectroscopy is a good method to probe the inter- and intra-molecular hydrogen bonding before and after the collapse of the polymer, from which the interaction between the polymer and water molecules can be further determined.^{74,105} Furthermore, the kinetics of the thermal processes is normally investigated by differential scanning calorimetry (DSC). Shibayama and coworkers reported that through measuring of the enthalpy change by DSC during the phase transition of PNIPAM, the number of associated water molecules (about 13) within one repeat unit of NiPAM can be evaluated.¹⁰⁶ Specially, by using MTDSC for a thermal kinetic study, the hysteresis of linear PNIPAM during the heating and cooling process was clearly detected.⁵³ The thermal response rate of PNIPAM homopolymers, PNIPAM/PEO block and graft copolymer were all investigated and compared.⁵⁴ It was found that the architecture played a role in the remixing rate of the polymer chains with water molecules. The homopolymer and block copolymer behaved quite similarly, whereas the graft copolymer showed faster rehydration rate than the others. This kind of architecture effect was also revealed when linear

PNiPAM chains were covalently attached to a fourth generation dendritic core.¹⁰⁷ This dendritic macromolecule exhibited a so-called double phase transition phenomenon due to the difference of chain packing density: densely packed inner PNiPAM segments collapse in the temperature range of 20–30 °C; less densely packed PNiPAM segments in the outer region collapse as free linear PNiPAM chains around 32 °C. A similar phenomenon was also reported when PNiPAM is densely grafted onto gold nanoparticles¹⁰⁸ or flat surfaces.¹⁰⁹ Additionally, high-frequency dielectric relaxation technique was used to study the temperature dependent hydration number of PNiPAM and its monomer.^{110, 111} The number of hydrated water molecules is found to be 5-6 per NiPAM monomer and 10-11 per unit of PNiPAM, which is consistent with the result from DSC measurements by Shibayama. Recently, electron paramagnetic resonance (EPR) spectroscopy was also employed as an efficient tool to investigate the collapse mechanism of PNiPAM hydrogel.¹¹² In this measurement, TEMPO was used as the spin probe and added to the polymer solution. Due to the amphiphilic character of TEMPO, it could be detected from both the hydrophobic and hydrophilic environments. Therefore, a picture of the thermally induced collapse of PNiPAM hydrogel on molecular level was described. It was demonstrated that the polymer didn't follow a homogeneous but a discontinuous collapse mechanism with a coexistence of collapsed and expanded network regions above the LCST.

Based on above discussion, various thermoresponsive polymers have been investigated, with most of them being linear homo- and block (co)polymers. Although some dendritic systems have been reported recently, their thermoresponsiveness was mostly imparted from the incorporated thermoresponsive units. For nearly all cases reported up to date, either broad transitions or significant hysteresis were involved, therefore, it still remains a challenge to develop ideal thermoresponsive macromolecules. They could show not only fast and sharp transitions, small hysteresis between heating and cooling, tunable LCST in the physiologic range with less environmental sensitivity, but also should be biocompatible and easy to be synthesized. Besides, the thermally induced phase transition mechanism of the thermoresponsive macromolecules has been investigated, but most of the studies are limited to linear PNiPAM. Compared to linear polymers, dendritic macromolecules contain more variable units and their sizes of individual molecules are on the

nanometer range. These unique characteristics, together with novel chemical structural design, may afford dendritic macromolecules improved thermoresponsiveness and interesting collapse mechanism. All these aspects formed the main aim of the present thesis.

1.3 Amphiphilic Polymers

In nature, many biological molecules such as phospholipids, cholesterol, and bile salt possess amphiphilic properties, which direct their specific functions in living systems. Synthetic surfactants are another kind of amphiphilic molecules that are commonly used in our daily life. Inspired by them, various kinds of amphiphilic polymers composed of both hydrophilic and hydrophobic units were chemically designed and synthesized. The beauty of these macromolecules is that they can self-assemble either in selected solvents, or in bulk, or at interfaces to form versatile superstructures, such as micelles, vesicles, cylinders, lamellae, etc.^{113–115} These assemblies are the result of the non-covalent interactions between the incompatible units in certain environment. Tuning the amphiphilicity (volume fraction of the units) or the architectures of the polymers, their self-assembly can be controlled. Therefore, these types of polymers are highly interesting and have been explored for many applications in material science and biomedicine areas.^{116–119}

Amphiphilic polymers contain homo-, block-, random- or alternating (co)polymers. Among them, amphiphilic block copolymers are the most investigated ones, which can contain linear¹²⁰ or non-linear (comb-like, star-shaped and dendritic) structures.¹²¹ Investigation of linear block copolymers have been well documented in several reviews.^{122–124} Here only amphiphilic dendronized copolymers and homopolymers will be discussed.

1.3.1 Amphiphilic Dendronized Block Copolymers

With the development of synthetic chemistry, non-linear amphiphilic block copolymers, especially polymers containing dendritic side groups attracted more and more attention. The three dimensional branched structures of dendritic molecules lead to interesting self-assembly behaviors.^{125,126} Up to nowadays, only few reports

are related to dendronized block copolymers due to their synthesis difficulties. Some examples are summarized in Figure 13. Xi and coworkers reported one kind of amphiphilic diblock copolymers based on linear PEO chains and Percec-type G1 dendrons prepared with the ATRP technique (Figure 13a).¹²⁷ The interfacial behaviors of these polymers at the air-water interface were investigated with the Langmuir-Blodgett trough, and various morphologies were observed at different compression stages. At lower pressure, only wormlike individual polymer chains were formed. Upon gradually increasing the pressure, the polymer chains arrayed parallel to result in an ordered structure, which was then bended and twisted by further compression. Finally, large 3D aggregates were formed at the collapse state of the film. Another kind of amphiphilic dendronized diblock copolymers bearing Percec-type dendronized polystyrene and comb-like PEO were synthesized *via* the ATRP method by Chen and coworkers (Figure 13b).¹²⁸ These polymers could form rich morphologies via self-assembly in a mixture of methanol and THF. A series of diblock copolymers containing linear PNiPAM and dendronized polymethacrylates (G1 and G2) were synthesized *via* the RAFT polymerization technique by our group (Figure 13c).^{51,129} Based on the thermoresponsiveness of PNiPAM, the linear block is switchable from hydrophilic to hydrophobic upon changing temperature. The thermally induced aggregation of these copolymers with varied block lengths and dendron generations were investigated. It was found that they can self-assemble into aggregates of different morphologies, including spherical objects, large compound micelles, sheet and irregular objects.

Though block copolymers are interesting materials, strict experimental conditions are normally required for their synthesis, as most of them were synthesized *via* living polymerization techniques including ionic, RAFT, ATRP, and so on. Whereas the syntheses of random copolymers and homopolymers are much more robust and conventional free radical polymerization can be applied. Therefore, homopolymers with amphiphilic properties are attractive.

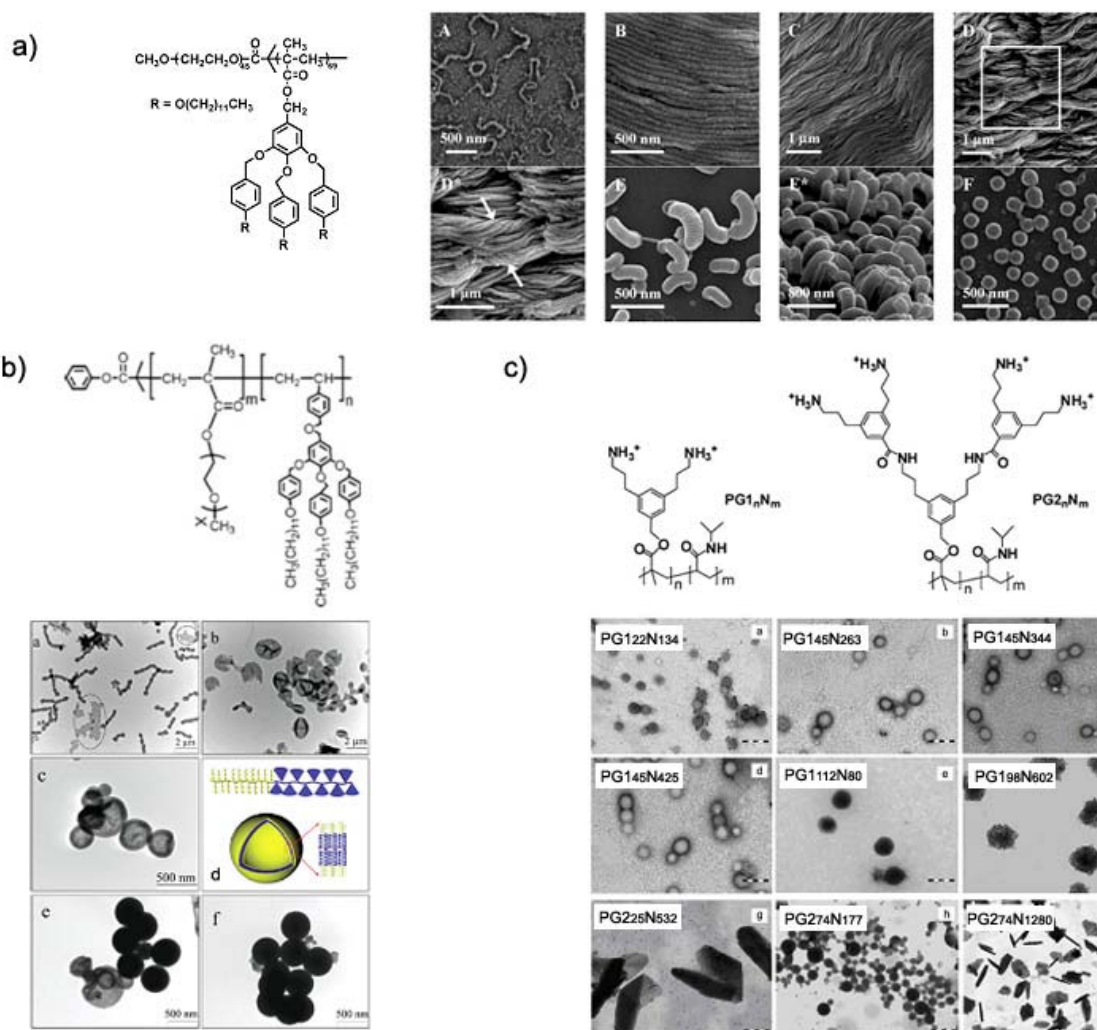


Figure 13. Chemical structures of various amphiphilic dendronized block copolymers and their self-assembled morphologies at interface (a)¹²⁷ or in solution (b) and (c).^{128,129}

1.3.2 Amphiphilic Homopolymers

A few amphiphilic linear homopolymers constructed by small molecular repeat units were reported and their self-organization behavior was studied. Examples are shown in Figure 14. Tang and coworkers reported a series of homopolymers constructed from hydrophiphilic amino acid pendants and hydrophobic conjugated polyacetylene (Figure 14a).¹³⁰ These polymers could form well-defined morphologies under different conditions *via* self-assembly, including rings, globules, cages as well as nanofibers. Homopolymers based on a polystyrene backbone, hydrophiphilic carboxylic acid and hydrophobic alkyl chain or benzyl group incorporated in the monomer unit were synthesized by Thayumanavan's group (Figure 14b).¹³¹ These polymers were

demonstrated to form both micelle and inverse micelle-like assemblies in different solvents.

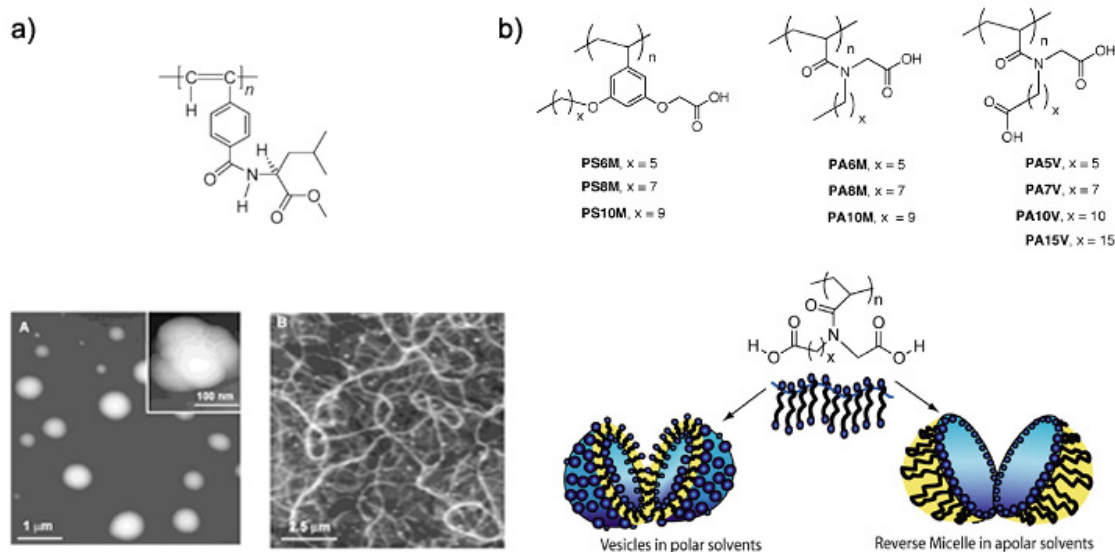


Figure 14. Amphiphilic homopolymers prepared by Tang *et al.*¹³⁰ (a) and Thayumanavan *et al.*¹³¹ (b).

Amphiphilic non-linear homopolymers with large repeat units were also reported. Cylindrical polymer brushes with poly(2-hydroxyethyl methacrylate)(HEMA) as the backbone and amphiphilic diblock side chains were synthesized *via* the ATRP technique by Müller *et al.* (Figure 15a).¹³² The amphiphilic side chains led to the formation of well-defined core-shell structures. The single wormlike unimolecular nanocylinders were clearly visualized by AFM. Homopolymers based on the dendronized polymer concept were prepared by our group.^{133,134} These polymers contain a conjugated backbone and Fréchet type benzyl ether dendrons as the hydrophobic units and OEG-covered dendrons as hydrophilic units, which were synthesized *via* Suzuki polycondensation (Figure 15b). The combination of hydrophobic and hydrophilic dendrons into one repeat unit around the backbone was assumed to lead to lengthwise segregation. This is quite different from amphiphilic block copolymers whose self-assembly normally follow perpendicular segregation along their backbone. These conjugated polymers could form a stable monolayer LB film at the air-water interface. Recently, by using the same method, another two amphiphilic dendronized homopolymers polyfluorene (PF) and poly(binaphthyl-*alt*-fluorene) (PBF) bearing OEG based dendrons as the hydrophilic groups and long alkyl chain based dendrons as the hydrophobic groups were developed by Bo, *et al.*

(Figure 15c)¹³⁵ They found that the configurations of the conjugated backbones played a very important role in the self-assembly of the polymers in DCM. Polymer PF with linear rodlike backbone conformation could self-assemble into nanosized wires, whereas PBF with folded rigid backbone conformation could form nanoparticles. But one obvious drawback is that these conjugated dendronized polymers have low molar masses due to experimental difficulties in Suzuki polycondensation. The polymerization degrees (DP_n) of the polymer in Figure 15b, of polymer PF and polymer PBF are about 20, 20 and 6, respectively. Besides, these polymers have no functional groups available for further modification.

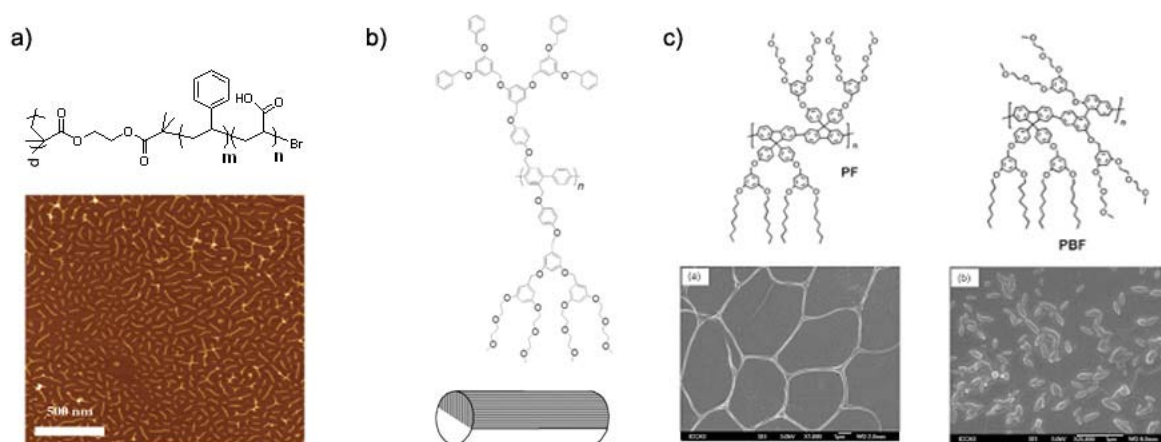


Figure 15. Amphiphilic homo-polymers prepared by Müller *et al.*¹³² (a) and Bo *et al.* (b) and (c).^{133,135}

In conclusion, amphiphilic homopolymers with small size repeat units and a flexible backbone are normally considered to be not useful for building well-defined suprastructures. One possible reason is that the closely packing of the hydrophobic and hydrophilic groups in each repeat unit hinders the phase separation. In contrast to conventional homopolymers, amphiphilic dendronized homopolymers are constructed from larger hydrophobic and hydrophilic dendrons, which may have the ability to show lengthwise phase segregate. Besides, the volume fraction (hydrophilic and hydrophobic balance) of the immiscible dendrons can be easily tuned by varying dendron generations. Nevertheless, only few examples of very short main chains with such architecture were reported. So, to design and prepare novel amphiphilic dendronized homopolymers is still a challenge.

1.4 Fabrication of Porous Polymer Films *via* the “Breath Figure” Technique

Nano and microporous films formed from self-assembly of polymers are interesting due to their potential applications in many areas as shown in Figure 16a. Normally, the fabrication of these films needs suitable templates, such as colloid crystals,^{136–138} meso-porous silica,^{139,140} microphase-separated block copolymers,^{141,142} etc. The disadvantages of using these templates include: 1) Inability to vary the pore size; 2) need of removing the templates. In contrast, the “breath figure” (BF) method is a low cost, efficient and easy technique to form porous polymer films.^{143,144} Furthermore, the porous morphologies can be easily controlled by changing the casting and “breath” conditions. The size of the pores can be in the range of 50 nm to 20 μm . Besides, no extra effort is needed to remove the water template as it can simply be evaporated. Therefore, the BF technique has been widely used for fabrication of polymer films with regular porous structures since its discovery^{145–149}. A typical example is shown in Figure 16b.

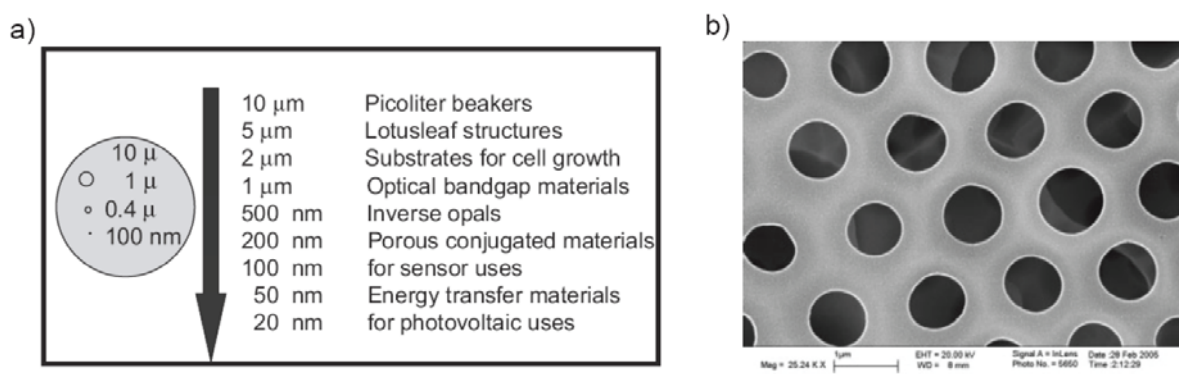


Figure 16. Potential applications of porous films with various pore sizes (a) and a typical example of a polymer film with ordered porous array (b).¹⁴³

The basic principle of the BF method is shown in Figure 17.¹⁵⁰ Moist air flowing over a polymer droplet in an organic solvent on a substrate causes the quick evaporation of the solvent, which results in a cold surface ($-6\sim 0\text{ }^{\circ}\text{C}$). This cold surface leads to the condensation of water from air into the droplets, which form a closely packed array on the liquid droplets surface. These droplets don't coalesce but sink into the polymer solution. The new generations of water droplets deposit on the top of the previous ones with time. After the evaporation of both solvent and water, an imprint of the water droplets with an ordered 3-D array in the dried polymer film is formed. The

mostly used solvents for the polymer solution include CS_2 , CH_3Cl , benzene and THF. The substrate can be either solid (glass, mica, silicon wafer, etc) or liquid (water). The regularity and size of the pores are influenced by several parameters, including the air flow rate and humidity, the concentration and molar mass of the polymer. If air flowing is too fast, the solution evaporates too rapidly and an unordered film will be obtained, as the water droplets have not gotten enough time for a regular arrangement. Normally, regular structures can be easily achieved under high humidity ($> 50\%$), and the pore size increases with a linear relation with the humidity.¹⁵¹

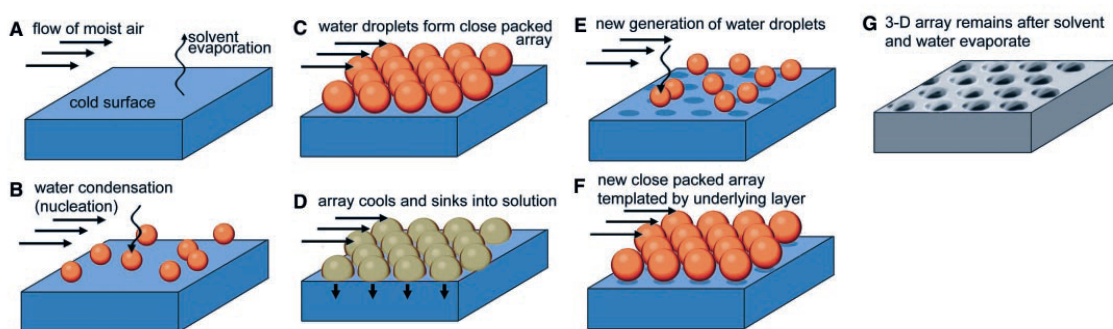


Figure 17. A model for the formation of ordered porous structures in polymer film.¹⁵⁰

The first polymers employed for this process are star polystyrene (SPS) and poly(*para*-phenylene)-block-PS(PPS).¹⁴⁹ Francois and coworkers indicated that the star-shaped polymers and block copolymers seemed to be necessary for the formation of honeycomb morphologies via the BF method, as no such arrays could be obtained from linear PS. But this viewpoint was proved to be not true by many following works in this area. Srinivasarao and coworkers reported that linear PS also could form regular porous films under certain conditions.¹⁵⁰ It was found that compared to star, block copolymers or functionalized linear polymers, less robust conditions (such as very high humidity $> 70\%$ and high polymer concentration) are required for the linear homopolymers and highly hydrophilic polymers to self-assemble into ordered porous array. To date, the structures of the polymer employed with the BF method become more and more diverse, including star-shaped,^{152,153} rod-coil block,¹⁵⁴ rigid-rod,¹⁵⁵ amphiphilic block,^{156,157} comb-like¹⁵⁸ as well as linear (co)polymers.¹⁵⁹ Recently, polymers with dendritic structures were also tested for this process as shown in Figure 18. Xi and coworkers reported that honeycomb patterned

porous films were formed on both solid and water surfaces *via* the BF method by using amphiphilic dendronized block copolymer as the precursor (Figure 18a).¹⁵⁴ The same group also studied the influence of the humidity and polymer concentration on the morphologies of the pores and discovered that the most ordered pattern was formed from the copolymer with a concentration of 1.00 mg/mL and around a humidity of 85%. Yan and coworkers reported the preparation of honeycomb patterned films based on amphiphilic hyperbranched poly(amidoamine)s (Figure 18b),¹⁶⁰ which form ordered morphologies on various substrates (quartz, glass, mica and gold) under a wide range of humidity (30% to 72%). Besides, by changing the polymer concentration, the thickness of the films can be tuned from nanometer to micrometer scale. Recently, a series of dendron-functionalized star-shaped polymers were prepared by Qiao and coworkers.¹⁵² The polymers were composed of Fréchet-type polyester dendrons with different generations (G1 to G4) and terminal groups (acetamide, hydroxyl and pentadecafluorooctanoyl) (Figure 17c). All these polymers were able to form porous films with the BF method, and both the dendron generation and the polarity of the functional groups had pronounced effects on the pore morphologies. By increasing the generation of the hydroxyl terminated polymer from G1 to G3, the regularity of the pores increased and the morphology changed into a thin-walled interconnected honeycomb film, but no ordered structures were obtained from all polymers with the G4 dendron. Polymers with G2 and G3 dendrons containing the most hydrophobic perfluoroalkyl end groups could form a novel highly ordered monolayer pores with extremely thin walls.

The BF technique has been proved to be an easy and economic technique for fabrication of porous polymer films for functional materials, and polymers with different chemical structures and architectures have been employed, but amphiphilic homopolymers has not yet been investigated. Besides, it was revealed that amphiphilic block copolymers can form porous films with their hydrophobic groups on the surface of the pores but the hydrophilic groups accumulated inside the walls of the holes.^{156,161} The formed microporous films could be good materials for cell adhesion. It can be expected that porous films obtained from amphiphilic homopolymers may also have this property. Therefore, to employ amphiphilic homopolymers to the BF process is interesting, not only to further expand the

diversity of the polymer structures for the formation of ordered porous film, but also to bridge amphiphilic homopolymers with functional materials.

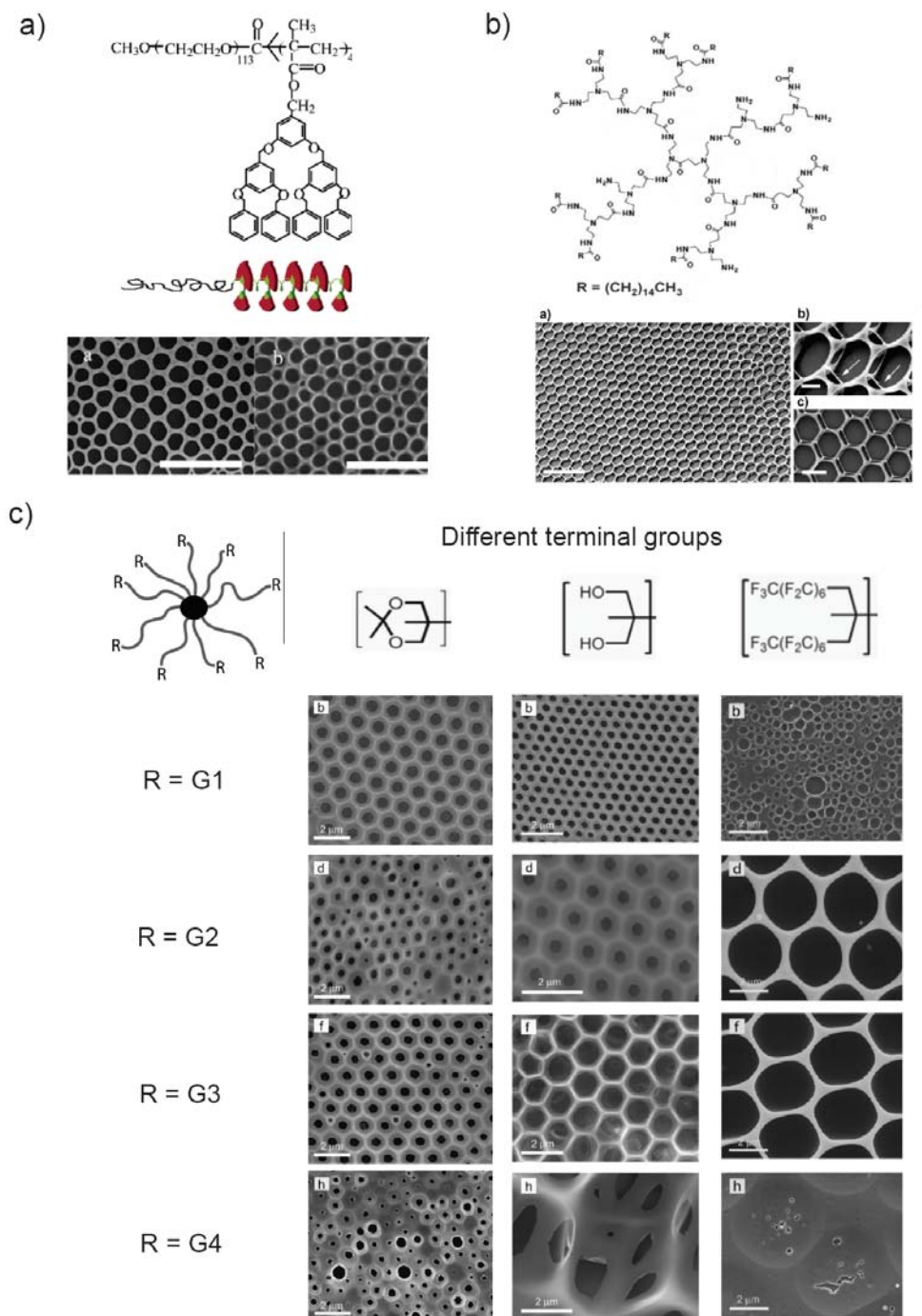


Figure 18. Porous films formed from block dendronized copolymer (a),¹⁵⁴ hyperbranched polymer (b),¹⁶⁰ and dendron functionalized star-shaped polymers (c).¹⁵²

2. Objectives and Considerations of the Thesis

Based on the above backgrounds, the main objective of this thesis is to develop novel dendritic macromolecules by cheap chemistry and easy synthesis, and carrying better functional properties, in order to bridge dendritic macromolecules and functional materials for possible applications. It can be divided into following parts:

- 1) Design and synthesis of liquid and water-soluble dendritic macromonomers which can be polymerized in aqueous solutions or even in bulk, in order to develop an economic and environmentally friendly process for achieving high molar mass and water-soluble dendronized polymers.
- 2) Combination of dendronization and thermoresponsiveness concepts to create novel dendronized polymers with characteristic thermoresponsiveness.
- 3) Investigation of the thermoresponsive behavior of the dendronized polymers with different methods to discover their special properties, including their phase transition behavior, thermally induced aggregation processes and chain collapse mechanism.
- 4) Synthesis of thermoresponsive dendrimers for comparing with the corresponding dendronized polymers.
- 5) Design and synthesis of amphiphilic dendronized homopolymers by incorporation of both hydrophilic and hydrophobic dendrons into each repeat unit.
- 6) Self-assembly of amphiphilic dendronized homopolymers into microporous films via the “breath figure” technique to make them candidates for material applications.

In order to achieve above objectives, OEG and its derivatives were selected as branching segments and gallic acid with three hydroxyl groups was chosen as branching point for the construction of dendrons. The chemical structure of the designed dendron is shown in Figure 19. Different from most of the reported dendrons for dendronized polymer synthesis which normally possess two-folded branching units here the dendron contains densely packed three-fold branch units.

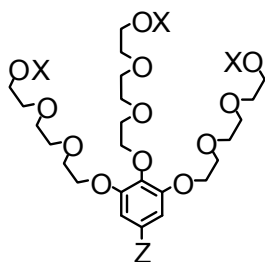


Figure 19. OEG based G1 dendron. X represents either a proton or an alkyl group, and Z represents a linkage point.

The selection of OEG and its derivatives is based on their several fascinating properties, such as low price, good water solubility, low T_g , low toxicity and high chemical stability. They have been thus incorporated into various systems for biomedicine and functional material applications. PEG has been either grafted onto the PAMAM surface to enhance dendrimer's biocompatibility^{162–164} and circulation time, or incorporated into dendrimer's interior part to improve the encapsulation ability.^{165,166} OEG-modified PPI dendrimers are water-soluble and can be used as a host-guest system.¹⁶⁷ Polymers with short OEG side chains are thermoresponsive and were designed for smart biocompatible materials.¹⁶⁸ PEG is also a good polymeric material for ion-conductivity due to its flexible nature, processability and lightness. Polymers containing linear OEG moieties were synthesized and complexed with lithium salts for application in lithium batteries.^{169–173} Ester-terminated dendrons and dendrimers containing internal OEG linkages were used for polyelectrolytes in solid-state batteries.¹⁷⁴ OEG-based dendrons,¹⁷⁵ dendrimers,¹⁷⁶ and hyperbranched polymers,¹⁷⁷ have also been developed for ion conducting materials.

Actually, the dendrons constructed by combination of short OEG chains and gallate have been widely reported. They were used 1) for preferential localization of guest molecules,¹⁷⁸ 2) for amphiphilic rotaxanes,¹⁷⁹ 3) for rendering chitosan water solubility for medical applications,¹⁸⁰ 4) for nanoparticle modification with fluorescence probes,¹⁸¹ and 5) as drug carriers.¹⁸² But surprisingly, most of these work stayed either on the G1 dendron level or combination with other branching units for higher generation dendrons construction, and only few reports deal with higher generation OEG dendrons.^{183–185}

With the present design, a three-fold dendron constructed totally by OEG segments will provide access to water-soluble or thermoresponsive dendronized polymers with either hydroxyl or alky-terminated peripheral groups. This water-soluble OEG-based dendron can be further used for the construction of amphiphilic dendronized homopolymers. The macromonomer route will be applied for the synthesis of different generation polymers. We hope to create novel dendritic macromolecules with well-defined chemical structures and superior properties from OEG units potentially useful for various applications.

3. OEG-Based Water-Soluble Dendronized Polymers

Based on previous discussion, triethylene glycol (TEG) is chosen as the segment to construct the first and second generation dendrons, aiming at achieving neutral, water-soluble and biocompatible dendronized polymers. The chemical structures of the targeted G1 and G2 polymers are shown in Figure 20.

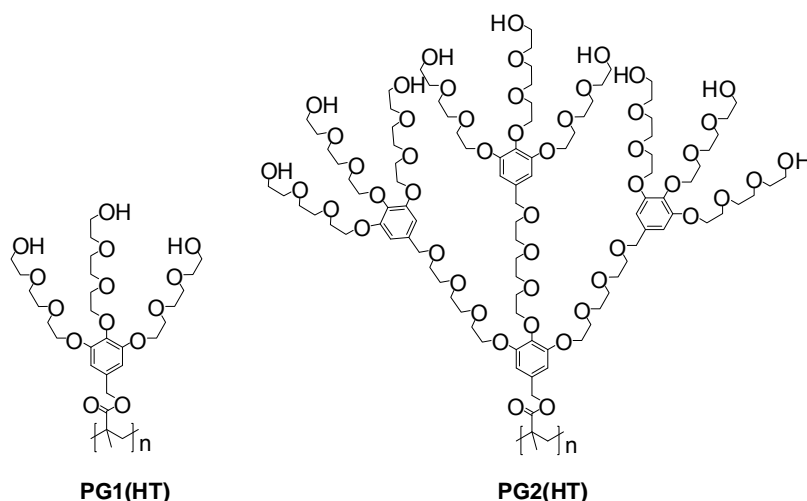


Figure 20. Chemical structures of the OEG based, hydroxyl-terminated water-soluble first and second generation dendronized polymers **PG1(HT)** and **PG2(HT)**. For the nomenclature: HT stands for hydroxyltriethyleneoxy.

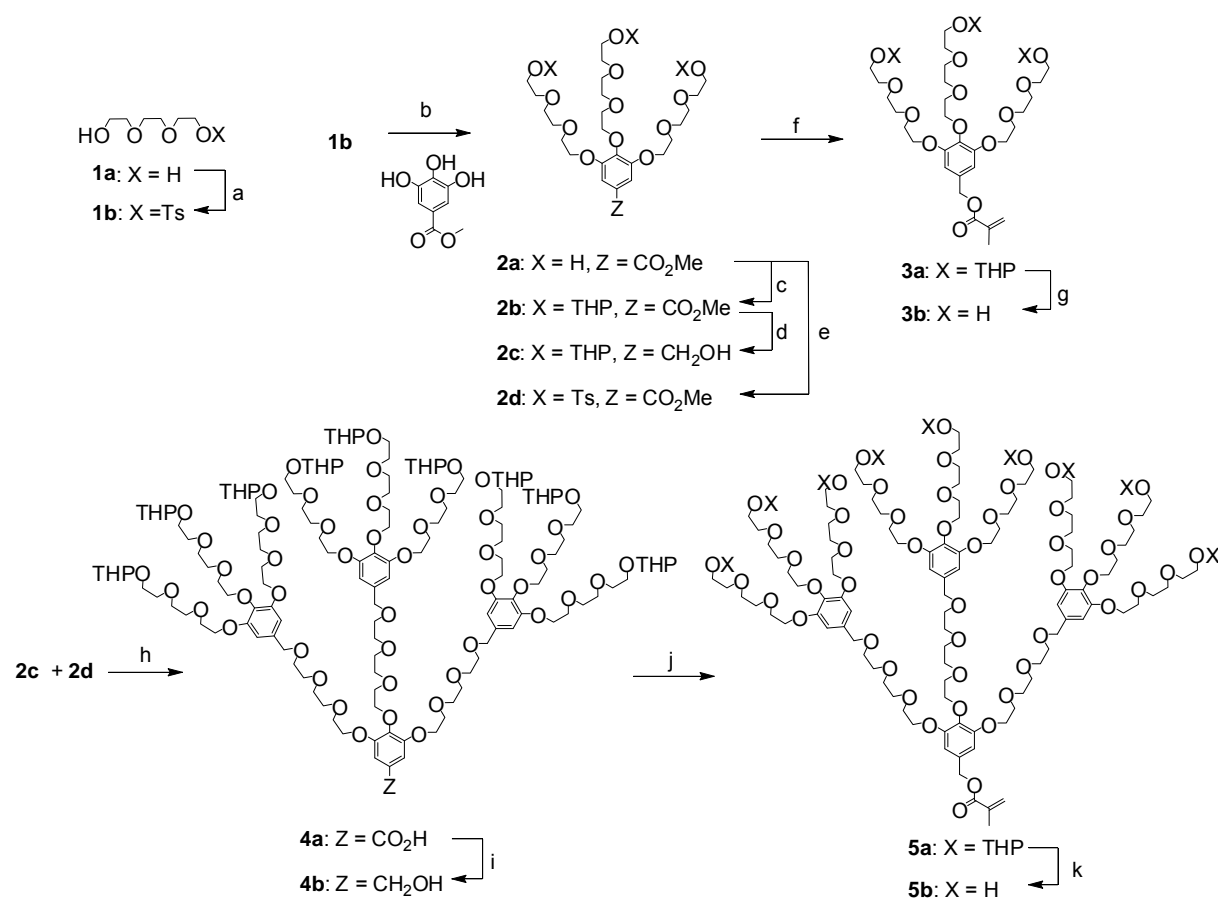
3.1 Synthesis of the Macromonomers

The synthetic procedures for the dendrons and macromonomers are summarized in Scheme 1. First, mono-tosylated TEG **1b** was synthesized according to an established method by using NaOH as the base and THF/H₂O as the mixed solvent.¹⁸⁶ Normally, the tosylation of ethylene glycol was carried out in pyridine, which leads to smelly reactions and difficulties for work up. The method used here is much easier and more convenient. The yield for this reaction is 60%, as it is unavoidable for the production of double-tosylated TEG byproduct. The product was then reacted with methyl gallate *via* Williamson etherification to afford hydroxyl-terminated dendron ester **2a**. In the next step, the three hydroxyl groups in **2a** were protected with tetrahydropyranyl (THP) to furnish **2b** so that compound **2c** with the only hydroxyl group at the focal point could be achieved after reduction. For the

reduction, the reagents NaBH_4 combined with LiCl or LiBH_4 itself were first used. Unfortunately, after several hours, the reactant still existed and no product was found. Then, the strong reduction agent LAH was applied, and **2b** was successfully reduced to **2c** after 3.5 h in a yield of 92%. After reaction with MAC, THP protected G1 macromonomer **3a** was obtained and it could be easily transferred to hydroxyl-terminated G1 macromonomer **3b** by de-protection with PTSA in MeOH.

For the synthesis of the G2 dendron, two routes were designed and tested: First, tosylation of the alcohol group of **2c**, and then etherification with the three hydroxyl terminal groups of G1 dendron **2a**; Second, in a reverse way, tosylation of the three hydroxyl groups of **2a** to furnish **2d**, and then reaction with the alcohol group of **2c**. The first route didn't work out due to the failure in tosylating the benzyl alcohol **2c**, though the reaction was tried in both basic and neutral conditions. There are two possible reasons: 1) the Lewis acid TsCl may lead to the deprotection of THP groups of **2c**; 2) TsCl may react with the activated aromatic ring *via* Friedel-Crafts substitution.¹⁸⁷ The second route was thus tested and proved to be successful. Tosylating the three hydroxyl groups at the periphery of **2a** worked well in a neutral media in the presence of KI and freshly prepared Ag_2O .^{188,189} Ag_2O was proved to be an excellent reagent to promote sulfonylation of alcohols in the presence of sulfonyl chloride, and KI can accelerate the reaction rate by converting *in situ* the tosyl chloride into the more reactive tosyl iodide. Compound **2d** was synthesized in a good yield (80%), which was reacted with **2c** in the presence of NaH, KI and 15-crown-5 to afford the G2 dendron. Surprisingly, G2 dendron acid **4a** was obtained instead of the methyl ester, which suggested the saponification happened in parallel. In this reaction, 15-crown-5 could enhance the activity of the sodium alkoxide intermediate by solvating the ion pair. This led to a rapid nucleophilic attack on tosylated compound, therefore, the efficiency of the etherification could be greatly improved.¹⁹⁰ For the reduction of **4a** with the carboxyl focal group, LAH was applied again but unsuccessfully. Then the method from Kokotos and co-workers^{191,192} was tried and proved successfully with an overall yield of 83%. It contained two steps: first, ethyl chloroformate was mixed with acid **4a** in dry THF to produce the mixed anhydride, which was then reduced to G2 alcohol **4b** by the addition of excess NaBH_4 . After reaction with MAC, THP protected G2 macromonomer **5a** was obtained. At the beginning, the same method as for the de-protection of G1 macromonomer was used

to transfer **5a** to **5b**. The reaction worked well as judged from a TLC analysis, but unluckily, the product could not be purified by conventional column chromatography due to its high polarity. It stayed inside the column even with MeOH as the eluent. Other methods (such as precipitation) for purification were also tried but the PTSA could not be removed completely. Then PPTS was chosen as the de-protection reagent as it could be easily removed by extraction between DCM and water. PPTS stayed in the water phase and the product stayed in the organic phase. After evaporation of the solvent, **5b** was achieved finally in acceptable purity.



Scheme 1. Synthesis of dendrons and the corresponding macromonomers. Reagents and conditions: a) NaOH, TsCl, THF, H₂O, 0~25 °C, 3 h (60%); b) K₂CO₃, KI, DMF, 80 °C, 24 h (83%); c) DHP, PPTS, DCM, -5 to 25 °C, 6 h (90%); d) LAH, THF, -5 to 25 °C, 3.5 h (92%); e) TsCl, Ag₂O, KI, DCM, 0 to 25 °C, 12.5 h (80%); f) MAC, DMAP, TEA, DCM, 0 to 25 °C, 4 h (92%); g) PTSA, MeOH, r.t., 2 h (82%); h) KI, 15-crown-5, NaH, THF, r.t., 12 h (57%); i) N-methylmorpholine, ethyl chloroformate, NaBH₄, THF, -15 to 25 °C (83%); j) MAC, DMAP, TEA, DCM, 0 to 25 °C, 5 h (83%); k) PPTS, MeOH, 50 °C, 10 h (88%). TsCl = 4-Toluenesulfonyl chloride; DHP = 3,4-dihydro-2H-pyran; LAH = lithium aluminum hydride; PTSA = *p*-

toluenesulfonic acid; PPTS = pyridinium toluenesulfonate; MAC = methacryloyl chloride; DMAP = *N,N*-dimethylaminopyridine; TEA = triethylamine.

All the steps were finished with good ($\geq 80\%$) or satisfactory yields (60% for the monotosylation of TEG and 57% for the synthesis of G2 dendron acid). All new compounds were characterized with ^1H and ^{13}C NMR spectroscopy as well as high resolution mass spectrometry. Some of the key compounds were further characterized by elemental analysis. The typical ^1H NMR spectra of all 4 monomers either with or without THP-protection are shown in Figure 21, which proves the successful synthesis and their high purity.

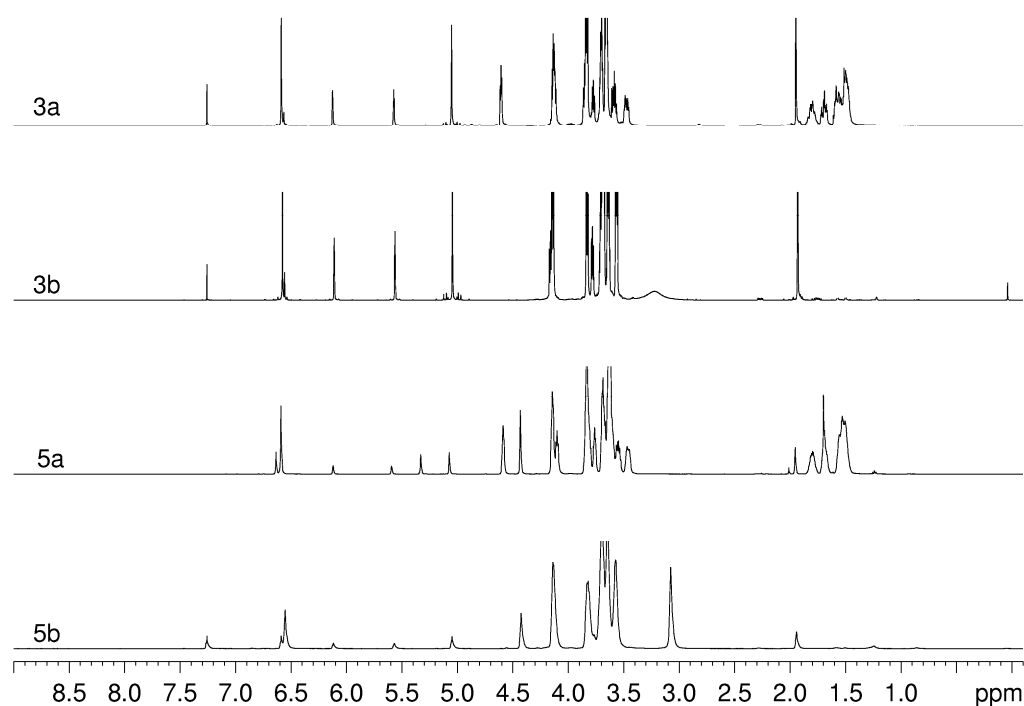


Figure 21. ^1H NMR spectra (500 MHz) of **3a** (in CDCl_3), **3b** (in CDCl_3), **5a** (in CD_2Cl_2) and **5b** (in CDCl_3) at room temperature.

3.2 Polymerization and Characterization

As discussed in the introduction part, most of the dendritic macromonomers reported until now are solid. They are hard to be polymerized in highly concentrated media or in bulk. But the macromonomers synthesized in the present work are all liquid,

especially, hydroxyl-terminated monomer **3b** and **5b** are also well water-soluble, which provides the chance to conduct polymerization in bulk and aqueous media. This is quite important for industry from economic and environmental consideration. Conventional radical polymerization was then carried out at 60 °C with either AIBN (for polymerization in bulk and DMF solution) or ACVA (for polymerization in aqueous solution) as the initiator. The details of the polymerization conditions are summarized in Table 1. Finally, polymers from **3a**, **3b** and **5a** were obtained with yields between 64% and 80% as colorless sticky gels, but the polymerization of **5b** failed. The possible reason is that purification of **5b** just by extraction is not enough to make it polymerizable. So, the hydroxyl terminated G2 polymer **PG2(HT)** was obtained by successful deprotection of THP protected G2 polymer with acetic acid. Whereas the **PG1(HT)** could be achieved either by direct polymerization of the hydroxyl-terminated monomer or by deprotection of the THP protected G1 polymer. The THP protected G1 and G2 polymers can be dissolved well in various solvents, such as CHCl₃, DCM, THF, DMF etc., while the hydroxyl-terminated polymers are well soluble in DMF and water. GPC characterization of THP-protected polymers failed. There was no signal detected from the elution either by using DMF or chloroform as the eluent. A possible reason could be the partial deprotection of the THP groups of the polymers in the GPC column, which led to their aggregation and then stick inside the supports of the GPC column. Instead, their molar masses were measured after deprotection into the corresponding hydroxyl-terminated polymers. From the GPC results in Table 1, several conclusions can be drawn: 1) It is easy to achieve G1 polymers with extremely high molar masses in various conditions; 2) Molar masses of polymers are higher (about 2 million) from bulk polymerization (entry 2) than in DMF solutions (entry 1 and 3, about 1 million); 3) The polymerization in either concentrated DMF solution (entry 3) with short time (5 hours) or in less concentrated DMF solution (entry 1) with long time (19 hours) led to similar molar mass polymers; 4) Interestingly, the highest molar mass polymer was obtained from the polymerization of hydroxyl-terminated monomer **3b** in water (entry 4) in only 3 hours, though much lower monomer concentration was used compared to all other cases; 5) For the polymerization of G2 monomer, polymers with similar molar masses were obtained, no matter the polymerization was proceeded for short (3 hours, entry 5) or long (15 hours, entry 6) time. Though their molar masses are much lower than G1 polymers, they are already high enough compared to other reported dendronized polymers. As

discussed in chapter 1.1.3, the low molar mass is a common problem for higher generation dendronized polymers prepared with the macromonomer route due to the large steric hindrance from the dendron and the low concentration of the polymerizable units even in bulk.

Table 1. Conditions and results for the polymerization of macromonomers **3a**, **3b**, **5a**, and **5b**.

Entry	Polymerization conditions ^a				Yield (%)	GPC ^b			T _g ^b (°C)
	Monomer	Solvent	[Monomer] (mol · L ⁻¹)	Time (h)		M _n × 10 ⁻⁶	DP _n ^c × 10 ⁻³	PDI	
1	3a	DMF	0.71	19	67	0.88	1.41	2.31	-47.1
2	3a	bulk	1.26	3.0	70	1.94	3.12	4.86	-46.5
3	3b	DMF	1.07	5.0	80	0.98	1.58	6.40	-48.1
4	3b	H ₂ O	0.49	3.0	78	5.81	9.37	2.93	-44.0
5	5a	bulk	0.37	3.0	64	0.30	0.13	2.40	-39.8
6	5a	bulk	0.37	15	68	0.29	0.13	4.52	-41.1
7	5b	H ₂ O	0.26	12	— ^d	— ^d	— ^d	— ^d	— ^d

^a Polymerization was carried out at 60 °C.

^b All GPC and T_g measurements were done for the hydroxyl-terminated polymers (see text).

^c DP_n = number-average degree of polymerization.

^d No polymer formed.

3.3 Polymerization Kinetics Study

The rotation of magnetic stirrer bar inside the polymerization media of hydroxyl-terminated G1 monomer **3b** stopped much earlier in water than in DMF, which suggests a dramatically faster polymerization rate in water. The polymerization kinetics of **3b** in both solvents was then studied *in-suit* by ¹H NMR spectroscopy to further clarify their differences. The samples were prepared by dissolving the monomers (0.2 g, 0.32 mmol) in DMF-d₆ (0.35 mL) with AIBN (1 mg) as the initiator and in D₂O (0.35 mL) with ACVA (1.4 mg) as the initiator, respectively. The solutions were then transferred into two NMR tubes. They were put into a big tube which was connected to a vacuum pump and a N₂ line. After de-oxygenation, the NMR tubes were carefully sealed and put into the NMR spectrometer (with a temperature controller). When the temperature was increased to 50 °C, the ¹H NMR spectra were

recorded at a desired interval. The conversions were determined from the integration ratios of the vinylic monomer signals at $\delta = 6.11$ versus the proton signal of the OCH_2 groups for both monomer and polymer at $\delta = 4.14$. The kinetic curves are then plotted as shown in Figure 22. $[M_0]$ and $[M_t]$ refer to the concentration of the macromonomer at the beginning and the time t of the polymerization, respectively. Curve *a* refers to the polymerization in D_2O . The steep slope proves the extraordinary fast rate of the polymerization. It took less than 30 min to reach a conversion of 85%. In contrast, the curve *b* resulted from the polymerization in DMF, which reflects a typical kinetics of conventional radical polymerization. It contained an induction period at the beginning, followed by “auto-accelerated” stage, and finally reached a plateau. It took about 3 h to reach the conversion of 85%. Why was the polymerization rate in aqueous solution so fast and extremely high molar mass polymers obtained? The same phenomenon was also noticed by the groups of Ito¹⁹³ and Percec¹⁹⁴ when styrene monomers with OEG pendent groups or dendritic macromonomers were polymerized in water and bulk, respectively. They pointed out that this unprecedented polymerization behavior is caused by the pre-organization of the monomers which formed certain “micelles” or supramolecular “reactors”. This leads to a locally high concentration of the polymerizable units, which substantially increases polymerization rate and molar mass of the polymer. We assume this is also the most possible reason for the phenomena discovered in the present work.

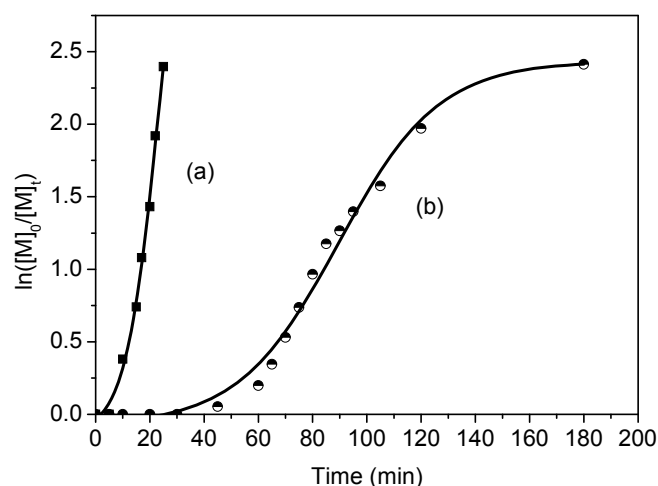


Figure 22. Kinetic plots of the polymerization of **3b** at 50 °C in D_2O (a) and DMF-d_6 (b) ($[\mathbf{3b}] = 0.60 \text{ mol}\cdot\text{L}^{-1}$, $[\text{AIBN}] = 11.5 \text{ mmol}\cdot\text{L}^{-1}$, $[\text{ACVA}] = 9.4 \text{ mmol}\cdot\text{L}^{-1}$).

The glass transition temperatures (T_g) of all polymers were measured by DSC (Table 1) to be in the range of -40 to -50 °C, which are much lower than other dendronized polymers developed by our group (normally in the range of 55-80 °C).^{27,28} These neural dendronized polymers with good water-soluble characteristics have the potential applications in industry as dispersants, stabilizers, biomaterials, etc. Furthermore, polymers with more functionality could be easily achieved by further modification of the densely packed hydroxyl groups at the periphery.

4. OEG-Based Thermoresponsive Dendritic Macromolecules

As mentioned in chapter 1.2.2, polymers based on OEG derivatives can show thermoresponsive properties. Though **PG1(HT)** and **PG2(HT)** are constructed by OEG segments, no phase transition could be observed from their aqueous solutions even when the temperature was increased to 90 °C, which is mostly due to the high hydrophilicity of the peripheral hydroxyl groups. In order to afford this kind of OEG-based dendronized polymers with thermoresponsiveness, a series of novel dendronized polymers were designed and synthesized by slight structure modification. In this chapter, the synthesis of these polymers is described and their thermoresponsive properties are systematically investigated and compared. Besides, their biocompatibilities were preliminarily tested with an *in vitro* cytotoxicity study. Additionally, the specific collapse mechanism of these polymers, related to their unique architecture, will also be illustrated in detail.

4.1 Methoxy-Terminated Thermoresponsive Dendronized Polymers

In principle, the LCST is dependent mostly on the overall hydrophilicity of a polymer, the lower the hydrophilicity, the lower the LCST. In order to reduce the hydrophilicity of **PG1(HT)** and **PG2(HT)**, their terminal hydroxy groups were substituted with methoxy groups (Figure 23). This alternation will not only reduce the hydrophilicity of the polymers, which may afford the polymers thermoresponsiveness, but also lead to their easier synthesis as unstable THP protection and its de-protection are not necessary any more.

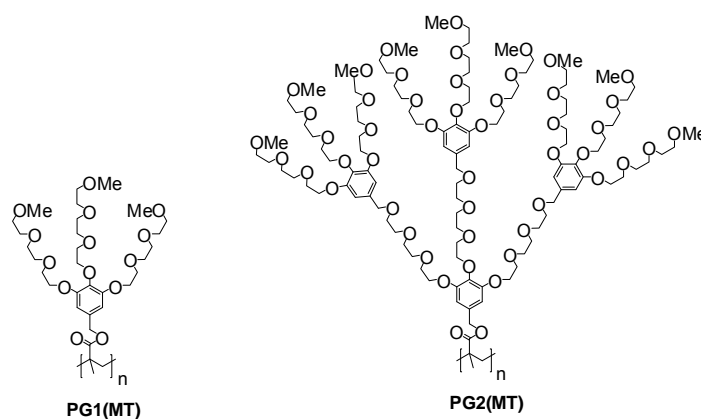
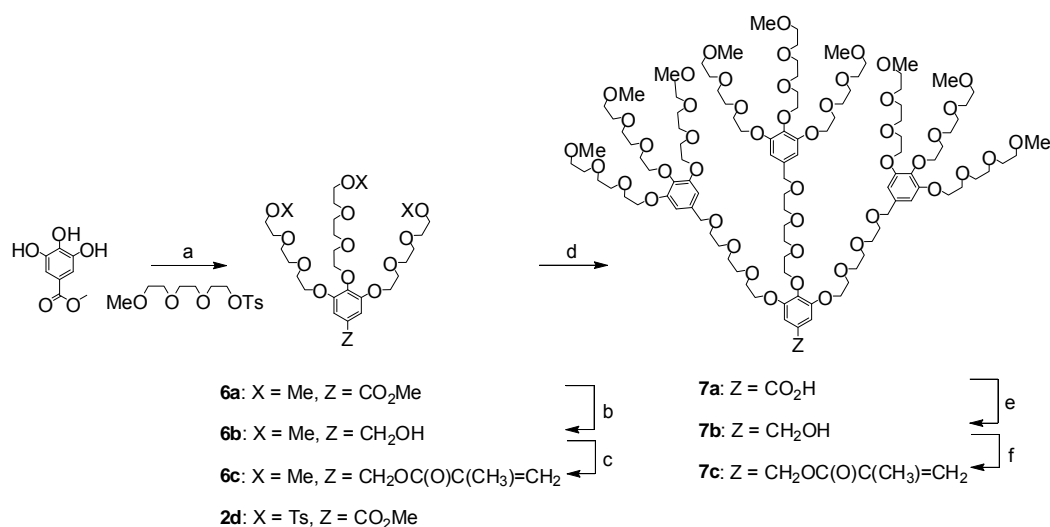


Figure 23. Chemical structures of methoxy-terminated dendronized polymers **PG1(MT)** and **PG2(MT)**. For the nomenclature: MT stands for methoxytriethyleneoxy.

4.1.1 Synthesis and Characterization

The synthesis procedures of the targeted macromonomers are described in scheme 2. First, tosylated mono-methoxy-terminated triethylene glycol (Me-TEG-Ts) was synthesized in much better yield (90%) by using the previous method. It was then attached to the three hydroxyl groups of the methoxy gallate *via* Williamson etherification to afford methoxyl-terminated G1 dendron ester **6a**. Reduction of **6a** with LAH furnished dendron alcohol **6b**, which was directly reacted with MAC to give G1 macromonomer **6c**. The same as before, etherification of dendron alcohol **6b** with the three tosylated groups of **2d** resulted in G2 acid **7a**. After reduction by Kakotos' protocol, G2 dendron alcohol **7b** was obtained, which was then transformed into G2 macromonomer **7c** by reaction with MAC.



Scheme 2. Synthesis procedures for G1 and G2 macromonomers **6c** and **7c**. Reagents and conditions: (a) Me-TEG-Ts, K₂CO₃, KI, DMF, 80 °C, 24 h (94%); (b) LAH, THF, -5~25 °C, 3 h (93%); (c) MAC, TEA, DMAP, DCM, 0~25 °C, 3 h (90%); (d) KI, 15-crown-5, NaH, THF, r.t., 24 h (44%); (e) i) *N*-methylmorpholine, ethyl chloroformate, THF, -15 °C, 1 h. ii) NaBH₄, -5 °C, 2 h (82%); (f) MAC, TEA, DMAP, DCM, 0~25 °C, 5 h (88%).

All the steps were finished with good yields, and all new compounds were characterized with ¹H and ¹³C NMR spectroscopy, high resolution mass spectrometry as well as elemental analysis. The ¹H NMR spectra of G1 and G2 macromonomers **6c** and **7c** are shown in Figure 24 to prove the success of the synthesis. Both G1 and G2 macromonomers are liquid and well soluble in water as well as in various organic solvents, such as DMF, DCM, THF, ethyl acetate, etc. Therefore, the polymerization

can be carried out in either organic or aqueous solutions or in bulk. The detailed polymerization conditions for all the macromonomers and the results are summarized in Table 2. Based on previous experience, polymers with high molar masses could be achieved both in bulk and aqueous solutions, here, the polymerization of G1 and G2 monomers were carried out in both media. Besides, G1 monomer also was polymerized in dilute DMF solution in order to get lower molar mass polymer for comparison of the solution behavior to that of higher molar mass polymers. As shown in Table 2, the highest and lowest yields were obtained from the polymerization of G1 monomer **6c** in bulk (74%) and in DMF solution (55%), respectively. The polymerization of G2 monomer **7c** in either water (63%) or in bulk (65%) within similar time gave to similar yields. The T_g of these polymers are all below $-80\text{ }^{\circ}\text{C}$, which are the lowest among the reported dendronized polymers.

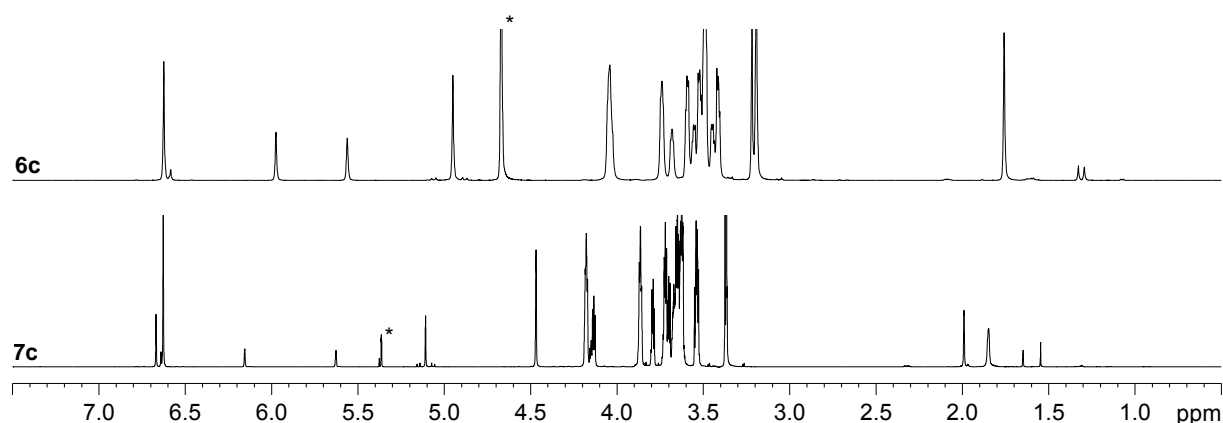


Figure 24. ^1H NMR spectra (500 MHz) of macromonomers **6c** in D_2O and **7c** in CD_2Cl_2 at room temperature. The solvent signals are marked with(*).

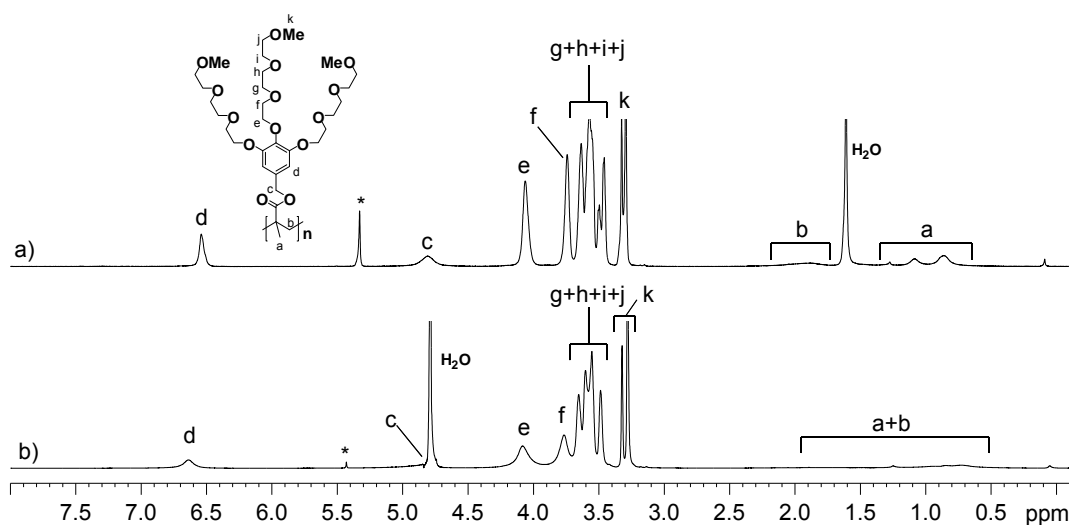
The molar masses of the polymers were determined by GPC with DMF as the eluent. The polymerization of **6c** in bulk was carried out for 4.5 h and extremely high molar mass (more than 2 million) polymer was obtained. A similar result was obtained from the polymerization of **6c** in aqueous solution after 15 h. As expected, G1 polymer with lower molar mass was obtained from the polymerization in DMF. G2 polymers with similar high molar masses (less than 1 million) were obtained by polymerization in aqueous solution and in bulk. The lower DP_n of the **PG2 (MT)** compared to **PG1(MT)** is also due to the same reason as explained previously: the low concentration of polymerizable unit in the G2 monomer and the large steric hindrance of the three-folded dendrons.

Table 2. Conditions and results for the polymerization of macromonomers **6c** and **7c**.

Entries	Polymerization conditions ^a				Yield (%)	GPC results ^b			LCST (°C)
	Monomer	Solvent	[Monomer] (mol · L ⁻¹)	Time (h)		$M_n \times 10^{-6}$	DP _n	PDI	
1 ^c	6c	DMF	1.06	7.0	55	0.48	720	2.54	63.2
2 ^d	6c	Water	0.48	15.0	60	2.00	3020	2.48	63.0
3 ^c	6c	Bulk	1.66 ^f	4.5	74	2.36	3560	4.92	62.6
4 ^d	7c	Water	0.30	15.0	63	0.82	350	2.49	63.6
5 ^c	7c	Bulk	0.47 ^f	14.0	65	0.71	300	2.55	64.4

^a All polymerizations were carried out at 60 °C. ^b All GPC measurements were done with DMF (1% LiBr) as eluent at 45 °C. ^c AIBN and ^d ACVA as initiator with a concentration of 0.5 wt% based on monomer. ^e The values were obtained taking the monomer densities into account which were determined to be 1.1 g·mL⁻¹ for both **6c** and **7c**.

The same as their macromonomers, both **PG1(MT)** and **PG2(MT)** can dissolve well in various organic solvents and in water. Their ¹H NMR spectra were recorded in both CD₂Cl₂ and D₂O, and the results from **PG1(MT)** with full assignment are shown in Figure 25. In CD₂Cl₂, the signals from the OEG units (e-k) are all sharp whereas the signals from the benzyl CH₂ group (c), the aromatic ring (d) and the backbone (a and b) are broad. Differently, the signals in D₂O appear much broader than in CD₂Cl₂, especially d, e, f, a and b which are close to the backbone. This indicates the limited mobility of the polymer in water compared to in CD₂Cl₂, and the mobility of the backbone is even less than that of the OEG pendent groups. Due to the bulk structure of G2 polymers, the signals close to or from the backbone couldn't be clearly resolved in both solvents, thus, the spectra of **PG2(MT)** are not shown here.

**Figure 25.** ¹H NMR spectra (500 MHz) of **PG1(MT)** (Table 2, entry 2; 4.0 wt%) in CD₂Cl₂ (a) and in D₂O (b) at room temperature.

The special structure characteristics of dendronized polymers are their large size and high rigidity. Here, AFM was applied to directly observe the individual chain morphologies of these OEG-based polymers. Polymers in chloroform were spin coated on mica surfaces and recorded with AFM in tapping mode. The images from **PG1(MT)** with low and high molar mass as well as **PG2(MT)** are shown in Figure 26a, b and c, respectively. All polymers exhibit homogeneous apparent heights and widths. The molar masses of these polymers were further proved by histographic contour lengths analysis. The chains of the high molar mass polymer are very long and most of them aggregate together, which cause difficulties for analysis of the individual chain length. Therefore, **PG1(MT)** with low molar mass (short chains) was selected for the analysis. Finally, 187 individual chains of **PG1(MT)** were selected and their average contour length is 142 nm (Figure 26d) which agrees well with GPC results ($DP_n = 720$). As the length of one stretched polymerizable units is about 2.5 Å, the counter length of one polymer chain at fully stretched conformation is calculated to be 180 nm from GPC result. **PG2(MT)** with shorter chain length are well separated from each other on mica surface and 174 chains could be easily selected for the analysis. Their average counter length is 96 nm, which is also similar with the results from GPC ($DP_n = 300$, contour length at fully stretched confirmation is 75 nm).

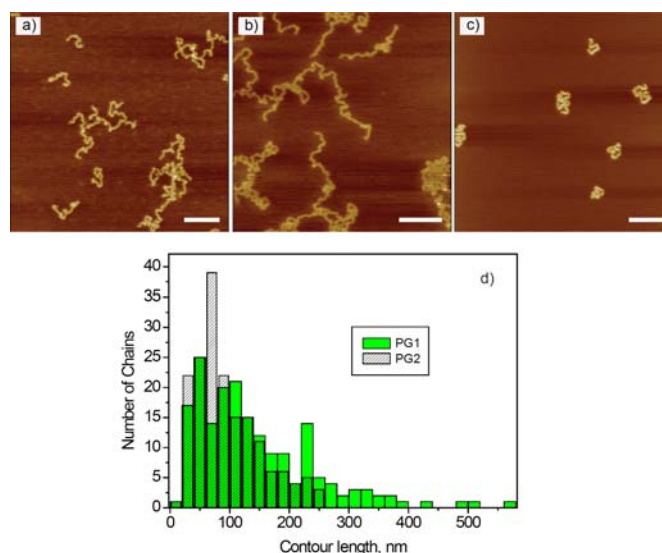


Figure 26. Tapping mode AFM images of **PG1(MT)** (a; Table 2, entry 1), **PG1(MT)** (b; Table 2, entry 2) and **PG2(MT)** (c; Table 2, entry 5) on mica and the contour length distributions of **PG1(MT)** and **PG2(MT)** (d). The scale bars in a-c are the same and corresponding to 100 nm. The Z scale is 2 nm for **PG1(MT)** (a and b) and 4 nm for **PG2(MT)** (c). Samples were prepared from chloroform solutions (3 mg/L for **PG1(MT)** and 4 mg /L for **PG2(MT)**) by spin coating (2000 rpm).

4.1.2 Thermoresponsive Behavior

These polymers are soluble in water, and transparent solutions are thus formed. But the clear solutions quickly become turbid when heated to certain temperature (LCST), and this process is fully reversible (Figure 27). This is a visual indication of the thermoresponsiveness of these polymers. The good solubility of these polymers at low temperature is believed to be due to hydrogen bonding between OEG units and water molecules.¹⁹⁵ Once the temperature is high enough, the hydrogen bonding is broken, and interactions between polymer chains are favored. At this stage, polymers behave more hydrophobic, consequently, they start to precipitate from water and form aggregates. The detailed thermoresponsive behavior of these dendronized polymers is investigated on microscopic level with proton NMR spectroscopy and macroscopic level with UV turbidimetry, DLS and optical microscopy.

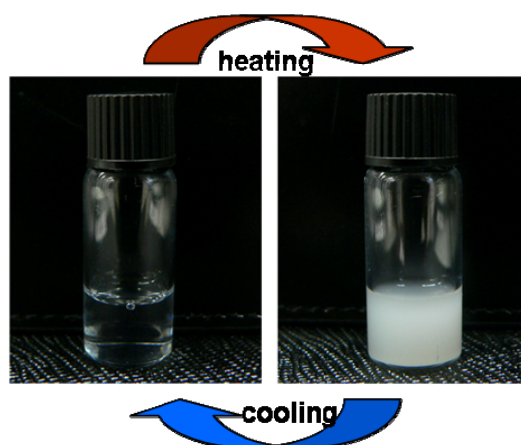


Figure 27. The reversible transitions from clear to turbid of **PG1(MT)** or **PG2(MT)** in water (concentration: 0.25 wt%) during heating and cooling processes.

Temperature dependent ^1H NMR spectroscopy

The thermally induced dehydration processes of the polymers were first monitored by temperature-dependent ^1H NMR spectroscopy. Figure 28a and b show the spectra of **PG1(MT)** and **PG2(MT)** with the same concentration (2 wt%) in D_2O at various temperatures. When the solution temperature increased to above 58 °C for **PG1(MT)** and 62 °C for **PG2(MT)**, respectively, all proton signals became broader and their heights decreased. For **PG1(MT)**, the clearest changes could be observed from the signal of the backbone (0.75-1.30 ppm, 1.80-2.20 ppm) and the aromatic ring (6.82

ppm). For **PG2(MT)**, the most pronounced changes could be found from the signal of the aromatic ring (6.82 ppm). These changes are due to the dehydration of the molecules, which lead to a reduced mobility of the polymer chains. It was found that the dehydration temperature is not strongly dependent on the polymer concentration. As shown in Figure 28 c and d, the decreases of the proton signal height start at about 58 °C for **PG1(MT)** with either lower (0.5 wt%) or higher (4 wt%) concentrations. But even when the solution temperature increased to much higher values, above their phase transition points, proton signals from the polymers are still detectable, which suggests the high mobility of polymer chains even after their dehydration. This is a common property for all these OEG based thermoresponsive dendronized polymers and more examples will be discussed in the following chapter.

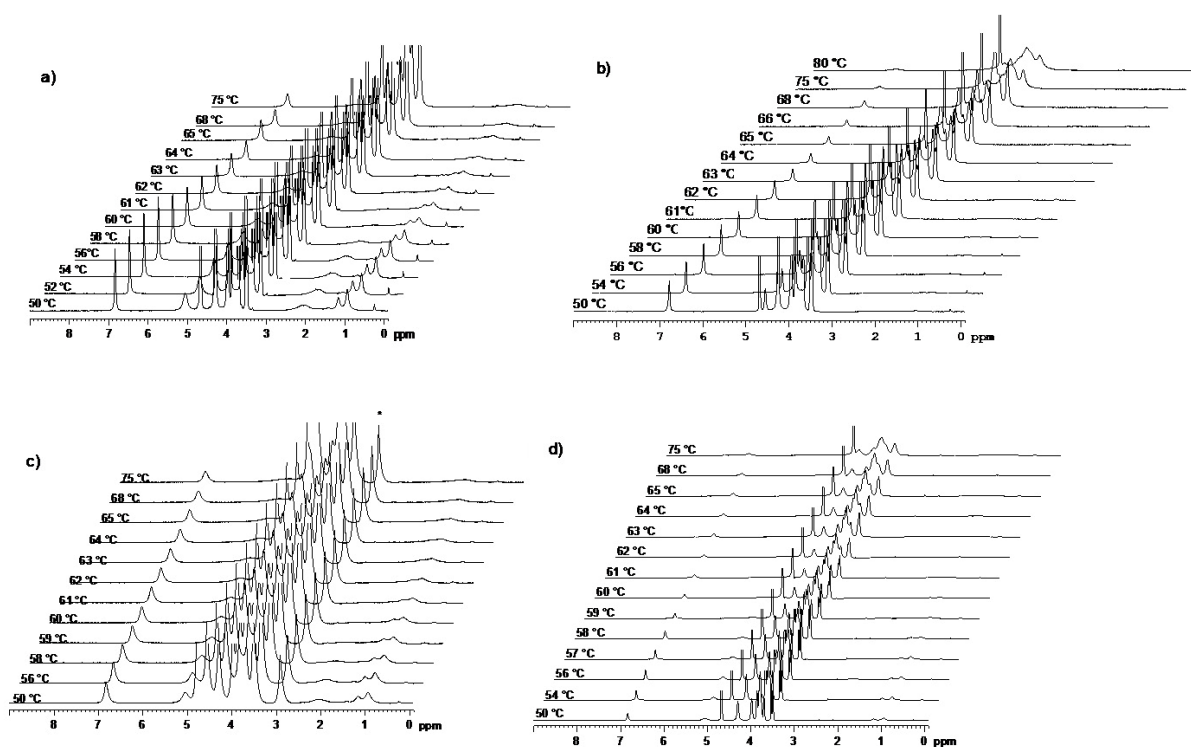


Figure 28. Temperature-dependent ^1H NMR spectra (500 MHz) of **PG1(MT)** (a, Table 1, entry 2; 2.0 wt %), **PG2(MT)** (b, Table 1, entry 5; 2.0 wt%), **PG1(MT)** (c, entry 2, Table 2, 0.5 wt%) and **PG1(MT)**(d, entry 2, Table 2, 4.0 wt%) in D_2O .

Turbidity measurements

Turbidity measurements were then applied to follow the phase transition processes of these polymers and for determination of their LCSTs. The transmittances of the aqueous polymer solutions at the wavelength of 500 nm were recorded as a function

of temperature by using a UV-vis spectrometer. The typical turbidity curves during heating and cooling from low and high molar mass **PG1(MT)** and **PG2(MT)** are all plotted in Figure 29a. At low temperature, the solutions were clear with 100% transmittances, once increased to certain temperatures, the transmittances started to decrease quickly and reached 0%, and kept on this value afterwards. This suggests the formation of stable and large aggregates which scatter the visible light sufficiently. The LCSTs were determined as the temperature reached at 50% transmittance. The following three points should be stressed: 1) All polymers show very sharp phase transitions (≤ 0.8 °C) and quite small hystereses (≤ 0.6 °C) between the heating and cooling processes; 2) The LCST for **PG1(MT)** (Table 2, entry 2) and **PG2(MT)** (Table 2, entry 5) are quite similar (63.0 °C and 64.4 °C). This indicates that the dendron generation has a quite limited influence on the phase transition of the polymers. These temperatures are all slightly higher than their corresponding dehydration temperatures measured from ^1H NMR spectroscopy, which means that the aggregation takes place closely after the dehydration of the polymer chains but not exactly at the same time; 3) The thermoresponsive behaviors of these polymers are independent of the molar mass. **PG1(MT)** with lower molar mass (Table 2, entry 1) also show very sharp phase transition and its LCST is 63.2 °C which is almost the same as the LCST of the high molar mass polymer (63.0 °C). The influence of polymer concentration on the thermoresponsiveness was also examined. Aqueous solutions of **PG1(MT)** (Table 2, entry 2) and **PG2(MT)** (Table 2, entry 5) with concentration from 0.05% to 2% or 4% were prepared and measured. The corresponding LCSTs versus concentrations are plotted in Figure 29b. The LCST differences are less than 2 °C for both **PG1(MT)** and **PG2(MT)** within the studied concentration range, which suggests their LCSTs are not so sensitive to concentrations. The corresponding turbidity curves (Figure 30) indicate that polymers with different concentrations all exhibit sharp phase transitions (≤ 1 °C), except the very dilute one (0.05 wt%).

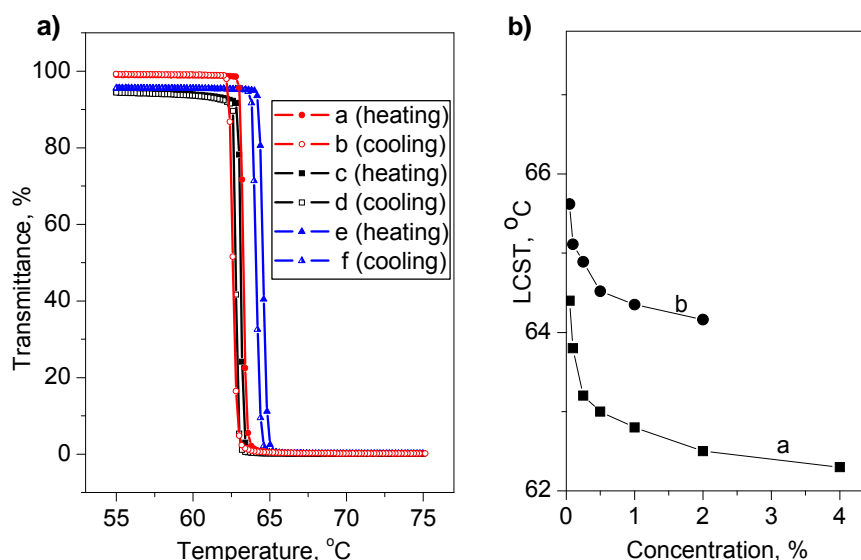


Figure 29. a) Plots of transmittance vs temperature for 0.25 wt% aqueous solutions of **PG1(MT)** and **PG2(MT)**. Heating and cooling rate = 0.2 °C/min. Curve *a* and *b*: **PG1(MT)** (Table 2, entry 1); curve *c* and *d*: **PG1(MT)** (Table 2, entry 2); curve *e* and *f*: **PG2(MT)** (Table 2, entry 5). b) Dependence of LCSTs on polymer concentrations. Curve *a*: **PG1(MT)** (Table 2, entry 2), and curve *b*: **PG2(MT)** (Table 2, entry 5).

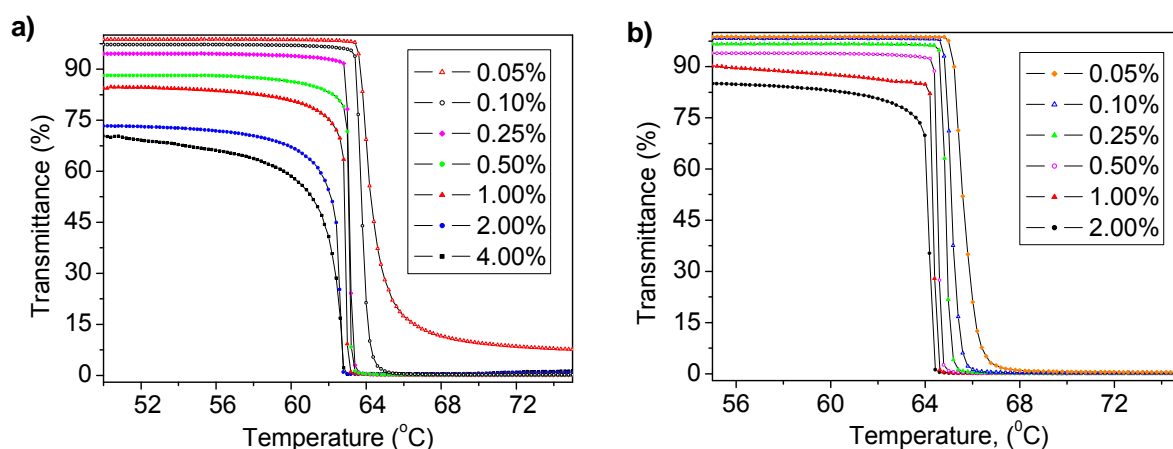


Figure 30. Plots of transmittance vs temperature for aqueous solutions of **PG1(MT)** (a, Table 2, entry 2) and **PG2(MT)** (b, Table 2, entry 4) at different concentrations. Heating rate = 0.2 °C/min.

From above results, it can be concluded that both the molar masses and concentrations of the polymers take negligible effects on their thermoresponsive properties in the investigated ranges. Similar results were also found from the OEG-based dendritic polyphosphazenes (Figure 10 in chapter 1.2.2) reported by Allcock⁸³. It is essential to have polymers with different molar masses or concentrations for

different applications, therefore, these non-sensitive characteristics are quite important and make these OEG-based dendronized polymers superior over other systems. It was found that the LCST of PNiPAM is not concentration dependent but molar mass dependent, and lower molar mass PNiPAM show much broader phase transition compared to high molar mass one.^{72,196} For the amphiphilic dendrimer with oligo(*p*-phenylene vinylene) core branches and OEG terminal chains synthesized by Dai and coworkers,⁹² its LCST decreased dramatically with the increasing of the concentration (~ 7 °C from 0.2 mmol/L to 15 mmol/L). As mentioned in chapter 1.2.2, Zhao and coworkers reported a series of polyacrylates and polystyrenics with OEG pendent groups. Their LCSTs are both molar mass and concentration dependent.⁸⁶

DLS measurements

The thermally induced aggregation of these polymers was further investigated by DLS to follow the temperature-dependence of the aggregate size. Both **PG1(MT)** and **PG2(MT)** with two different concentrations (0.05 and 0.25 wt%) were prepared and the results are plotted in Figure 31. All polymer solutions were fully transparent at 25 °C by visual inspection and the hydrodynamic diameters (D_h) were around 22, 34 and 27 nm for **PG1(MT)** ($DP_n = 720$), **PG1(MT)** ($DP_n = 3020$) and **PG2(MT)** ($DP_n = 300$), respectively (see insert in Figure 31a). With increasing temperature all aggregate sizes showed a sharp transition around LCST and reached surprisingly large values (a few micrometers), except for **PG1(MT)** at low concentration, where particles of sizes of only around 200 nm were formed (curve a). This is quite different from conventional linear thermoresponsive polymers, the sizes are about several hundred nanometers. In contrast, both concentrations of **PG2(MT)** above LCST gave nearly the same aggregate sizes in the range of 2-4 μm (compare curves *b* and *c*). The effect of molar mass of **PG1(MT)** on aggregate size was not pronounced in the range investigated (compare curves *d* and *e*). Further increase of temperature reduced slightly the aggregate size due to further dehydration of the aggregates, but it still remained in the micrometer range.

The development of aggregate size with temperature is shown in Figures 31b and c. In the following, **PG1(MT)** will be discussed first. For highly concentrated solutions ($DP_n = 3020$) at 25 °C, less than 3% of large aggregates in the size range of 190 nm to 4.8 μm coexisted with small particles (31 nm), with the latter expected to be of the

size for single chains of the given molar mass. At 62 °C, thus, right below the LCST, a small amount (ca. 6 %) of large aggregates (4.5 μm) was observed and the small aggregates (ca. 94 %) increased in their size to approximately 56 nm. At 63 °C, thus, right at the LCST, the size of both kinds of aggregates (45 nm and 4.4 μm) remained unchanged but the ratios between them changed to the advantage of the larger one (83 %). Finally, at 65 °C all small aggregates disappeared and the large aggregates sorted themselves into two differently sized classes (2.5 and 5.0 μm). Due to the instrument's cut-off (see Experimental Section) possibly existing even larger aggregates could not be detected. For **PG2(MT)** the aggregate size development with temperature resembled very much that of **PG1(MT)**. At room temperature, less than 2% of large aggregates in the range of 4.8 μm were found to be present together with the presumed unimers (26 nm). Right below the LCST (64 °C) aggregates of two different sizes (26 nm and 850 nm) coexisted, with the smaller ones being the majority (98 %). Around the LCST (65 °C), the size of the small aggregates remained nearly constant (24 nm), while the larger ones not only increased significantly in size (1.8 μm) but also in abundance (50%). Finally, above LCST (66 °C) only broadly distributed large aggregates (2.7 μm) were observed.

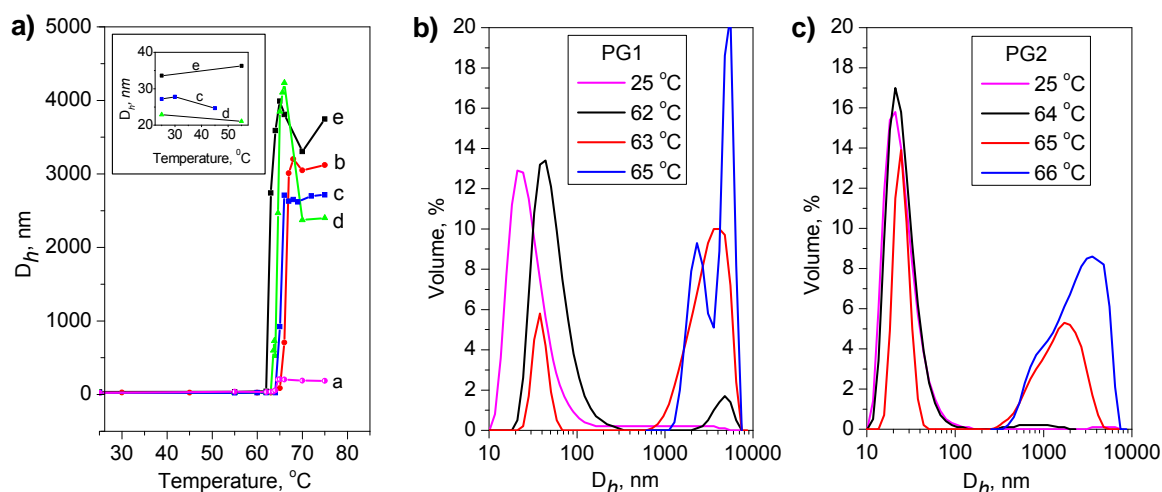


Figure 31. Plots of hydrodynamic diameters (D_h) of the aggregates from **PG1(MT)** and **PG2(MT)** in aqueous solution as a function of temperature from DLS measurements (a). Curve a: **PG1(MT)** (Table 2, entry 2), 0.05 wt%. Curve b: **PG2(MT)** (Table 2, entry 5), 0.05 wt%. Curve c: **PG2(MT)** (Table 2, entry 5), 0.25 wt%. Curve d: **PG1(MT)** (Table 2, entry 1), 0.25 wt%. Curve e: **PG1(MT)** (Table 2, entry 1), 0.25 wt%. Volume distribution of particle sizes from **PG1(MT)** (Table 2, entry 2; 0.25 wt%) (b) and **PG2(MT)** (Table 2, entry 5; 0.25 wt%) (c) from DLS measurements.

Optical microscopy

Based on the DLS measurements, these polymers with dendritic structures could form micrometer aggregates, which may allow to following their aggregation process directly by optical microscopy. For these measurements, special samples need to be prepared in order to avoid water evaporation while heating the solution. After several attempts, a concavity slide was finally selected to keep a drop of polymer solution under the optical microscope, which was covered by a thin cover slip. The cover slip was carefully pasted around its edge to the slide with a glue. In this way, the samples could be reused for many times. The slide was then put onto a heating stage under the lens of the OM. The whole aggregation and de-aggregation processes induced by heating and cooling were recorded by a video-camera with a high-resolution (x 50 times) CCD camera in time intervals of one second to gain a detailed picture of these processes (for the video, please follow the web linkage, <http://pubs.acs.org/doi/suppl/10.1021/ma800129w>). The OM images recorded from **PG1(MT)** (0.25 wt%) around its LCST are shown in Figure 32a to d. The images from **PG2(MT)** with lower (0.05 wt%) and higher (0.25 wt%) concentrations are shown in Figure 32e and f, respectively, aiming at gaining information on the concentration dependence of the aggregate morphologies. Below their LCSTs, no objects were observed for all samples as shown in Figure 32a. When the solutions were heated to their LCSTs, different aggregation processes were observed from **PG1(MT)** and **PG2(MT)** solutions. At 63 °C, aggregates with irregular shape and small sizes were observed from **PG1(MT)** (Figure 32b), and they changed into more complex and larger ones at 64 °C (Figures 24c). When cooled back to 63 °C, even larger aggregates were formed (Figure 32d), and kept on growing before completely disappearing at 62 °C (see video). In contrast, aggregates with uniform spherical shape were formed from **PG2(MT)** at 65 °C (Figure 32e and f). Their sizes are around 1-3 micrometer, which is in good agreement with the results from DLS. The number of the aggregates formed from low concentration solution is less than from the high concentration one, but their morphologies are irrespective to the concentration. These regular aggregates with stable shape and size could always be observed during the heating and cooling process and disappeared once the temperature dropped below their LCSTs (see video). The above processes were repeated for several times and proved to have good reproducibility.

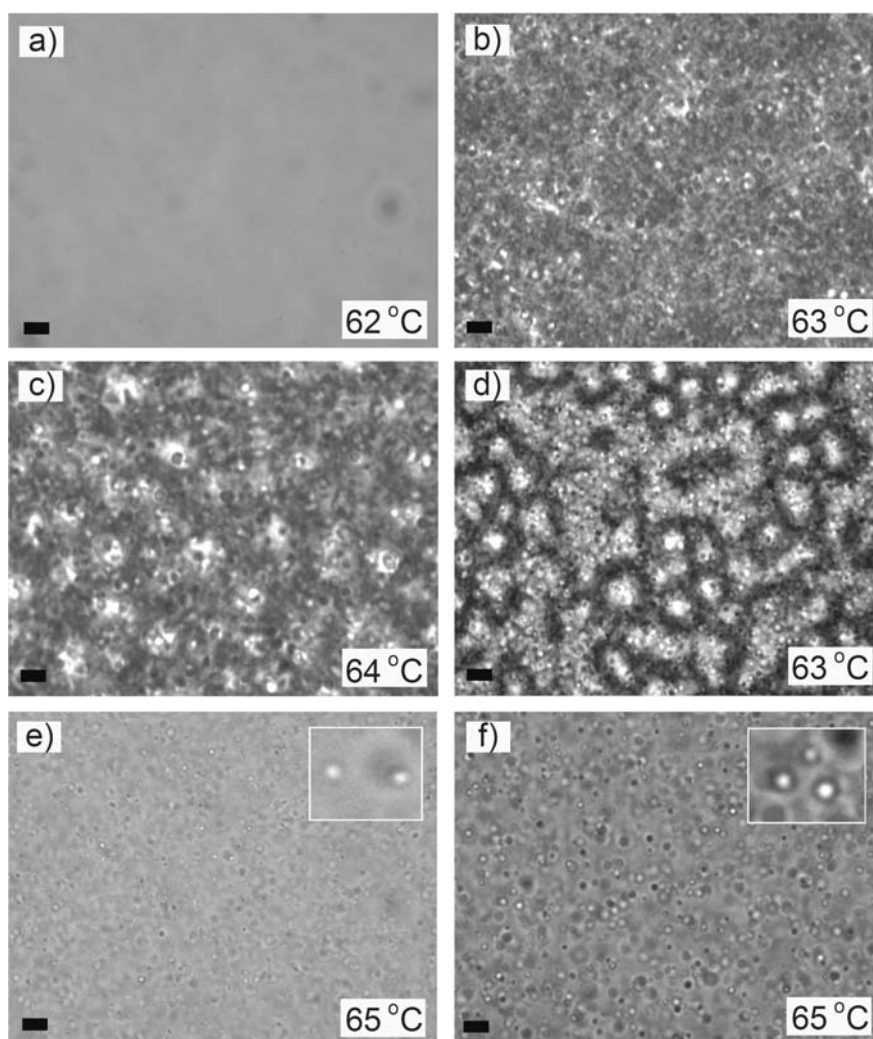


Figure 32. Optical micrograph of the aggregates from aqueous solutions of **PG1** (Table 2, entry 2) and **PG2** (Table 2, entry 5). All images have the same scale bar of 10 μm . (a) **PG1** (0.25 wt%), after heating to 62 $^{\circ}\text{C}$ (some dust particles to be seen); (b) **PG1** (0.25 wt%), after further heating to 63 $^{\circ}\text{C}$ and (c) to 64 $^{\circ}\text{C}$; (d) the same sample after cooling to 63 $^{\circ}\text{C}$; (e) **PG2** (0.05 wt%), 65 $^{\circ}\text{C}$; (f) **PG2** (0.25 wt%), 65 $^{\circ}\text{C}$. Images (e) and (f) contain inserts with 4 times enlarged features. Note that the white features are the ones in focus.

The reason for these unusual large aggregates formed from these dendronized polymers is still under discussion. It was reported that the self-assembly of rod-coil block copolymers could result to stable and well-defined aggregates with size scale in the tens of micrometers.¹⁹⁷ Specially, the size of the aggregates tends to decrease with the decreasing of the fraction of the rigid-rod block. This gives us a hint that the rigidity of the polymer plays a role on the large aggregates formation. Besides, the thermally induced aggregation process of **PG1(MT)** is similar to that of conventional

linear polymers, but **PG2(MT)** behaves quite differently. This difference is also not clearly understood. Based on their structures, the different rigidity and thickness of these two polymers may show effects on their self-organization behaviors.

In the present work, OEG-based dendronized polymers with good solubility, high molar mass and unique thermoresponsive properties were successfully prepared in gram scales with cheap and easy chemistry. All the advantages make them interesting candidates for various material applications. The large sizes of the aggregates make their aggregation processes possible to be directly monitored by OM, which contributes to a better understanding of the thermally induced aggregation process.

4.2 Thermoresponsive Dendronized Polymers with Tunable LCSTs

Though **PG1(MT)** and **PG2(MT)** exhibit many unique thermoresponsive properties, one obvious disadvantage is that their LCSTs are too high for bio-applications. Therefore, it is necessary to develop dendronized polymers with much lower LCSTs. Based on the fact that polymers with relative high hydrophobicity normally have lower LCSTs, the following work was continued with structure modifications. There are three structural parameters that can be changed within the present system, including the peripheral groups of the dendron, the length of the OEG segments and the dendron generations.

Based on these structural variations, Ghose's increment method¹⁹⁸ was applied first for the calculation of hydrophilicity values ($\log P$, with $P = [\text{solute}]_{\text{n-octanol}}/[\text{solute}]_{\text{water}}$; a larger $\log P$ value corresponding to a higher hydrophobicity), aiming at understanding of the relationship between the structure and hydrophobicity. Changing the terminal groups from methoxy to ethoxy or the TEG segments to DEG ones, different PG1 and PG2 polymers were designed. A third generation (G3) polymer with ethoxy-terminal groups is also targeted. All their chemical structures together with **PG1(MT)** and **PG2(MT)** are shown in Figure 33. The calculated $\log P$ values of these polymers are also listed. The hydrophobicity of PG1 and PG2 are increased by changing the terminal groups from methoxy to ethoxy or the TEG segments to DEG ones. The

most hydrophobic polymers are those with ethoxy terminal groups. It is not meaningful to compare the $\log P$ values between G1 and G2 polymers, as the architecture effect may not be negligible. With the present structure design, we hope that dendronized polymers with various LCSTs in a more attractive temperature range (32–45 °C) can be obtained.

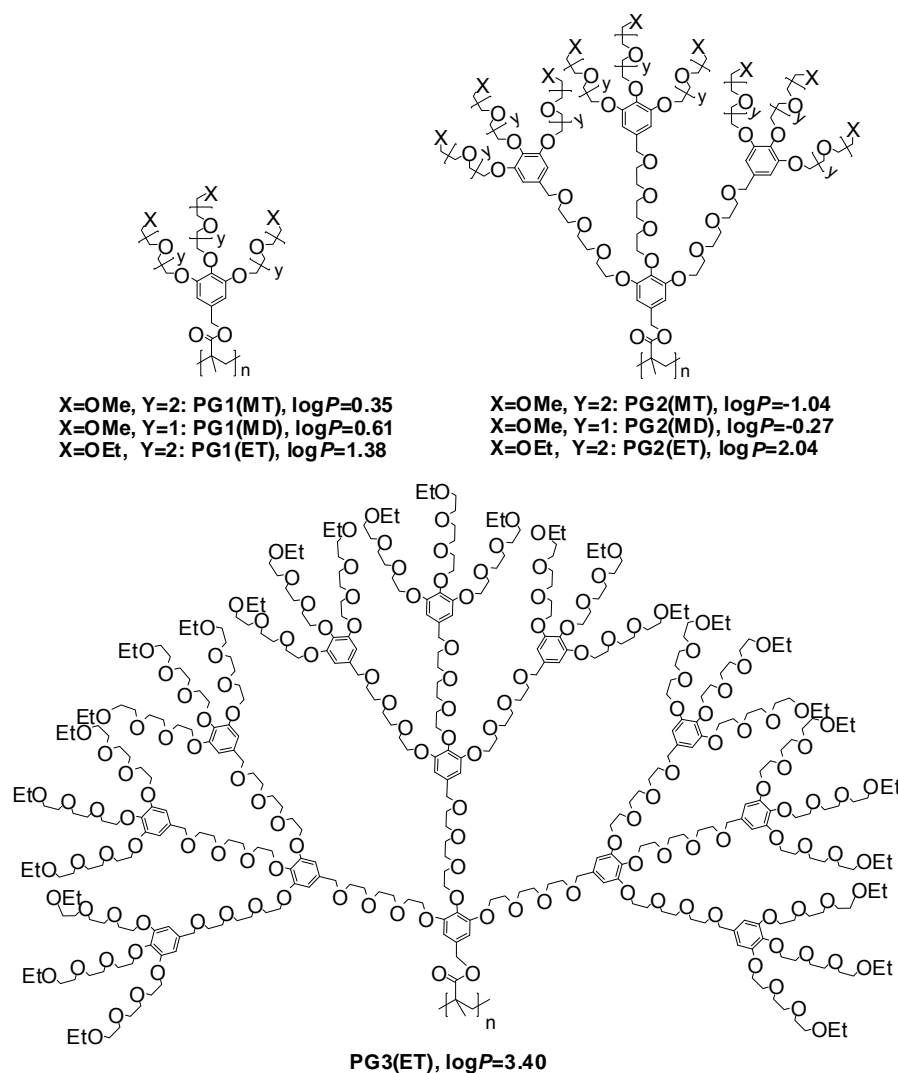


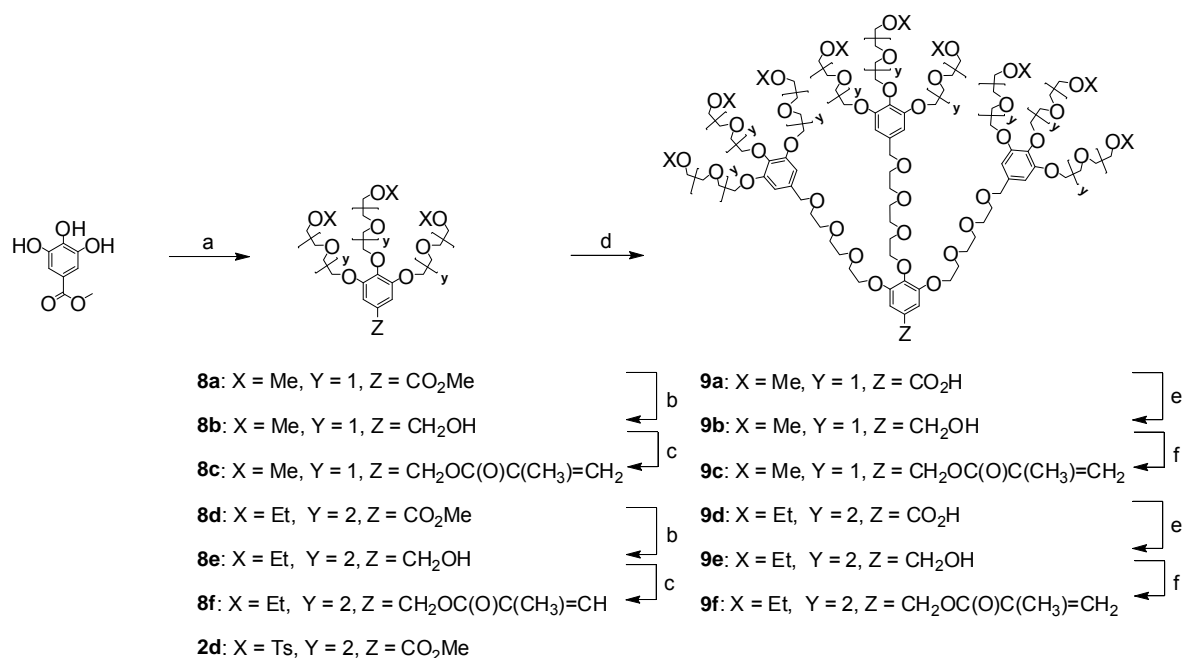
Figure 33. Chemical structures of the dendronized polymers **PG1(MT)** and **PG2(MT)** synthesized in chapter 4.1, as well as **PG1(MD)**, **PG2(MD)**, **PG1(ET)**, **PG2(ET)**, **PG3(ET)** designed in this chapter. Calculated $\log P$ values are also given.

4.2.1 Synthesis and Characterization

Synthesis of G1 and G2 macromonomers

A similar synthetic method to the previous chapter was applied again for the synthesis of all G1 and G2 macromonomers as shown in Scheme 3, but the starting materials were different. For the methoxy terminated dendrons with DEG segments

at the periphery, the synthesis started with the Williamson etherification of tosylated diethylene glycol monomethyl ether (Me-DEG-Ts) with gallate to afford G1 dendron alcohol **8b**. It was then reacted with MAC to furnish G1 macromonomers **8c** or with **2d** to give the G2 dendron acid **9a**, respectively. After reduction and then reaction with MAC, G2 macromonomer **9c** was obtained from **9a**. The ethoxy-terminated macromonomers **8f** and **9f** were also obtained with the same synthetic procedures, but the starting material was tosylated triethylene glycol monoethyl ether (Et-TEG-Ts). In summary, all G1 monomers were achieved in 3 steps and G2 monomers were then obtained by another 3 steps from **2d** and **8b** or **8e**. The overall yields for the synthesis of macromonomers **8c**, **8f**, **9c** and **9f** are 73, 70, 26 and 25%, respectively, which proved the high efficiency of the synthesis.

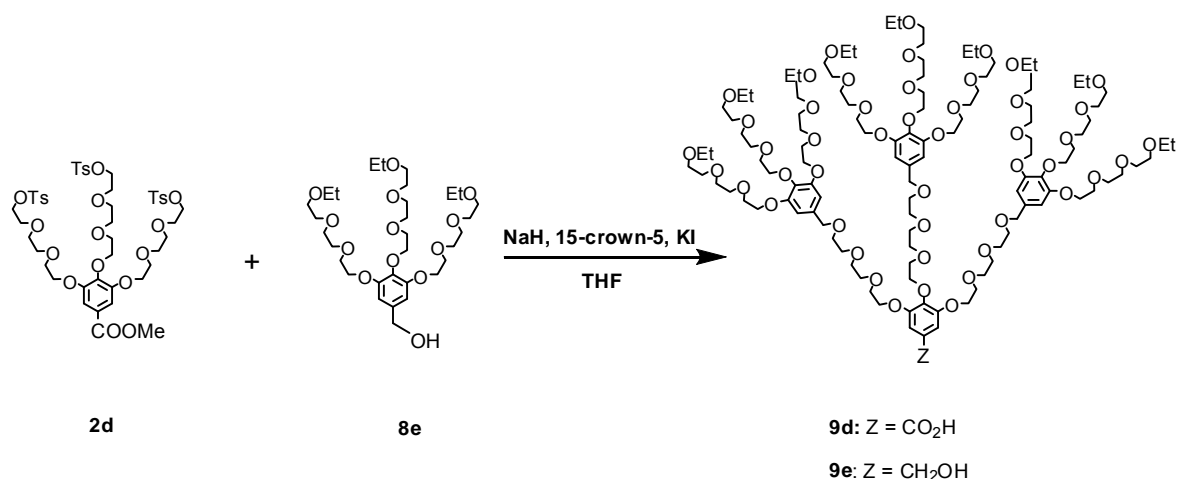


Scheme 3. Synthesis procedures for G1 and G2 macromonomers **8c**, **8f** and **9c**, **9f**. Reagents and conditions: (a) Me-DEG-Ts or Et-TEG-Ts, K₂CO₃, KI, DMF, 80 °C, 24 h (83–87%); (b) LAH, THF, -5~25 °C, 3 h (91–92%); (c) MAC, TEA, DMAP, DCM, 0~25 °C, 3 h (92%); (d) KI, 15-crown-5, NaH, THF, r.t., 24 h (48–50%); (e) i) *N*-methylmorpholine, ethyl chloroformate, THF, -15 °C, 1 h. ii) NaBH₄, -5~25 °C, 4 h (81–82%); (f) MAC, TEA, DMAP, DCM, 0~25 °C, 5 h (83–85%).

Synthesis of G3 macromonomer

In order to systematically study the dendron generation effect on their LCSTs, the third generation polymer is necessary to be synthesized. But the previous procedures

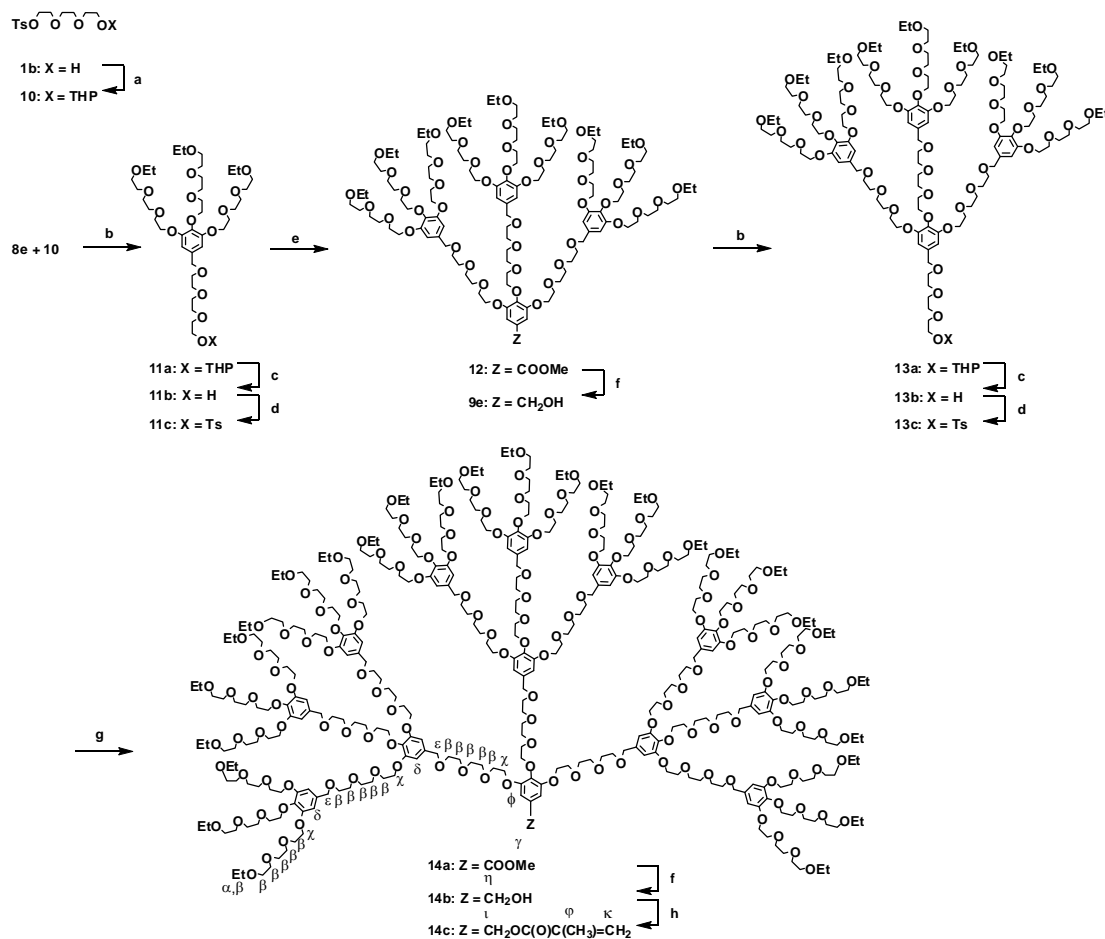
applied for G1 and G2 dendrons could not be used any more due to purification difficulties and low yield. As shown in Scheme 4, the key step for the synthesis of the G2 dendron is etherification of the G1 dendron ester **2d** with the dendron alcohol **8e** to afford directly the G2 acid, which was then reduced into G2 dendron alcohol **9e**. Though this reaction works well, the yield is normally below 50%. The reason for this relative low yield is the incomplete attachment of **8e** to **2d** in the presence of NaH. The products not only contain the desired 3:1 coupling compound, but also the 2:1 and 1:1 by-products. Due to the similarly high polarity of the product and by-products, the purification became tedious and normally 2-3 times column chromatographic separation was necessary to get the pure product. Modification of the reaction conditions didn't improve the yields obviously. For the synthesis of G3 dendron, with the same strategy, which means to make the coupling between the G2 alcohol **9e** and the tosylated G1 **2d**, the yield is expected to be even lower and purification becomes extremely tedious. To get enough G3 macromonomer for polymerization may not be possible. Therefore, a new synthetic route was then designed as shown in Scheme 5. The key improvement was to synthesize the modified dendron **11c** with one tosylated TEG tail, which can be used to react with the three phenyl groups of methyl gallate *via* Williamson etherification in the presence of K_2CO_3 , to form the G2 dendron. In this way, one can avoid the tedious etherification between **2d** and **8e** with NaH as base.



Scheme 4. Synthesis of G2 alcohol *via* the previous route (see Scheme 3).

The whole new procedures for the synthesis of G2 dendron alcohol **9e** and G3 macromonomer are outlined in Scheme 5. Starting from the monotosylated TEG synthesized in previous work (Chapter 3.1), the other hydroxyl group of TEG was

protected with THP to afford compound **10** which was then reacted with G1 dendron alcohol **8e** in the presence of NaH, 15-crown-5 and KI to give the dendron with one THP protected TEG tail **11a**. After deprotection with PPTA in MeOH, and followed by tosylation, compound **11c** with tosylated OEG tail was obtained. Etherification of **11c** with methyl gallate furnished the G2 dendron ester **12** in an excellent yield (92%). This is quite different from the previous method, the using of NaH as the base led to the hydrolysis of the dendron ester directly to acid. As there was no 2:1 or 1:1 by-product formed, the purification of **12** was quite easy and only one time column chromatography is sufficient to get a pure product. In the following, this dendron ester **12** was easily reduced to alcohol **9e** by LAH with good yield (88%). By using this new method, dendron alcohol **9e** was synthesized on a 20 g scale with an overall yield of 45% from G1 dendron. The synthesis efficiency has been greatly improved compared to the previous method (the overall yield was about 25%). This made us optimistic for a higher generation dendron synthesis. Following a similar procedure, **9e** was converted to **13a** via etherification with compound **10**. After de-protection and tosylation, G2 dendron with tosylated TEG tail **13c** was obtained. The etherification of **13c** with methyl gallate to furnish G3 dendron ester **14a** was carried out by using Cs₂CO₃ as the base, and the reaction was continued for 2 days. The crude product was first purified by column chromatography, but due to the existence of 2:1 and 1:1 by-products whose polarity are similar to the 3:1 product, the obtained compound was not pure enough. Based on the different molar mass of the by-products and product, recycling HPLC was used for further purification. Finally, highly pure **14a** was achieved on gram scale and with a yield of 30%. It was then reduced to alcohol **14b** by LAH in also good yield (78%). After reaction with MAC, G3 macromonomer **14c** was finally obtained.



Scheme 5. Synthesis procedures. Reagents and conditions: (a) DHP, PPTS, TEG, -5~25 °C, 12 h (98%); (b) KI, 15-crown-5, NaH, THF, r.t., 12 h, (94~96%); (c) PPTA, MeOH, 2 h (89~91%); (d) NaOH, TsCl, THF, H₂O, 0~25 °C, 3 h (82~83%); (e) methyl gallate, K₂CO₃, KI, DMF, 80 °C, 24 h (92%); (f) LAH, THF, -5 °C, 1.5 h (78~88%); (g) methyl gallate, Cs₂CO₃, KI, DMF, 80 °C, 48 h (30%); (h) MAC, DMAP, TEA, -5~25 °C, 4 h (86%).

All the new compounds were characterized by ¹H and ¹³C NMR spectroscopy and high resolution mass spectrometry as well as elemental analysis. Typical ¹H NMR spectra of the macromonomers **8c**, **9c**, **8f** and **9f** are shown in Figure 34 and 35, respectively. The ¹H NMR spectra of G3 dendrons **14a**, **14b** and macromonomer **14c** with full assignment are shown in Figure 36. For signal assignment, see Scheme 5.

Polymerization and characterization

These new macromonomers are also viscous oils and dissolve well in various organic solvents as well as in water. Conventional free radical polymerization techniques were applied for their polymerization. In order to get polymers with molar

mass as high as possible, they were all polymerized in bulk with AIBN as the initiator. But the polymerization of **8c** in bulk or concentrated DMF solution always led to too high molar mass polymers which became a sticky gel and could not be dissolved in any solvent. Therefore, **8c** was then polymerized in less concentrated DMF solution and stopped after a short time (4h) to achieve lower molar mass polymer. For the polymerization of G3 macromonomer **14c**, about 300 mg monomer was used and the polymerization was first conducted for 12 h under 65 °C. Only a slight viscosity increase of the mixture was observed, which suggests either low conversion of the monomer or low molar mass of the polymer formed. Therefore, the mixture was stirred for another 6 h at 80 °C. The viscosity of the reaction media increased obviously but the magnetic stirrer bar was still able to stir slowly. It is clear that the polymerization was successful but short polymer chains were supposed to be obtained. Details of the polymerization conditions for all monomers are summarized in Table 3. After purification by column chromatography with CH₂Cl₂ as the eluent, polymers **PG1(MD)**, **PG2(MD)**, **PG1(ET)**, **PG2(ET)** and **PG3(ET)** were all obtained as colorless gels (their ¹H NMR spectra are shown in Figure 34, 35 and 36, respectively). They have the same solubility as their monomers. The yields were between 50 to 68%, except a yield of 28% for **8c** from DMF solution. The molar masses of these polymers were measured by GPC and the results are shown in Table 3. The same as before, high molar mass polymers were achieved and the polymerization degree of G1 polymers are always higher than G2. Though the polymerization were carried out under the same conditions, the polymerization degree of **PG2(MD)** (DP_n = 303) is obviously higher than **PG2(ET)** (DP_n = 139). **PG3(ET)** with much lower molar mass (M_n = 1.21 × 10⁵ g mol⁻¹) was obtained from G3 macromonomer. The DP_n and DP_w were then calculated to be 16 and 58, respectively. These results supported the viewpoint that higher molar mass polymer could be easily achieved from lower molar mass macromonomer with higher polymerizable unit concentration and less steric hindrance. Another typical example is the amide based dendronized polymers developed in our group.^{27,28,199,200} Polymers with DP_n = 300 still could be reached with the G3 macromonomer carrying dendrons with molar mass of about 2300-2500. Whereas only oligomers could be obtained with the G4 macromonomer with the molar mass about 4900-5300 or 6300. Considering the G3 macromonomer **18c** synthesized in the present work which carries bulky threefold branching units with a molar mass of about 7700, it is already out of expectation that it could be polymerized.

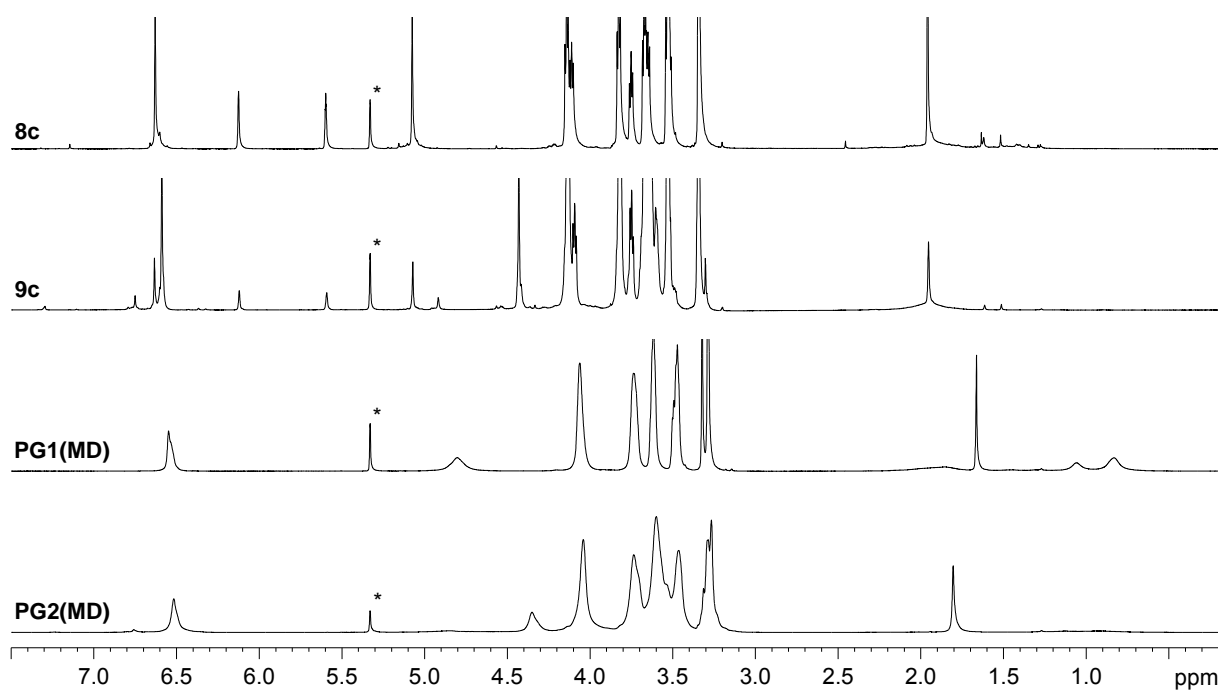


Figure 34. ^1H NMR spectra (500 MHz) of the macromonomers **8c**, **9c** and their corresponding polymers **PG1(MD)**, **PG2(MD)** in CD_2Cl_2 at room temperature. The signals from CD_2Cl_2 are marked as (*).

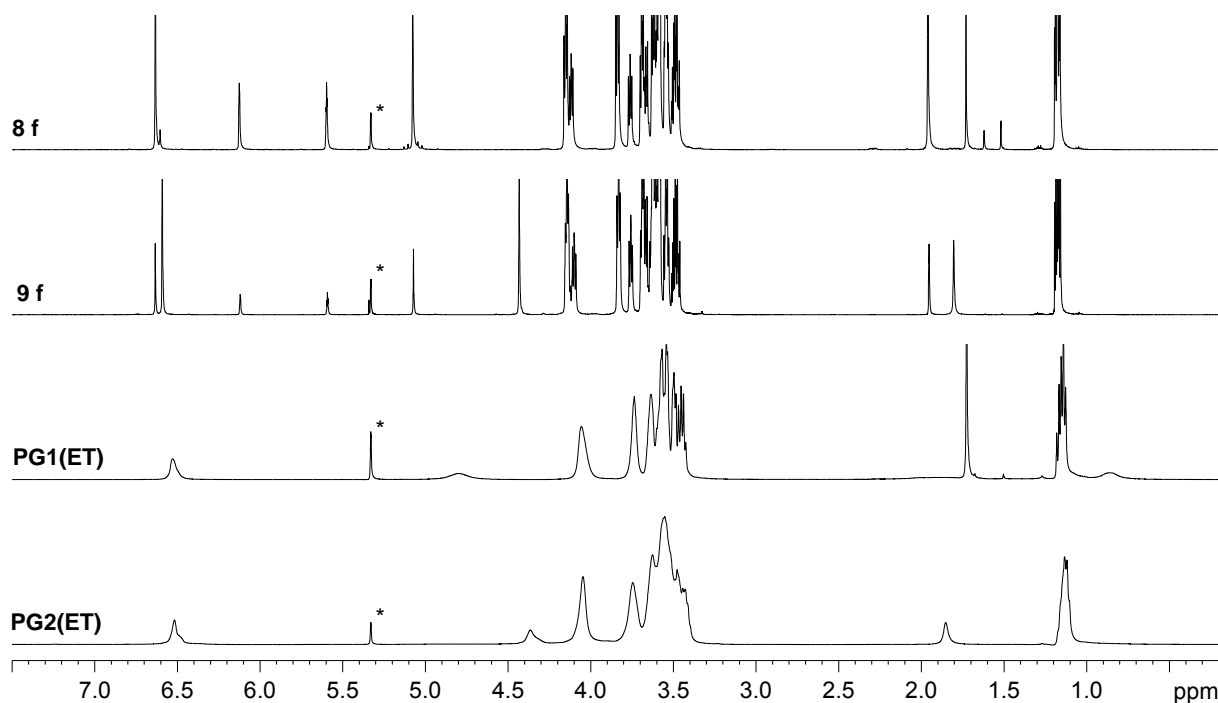


Figure 35. ^1H NMR spectra (500 MHz) of the macromonomers **8f**, **9f** and their corresponding polymers **PG1(ET)**, **PG2(ET)** in CD_2Cl_2 at room temperature. The signals from CD_2Cl_2 are marked as (*).

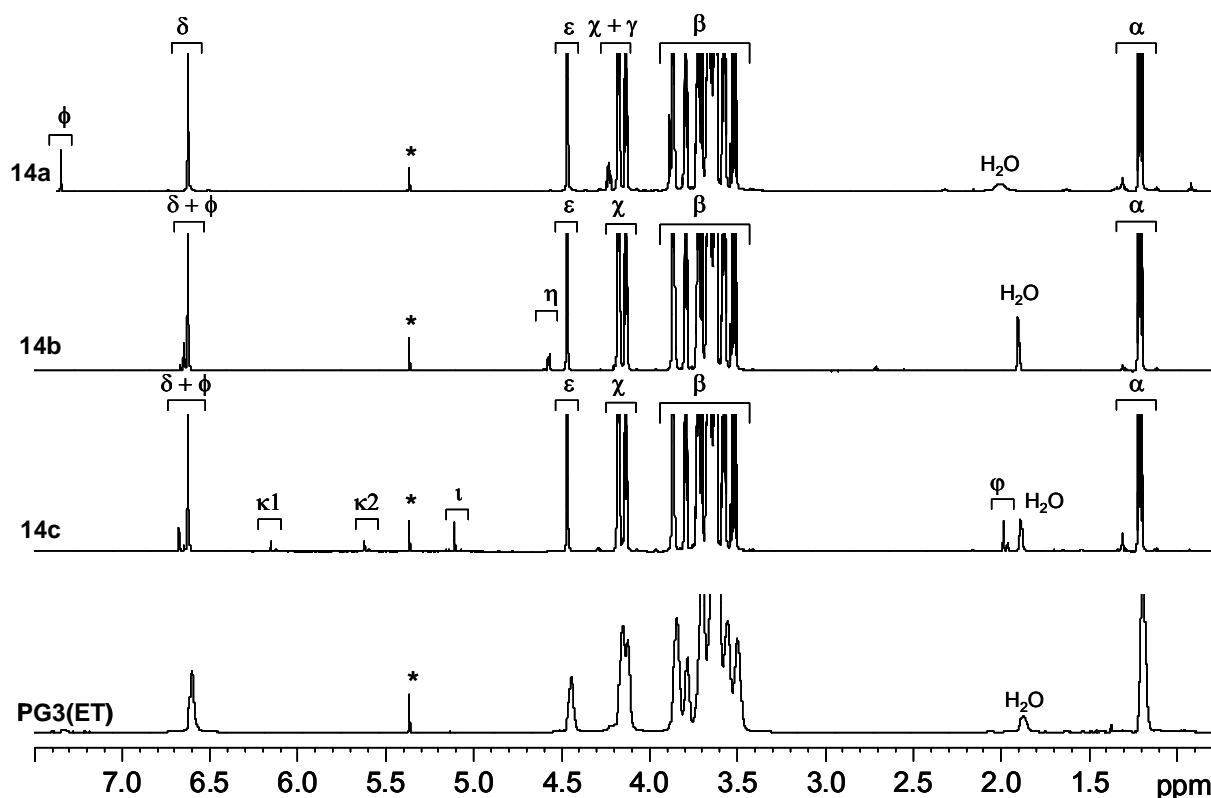


Figure 36. ^1H NMR spectra (700 MHz) of G3 dendrons **14a** (a), **14b** (b), **14c** (c) and polymer **PG3(ET)** in CD_2Cl_2 at room temperature. The signals from CD_2Cl_2 are marked (*).

Table 3. Conditions for and results of the polymerization of all macromonomers.

Entries	Polymerization conditions				Polymer Yield (%)	GPC results ^c			LCST (°C)
	Monomer	Solvent	[Monomer] (mol · L ⁻¹) ^d	Time (h)		M_n × 10 ⁻⁶	DP _n	PDI	
1	8c ^a	DMF	1.10	4.0	28	0.45	843	1.90	43.3
2	9c ^a	Bulk	1.56	3.0	68	0.72	1023	3.15	33.2
3	8f ^a	Bulk	0.56	24.0	61	0.59	303	2.63	48.5
4	9f ^a	Bulk	0.44	24.0	62	0.34	139	3.14	36.0
5	14c ^b	Bulk	0.14	18.0	50	0.12	16	3.60	34.0

^a Polymerizations were carried out at 60 °C and AIBN as initiator with concentration 0.5 wt% based on monomer. ^b Polymerization was carried out at 65 °C for 12 h, then at 80 °C for 6 h. ^c All GPC measurements were done in DMF (1% LiBr) as eluent at 45 °C. ^d The values were obtained by calculation from the monomer density (1.1 g·mL⁻¹ for all monomers).

AFM was applied to directly visualize the individual polymer chains of **PG3(ET)** on substrate (mica). One of the images recorded is shown in Figure 37. As expected, an individual polymer chain adopts cylindrical shape with quite short chain length. But

surprisingly, the apparent height of this polymer, estimated from the height profile of each polymer chain is about 9 angstroms, which is much smaller than the height of “normal” dendronized polymers,²⁶ where an apparent height for PG3 is in the range of 3 nanometers. This may be due to both the high polarity and high flexibility of the polymer, which lead to a collapse of the polymer on the polar substrate.

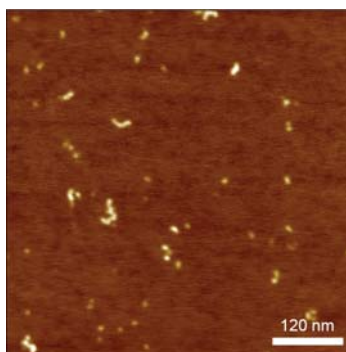


Figure 37. Tapping mode AFM image of **PG3(ET)**. Sample was prepared from chloroform solutions (4 mg/L) by spin coating (2000 rpm). The Z scale is 2 nm.

4.2.2 Thermoresponsive Behavior

The same as for **PG1(MT)** and **PG2(MT)**, when these new polymers were dissolved in water and heated to certain temperatures, the clear solutions will turn to be turbid within a few seconds. But much lower temperatures are needed for their phase transitions. The thermoresponsive behavior of these polymers were then studied and compared. Based on the fact that the molar mass of these OEG dendronized polymers doesn't show pronounced influence on their thermoresponsive behaviors (chapter 4.1), the results from **PG3(ET)** with low molar mass can be reasonably compared to that of **PG1(ET)** and **PG2(ET)** with relatively high molar masses.

Temperature dependent ^1H NMR spectroscopy

The dehydration processes of **PG1(ET)**, **PG2(ET)** and **PG3(ET)** were monitored by temperature dependent ^1H NMR spectroscopy, and the spectra from 25 °C to 65 °C were recorded as shown in Figure 38. The same as for **PG1(MT)** and **PG2(MT)** discussed before (in chapter 4.1.2), the proton signals from **PG1(ET)** and **PG2(ET)** start to change at 32 °C and 34 °C, respectively, including the decrease of the height and the broadening of the peaks, which indicates dehydration of the polymer chains. In contrast, the proton signals from **PG3(ET)** show only slight change around 34 °C, though the transparent solution already turned to be turbid at this temperature. Further increase of the temperature didn't show much influence on the height change

of the proton signals. Even at 65 °C, the proton signals are still sharp with quite high intensities. This phenomenon is quite different from the case of PNIPAM¹⁰⁴ and the linear OEG based polymers.⁸⁴ The small change of the proton signals with the increase of temperature suggests the high mobility of the PG3 chains. On the other hand, maybe not all the OEG units within the molecule were involved in the dehydration process, at least not simultaneously.

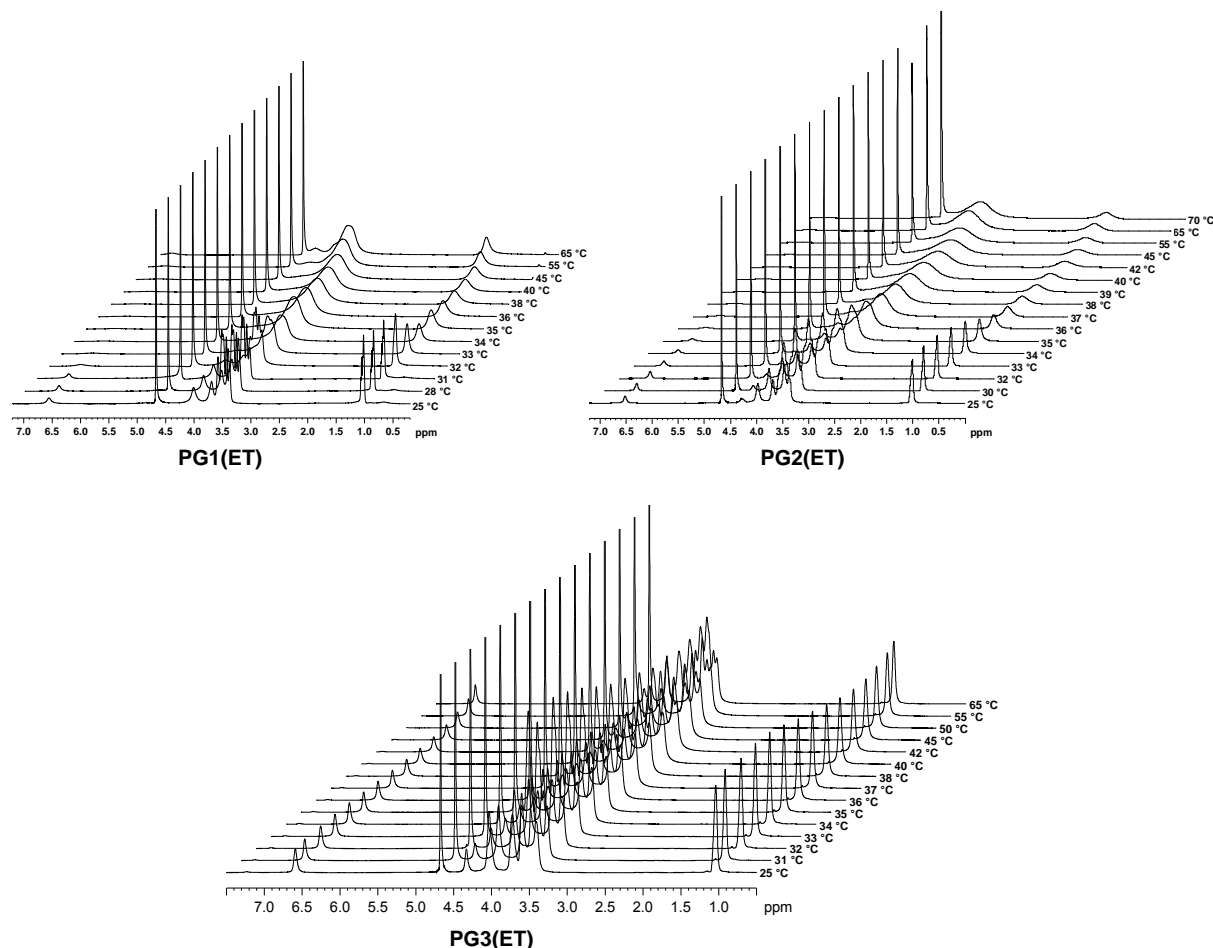


Figure 38. ¹H NMR spectra (500 MHz) of **PG1(ET)**, **PG2(ET)** and **PG3(ET)** in D₂O from 25 °C to 65 or 70 °C.

Turbidimetry

The thermoresponsive behavior of these polymers was then followed by turbidity measurement, aiming at the determination of their LCSTs and study of their phase transition behaviors. The results are shown in Figure 39. For comparison, the turbidity curves of **PG1(MT)** and **PG2(MT)** are also combined inside. From these curves, there are several conclusions which can be drawn: 1) The LCSTs of these polymers with slight structure variations cover a broad temperature range from about 33 °C to 64 °C. **PG1(MD)**, **PG2(MD)**, **PG1(ET)**, **PG2(ET)** and **PG3(ET)**, all with low

hydrophilicity (high $\log P$ value), have the LCSTs 43.3, 48.5, 33.2, 36.0 and 34 °C, respectively. These values are much lower than the LCSTs of **PG1(MT)** and **PG2(MT)**; 2) changing the end group from methoxy to ethoxy shows more strong effects on decreasing the LCSTs (about 30 °C) than changing the length of the OEG segments from TEG to DEG (about 20 °C); 3) The dendron generations didn't show a pronounced effect on the LCSTs. Variation of the generations of ethoxy terminated polymers from G1 to G3 resulted in slight changes of the LCSTs (≤ 5.2 °C). For the other 4 polymers, the LCST difference between G1 and G2 are all less than 5 °C. This is quite different from the thermoresponsive dendrimers synthesized by Kono and co-workers.⁹⁰ In their work, a clear dependence of the LCSTs on the dendrimer generation was observed (from G3 to G5, the LCST changed from 45 to 78 °C).; 4) All of them show quite sharp transition ($\Delta T \leq 0.8$ °C) and small hysteresis ($\Delta T \leq 0.6$ °C) between heating and cooling processes. All these results prove the successful design of the structures, and dendronized polymers with unique thermoresponsive properties and tunable LCSTs were obtained. Among them, **PG1(ET)**, **PG2(ET)** and **PG3(ET)** with the LCST quite close to body temperature may be highly interesting for bio-applications.

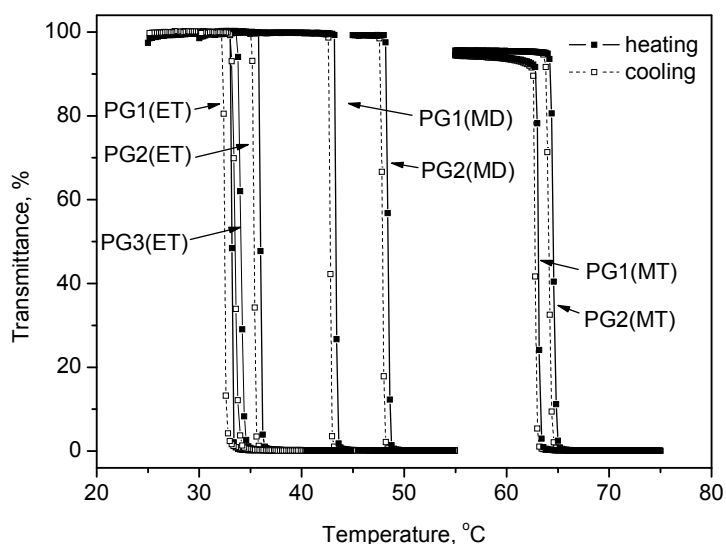


Figure 39. Plots of transmittance vs temperature for 0.25 wt% aqueous solutions of **PG1(ET)**, **PG2(ET)**, **PG3(ET)**, **PG1(MD)**, **PG2(MD)**, **PG1(MT)** and **PG2(MT)**. Heating and cooling rate = 0.2 °C/min.

Surface tension measurements

Surface tension measurements were carried out to substantiate the relationship between the LCSTs and the hydrophilicity of the polymers. These measurements

were based on the pendant drop method, and polymer aqueous solutions with the same concentration (0.25 wt%) as for the turbidity measurements were used. One drop of each polymer solution was sucked to form a well-shaped bubble and the measurements started when the bubble became relatively stable. The surface tension of the polymer at the air-water interface was then continuously measured until 1500 sec. The results are shown in Figure 40a. The stable values recorded at 1500 sec were determined and taken as the surface tension of these polymers. These surface tensions were then plotted versus the LCSTs of the corresponding polymers (Figure 40b). It is known that a higher surface tension value is related to a higher hydrophilicity of the substance. It is clear from Figure 40b that the surface tensions have an almost linear relationship with the LCSTs of the polymers, the higher the surface tension, the higher the LCSTs, which is just as expected.

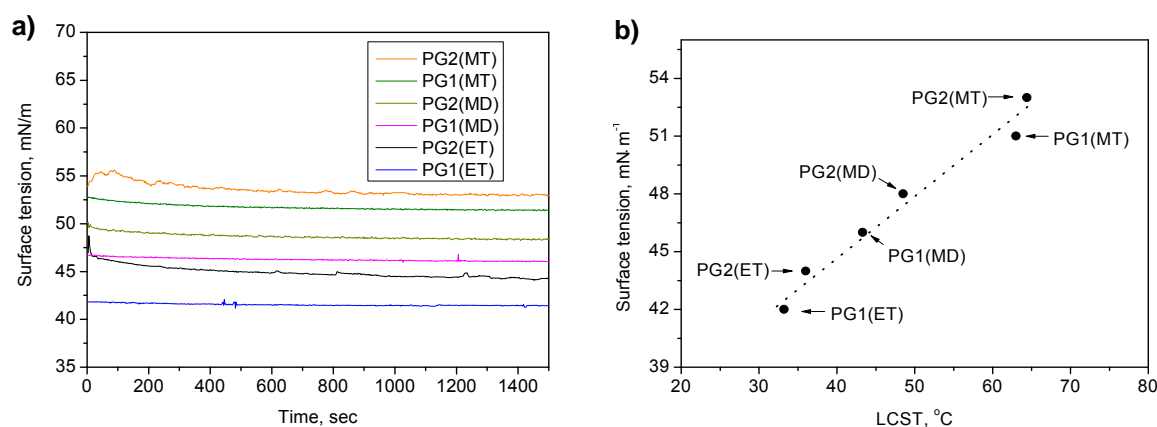


Figure 40. a) Surface tension vs time for pendant drops formed at the air–water interface and b) Plots of surface tension vs LCST of 0.25 wt% aqueous solutions of **PG1(ET)**, **PG2(ET)**, **PG1(MD)**, **PG2(MD)**, **PG1(MT)** and **PG2(MT)**. The linear line in (b) is a guide to the eyes.

“Salt-out” effects

When thermoresponsive polymers are used for biomedical applications, it is important to consider the influence of the salts on their thermal behavior. It has long been known that the LCSTs of thermoresponsive polymers can be tuned by addition of salts. Some reported examples are PNiPAM,^{201,202} poly(vinyl methyl ether)²⁰³ and poly(organophosphazenes) with methoxypoly(ethylene glycol) and amino acid esters as side groups,²⁰⁴ and so on. These salt effects on the LCSTs of polymers are due to a change of the polymer–water interaction by salts. There are two kinds of salts which are called to be water structure maker and breaker, respectively. The former one can

decrease the hydrogen bonding between water and polymer molecules, resulting in a decrease of the LCST, so called “salt out” effect, whereas the later one can enhance the interaction between water and polymers, resulting in a increase of the LCST, so called “salt in” effect. Most of the inorganic salts are water structure makers, and NaCl is a typical example. In the present work, this salt out effect was also examined with these OEG based polymers. For this purpose, phosphate buffer solutions (PBS) of **PG1(MD)** and **PG2(MD)** (0.25 wt%) mixed together with different amounts of NaCl (from 0.09 mol/L to 0.6 mol/L) were prepared and measured with UV-vis spectrometry. The resulting turbidity curves are shown in Figure 41a and b. The addition of salt did not show obvious influence on the sharpness of the phase transitions but show great influence on their LCSTs. As shown in Figure 41c, the LCSTs decrease linearly with increasing salt concentrations. So, NaCl is also working as a water structure maker in these OEG-based polymer solutions.

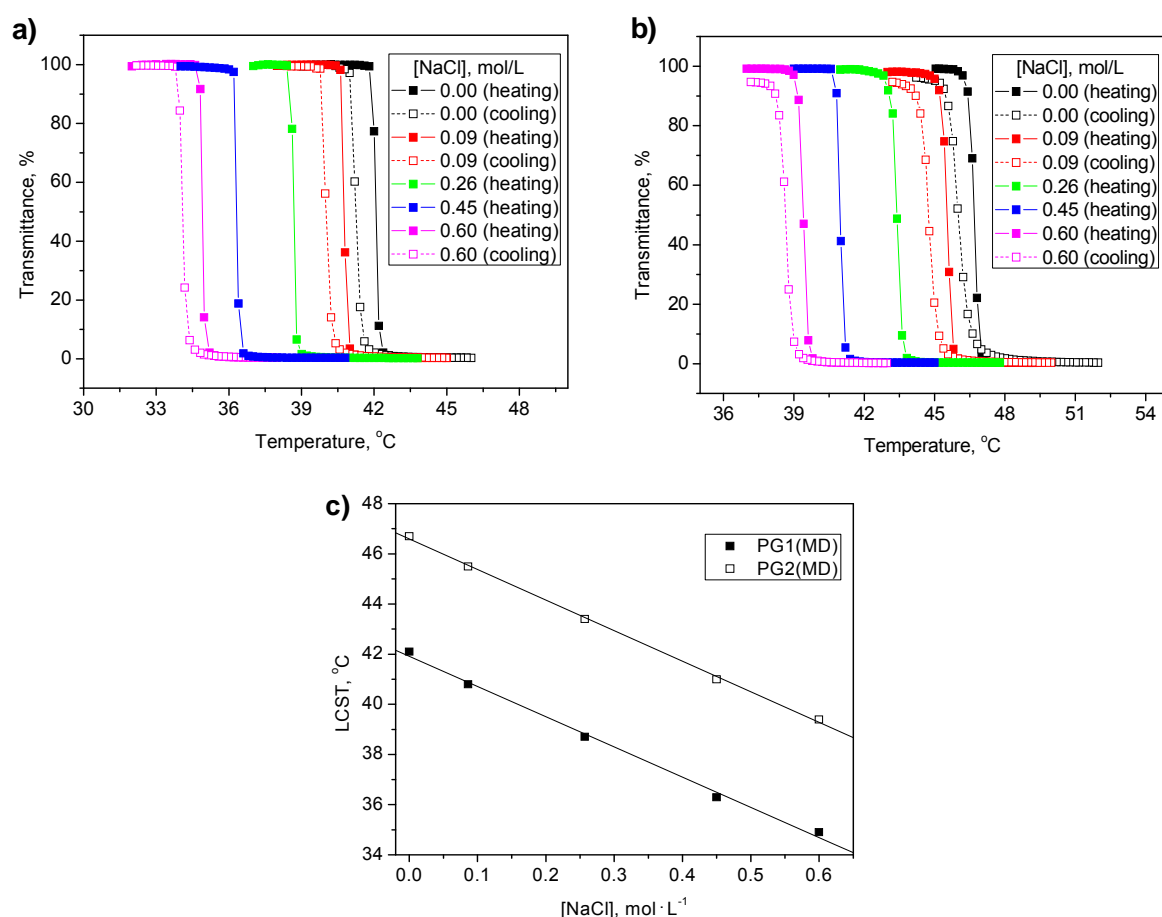


Figure 41. Plots of the temperature against the transmittance of **PG1(MD)** (a) and **PG2(MD)** (b) in 20 mM sodium PBS (0.25 wt%, PH 7.0) with the presence of different concentration of sodium chloride. (c) LCST dependence of **PG1(MD)** and **PG2(MD)** on NaCl concentration in PBS (pH 7.0).

Thermally induced aggregation

Furthermore, in a collaboration with Professor Ballauf's group, the thermally induced aggregation process of **PG2(ET)** was followed by DLS and the morphologies of the aggregates were further studied by static light scattering as well as *cryo*-TEM.²⁰⁵ As shown in Figure 42, when the temperature increased from 20 °C to the LCST of the polymer, the radius (R_h) of the particles increased from about 18 nm (for an individual polymer chain) subsequently to about 317 nm (for aggregates). Then they kept on increasing to a maximum value (more than 500 nm). Further increase of the temperature led to slight shrinking of the aggregates but soon the curve arrived at a plateau. This aggregation process is fully reversible. It was also found that the size of the aggregates is dependent on the heating rate, and faster heating resulted in a smaller particle size. From the insert of Figure 34, aggregates with quite narrow size distribution were formed at 40 °C. Additionally, R_g of the individual molecule (at low temperature) and the aggregates (above LCST) were determined with static light scattering. The R_g/R_h values at the two conditions were then calculated to be 1.2 (corresponds to a flexible coiled chain²⁰⁶) and 0.7 (corresponds to a uniform sphere²⁰⁷). These data prove that the polymer chains in aqueous solution follow an interesting coil to mesoglobule transition upon reaching the LCST.

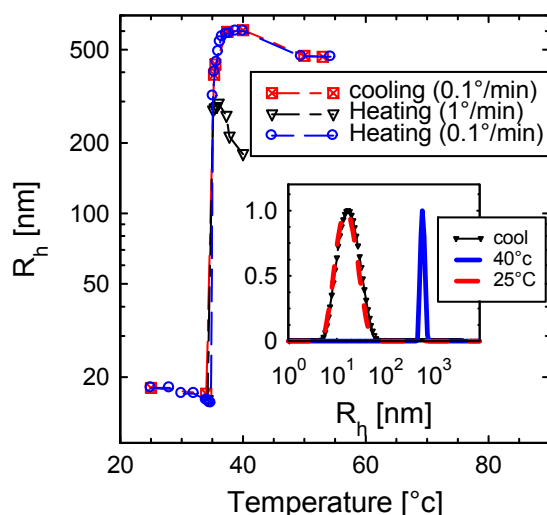


Figure 42. Hydrodynamic radius R_h of the **PG2 (ET)** as a function of temperature. The solution (0.016 wt%) was heated from 20 °C to 55 °C. The R_h were measured after equilibrium had been reached at each temperature. Heating and cooling was done using rates of 0.1 °C/min and 1 °C/min, respectively. The inset shows the corresponding particle size distribution at the heating and cooling rate of 0.1 °C/min calculated from CONTIN fits at 25 °C and 40 °C and again at 25 °C after cooling to the respective temperature.

This transition was also confirmed by *cryo*-TEM. As shown in Figure 43, at 25 °C, individual polymer chains with small size were observed (Figure 43 A) whereas stable mesoglobules with spherical shape were clearly formed at 60 °C (Figure 43 B). All the thermal aggregation behavior of **PG2(ET)** are similar to that of **PG2(MT)** discussed in chapter 4.1.

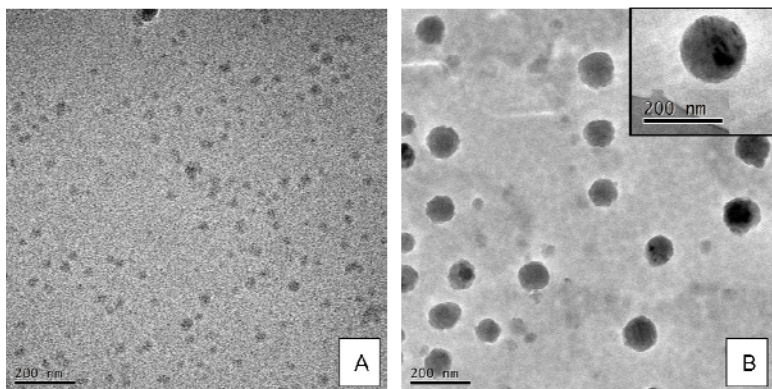


Figure 43. *Cryo*-TEM images of **PG2(ET)** at different temperatures. (A) Image taken at a solution temperature of 25° C. The individual dendrons are clearly visible. (B) At 60° C the dendronized polymer chains aggregate and form stable spherical mesoglobules. The inset shows the individual single mesoglobule.

4.2.3 *In Vitro* Cytotoxicity Study

One important parameter for these OEG-based dendronized polymers is their biocompatibility when considering their application in bio-related areas. Though PEG is believed to be a biocompatible substance, the polymers synthesized in present work contain some other units besides the OEG segments, such as the aromatic rings and PMMA backbone. Certainly, specific architecture effects should be also considered, even including their molar masses. Therefore, an *in vitro* cytotoxicity study of these polymers was then carried out with the CCK-8 assay and B16F1 cell line. All G1 (**PG1(HT)**, **PG1(MT)**, **PG1(MD)**, **PG1(ET)**) and G2 (**PG2(HT)**, **PG2(MT)**, **PG2(MD)**, **PG2(ET)**) polymers with low to high concentrations (1 – 200 $\mu\text{g mL}^{-1}$) were cultured together with the cells for 2 days under 37 °C, and then treated with CCK-8 solution for another 3 h. The cell viability was calculated and plotted as shown in Figure 44. The cell viability for each polymer is always around 100%, which means these polymers caused nearly no cell death even at high concentrations. From the optical microscopic images of the cells (Figure 45), no difference of the cell

morphologies was found compared to the control cells, which also suggests the non-toxic characteristic of these polymers.

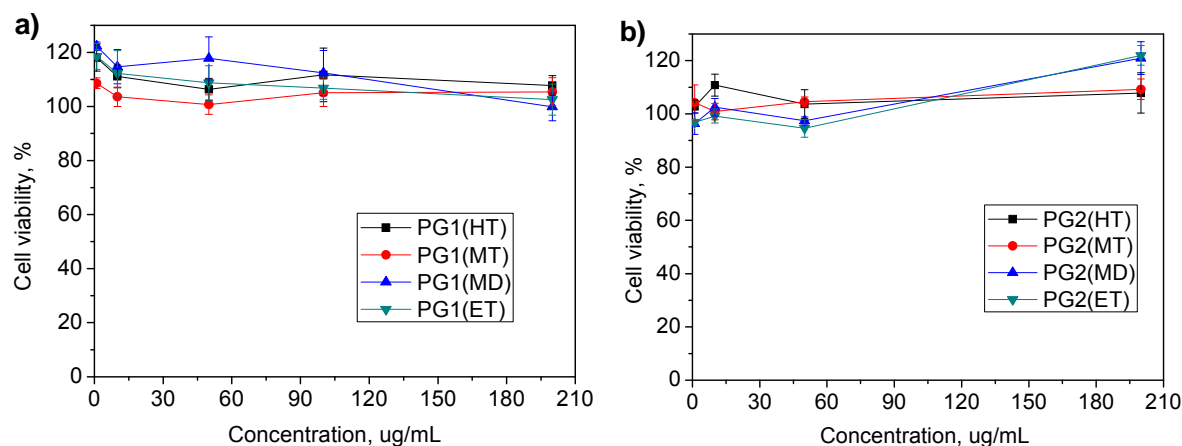


Figure 44. *In vitro* cytotoxicity of G1 (a) and G2 (b) dendronized polymers to B16F1 cells by CCK-8 assay. Data are mean values plus/minus standard deviation of four samples/cultures.

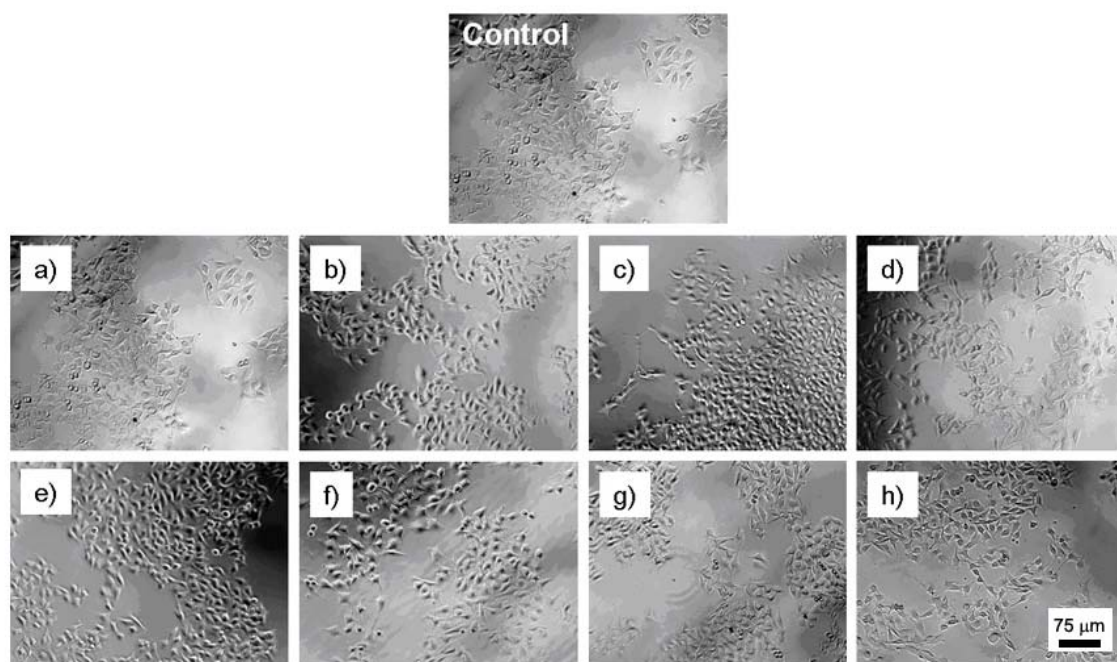


Figure 45. Microscopic images of B16F1 cells after incubation with untreated cells, and polymer solutions ($200 \mu\text{g mL}^{-1}$) **PG1(HT)** (a), **PG2(HT)** (b), **PG1(MT)** (c), **PG2(MT)** (d), **PG1(MD)** (e), **PG2(MD)** (f), **PG1(ET)** (g) and **PG2(ET)** (h) at 37°C for 48 h. The scale bars are the same for all images.

In summary, a series of OEG-based thermoresponsive dendronized polymers (from G1 to G3) with high to acceptable molar masses and well-defined structures were successfully synthesized. A new improved synthetic route was designed and proved

to be quite efficient, which leads to easy and large scale synthesis of G2 dendrons, and the access of G3 dendron. These dendronized polymers show not only unique thermoresponsive properties, but also their LCSTs can be tuned by slight structure variation. Their LCSTs are less sensitive to molar masses and concentration of the polymers, as well as dendron generation. Besides, these polymers with higher generations show special thermally induced dehydration and aggregation processes, which are different from conventional linear counterparts. With all these properties and their good biocompatibility, these polymers are certainly attractive for both fundamental researches and material applications.

4.3 Thermoresponsive Dendrimers

Based on the thermoresponsive dendronized polymers, we start to think whether their unique thermoresponsive behavior comes from their special cylindrical polymer structure or from the dendron itself. To clarify this point, dendrimers with well-defined spherical shape constructed by exactly the same dendrons as these polymers were designed. Their chemical structures are shown in Figure 46. 1,1,1-Tris(4-hydroxyphenyl)ethane (THPE) with three hydroxyl groups was selected as the core point, and OEG based G1 and G2 dendrons with either ethoxy or methoxy end-groups were chosen as the branch units, aiming at achieving various LCSTs.

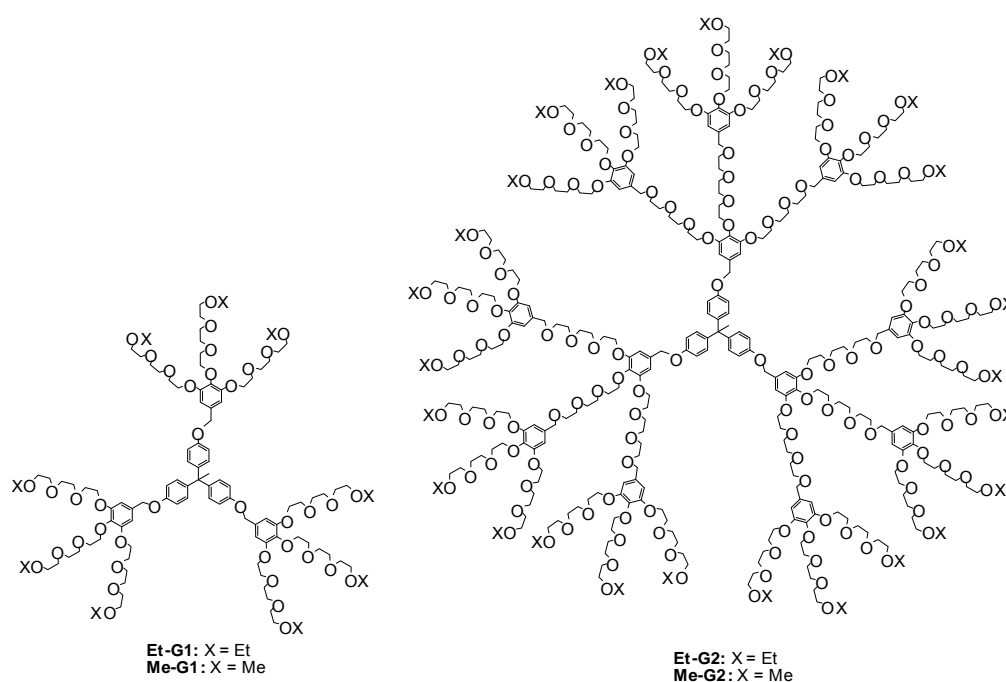
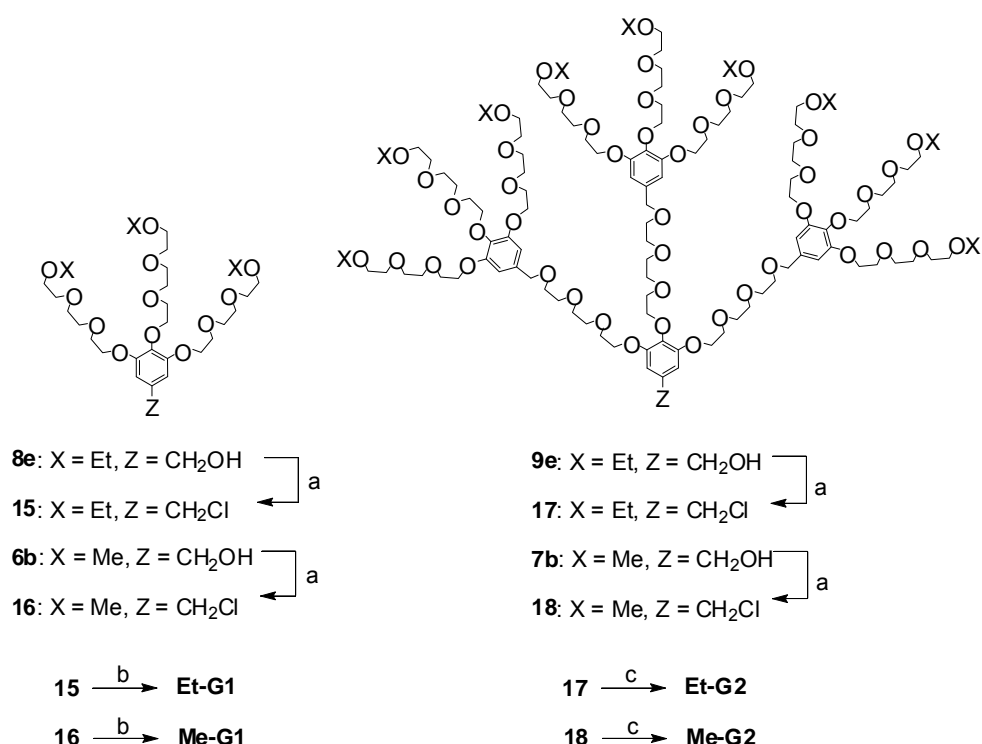


Figure 46. Chemical structures of the targeted dendrimers **Et-G1**, **Me-G1**, **Et-G2** and **Me-G2**.

4.3.1 Synthesis and Characterization

The synthetic steps for the dendrimers are summarized in Scheme 6. Dendrons **8e**, **6b**, **9e** and **7b** synthesized previously with different generation and end-groups were converted into dendron chlorides **15**, **16**, **17**, and **18**, respectively, by chlorination with SOCl_2 in concentrated DCM solution with DMAP as proton trap.²⁰⁸ Then G1 dendrimers **Et-G1** and **Me-G1** were obtained with high yield ($\geq 88\%$) by Williamson etherification of compound **15** or **16** with THPE in the presence of K_2CO_3 and KI. For synthesis of the G2 dendrimer, at the beginning, the same method as for G1 was applied, however, the reaction didn't work well and the targeted product was obtained with quite low yield ($\sim 5\%$). Most of the products were dendrimers with one or two dendrons attached to the core. Due to the large steric hindrance of the bulky G2 dendrons, the connection efficiency between the dendron chloride and the hydroxyl groups of the core was reduced. Therefore, Cs_2CO_3 was used instead of K_2CO_3 , and the reaction time was extended to two days. Finally, dendrimers **Et-G2** and **Me-G2** were obtained in satisfactory yields ($\geq 73\%$). In order to get the most pure products for analysis, some of the G2 dendrimers were further purified with HPLC.



Scheme 6. Synthesis procedures for dendrimers **Et-G1**, **Me-G1**, **Et-G2** and **Me-G2**. Reagents and conditions: (a) SOCl_2 , DMAP, DCM, r.t., 4 h (72~84%); (b) THPE, K_2CO_3 , KI, DMF, 80 °C, 24 h (88~90%); (c) THPE, Cs_2CO_3 , KI, DMF, 80 °C, 48 h (73~74%).

All dendron chlorides and dendrimers were characterized with ^1H and ^{13}C NMR spectroscopy and high resolution mass spectrometry, as well as elemental analysis to prove the successful synthesis and their high purity. Typical ^1H NMR spectra of all dendrimers are shown in Figure 47.

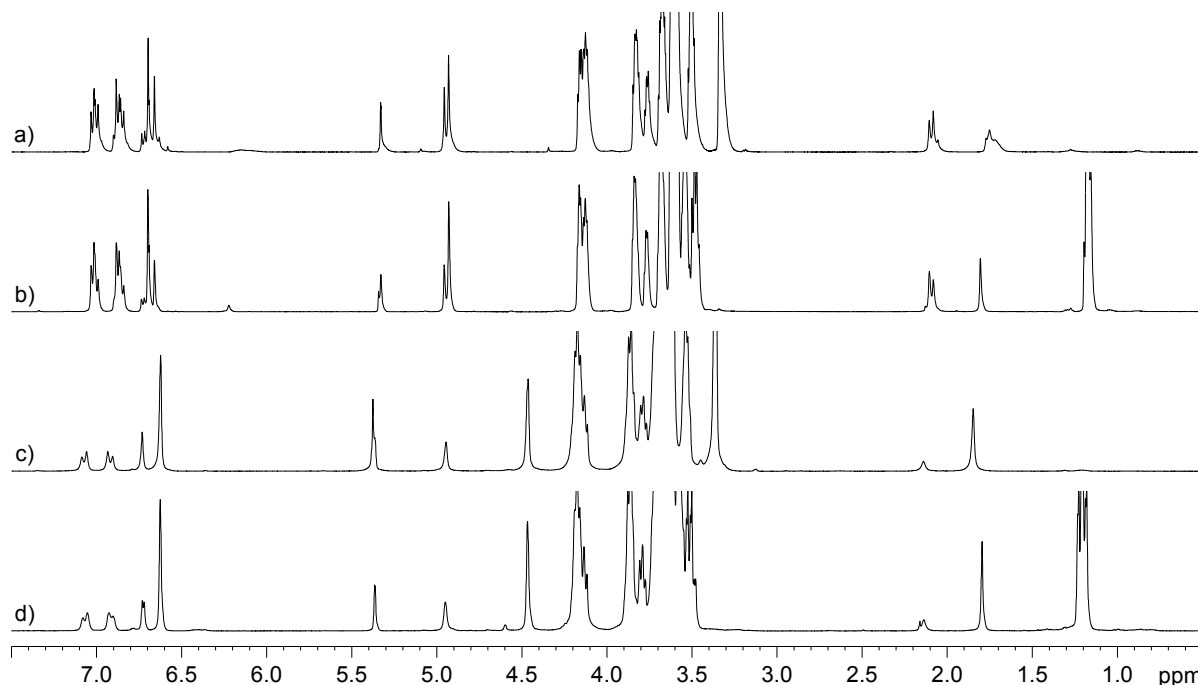


Figure 47. ^1H NMR spectra (500 MHz) of **Me-G1** (a), **Et-G1** (b), **Me-G2** (c) and **Et-G2** (d) in CD_2Cl_2 at room temperature.

4.3.2 Thermoresponsive Behavior

These OEG-based dendrimers also show thermosensitive properties when their aqueous solutions are heated above certain temperatures. Their phase transition curves from turbidimetry are plotted in Figure 48. The same as for dendronized polymers, these dendrimers with different generations (G1 or G2) and terminal groups (methoxy or ethoxy) also show different LCSTs in a range from 27 °C to 65 °C. The LCSTs of the ethoxy-terminated dendrimers (27 °C for **Et-G1** and 36 °C for **Et-G2**) are much lower than the methoxy-terminated ones (51 °C for **Me-G1** and 64 °C for **Me-G2**). But differently, the generation of the dendrimers shows stronger effect on the LCSTs, as the LCST of **Me-G1** is about 15 °C lower than **Me-G2** and the LCST of **Et-G1** is about 10 °C lower than **Et-G2**, whereas the values between G1 and G2 polymers is normally less than 5 °C. The possible reason is that the existing of the hydrophobic core in G1 dendrimer occupies certain high percentage of the structure, which decreases the overall hydrophilicity of the dendrimer. But for the G2 dendrimer,

the core only occupies a small part of the whole structure, which doesn't affect the overall hydrophilicity of the dendrimer. Therefore, all G2 dendrimers show similar LCSTs as their corresponding dendronized polymers. These results further prove that the LCSTs of these OEG-based dendritic macromolecules are independent of the molar mass. Besides, all these dendrimers also show sharp ($\leq 1^\circ\text{C}$) and fully reversible phase transitions. The hystereses between heating and cooling are also quite small ($\leq 0.8^\circ\text{C}$). Furthermore, unlike the thermoresponsive dendrimers reported by Kono,⁹⁰ the aggregation of these dendrimers exhibits a high thermal stability. Once the transmittances of the dendrimers decreased to 0% at the LCSTs, they kept on this value when further heated to high temperatures.

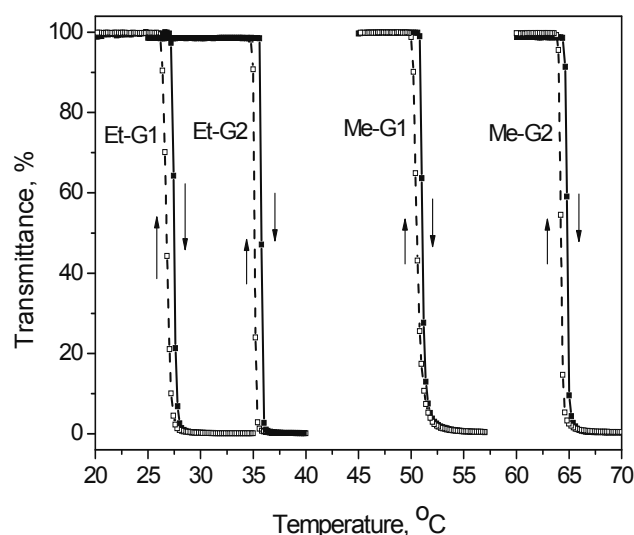


Figure 48. Plots of transmittance vs temperature (500 nm, $0.2^\circ\text{C}/\text{min}$; solid line: heating; dashed line: cooling) for 0.25 wt% aqueous solutions of dendrimers.

The influence of the dendrimer concentration on their phase transition behavior was also studied. Solutions of **Me-G1** and **Me-G2** with concentration ranging from 0.05 wt% to 2 wt% were prepared and measured. Their turbidity curves are shown in Figure 49a and b, and the LCSTs vs dendrimer concentrations are plotted in Figure 49c. For comparison, the results from dendronized polymers are also plotted together. It was found that unlike dendronized polymers, the concentration show more dramatic effects on the LCSTs of the dendrimers, the higher the concentration, the lower the LCSTs. The LCST of **Me-G1** and **Me-G2** decreased about 5°C and 7°C

°C, respectively, when the concentration changed from 2 wt% to 0.05 wt%. Whereas the LCSTs of both dendronized polymers **PG1(MT)** and **PG2(MT)** only decreased about 1 °C within the same investigated concentration range as for the dendrimers. Besides, the same as for dendronized polymers, the sharpness of the phase transition is less dependent on the concentration. Broad phase transition is only observed in very dilution solutions (0.05 wt%).

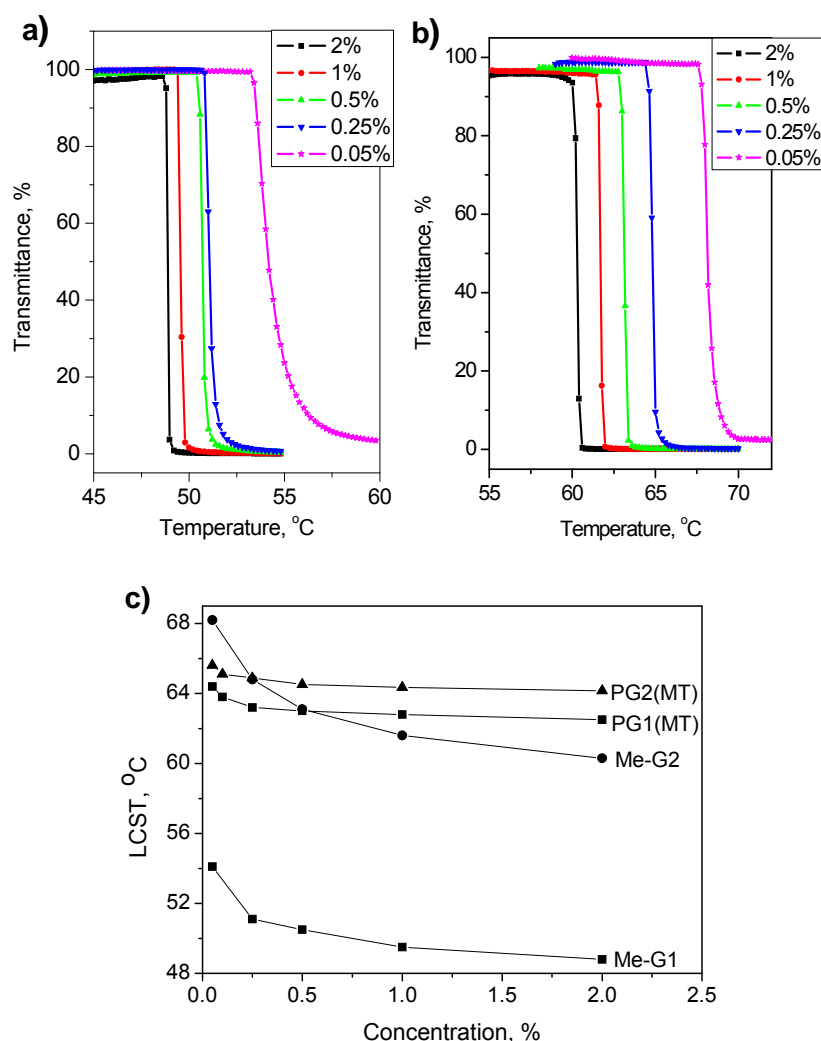


Figure 49. Plots of transmittance vs temperature for aqueous solutions of **Me-G1** (a) and **Me-G2** (b) at different concentrations. c) Dependence of LCSTs on concentrations of dendrimers and dendronized polymers.

The thermally induced aggregation processes of the dendrimers were also followed by DLS measurements. As shown in Figure 50a, the sizes of the individual dendrimer molecules are about 3-4 nm at room temperature. When the temperature increased to their LCSTs, large aggregates were formed as for dendronized polymers, and the

hydrodynamic diameters of these aggregates increased abruptly to several micrometers. The volume distributions of the aggregates at room temperature, around and above the LCSTs are shown in Figure 42b and c, respectively. Comparing to the corresponding polymers, the aggregates formed from these dendrimers showed much narrower size distribution once they were formed (Figure 42b and c), which may be due to the mono-dispersity of dendrimer macromolecules.

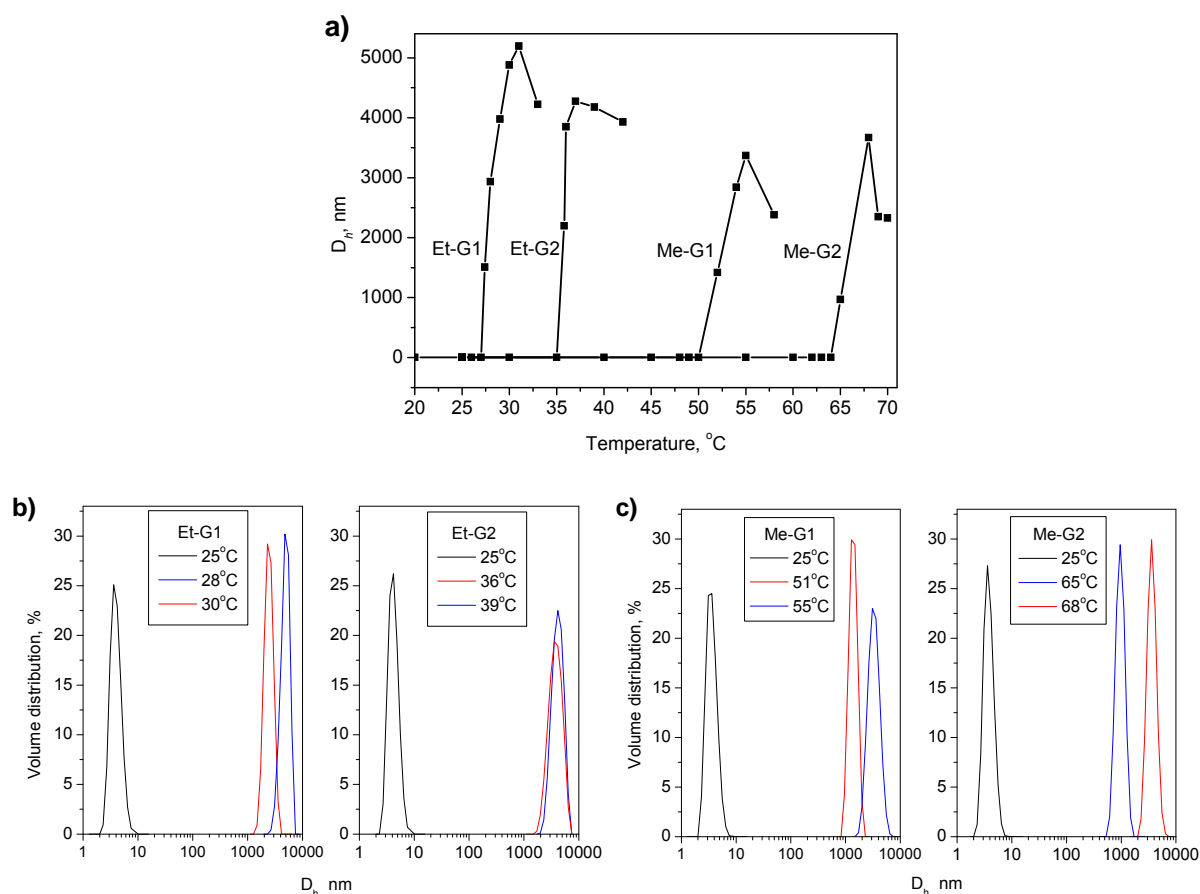


Figure 50. Plots of hydrodynamic diameters (D_h) of the aggregates from **Et-G1**, **Et-G2**, **Me-G1** and **Me-G2** in aqueous solution as a function of temperature obtained from DLS measurements.

The aggregation process of **Et-G2** was also recorded by optical microscopy (see movie at <http://www.rsc.org/suppdata/CC/b8/b814192d/index.sht>). The typical image of the aggregates formed in aqueous solution is shown in Figure 51a. The same as **PG2(MT)**, aggregates with uniform spherical shape were also obtained above the LCST. Their sizes are around 3~4 μm , which are similar to the results measured from DLS. The sizes of the spherical particles were constant whenever the temperature was increased above the LCST and the particles disappeared suddenly below the LCST. The morphologies of the aggregates in dry state were measured by AFM. For

preparing the samples, a **Et-G2** solution was pre-heated to about 50 °C. Then one drop of the turbid solution was spin-coated on a pre-heated HOPG surface. The resulted morphologies of the aggregates are shown in Figure 51b. Clearly, aggregates with similar well-defined spherical shape as seen by optical microscopy were observed by AFM. From the cross section analysis (Figure 51c), the average size of the aggregates is around 30 nm (height) x 1 μm (width). It is reasonable that aggregates with smaller size were observed from AFM as compared to OM, as the aggregates formed from solutions may contain more water than in dry substrate.

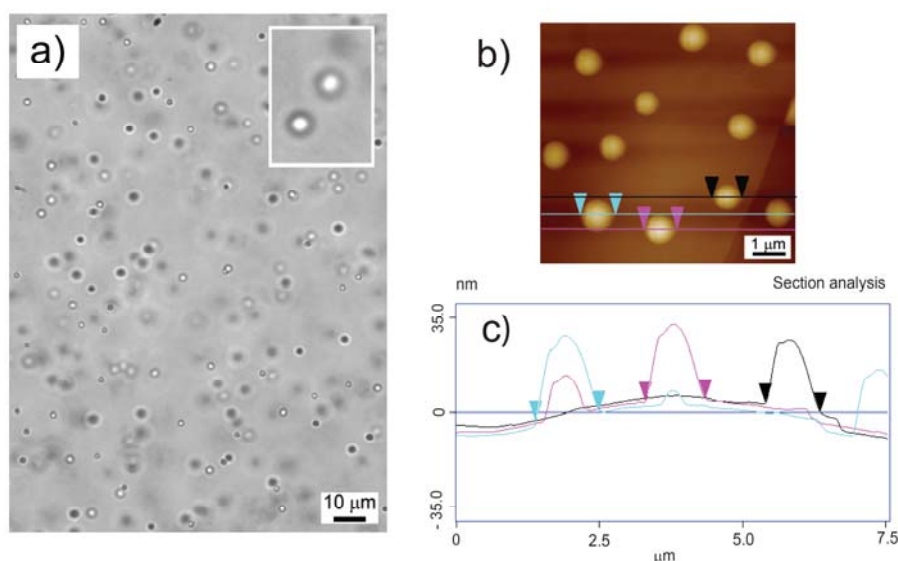


Figure 51. a) Optical micrograph of the aggregates in 0.25 wt% aqueous solutions of **Et-G2**. Note that the white features are the ones in focus. The inset: four-time enlarged feature. b) Tapping mode AFM image of the aggregates on HOPG from 0.25 wt% aqueous solutions of **Et-G2**. c) Cross-sectional profile of AFM image in (b).

4.3.3 *In Vitro* Cytotoxicity Study

In vitro cytotoxicity measurements were carried out to test the biocompatibility of these dendrimers. Dendrimer solutions with different concentrations were prepared and cultured with two cell lines (B16F1 and HaCat) for 48 h at 37 °C. PEG was also tested for comparison. The CCK-8 assay was then used to determine the cell viability. The results are shown in Figure 52a and b. The cell viability in presence of **Me-G1** (50 $\mu\text{g mL}^{-1}$) decreased to about 50% for B16F1 cells and 75% for Hacat cells, and in presence of **Et-G1** (10 $\mu\text{g mL}^{-1}$) decreased to about 40% for B16F1 cells and 50% for Hacat cells. From Figure 53, the morphologies of the B16F1 cells after treating with G1 dendrimers also changed when comparing to the control cells. These results

indicate that both of the G1 dendrimers show certain toxicity. The possible reason is the presence of the hydrophobic aromatic core which is expected to exhibit toxicity. A certain part of the toxic core units are exposed outside the dendrimer structures, which caused the death of the cells. Different from G1 dendrimers, both **Me-G2** and **Et-G2** caused almost no cell death like PEG even at high concentrations. The morphologies of the B16F1 cells after incubation with G2 dendrimers also show no difference with the control cells. G2 dendrimers contain large G2 OEG-based dendrons that can cover the toxic core sufficiently. Therefore, the whole G2 dendrimers show non-toxic properties. This is one of the main advantages of these OEG-based dendrimers when compared to other systems.

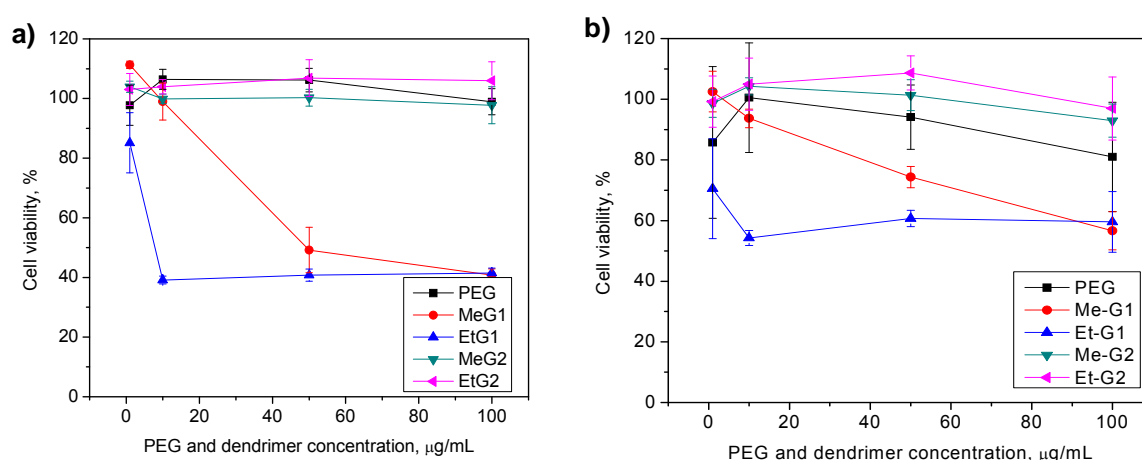


Figure 52. Cytotoxicity of dendrimers to B16F1 (a) and HaCat cells (b) by CCK-8 assay. Data are mean values plus/minus standard deviation of four samples/cultures.

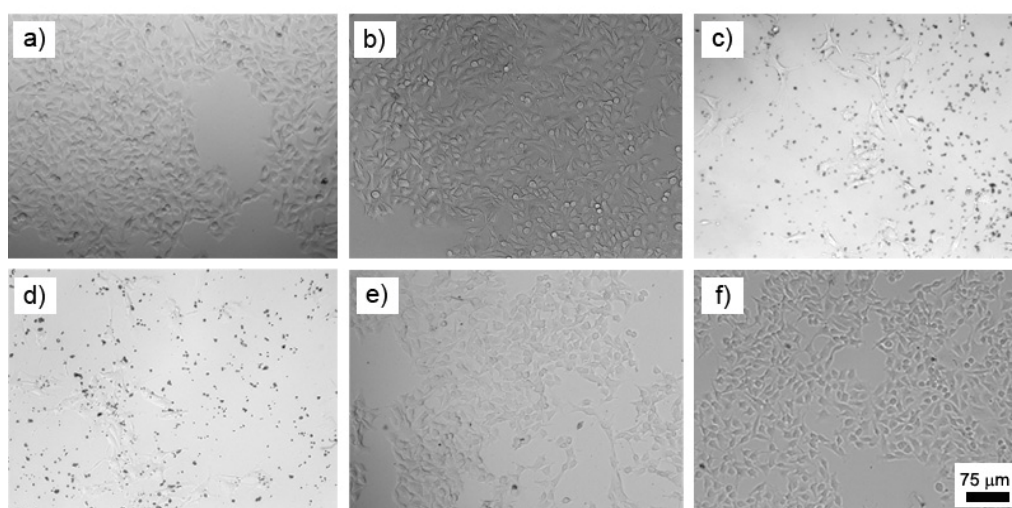


Figure 53. Microscopic images of B16F1 cells after incubation with untreated cells (a), PEG (b), Me-G1 (c), Et-G1 (d), Me-G2 (e) and Et-G2 (f) solutions (100μg/mL) at 37 °C for 48 h.

In contrast to other thermoresponsive dendrimers, the thermoresponsiveness of these OEG-based dendrimers comes from the OEG branch units, but not by introduction of thermoresponsive moieties. They show superior thermoresponsive properties (high thermal stability, sharp phase transition and small hysteresis) than most other systems. But differing from dendronized polymers, their LCSTs are both generation and concentration dependent. They can also form uniform spherical, large aggregates as the corresponding polymers. The reason is still not so clear and needs to be further investigated. The **Et-G2** dendrimer with good biocompatibility and LCST around body temperature (36°C) could be an attractive structure for bio-related applications.

4.4 Collapse Mechanism of Thermoresponsive Dendronized Polymers

As mentioned before, the LCST of an OEG groups containing polymer depends normally on its over-all hydrophilicity. This rule also applies to the OEG-based dendronized polymers of the same generation (Figure 54). For PG1, the calculated $\log P$ values have the order: **PG1(MT)** < **PG1(MD)** < **PG1(ET)**, which fits well to their LCST order: **PG1(MT)** > **PG1(MD)** > **PG1(ET)**. The same rule applies to PG2. But this rule doesn't fit to the polymers of different generations. Though the $\log P$ values of **PG1(ET)**, **PG2(ET)** and **PG3(ET)** are quite different, their LCSTs are quite similar, which suggests that the LCSTs of these polymers not only depend on the hydrophilicity but also on their architectures. The main structural characteristic of dendronized polymers differing from conventional linear counterparts is their sizeable thickness, which is tunable by the pendent dendron generations. It is interesting to know what a role the thickness plays on the phase transitions. The overall hydrophilicity of these polymers can be tuned not only by the peripheral groups and the length of the OEG segment, but also by varying the dendron generation. These structure variations show quite different effects on the LCSTs of the polymers. As shown in Figure 54, changing the peripheral groups from methoxy to ethoxy or the segment lengths from TEG to DEG, the apparent LCSTs decreased greatly about 30 and 20 degrees, respectively. In contrast, variation of the dendron generation from G1 to G3 had quite little influence on their LCSTs (≤ 3 °C). This interesting contrast

proves that, compared to the periphery part, the interior part of the dendrons contribute less to the phase transitions. This phenomenon can not be observed from conventional linear polymers where “no” thickness exists.

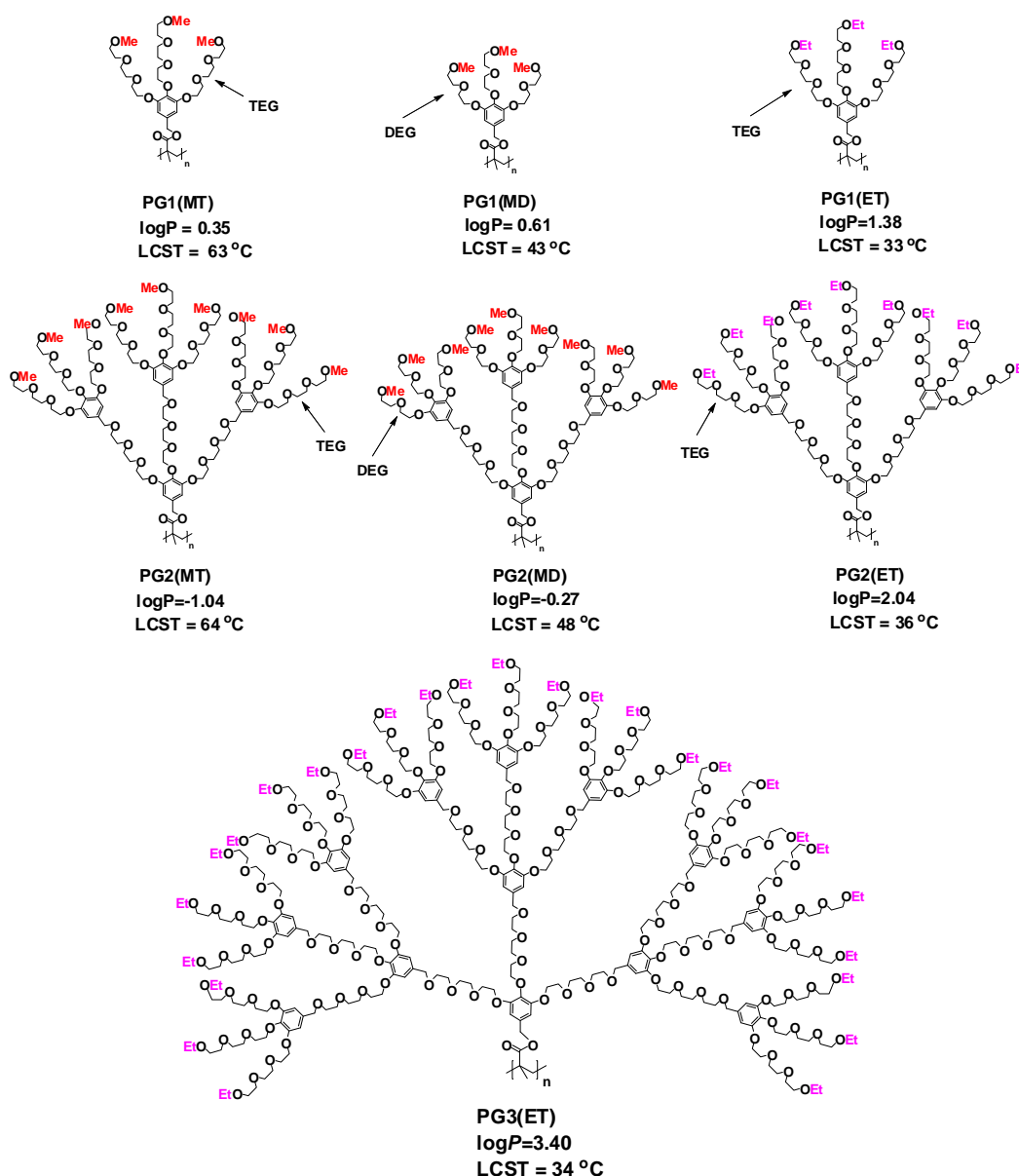


Figure 54. Chemical structures, calculated hydrophilicity values as well as LCSTs of all thermoresponsive dendronized polymers synthesized in the present work.

4.4.1 Doubly Dendronized Polymer with Interior Hydrophobic and Peripheral Hydrophilic Dendrons

In order to test the above conjecture on the collapse pattern, a novel G2 polymer **PG2(ETalkyl)** was designed (Figure 55). It has a similar structure to **PG2(ET)**, but contains a different interior part which is totally substituted by a hydrophobic alkyl

dendron. The LCST difference of this polymer and **PG2(ET)** will provide an answer to the question whether the interior part of a dendronized polymer contributes significantly to the phase transitions.

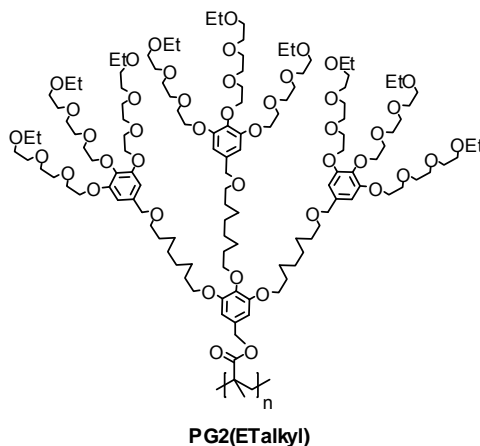
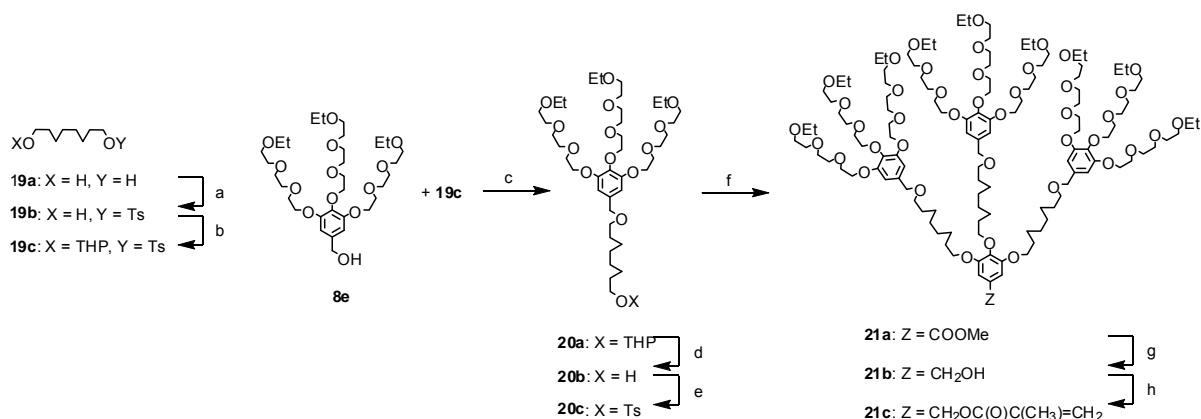


Figure 55. Chemical structure of the doubly dendronized polymer **PG2(ETalkyl)**.

The synthesis of this inside octane-based and outside OEG-based dendron follows a similar method which is described in Scheme 5. The details are summarized in Scheme 7. Compound **19c** was synthesized from octane-1,8-diol in two steps: mono-tosylation and THP protection. It was then converted into compound **20a** with one THP protected octane tail by etherification with the OEG based G1 dendron alcohol **8e** (chapter 4.2) in the presence of NaH. After de-protection and tosylation, compound **20c** was achieved. It was then reacted with gallate *via* Williamson etherification to afford the G2 dendron ester **21a**. Followed by reduction with LAH and esterification with MAC, the targeted macromonomer **21c** was obtained on gram scale. Except the first step (with a yield 56%), all others were finished with easy purifications and high yields ($\geq 83\%$). All the new compounds were characterized with ^1H and ^{13}C NMR spectroscopy and high resolution mass spectrometer, as well as elemental analysis. The ^1H NMR spectrum of macromonomer **21c** is shown in Figure 56.



Scheme 7. Synthesis procedures. Reagents and conditions: (a) NaOH, TsCl, THF, H₂O, 0~25 °C, 3 h (56 %); (b) DHP, PPTS, -5~25 °C, 4.5 h (86%); (c) KI, 15-crown-5, NaH, THF, r.t., 12 h (96%); (d) PTSA, MeOH, r.t. 2 h (90%); (e) TsCl, TEA, DMAP, DCM, -5~25 °C, 3 h (89%); (f) methyl gallate, K₂CO₃, KI, DMF, 80 °C, 24 h (83%); (g) LAH, THF, -5 °C~25 °C, 2.5 h (95%); (h) MAC, DMAP, TEA, DCM, -5~25 °C, 3 h (84%).

The macromonomer **21c** is liquid, which allows to conducting polymerization in bulk. Polymer **PG2(ETalkyl)** with a molar mass $M_n = 3.3 \times 10^5$ and PDI = 3.8 (from GPC) was obtained within three hours at 60 °C, but it became an insoluble gel-like compound when the polymerization was carried out for an elongated time (such as 14 hours), presumably due to the extremely high molar mass of the polymer.

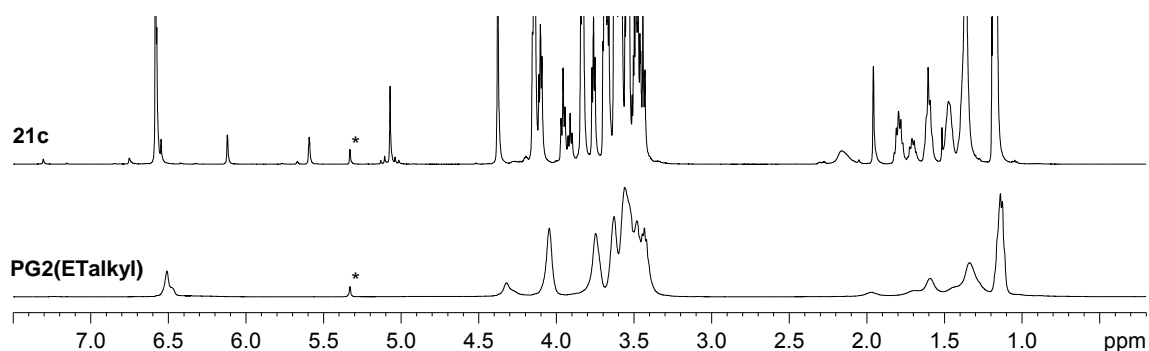


Figure 56. ¹H NMR spectra (500 MHz) of the macromonomer **21c** and its corresponding polymer **PG2(ETalkyl)** in CD₂Cl₂. The signals from CD₂Cl₂ are marked as (*).

4.4.2 Thermoresponsive Behavior

Polymer **PG2(ETalkyl)** is water-soluble at room temperature and exhibits a LCST. The transition curves from turbidimetry are shown in Figure 57a. The same as its

counterpart **PG2(ET)**, the phase transitions in both heating and cooling process are very sharp and the hysteresis is quite small. Its LCST is 31 °C. Although the overall hydrophilicity of this polymer was greatly decreased by incorporation of the alkyl-based hydrophobic interior dendron instead of the hydrophilic OEG-based dendron, the LCST difference between **PG2(ETalkyl)** and **PG2(ET)** is only 5 °C. This result also supports the assumption that the phase transitions of these polymers are dominated by the peripheral parts, and most of the interior parts show negligible effects. Therefore, the LCSTs of these dendronized polymers are controlled mainly not only by its over-all hydrophilicity but also by the arrangement of the hydrophobic and hydrophilic units within the structures. The hydrodynamic sizes of the aggregates were followed by dynamic light scattering measurements (Figure 57b), and the results show no clear difference if compared to that from **PG2(ET)**.

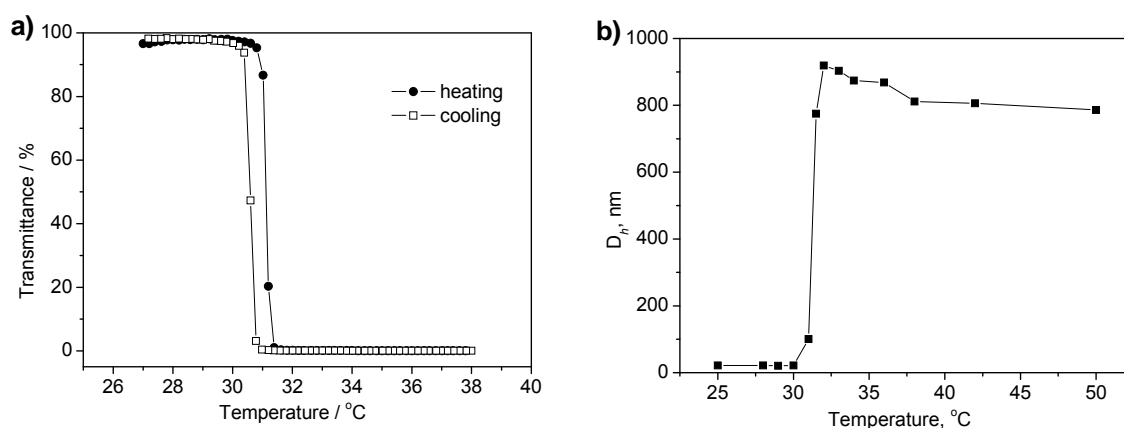


Figure 57. (a) Plots of transmittance vs temperature for 0.25 wt% aqueous solutions of **PG2(ETalkyl)**. Heating and cooling rate = 0.2 °C/min. (b) Hydrodynamic diameter of aggregates as a function of temperature measured from the same solution.

4.4.3. Study of the Collapse Mechanism via EPR Spectroscopy

In order to prove the above viewpoint and further understand the chain collapse mechanism, conventional continuous wave (CW) EPR spectroscopy was utilized as a simple and efficient tool to monitor the molecular environments of the dendronized polymer chains during the phase transitions. Paramagnetic tracer molecules, so called “spin probes”, are added into the system. These probes can physically interact with the molecules in the medium, which are dependent on the local polarity/hydrophilicity. The electron density in the spin probes is redistributed with the presence of local dipoles or hydrogen bonding, and the shape and hyperfine splitting

of the EPR signals will be affected at the same time. The changes in hyperfine splitting most strongly affect the signals at high magnetic field, from which the chemical environment of the polymers can be analyzed.

The EPR measurements were done with the supports from Professor Spiess's group. Based on the previous work,¹¹² TEMPO was selected as the spin probe. As shown in Figure 58, it contains both hydrophilic (N-O group) and hydrophobic (hydrocarbon ring) parts, which make this compound distributed in both hydrophobic and hydrophilic environments. This means, re-distribution of the probe in different environment and signal intensity changes during the phase transitions should reflect the proportions of hydrophilic and hydrophobic phases. Therefore, EPR spectroscopy of TEMPO in the media could provide insight into the chain collapse process on molecular level. **PG1(ET)**, **PG2(ET)** and **PG3(ET)** as well as **PG2(Etalkyl)** were used for the measurements. The polymer solutions of concentration 10 wt% were prepared to get strong EPR signals, and 0.2 mM spin probe were used to get good signal to noise ratio.

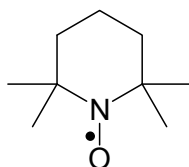


Figure 58. Chemical structure of TEMPO.

Two temperatures, one below (15 °C) and one above (65 °C) the LCST of **PG1(ET)**, were selected to test the feasibility of this method, and the recorded spectra are shown in Figure 59a. The polymer dissolved well in water below its LCST and only a hydrophilic environment existed, therefore, no peak splitting was found in the spectrum. But at 65°C, the high field signal split apparently into two well-defined components (denoted A and B), which should be related to the hydrophobic and hydrophilic environments formed from the polymer above its LCST. B peak related to the fraction of TEMPO in collapsed regions and A peak related to the fraction in the water swollen polymer and water regions. For detailed investigation, the EPR spectra of the **PG1(ET)** solution at different temperatures were recorded during the slow heating from 15 to 65 °C, and only the spectra at high magnetic fields are shown here (Figure 59b). Below the LCST, only A peak was detected. When the temperature increased to the LCST, the B peak appeared which is correspondent to the formation

of hydrophobic regions from collapsed polymer chains. Further heating resulted in intensity increase of B peak compared to A peak. The ratio of peak A and B at different temperature is a direct measure of the fraction of swollen and collapsed regions. It is clear that the polymer chains continue dehydration even at temperatures much higher than its LCST. Different from turbidimetry, which only provides the information of polymer aggregation at macroscopic level, EPR spectroscopy provides a more detailed pattern of polymer chain collapse at molecular level.

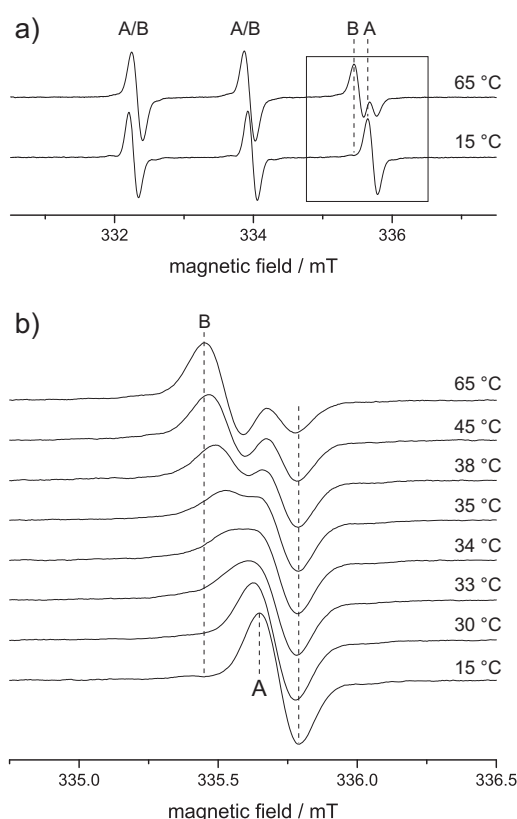


Figure 59. a) CW EPR spectra (X-band, microwave frequency ~ 9.3 GHz) for 0.2 mM TEMPO in an aqueous solution of 10 wt% EtPG1 recorded at 15 °C and 65 °C and b) detailed plot of the high field transition line ($m_1 = -1$, marked by a rectangle in a)) at selected temperatures. The contribution to the high field peak at 335.4 mT, denoted B, originates from TEMPO molecules in a hydrophobic environment, while nitroxides in a hydrophilic surrounding give rise to the contribution A. The broken lines at the outer extrema of the peak serve as guides to the eye.

To further investigate the structure effects on the polymer chain collapse, the temperature dependent EPR spectra of other three polymers were recorded (Figure 60). The solid lines under the numbers indicate their corresponding LCSTs. Though

the LCSTs of these ethoxy-terminated polymers are similar, their EPR spectra are quite different. For **PG2(ET)** (Figure 60a), when the temperature increased to the LCST, the signal became broad but there was no individual B peak clearly appearing. This suggests that, though the dehydration happened, many water molecules were entrapped in the aggregates, so most of TEMPO molecules still stayed in the hydrophilic regions. With increasing temperature, water molecules were expelled gradually out of the aggregates. More and more TEMPO molecules were entrapped into the collapsed region which led to the intensity increase of the B signal. At 65 °C, B signal became slightly stronger than A, but peak A still possessed quite high intensity at this stage, which means this polymer still contained hydrophilic regions inside. While for **PG2(Etalkyl)**, the B peak appeared clearly at the LCST (Figure 60b), which means once the aggregates formed, they contained quite less water molecules but kept an intensively hydrophobic environment. At 65 °C, the B peak is so strong and the A peak is negligible small. This means the formation of many hydrophobic regions and most of TEMPO was trapped inside. This is quite different from **PG2(ET)** which contains a hydrophilic interior dendron. Why the aggregations of these two polymers started at similar temperature but their dehydrations behaved so differently? The most possible reason is that the phase transition is dominated by the peripheral groups but not the interior part. The interior units of **PG2(ET)** were less dehydrated which always provided certain hydrophilic regions. This could be further proved from the spectra of **PG1(ET)** which has no dendron core. It was found that, just at 2 °C higher than the LCST, the B peak became stronger than A, which means the aggregates also contained less water. Finally at 65 °C, quite strong B peak remained with a negligible A peak which also means an intense hydrophobic environment was formed similar to **PG2(Etalkyl)**. Similar results as **PG2(ET)** were obtained from **PG3(ET)**, which contains even hydrophilic interior G2 dendrons (Figure 60c). The EPR signal became broad at the LCST of **PG3(ET)**, then the B peak appeared around 40°C and its intensity increased gradually with temperature. The intensity of B peak became stronger than that of A peak at the temperature about 10 °C higher than its LCST.

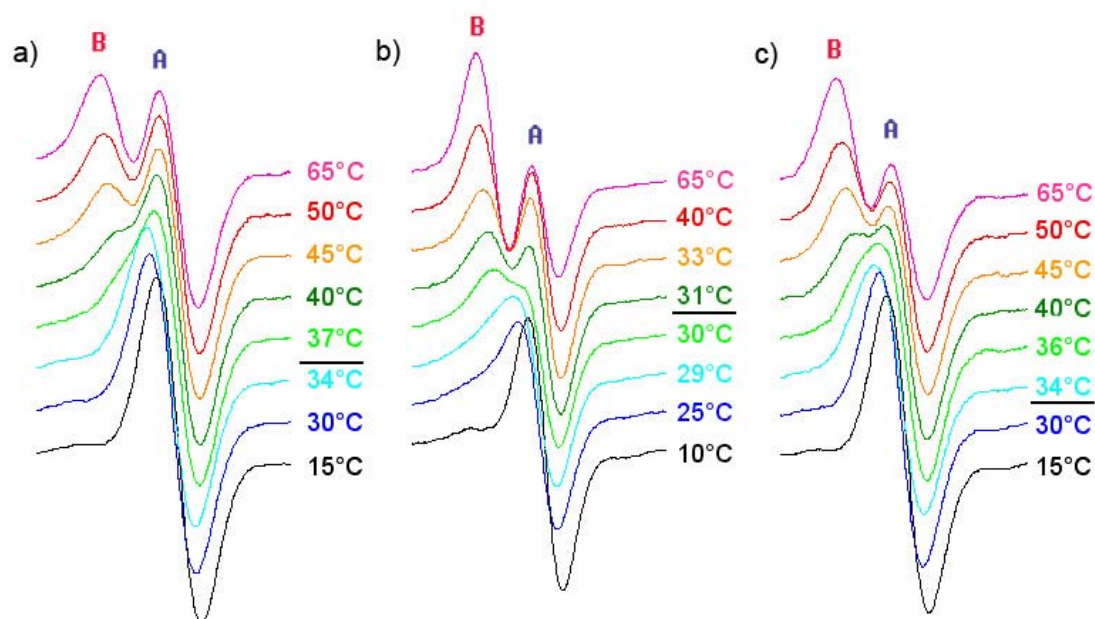


Figure 60. Temperature dependent EPR spectroscopy of **PG2(ET)** (a), **PG2(Etalkyl)** (b) and **PG3(ET)** (c). The solid lines under the numbers indicate their corresponding LCSTs.

In conclusion, both turbidimetry and EPR spectroscopy prove that the increase of polymer's thickness shows only small effects on the thermal behavior of dendronized polymers. Their thermoresponsiveness is dominated by the peripheral units. Above the LCST, the interior part of the polymer which contains OEG dendron(s) provides a hydration environment covered with a collapsed outer-layer, which makes the dendronized polymer as a nano-cylindrical container.

5. Amphiphilic Dendronized Homopolymers

Based on the successful synthesis of water-soluble and insoluble dendrons in our group, it is interesting to use them as building units for the construction of amphiphilic dendronized polymers. By introduction of hydrophilic OEG-based and hydrophobic 4-aminoproline-based dendrons^{30,209} into a macromonomer, a series of novel amphiphilic homopolymers based on the dendronized polymer concept were designed. Their chemical structures are shown in Figure 61. This structure design is based on the following considerations: 1) The hydrophilicity of the polymers could be easily tuned *via* changing the dendron generation; 2) The introduction of the lysinol unit not only connects these two different dendrons together, but also provides a space for their segregation; 3) The existing of the chiral centers may induce helical conformation of the polymer; 4) OEG dendron may afford the polymer thermoresponsiveness and also bio-compatibility. Here the synthesis of these polymers, their secondary structures and thermoresponsive behaviors will all be described. Furthermore, their self-assembly into porous films *via* the breath figure technique will be illustrated in detail.

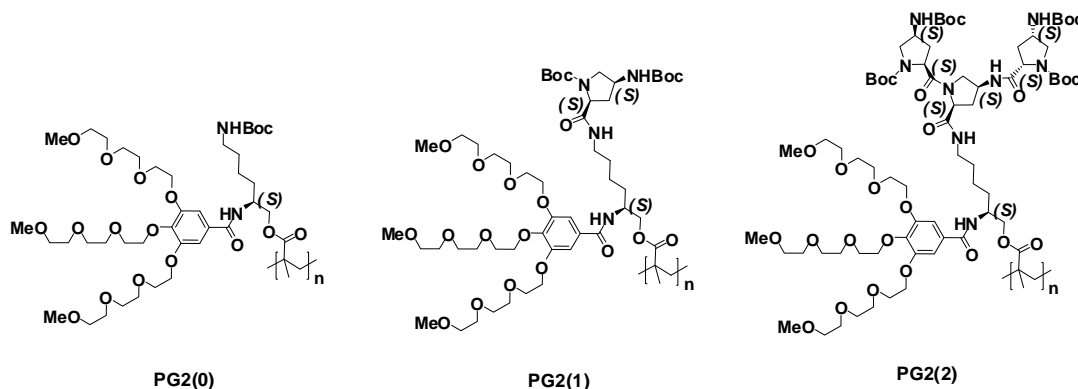
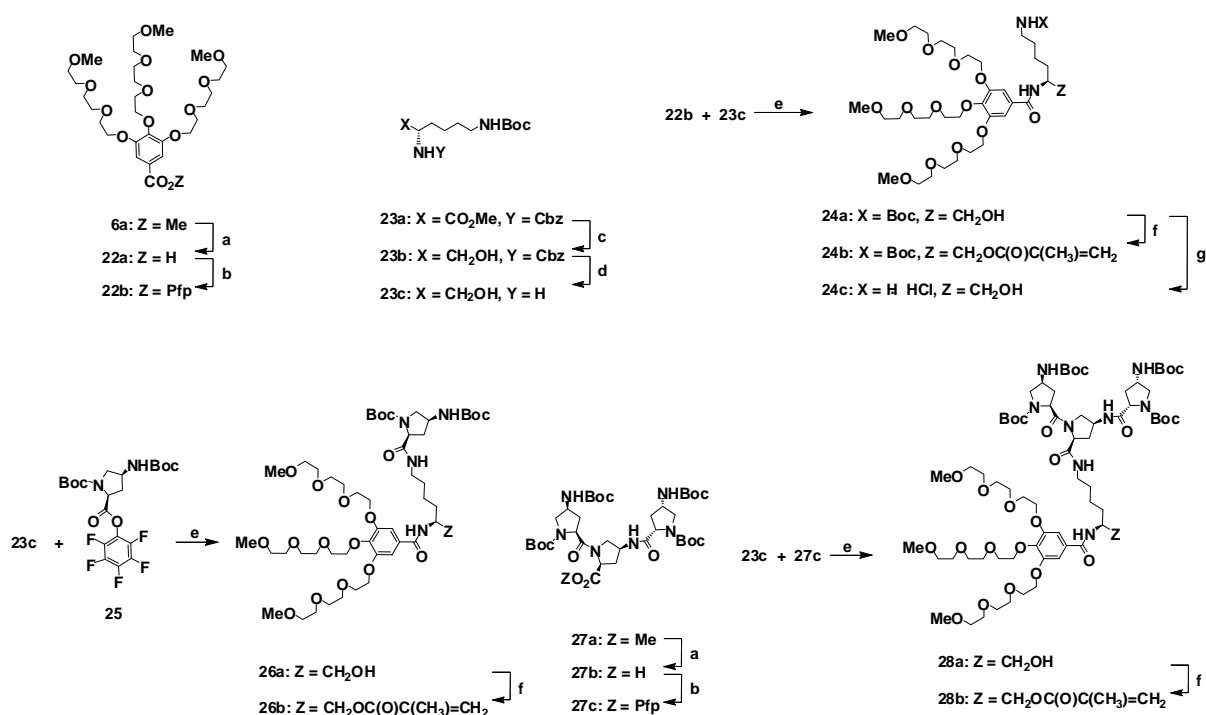


Figure 61. Chemical structures of the amphiphilic dendronized polymethacrylates **PG2(0)**, **PG2(1)** and **PG2(2)** designed in this work

5.1 Synthesis and Characterization

In order to achieve high molar mass and to keep a well-defined chemical structure, the macromonomer route was selected to synthesize the amphiphilic polymers. The detailed synthetic sequences to the macromonomers are delineated in Scheme 8. First, the methoxy terminated OEG dendron ester **6a** was converted to acid **22a** *via*

hydrolysis with $\text{LiOH}\cdot\text{H}_2\text{O}$. After reaction with pentafluorophenol in the presence of DCC, **22a** was converted to active ester **22b**. The commercially available benzyloxycarbonyl (Cbz) and *tert*-butyloxycarbonyl (Boc) protected lysinol ester **23a** was selected as the connection unit. After reduction with LiBH_4 and dehydrogenation, **23c** was obtained. The dendron active ester **22b** was then successfully attached to the lysinol amine **23c** via amide coupling to afford compound **24a**. It was then either reacted with MAC to get the macromonomer **24b** or deprotected with concentrated HCl to achieve the amine **24c**. Amide coupling of **23c** and G1 proline active ester **25** synthesized before afforded the amphiphilic dendron alcohol **26a** which was then reacted with MAC to furnish the macromonomer **26b**. Similar with previous procedures, from G2 proline ester **27a**, followed by hydrolysis and condensation reaction, G2 proline active ester **27c** was synthesized. It was then attached to amine **23c** via amide coupling to afford the amphiphilic dendron alcohol **28a**. After reaction with MAC, amphiphilic macromonomer **28b** was successfully synthesized. All the steps were performed with high yield ($\geq 80\%$) and easy purification.



Scheme 8. Synthesis procedures. Reagents and conditions: (a) $\text{LiOH}\cdot\text{H}_2\text{O}$, MeOH, H_2O , $-5\sim 25\text{ }^\circ\text{C}$, 6 h (85~91%); (b) DCC, pentafluorophenol, DCM, 12 h, $-15\sim 25\text{ }^\circ\text{C}$ (80~90%); (c) LiBH_4 , THF, $-5\sim 25\text{ }^\circ\text{C}$, over night (93%); (d) Pd/C, ethanol, ethylacetate, 3 bar of H_2 , $25\text{ }^\circ\text{C}$, over night, (93%); (e) DiPEA, DCM, over night, $-15\sim 25\text{ }^\circ\text{C}$ (85~87%); (f) MAC, DMAP, TEA, $-5\sim 25\text{ }^\circ\text{C}$, 4 h (83~90%). DCC = N,N'-Dicyclohexylcarbodiimide, DiPEA = diisopropylethylamine.

All new compounds were characterized by ^1H and ^{13}C NMR spectroscopy, high resolution mass spectrometry as well as elemental analysis. Most of the products were synthesized with high purity.

Free radical polymerization of the liquid macromonomer **24b** was carried out in bulk and high molar mass polymer **PG2(0)** was obtained. For the solid macromonomers **27b** and **29b**, the polymerization were carried out in highly concentrated DMF solutions, and the respective polymers **PG2(1)** and **PG2(2)** with lower DP_n were obtained. But their molar masses are much higher than the conjugated amphiphilic dendronized homopolymers synthesized previously by the Suzuki polycondensation method.¹³³ Besides, with the Boc-protected lysinol unit or the hydrophobic proline G1 dendron incorporated into the OEG dendron, **PG2(0)** and **PG2(1)** are still very hydrophilic, and highly water soluble. When more hydrophobic G2 proline dendron was incorporated, the corresponding polymer **PG2(2)** is not soluble in water anymore.

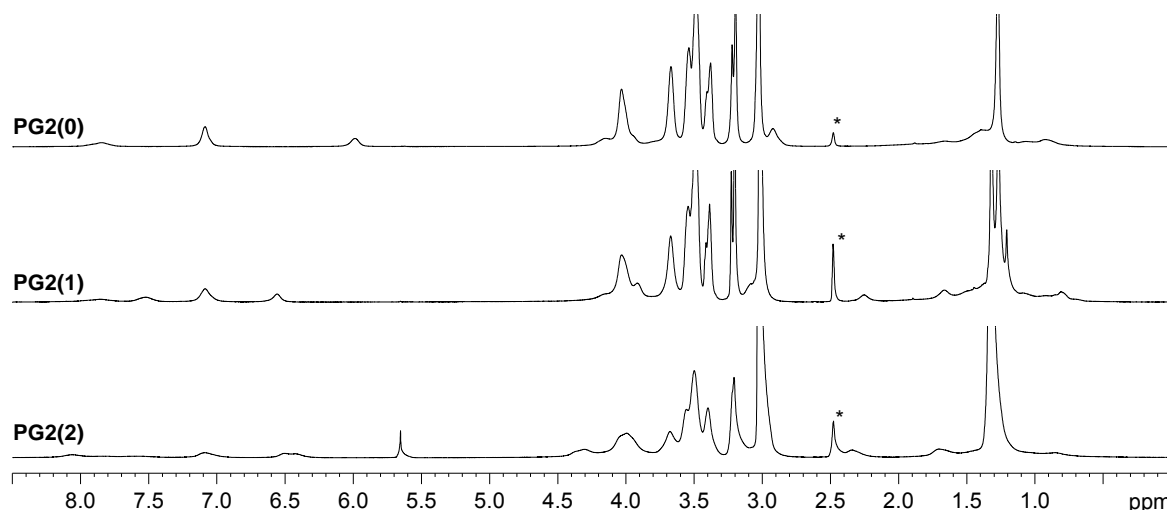


Figure 62. ^1H NMR spectroscopy of **PG1(0)**, **PG1(1)** and **PG1(2)** in DMSO at 80°C. The signals from DMSO are marked as (*).

Table 4. Conditions for and results of the polymerization of macromonomers.

Entries	Polymerization conditions			Yield (%)	GPC results ^c		
	Monomer	Solvent	Time (h)		$M_n \times 10^{-5}$	DP_n	PDI
1	24b ^a	Bulk	18	65	4.6	516	2.3
2	26b ^b	DMF	17	60	2.6	236	2.9
3	28b ^a	DMF	14	40	1.4	92	2.5

^a Polymerizations were carried out at 60 °C and ^b at 80 °C with AIBN as the initiator (0.5 wt% based on monomer). ^c All GPC measurements were done in DMF (1% LiBr) as eluent at 45 °C.

5.2 Thermoresponsive Behavior

PG2(0) and **PG2(1)** are soluble well in water at room temperature, but also show thermoresponsiveness at elevated temperatures. Their turbidity curves are shown in Figure 63. The LCSTs of **PG2(0)** and **PG2(1)** were determined to be 46.7 and 37.7 °C, respectively. Obviously, the LCSTs of the resulted polymers are much smaller than **PG1(MT)**. This indicates that the hydrophobic G1 proline dendron, which is arranged beside the OEG dendron in each repeat unit, contributed significantly to the thermally-induced aggregation. This is quite different from **PG2(ETalkyl)** discussed before: by changing the interior hydrophilic groups to hydrophobic alkyl units, the LCST of the polymer only slightly changes. Besides, the sharpness of the phase transition of **PG2(0)** remains the same as **PG1(MT)** (Figure 63a), but introduction of G1 proline dendron in the case of **PG2(1)** leads to much broader phase transitions and obviously hysteresis between heating and cooling processes as shown in Figure 63b.

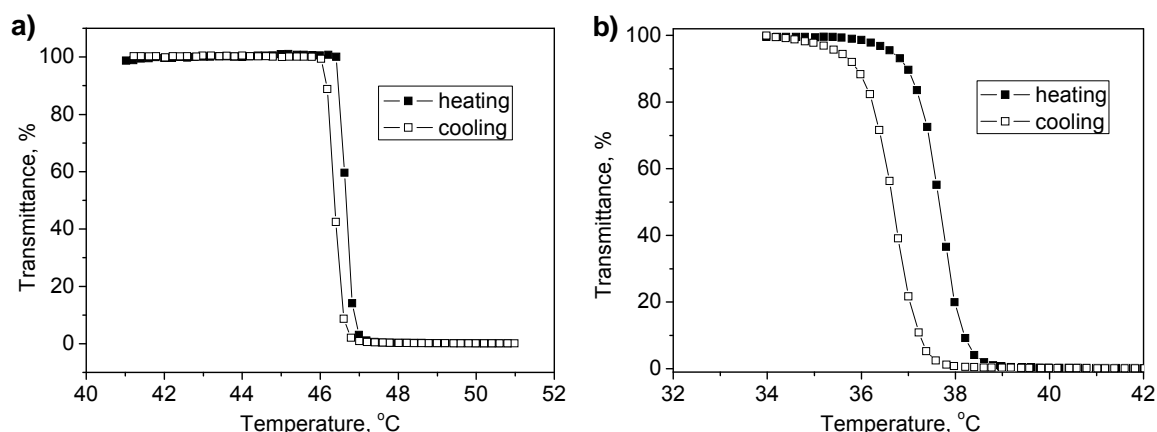


Figure 63. Plots of transmittance vs temperature for 0.25 wt% aqueous solutions of **PG2(0)** and **PG2(1)**. Heating and cooling rate = 0.2 °C/min.

5.3 Secondary Structure Analysis

The secondary structures of these polymers were investigated with optical rotation (OR) and circular dichroism (CD) spectroscopy, and the results are summarized in Table 5 and Figure 64. The OR values of all polymers are all smaller than that of their corresponding monomers. Though the differences are not so pronounced due to the

relatively high rigidity of the dendronized polymers,^{30,210} these results nevertheless suggest polymers and monomers adopt different conformations, and the polymers possibly possess ordered secondary structures. To further characterize their conformation, CD spectroscopy was applied, and the spectra of methanolic solutions at room temperature are shown in Figure 64. All polymers show different CD spectra compared to their monomers, which demonstrates that the polymers adopt ordered secondary structures. Comparing the CD spectra of different polymers, one can conclude that introduction of the chiral proline dendron doesn't enhance the chirality of the corresponding polymers.

Table 5. Specific rotations of all monomers and polymers.^a

Sample	$[\alpha]^{25}_D(\text{deg})$	
	Monomer	Polymer
G2(0)	-14.4	-3.2
G2(1)	-40.1	-10.8
G2(2)	-42.7	-19.3

^a) All measurements were done at 25 °C with a 1 dm cuvette in MeOH.

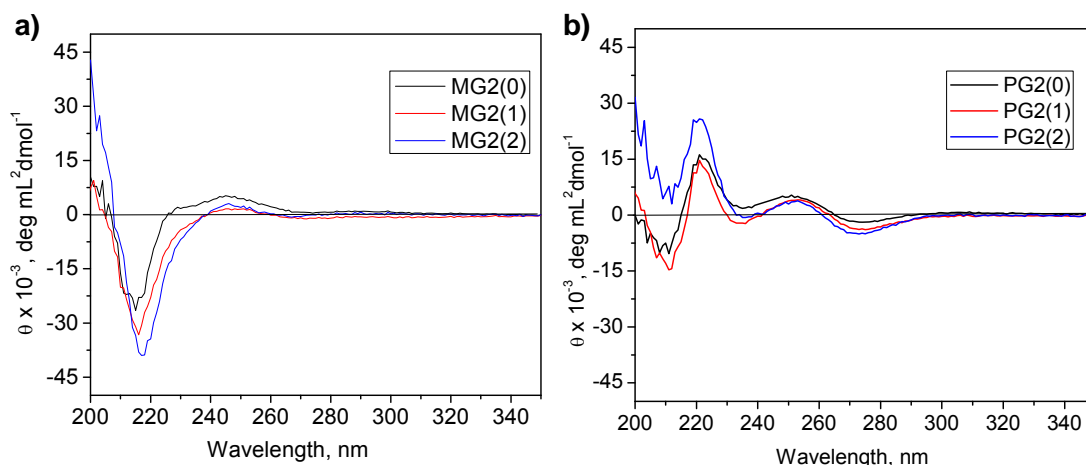


Figure 64. CD spectra of all monomers and polymers in MeOH at 25 °C: a) All monomers; b) All polymers.

5.4 Fabrication of Porous Films with the “Breath Figure” Technique

The self-assembly of these polymers into porous films with the BF method on a mica surface was studied. It is known that several parameters will influence the morphologies of the porous film, including the humidity, polymer concentration,

flowing rate of the gas, substrate, hydrophilicity and structure of the polymers. It was found that though several kinds of polymers could form micro-porous honeycomb films *via* this technique, the basic principle is still not fully understood, and different conditions are required for different polymers. The whole procedures and conditions for the preparation of the films in the present work are as follows: in a small chamber with 70% humidity, about 20 μL of the polymer solution (10 mg/mL) in chloroform was dropped onto the mica surface (1 x 1 cm). After evaporation of all the solvent and water, the films with cavities were formed and the porous morphologies were investigated by SEM (Figure 65). The films formed from **PG2(0)** and **PG2(1)** are all transparent. No porous film formed from **PG2(0)** and only a flat film was observed (Figure 65a). Some holes appeared from **PG2(1)**, but they are either irregular or with quite small size (Figure 65b). This result may be due to the high hydrophilicity of these two polymers, which destabilize the water droplets on the polymer surface and most of the water droplets were entrapped into the polymers. The hydrophobic polymers **ProG1** and **ProG2** (Figure 5, polymer 3) were also tested and turbid films were obtained on the mica surface. As shown in Figure 65c and d, both polymers could form porous film, but the sizes of the porous are widely distributed. Differently, films prepared from **PG2(2)** under the same condition as for the previous samples were regularly porous with round shaped pores with 1 μm size (Figure 65e), together with several holes of smaller size and irregular shape.

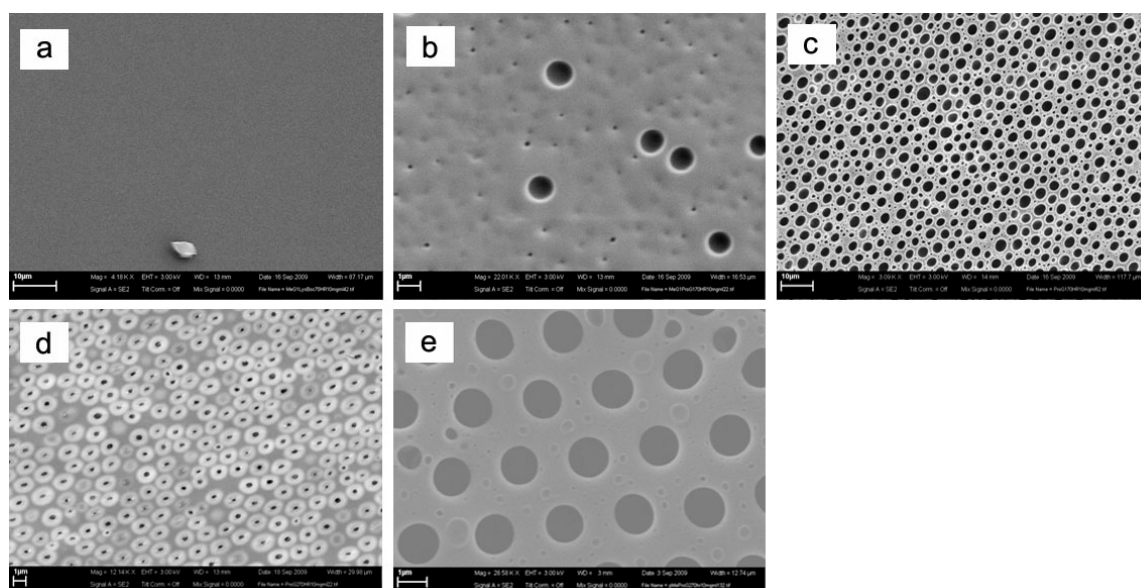


Figure 65. SEM images of porous films on mica surface cast from different dendronized polymer solutions: a) **PG2(0)**; b) **PG2(1)**; c) **ProG1**; d) **ProG2**; e) **PG2(2)**.

Additional experimental conditions were applied to examine their influences on the formation of the porous films, so samples were prepared with lower concentration and under lower humidity, respectively. When decreasing the polymer concentration to 5 mg/mL or the humidity to 60%, though porous films were still formed, all of the pores were not in ordered arrays (Figures 66a and b). On the other side, when small amounts of the hydrophobic G1 proline polymer (10 wt%) was mixed with **PG2(2)**, a flat film with much more regularly arranged holes with about 1 μm size was obtained (Figure 66c).

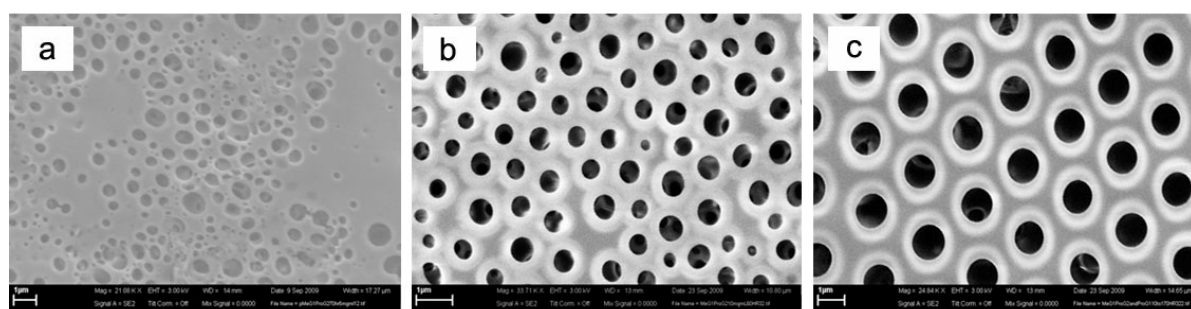


Figure 66. SEM images of porous films on mica surface cast from **PG2(2)** under different conditions: a) 5 mg/mL, 70% humidity; b) 10 mg/mL, 60% humidity; c) mixed together with **ProG1** (10 wt%), 10 mg/mL, 70% humidity.

In conclusion, a series of amphiphilic dendronized homopolymers based on OEG and proline units were prepared by the macromonomer route. The water-solubility of these polymers is tunable by the generation of the hydrophobic proline dendron. The polymers with or without G1 proline dendron are water-soluble and thermoresponsive, but the polymer carrying the G2 proline dendron is water insoluble. The arrangement of the hydrophobic and hydrophilic units within these polymers shows significant influences on the thermoresponsiveness: with hydrophobic units connected side-by-side to the hydrophilic units, phase transitions become very broad, and the LCST decreases greatly. The secondary structures of the polymers were characterized with OR and CD spectroscopy, and it was found that the ordered structures aroused from the densely packing and chirality of the lysinol core unit. These polymers were employed to fabricate porous films with the BF technique, and only the most hydrophobic **PG2(2)** could self-assemble into an ordered pattern under proper conditions. Though less robust conditions are needed, the present results provide the first successful example to form ordered porous films by using amphiphilic homopolymers.

6. Conclusions and Outlook

From all the above discussions, several conclusions can be finally drawn as summarized in the following together with some outlook (all the chemical structures of the dendritic macromolecules are listed in pages 101 and 102):

- 1) A series of OEG-based first and second generation water-soluble [**PG1(HT)** and **PG2(HT)**] and thermoresponsive dendronized polymers [**PG1(MT)**, **PG2(MT)**, **PG1(MD)**, **PG2(MD)**, **PG1(ET)** and **PG2(ET)**] with three-fold branching units and various peripheral groups were designed and synthesized. Different from other dendronized polymers, the novel structure design allows their synthesis to be performed in organic and aqueous solutions as well as in bulk. High molar mass G1 and G2 polymers were obtained *via* free radical polymerization of their corresponding macromonomers either in bulk or in aqueous solutions.
- 2) **PG1(HT)** and **PG2(HT)** are fully water-soluble. Their peripheral hydroxyl functional groups provide an opportunity for further modifications for different application purposes.
- 3) Dendronized polymers with methoxy or ethoxy terminal groups are thermoresponsive and show tunable LCSTs in a temperature range from 33°C to 64°C. All exhibit unique thermoresponsive behavior above the LCSTs, including extremely fast phase transitions and negligible hystereses between heating and cooling processes. Their thermoresponsive behavior is less sensitive to molar mass, polymer concentration and also dendron generations. But their LCSTs decrease linearly with linear increase of added salt concentration. Both PG1 and PG2 polymers in water could form large aggregates with micrometer sizes above their LCSTs, but the morphologies of the aggregates from PG1 are irregular, while uniform spherical objects were observed from PG2. *In vitro* cytotoxicity study proved these polymers to be non-toxic to cells.

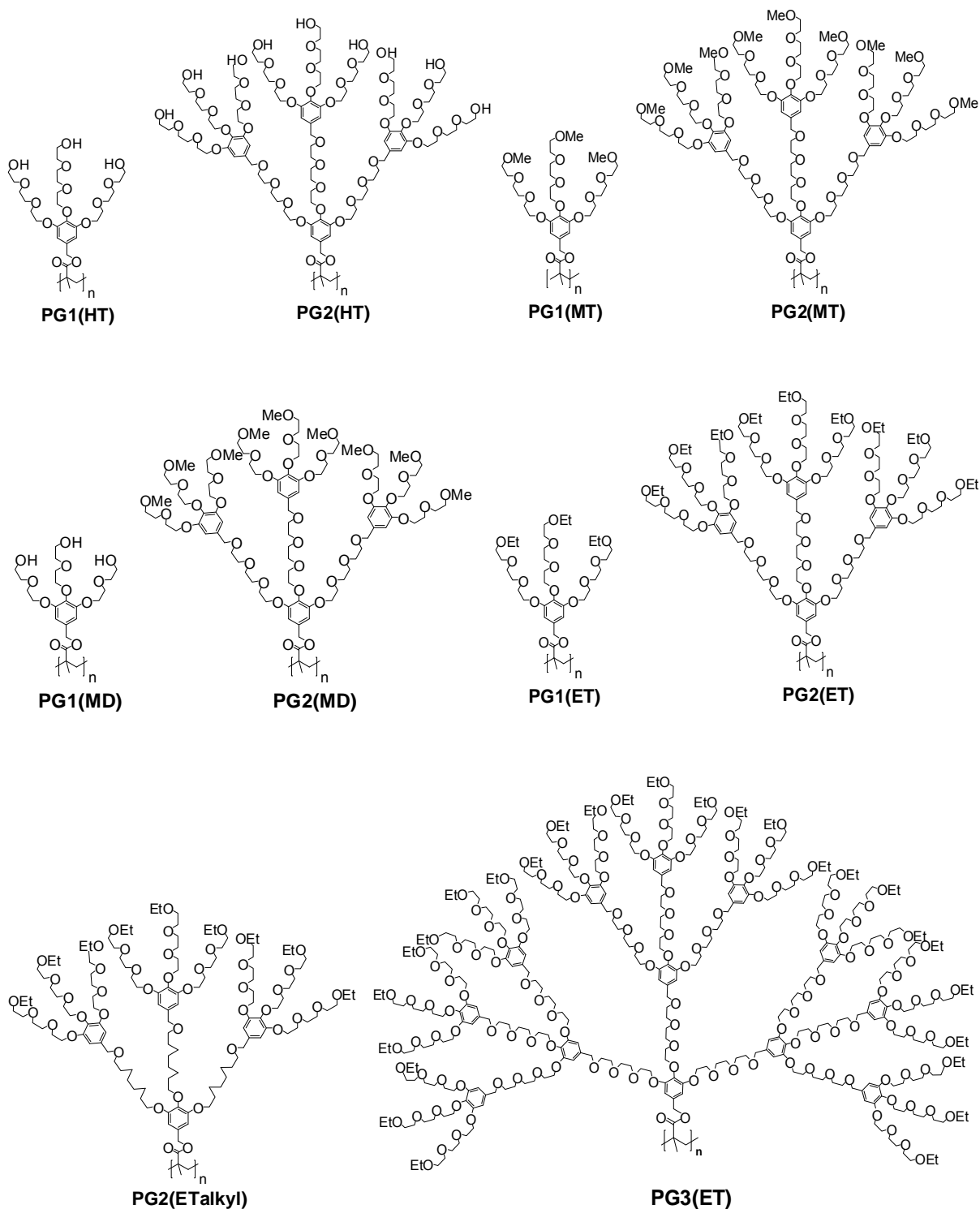
- 4) Thermoresponsive dendrimers **Me-G1**, **Me-G2**, **Et-G1** and **Et-G2**, constructed with the same dendrons as for the dendronized polymers, were prepared. They also exhibit unique thermoresponsive behavior with fast transitions and small hystereses, but different from the polymer counterparts, their LCSTs are obviously concentration and dendron generation dependent.
- 5) An improved synthetic strategy was developed to ease the synthesis of OEG-based G2 dendrons, which afforded the synthesis of G2 dendron on 20 gram scales with excellent yields and easy purification. With this improved procedure, ethoxy-terminated G3 dendronized polymer **PG3(ET)** was successfully prepared. It shows similar thermal behavior as the lower generation counterparts, which suggests that the thickness of the dendronized polymers was less influence on the thermoresponsiveness.
- 6) The doubly dendronized polymer **PG2(ETalkyl)** was synthesized. It shows a similar LCST as **PG1(ET)**, **PG2(ET)** and **PG3(ET)**, which proves that the interior parts of the dendronized polymers contribute less to the phase transitions than the exterior parts. Temperature dependent ^1H NMR spectroscopy, together with EPR spectroscopy, further proved that the aggregation of **PG2(ET)** and **PG3(ET)** originates mostly from the collapse of their peripheral groups, while the interior parts are less dehydrated around the LCSTs.
- 7) All OEG-based dendritic macromolecules can be used for the fabrication of smart and ionic conductive materials. With exception of the G1 dendrimers, all these macromolecules are non-toxic to cells, therefore, they are potentially useful for drug delivery.
- 8) OEG- and proline-based amphiphilic dendronized homopolymers **PG2(0)**, **PG2(1)** and **PG2(2)** were synthesized. They possess ordered secondary structures due to the chiral center in the lysinol unit and the dense packing of the dendrons around the backbone. Similar to **PG1(MT)**, **PG2(0)** and **PG2(1)** also show thermoresponsive properties, but their LCSTs are much lower and the phase transitions much broader. This suggests the arrangement of the

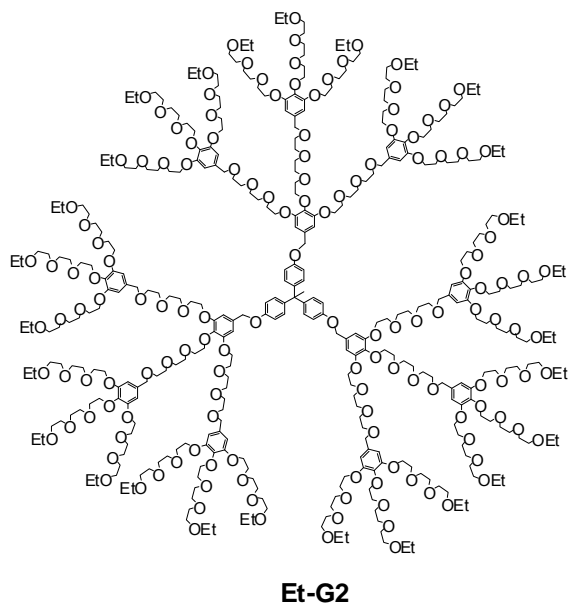
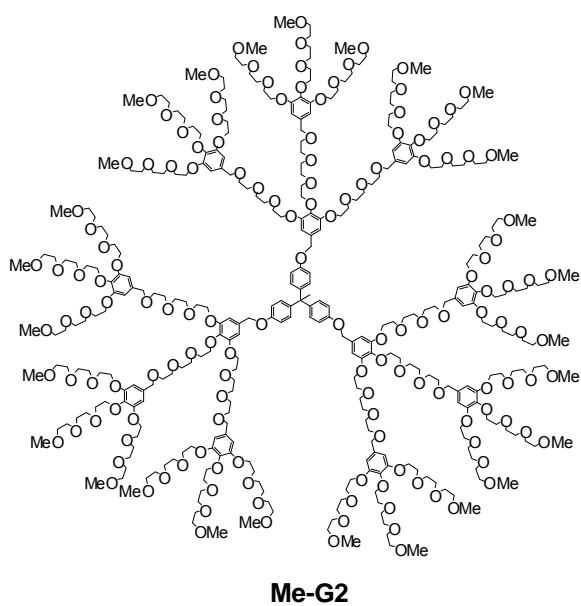
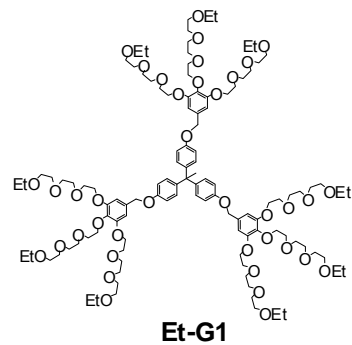
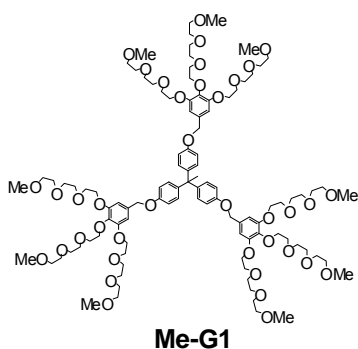
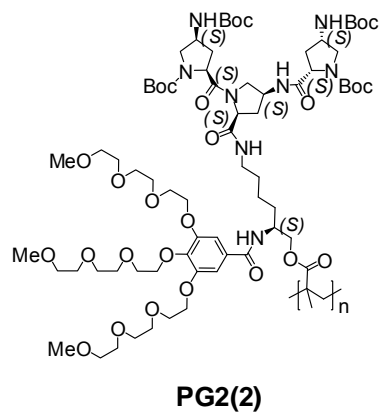
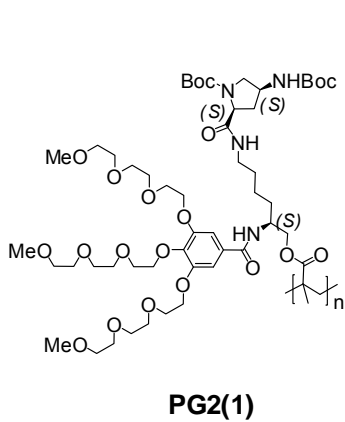
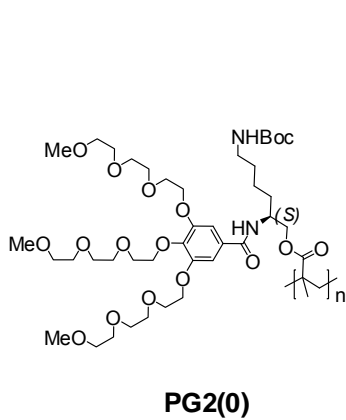
hydrophilic and hydrophobic dendrons affects dramatically the thermoresponsiveness of the polymers.

- 9) **PG2(2)** of a concentration of 10 mg/mL in chloroform can form ordered porous films on mica surfaces under 70% humidity by utilizing the BF technique, while **PG2(0)** and **PG2(1)** can not, which indicates that the hydrophobicity of the polymers and proper conditions are essential for the formation of an ordered pattern.
- 10) Due to the limited time available for this thesis work, some other interesting aspects of the amphiphilic dendronized homopolymers have not yet been investigated, such as their lengthwise segregation behavior in bulk, in solutions, or at air-water interfaces to build suprastructures. Further more, the direct visualization of the individual polymer chain's helical structures needs to be studied, and possible applications of the ordered porous films formed from **PG2(2)** for cell adhesions would be another interesting topic to investigate.

7. List of All the Dendritic Macromolecules Synthesized in This Thesis Work

All water-soluble and thermoresponsive dendronized polymers



All thermoresponsive dendrimersAll amphiphilic dendronized homopolymers

8. Experimental Part

8.1 Materials

Azobis(isobutyronitrile) (AIBN) was recrystallized twice from methanol. Tetrahydrofuran (THF) was refluxed over lithium aluminum hydride (LAH) and dichloromethane (DCM) was distilled from CaH_2 for drying. Linear PEG ($M_n = 5600$) was purchased from Aldrich. B16F1 cells (mouse melanoma) and HaCat cells (human keratinocyte) were obtained from the American Type Culture Collection (Manassas, VA). Cells were cultured in Dulbecco's modified Eagle's medium supplemented with 10% FBS and antibiotics (Life Science, Grand Island, NY), and maintained in sub-confluency. Cell Counting Kit-8 (CCK-8) was purchased from Probiol GmbH (Munich, Germany). Other reagents and solvents were purchased at reagent grade and used without further purification. All reactions were run under a nitrogen atmosphere. Macherey-Nagel pre-coated TLC plates (silica gel 60 G/UV₂₅₄, 0.25 mm) were used for thin-layer chromatography (TLC) analysis. Silica gel 60 M (Macherey-Nagel, 0.04-0.063 mm, 230-400 mesh) was used as the stationary phase for column chromatography.

8.2 Instrumentation and Measurements

NMR spectroscopy

^1H and ^{13}C NMR spectra were recorded on Bruker AV 500 (^1H : 500 MHz, ^{13}C : 125 MHz) or Bruker 700 (^1H : 700 MHz, ^{13}C : 175 MHz) spectrometers, and chemical shifts are reported as δ values (ppm) relative to internal Me_4Si .

Mass spectrometry

High-resolution MALDI-TOF-MS and ESI-MS analyses were performed by the MS service of the Laboratorium für Organische Chemie, ETH Zürich, on IonSpec Ultra instruments.

Elemental analysis

Elemental analyses were performed by the Mikrolabor of the Laboratorium für Organische Chemie, ETH Zürich. The samples were dried rigorously under vacuum prior to analysis.

Gel permeation chromatography (GPC) measurements

GPC measurements were carried out on a PL-GPC 220 instrument with 2×PL-Gel Mix-B LS column set (2×30 cm) equipped with refractive index (RI), viscosity, and light scattering (LS; 15 ° and 90 ° angles) detectors, and DMF (containing 1 g·L⁻¹ LiBr) as eluent at 45 °C. Universal calibration was performed with poly(methyl methacrylate) standards in the range of $M_p = 2680$ to 3900000 (Polymer Laboratories Ltd, UK).

Differential scanning calorimetry (DSC) measurements

DSC were performed on a DSC Q1000 differential scanning calorimeter from TA Instruments in a temperature range of -80 ~ +200 °C with a heating rate of 10 °C·min⁻¹. Samples of a total weight ranging between 3 - 10 mg were closed into aluminum pans of 40 µL, covered by a holed cap, and analyzed under a nitrogen atmosphere. The glass transition temperature (T_g) was determined in the second heating run.

UV/vis turbidity measurements

Turbidity measurements were carried out for the LCST determination on a Varian Cary 100 Bio UV/vis spectrophotometer equipped with a thermostatically regulated bath. Solutions of the polymers or dendrimers in de-ionized water or in pH 7 sodium phosphate buffer solution were filtered with a 0.45 µm filter before adding into a cuvette (path length 1 cm), which was placed in the spectrophotometer and heated or cooled at a rate of 0.2 °C·min⁻¹. The absorptions of the solution at $\lambda = 500$ nm were recorded every minute.

Surface tension measurements

Surface tension of the polymers at the air-water interface was measured *via* the pendent drop method using PAT1 (Sinterface Technologies, Berlin, Germany). For each experiment, one drop of the polymer aqueous solution (0.25 wt %) with a constant volume of 35 mm³ was set at 22 °C. The surface tension as a function of

time was then determined according to Laplace-Gauss equation. The surface tension value was selected after the equilibrium.

Dynamic light scattering (DLS) measurements

DLS measurements were performed with a Zetasizer Nano (Malvern, UK) instrument using a light scattering apparatus equipped with a He-Ne (633 nm) laser. The measurements were made at the scattering angle of $\theta = 173^\circ$ (backscattering detection). Solutions of the dendrimers and dendronized polymers for DLS measurements were filtrated with a 0.45 μm filter prior to use. The hydrodynamic diameters (D_h) were calculated according to the volume size distribution.

Continuous wave electronic paramagnetic resonance (CWEPR)

CWEPR spectra were recorded on a Miniscope MS200 (Magnettech, Berlin, Germany) benchtop spectrometer working at X-band ($\nu_{\text{mw}} \sim 9.4$ GHz) with a modulation amplitude of 0.04 mT, a sweep width of 8 mT, a sweep time of 30 s, and a microwave power of 12.5 mW. The temperature was adjusted with the temperature control unit TC H02 (Magnettech), providing an electronic adjustment in steps of 0.1 $^\circ\text{C}$ in the range of -170 $^\circ\text{C}$ to 250 $^\circ\text{C}$. The polymer solutions were ramp heated to a maximum temperature of 65 $^\circ\text{C}$, then decreased stepwise for the actual measurements.

Optical rotation measurement (OR)

Optical rotation values were measured on a Perkin-Elmer 241 polarimeter with a 1-dm cuvette.

Circular dichroism (CD)

Circular dichroism measurements were performed on a JASCO J-715 spectropolarimeter with a thermo-controlled 1-mm quartz cell (5 accumulation, continues scanning mode, scanning speed 20 $\text{nm}\cdot\text{min}^{-1}$, data pitch: 1 nm, response: 1 sec, band width: 5.0 nm).

Atom force microscope (AFM) measurements

The AFM measurements were carried out on a Nanoscope[®] IIIa Multi Mode Scanning probe microscope (from Digital Instruments, San Diego, CA) operated in the tapping

mode with an “E” scanner (maximal scan range 10 μm x 10 μm) and operated in the tapping mode at room temperature in air. Olympus silicon OMCL-AC160TS cantilevers (from Atomic Force F&E GmbH, Mannheim, Germany) were used with a resonance frequency between 200 and 400 kHz and a spring constant around 42 N/m. The samples were prepared by spin-coating (2000 rpm) the polymer (3–4 mg/L chloroform) or dendrimer (0.25 wt% water) solutions onto freshly cleaved mica or HOPG (from PLANO W. Plannet GmbH, Wetzlar, Germany). For the contour length analysis AFM images were taken with a scan size of 600 nm x 600 nm (corresponding to 512 x 512 pixels). The contour length of individual polymer chains was determined by manually drawing lines with a step length of about 5 nm along the polymer chains using the software Image J (version 1.34s). The error for determination of the chain length is $\pm 2.6\%$ or less when repeated measurements were done on the same polymer chain.

Optical microscopy (OM)

Optical microscopy images were recorded on a Leica DMRX instrument (objective lens $\times 50$) equipped with a halogen-lamp and a color CCD camera (Leica DFC480) connected to an imaging and processing system. A hot-stage from Mettler (model FP82TM) was used. About 50 μL of the polymer or dendrimer aqueous solutions (0.25 wt%) were sealed inside a concavity slide, and the aggregation process was recorded every second with heating and cooling rates of $0.5\text{ }^{\circ}\text{C}\cdot\text{min}^{-1}$. Recording program for the movie of the thermoresponsive aggregation (heating and cooling) processes of **PG1(MT)** (Table 2, entry 2) in chapter 4.1 is: started from $62\text{ }^{\circ}\text{C}$ with heating rate $0.5\text{ }^{\circ}\text{C}\cdot\text{min}^{-1}$ to $64\text{ }^{\circ}\text{C}$, kept at $64\text{ }^{\circ}\text{C}$ for 1 minute, and then cooled at a rate of $0.5\text{ }^{\circ}\text{C}\cdot\text{min}^{-1}$ to $62\text{ }^{\circ}\text{C}$. The total recording time is 9 minutes, and then compressed with Adobe Premiere into 35 seconds. Recording program for the movie of the thermoresponsive aggregation (heating and cooling) processes of **PG2(MT)** (Table 1, entry 5) is: started from $63\text{ }^{\circ}\text{C}$ with heating rate $0.5\text{ }^{\circ}\text{C}\cdot\text{min}^{-1}$ to $65\text{ }^{\circ}\text{C}$, kept at $65\text{ }^{\circ}\text{C}$ for 1 minute, and then cooled at a rate of $0.5\text{ }^{\circ}\text{C}\cdot\text{min}^{-1}$ to $63\text{ }^{\circ}\text{C}$. The total recording time is 9 minutes, and then compressed with Adobe Premiere into 34 seconds. Recording program for the movie of the thermoresponsive aggregation (heating and cooling) processes of **Et-G2** in chapter 4.3 is: heating from 35 to $37\text{ }^{\circ}\text{C}$, $0.5\text{ }^{\circ}\text{C}\cdot\text{min}^{-1}$, and then cooling from 37 to $35\text{ }^{\circ}\text{C}$, $0.5\text{ }^{\circ}\text{C}\cdot\text{min}^{-1}$. The total recording time

was 8 minutes. The movie was compressed into 36 seconds with Windows Movie Maker.

Scanning electron microscopy (SEM)

SEM images were obtained on a Zeiss Leo 1530 field-emission SEM operated at 3 kV with secondary electron detection.

8.3 Synthesis

General procedure for tosylation with NaOH as the base and in THF/H₂O mixed solvent (A). TsCl in THF was added dropwise to the mixture of NaOH aqueous solution, alcohol in THF at 0 °C. The solution was stirred for another 3 h. After evaporation of the solvent, the residue was dissolved in DCM and washed with brine. After drying over MgSO₄, purification by column chromatography afforded the product.

General procedure for Williamson etherification with K₂CO₃ (B). A mixture of methyl gallate, tosylated OEG, KI, and potassium carbonate (K₂CO₃) in dry DMF was stirred at 80 °C over 24 h. After removal of DMF in vacuo, the residue was dissolved in DCM and washed sequentially with saturated NaHCO₃ and brine. After drying over MgSO₄, purification by column chromatography afforded the product.

General procedure for reduction of ester to alcohol with LAH (C). Lithium aluminum hydride (LAH) was added to a solution of dendron esters in dry THF at -5 °C. The mixture was stirred for 30 min, then warmed to r.t. and stirred for another several hours. The reaction was quenched by successive dropwise addition of water, 10% NaOH, and water. The resulting precipitate was filtered and THF evaporated. The residue was dissolved in DCM and washed with brine. After drying over MgSO₄, purification by column chromatography afforded the product as colorless oil.

General procedure for synthesis of macromonomer (D). Methacryloyl chloride (MAC) was added dropwise to a mixture of dendron alcohol, TEA and DMAP in dry DCM at 0 °C over 5 min. The mixture was stirred for several hours at r.t. and then

quenched with MeOH. After washing successively with aqueous NaHCO_3 solution and brine, the organic phase was dried over MgSO_4 . Purification by column chromatography afforded the product.

General procedure for etherification with NaH (E). Tosylated compound in dry THF was added dropwise to a mixture of dendron alcohol, KI, 15-crown-5, and NaH in dry THF. The mixture was stirred for 12 h at r.t. before dropwise addition of MeOH to quench the excess NaH. After evaporation of solvent, the residue was dissolved in DCM and successively washed with NaHCO_3 and brine. After drying over MgSO_4 , purification by column chromatography afforded the product.

General procedure for reduction of dendron acid to alcohol with kokotos' method (F). *N*-Methylmorpholine and ethyl chloroformate were added sequentially to a solution of G2 acid in dry THF at $-15\text{ }^\circ\text{C}$, and the mixture was stirred for 1 h. Then NaBH_4 was added at $-5\text{ }^\circ\text{C}$ and the reaction mixture stirred for another several hours. Water was added to quench the reaction and THF then evaporated. The residue was dissolved in DCM, and washed successively with saturated NaHCO_3 and brine. After drying over MgSO_4 , purification by column chromatography afforded the product.

General procedure for THP deprotection with PTSA (G). *p*-Toluenesulfonic acid (PTSA) was added to a solution of THP protected compound in MeOH and the mixture stirred for 2 h at r.t. After evaporation of MeOH, the residue was dissolved in DCM and successively washed with saturated NaHCO_3 solution and brine. After drying over MgSO_4 , purification by column chromatography afforded the product.

General procedure for polymerization in DMF solution (H). The required amounts of the monomer and AIBN (0.5 wt % to the monomer) were dissolved in DMF inside a Schlenk tube. The solution was thoroughly deoxygenated by several freeze-pump-thaw cycles and then stirred under certain temperature for the desired time. After cooling to r.t., the polymer was dissolved in DCM and purified by column chromatography with DCM as eluent. The hydroxyl group covered polymers were dissolved in water, and the aqueous phase was washed with DCM before to lyophilization.

General procedure for polymerization in bulk (I). The required amounts of the monomer and AIBN (0.5 wt % to the monomer) were added to a Schlenk tube. The mixture was thoroughly deoxygenated by several freeze-pump-thaw cycles and then stirred under certain temperature for the desired time. The purification of the polymer followed the same process as in procedure **H**.

General procedure for polymerization in aqueous solution (J). The required amounts of the monomer and 4,4'-azobis(4-cyanovaleric acid) (ACVA) (0.7 wt % to the monomer) were dissolved in water inside a Schlenk tube. The solution was thoroughly deoxygenated by several freeze-pump-thaw cycles and then stirred at certain temperature for desired time. The purification of the polymer followed the same process as in procedure **H**.

General procedure for deprotection of THP from dendronized polymers (K). The corresponding THP-protected polymer was dissolved in a mixture of THF, water and AcOH (2:1:4), and the solution was stirred for 3 days at r.t. After removal of the solvent *in vacuo*, the deprotected polymer was dissolved in water and lyophilized.

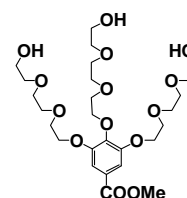
8.3.1 Compounds of Chapter 3.1

2-(2-(2-hydroxyethoxy)ethoxy)ethyl 4-methylbenzenesulfonate (**1b**).

According to general procedure **A** from TsCl (42.30 g, 0.22 mol) in THF (150 mL), triethylene glycol (100.00 g, 0.67 mol), NaOH solution (13.30 g NaOH in 50 mL water) and THF (100 mL), purification by column chromatography with DCM / MeOH (30:1, v/v) afforded **1b** as colorless oil (40.20 g, 60%).

Methyl 3,4,5-tris(2-(2-(2-hydroxyethoxy)ethoxy)ethoxy)benzoate (**2a**).

According to general procedure **B** from methyl gallate (18.15 g, 98.57 mmol), **1b** (120.00 g, 394.27 mmol), KI (12.62 g, 78.85 mmol), K₂CO₃ (136.23 g, 985.70 mmol) and dried DMF (150 mL), purification by column chromatography with DCM / MeOH (15:1, v/v)

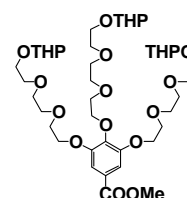


afforded **2a** as yellow oil (95.0 g, 83%). ¹H NMR (CDCl₃): δ = 3.07 (s, 1H, OH), 3.59 (m, 6H, CH₂), 3.66 (m, 6H, CH₂), 3.71 (m, 12H, CH₂), 3.82 (t, 2H, CH₂), 3.87 (m, 7H, CH₂ + CH₃), 4.20 (t, 4H, CH₂), 4.26 (t, 2H, CH₂), 7.28 (s, 2H, CH). ¹³C NMR (CDCl₃):

δ = 52.39, 61.68, 61.83, 68.87, 69.68, 70.45, 70.53, 70.68, 70.73, 70.94, 72.64, 72.81, 72.88, 109.02, 125.23, 142.46, 152.34, 166.72. HR-MS (MALDI): m/z calcd. for $C_{26}H_{44}O_{14}$ $[M + Na]^+$ 603.27; found 603.2633.

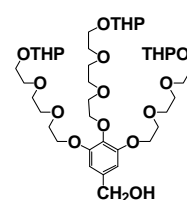
Methyl 3,4,5-tris(2-(2-(2-(tetrahydro-2H-pyran-2-yloxy)ethoxy)ethoxy)ethoxy) benzoate (2b).

3,4-Dihydro-2H-pyran (DHP) (26.08 g, 310.01 mmol) and pyridinium toluenesulfonate (PPTS) (7.79 g, 31.00 mmol) were added to a solution of **2a** (30.00 g, 51.67 mmol) in dry DCM at $-5\text{ }^{\circ}\text{C}$, and the mixture was stirred for another 6 h at r.t. After successive washing with aqueous NaHCO_3 solution and brine, the organic phase was dried over MgSO_4 . Purification by column chromatography with hexane / ethyl acetate (1:5, v/v) afforded **2b** as slightly yellow oil (38.50 g, 90%). ^1H NMR (CDCl_3): δ = 1.49 (m, 6H, CH_2), 1.55 (m, 6H, CH_2), 1.68 (m, 3H, CH_2), 1.79 (m, 3H, CH_2), 3.47 (m, 3H, CH_2), 3.58 (m, 3H, CH_2), 3.66 (m, 12H, CH_2), 3.68 (m, 6H, CH_2), 3.78 (t, 2H, CH_2), 3.85 (m, 13H, CH_2), 4.18 (m, 6H, CH_2), 4.60 (s, 3H, CH), 7.27 (s, 2H, CH). ^{13}C NMR (CDCl_3): δ = 19.64, 25.57, 30.71, 52.31, 62.37, 66.79, 69.00, 69.77, 70.69, 70.73, 70.83, 71.01, 72.58, 99.09, 109.15, 125.08, 142.71, 152.45, 166.73. HR-MS (MALDI): m/z calcd. for $C_{41}H_{68}O_{17}$ $[M + Na]^+$ 855.45; found 855.4363.



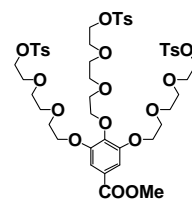
3,4,5-Tris(2-(2-(2-(tetrahydro-2H-pyran-2-yloxy)ethoxy)ethoxy)ethoxy) benzyl alcohol (2c).

According to general procedure C from LAH (2.60 g, 68.43 mmol), **2b** (38.0 g, 45.62 mmol) in dry THF (300 mL). The mixture was stirred for another 3 h at r.t. The reaction was quenched by dropwise addition of water (15 mL), 10% NaOH (45 mL), and water (40 mL). Purification by column chromatography with DCM / MeOH (20:1, v/v) afforded **2c** (33.60 g, 92%) as colorless oil. ^1H NMR (CDCl_3): δ = 1.55 (m, 6H, CH_2), 1.58 (m, 6H, CH_2), 1.68 (m, 3H, CH_2), 1.80 (m, 3H, CH_2), 3.47 (m, 3H, CH_2), 3.58 (m, 3H, CH_2), 3.65 (m, 12H, CH_2), 3.68 (m, 6H, CH_2), 3.76 (t, 2H, CH_2), 3.82 (m, 10H, CH_2), 4.11 (t, 2H, CH_2), 4.14 (t, 4H, CH_2), 4.54 (s, 2H, CH_2), 4.60 (t, 3H, CH), 6.60 (s, 2H, CH). ^{13}C NMR (CDCl_3): δ = 19.60, 25.56, 30.69, 62.36, 65.30, 66.80, 69.03, 69.97, 70.68, 70.81, 70.85, 70.97, 72.42, 99.09, 106.74, 136.92, 137.91, 152.83. HR-MS (MALDI): m/z calcd. for $C_{40}H_{68}O_{16}$ $[M + Na]^+$ 827.45; found 827.4414.

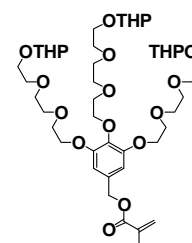


Methyl 3,4,5-tris(2-(2-(2-(tosyloxy)ethoxy)ethoxy)ethoxy)benzoate (2d).

p-Tosyl chloride (TsCl) (15.76 g, 82.67 mmol) was added to a mixture of **2a** (8.00 g, 13.78 mmol), freshly prepared Ag₂O (14.37 g, 62.01 mmol), KI (13.23 g, 82.67 mmol) in dry DCM (200 mL) at 0 °C. The mixture was stirred for 30 min, and then warmed to r.t., and stirring was continued for another 12 h at r.t. After washing with brine, the organic phase was dried over MgSO₄. Purification by column chromatography with DCM / MeOH (30:1, v/v) afforded **2d** (11.50 g, 80%) as colorless oil. ¹H NMR (CDCl₃): δ = 2.36 (s, 9H, CH₃), 3.52 (m, 8H, CH₂), 3.61 (m, 12H, CH₂), 3.70 (t, 2H, CH₂), 3.77 (m, 4H, CH₂), 3.82 (s, 3H, CH₃), 4.08 (m, 10H, CH₂), 4.13 (t, 2H, CH₂), 7.23 (s, 2H, CH), 7.26 (d, 6H, CH), 7.72 (d, 6H, CH), ¹³C NMR (CDCl₃): δ = 21.73, 52.32, 61.80, 68.77, 68.80, 68.96, 69.40, 69.48, 69.51, 69.75, 70.38, 70.53, 70.74, 70.83, 70.86, 72.51, 109.03, 125.09, 128.04, 130.00, 133.02, 142.60, 145.00, 145.05, 152.41, 166.65. HR-MS (MALDI): m/z calcd. for C₄₇H₆₂O₂₀S₃ [M + Na]⁺ 1065.30; found 1065.291.

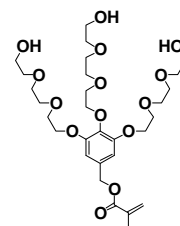
**3,4,5-Tris(2-(2-(2-(tetrahydro-2H-pyran-2-yloxy)ethoxy)ethoxy)ethoxy)benzyl methacrylate (3a).**

According to general procedure **D** from MAC (1.17 g, 11.18 mmol), **2c** (6.00 g, 7.45 mmol), TEA (3.01 g, 29.80 mmol), DMAP (0.15 g) and dry DCM (80 mL), the mixture was stirred for another 4 h at r.t., purification by column chromatography with DCM / MeOH (20:1, v/v) afforded **3a** (6.0 g, 92%) as colorless oil. ¹H NMR (CDCl₃): δ = 1.50 (m, 6H, CH₂), 1.56 (m, 6H, CH₂), 1.69 (m, 3H, CH₂), 1.80 (m, 3H, CH₂), 1.95 (s, 3H, CH₃), 3.48 (m, 3H, CH₂), 3.60 (m, 3H, CH₂), 3.66 (m, 12H, CH₂), 3.70 (m, 6H, CH₂), 3.77 (t, 2H, CH₂), 3.84 (m, 10H, CH₂), 4.13 (m, 6H, CH₂), 4.61 (t, 3H, CH), 5.05 (s, 2H, CH₂), 5.57 (m, 1H, CH₂), 6.13 (m, 1H, CH₂), 6.59 (s, 2H, CH). ¹³C NMR (CDCl₃): δ = 18.32, 19.45, 25.39, 30.53, 62.17, 66.36, 66.60, 68.89, 69.69, 70.50, 70.54, 70.63, 70.81, 72.29, 98.90, 107.88, 125.81, 136.15, 138.14, 152.64, 167.11. HR-MS (MALDI): m/z calcd. for C₄₄H₇₂O₁₇ [M + Na]⁺ 895.48; found 895.4678.

**3,4,5-Tris(2-(2-(2-hydroxyethoxy)ethoxy)ethoxy) benzyl methacrylate (3b).**

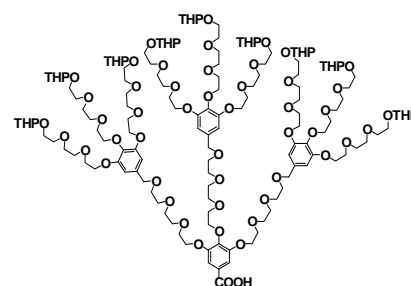
According to general procedure **G** from PTSA (1.31 g, 6.87 mmol), **3a** (4.00 g, 4.58 mmol) and MeOH (50 mL), purification by column chromatography with DCM / MeOH (10:1, v/v) afforded **3b** (2.30 g, 82%) as colorless oil. ¹H NMR (CDCl₃): δ = 1.93 (m,

3H, CH₃), 3.56 (m, 6H, CH₂), 3.64 (m, 6H, CH₂), 3.69 (m, 12H, CH₂), 3.78 (t, 2H, CH₂), 3.83 (t, 4H, CH₂), 4.16 (m, 6H, CH₂), 5.04 (s, 2H, CH₂), 5.56 (m, 1H, CH₂), 6.11 (m, 1H, CH₂), 6.58 (s, 2H, CH). ¹³C NMR (CDCl₃): δ = 18.51, 61.60, 61.78, 66.53, 68.87, 69.74, 70.42, 70.47, 70.50, 70.61, 70.62, 70.92, 72.47, 72.78, 72.83, 107.81, 126.08, 131.81, 136.30, 138.19, 152.69, 167.32. HR-MS (MALDI): m/z calcd. for C₂₉H₄₈O₁₄ [M + Na]⁺ 643.30; found 643.2947.



3,4,5-Tris(2-(2-(2-(3,4,5-tris(2-(2-(2-(tetrahydro-2H-pyran-2-yloxy)ethoxy)ethoxy)benzyloxy)ethoxy)ethoxy)ethoxy)benzoic acid (4a).

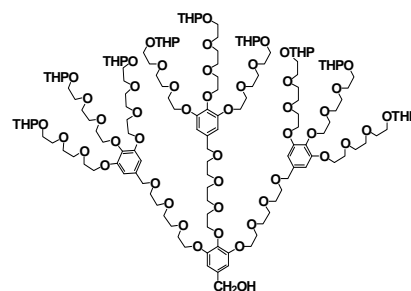
According to general procedure **E** from **2d** (2.94 g, 2.82 mmol) in dry THF (50 mL), a mixture of **2c** (7.50 g, 9.32 mmol), KI (0.27 g, 1.69 mmol), 15-crown-5 (2.06 g, 9.35 mmol), NaH (0.67 g, 27.90 mmol) in dry THF (200 mL), purification by column chromatography with DCM / MeOH (15:1, v/v) afforded **4a** (4.70 g, 57%) as slightly



yellow oil. ¹H NMR (CD₂Cl₂): δ = 1.53 (m, 36H, CH₂), 1.68 (m, 9H, CH₂), 1.80 (m, 9H, CH₂), 3.47 (m, 9H, CH₂), 3.55 – 3.71 (m, 87H, CH₂), 3.76 (t, 8H, CH₂), 3.84 (m, 34H, CH₂), 4.09 – 4.18 (m, 24H, CH₂), 4.42 (s, 6H, CH₂), 4.60 (t, 9H, CH), 6.59 (s, 6H, CH), 7.31 (s, 2H, CH). ¹³C NMR (CD₂Cl₂): δ = 19.70, 25.63, 30.76, 62.24, 66.75, 68.78, 68.86, 69.63, 69.68, 69.73, 69.87, 70.47, 70.57, 70.65, 70.71, 70.79, 70.86, 72.41, 72.42, 72.52, 73.20, 99.05, 106.79, 106.82, 109.01, 125.41, 134.19, 137.60, 142.42, 152.38, 152.70, 167.32. HR-MS (MALDI): m/z calcd. for C₁₄₅H₂₄₀O₅₉ [M + Na]⁺ 2948.58; found 2948.557.

3,4,5-Tris(2-(2-(2-(3,4,5-tris(2-(2-(2-(tetrahydro-2H-pyran-2-yloxy)ethoxy)ethoxy)benzyloxy)ethoxy)ethoxy)ethoxy)benzyl alcohol (4b).

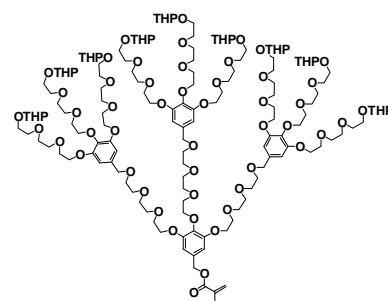
According to general procedure **F** from *N*-methylmorpholine (0.58 g, 5.72 mmol), ethyl chloroformate (0.62 g, 5.72 mmol), **4a** (4.20 g, 1.43 mmol) and NaBH₄ (0.43 g, 11.44 mmol), the mixture was stirred for another 2 h after the addition of NaBH₄, purification by column chromatography with DCM / MeOH (20:1, v/v) afforded **4b** (3.46 g, 83%) as colorless oil. ¹H NMR (CDCl₃):



δ = 1.53 (m, 36H, CH₂), 1.68 (m, 9H, CH₂), 1.80 (m, 9H, CH₂), 3.47 (m, 9H, CH₂), 3.52 – 3.69 (m, 87H, CH₂), 3.76 (t, 8H, CH₂), 3.83 (m, 34H, CH₂), 4.09–4.20 (m, 24H, CH₂), 4.43 (s, 6H, CH₂), 4.53 (s, 2H, CH₂), 4.59 (t, 9H, CH), 6.59 (s, 6H, CH), 6.61 (s, 2H, CH). ¹³C NMR (CD₂Cl₂): δ = 19.58, 25.50, 30.64, 59.12, 61.94, 62.11, 64.74, 66.27, 66.61, 68.36, 68.70, 68.91, 69.52, 69.72, 69.76, 70.45, 70.53, 70.57, 70.74, 72.30, 73.04, 98.93, 105.93, 106.72, 131.00, 134.05, 137.27, 152.58. HR-MS (MALDI): m/z calcd. for C₁₄₅H₂₄₂O₅₈ [M + Na]⁺ 2934.60; found 2934.5879.

3,4,5-Tris(2-(2-(2-(3,4,5-tris(2-(2-(2-(tetrahydro-2H-pyran-2-yloxy)ethoxy) ethoxy) ethoxy)benzyl)ethoxy)ethoxy)ethoxy)benzyl methacrylate (5a).

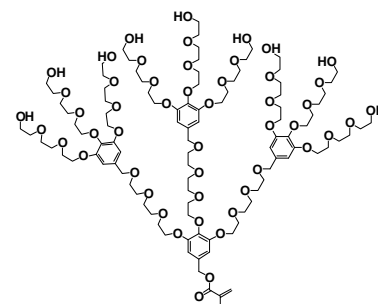
According to general procedure **D** from MAC (0.70 g, 6.69 mmol), **4b** (3.90 g, 1.34 mmol), TEA (0.68 g, 6.69 mmol), DMAP (0.15 g), the mixture was stirred for 5 h, purification by column chromatography with ethyl acetate / MeOH (10:1, v/v) afforded **5a** (3.30 g, 83%) as colorless oil. ¹H NMR (CD₂Cl₂): δ = 1.53 (m, 36H, CH₂),



1.68 (m, 9H, CH₂), 1.80 (m, 9H, CH₂), 1.95 (s, 3H, CH₃), 3.47 (m, 9H, CH₂), 3.53–3.70 (m, 87H, CH₂), 3.76 (t, 8H, CH₂), 3.83 (m, 34H, CH₂), 4.09–4.14 (m, 24H, CH₂), 4.43 (s, 6H, CH₂), 4.59 (t, 9H, CH), 5.07 (s, 2H, CH₂), 5.60 (s, 1H, CH₂), 6.12 (s, 1H, CH₂), 6.60 (s, 6H, CH), 6.64 (s, 2H, CH). ¹³C NMR (CD₂Cl₂): δ = 18.27, 19.73, 25.64, 30.78, 62.25, 66.45, 66.74, 68.81, 68.86, 69.65, 69.81, 69.86, 70.59, 70.67, 70.71, 70.88, 72.44, 73.20, 99.06, 106.79, 107.47, 125.57, 131.86, 134.16, 136.54, 137.62, 138.20, 152.72, 152.78, 167.07. HR-MS (MALDI): m/z calcd. for C₁₄₉H₂₄₆O₅₉ [M + Na]⁺ 3002.62; found 3002.606

3,4,5-Tris(2-(2-(2-(3,4,5-tris(2-(2-(2-hydroxyethoxy)ethoxy)ethoxy)benzyl-oxy) ethoxy)ethoxy)ethoxy)benzyl methacrylate (5b).

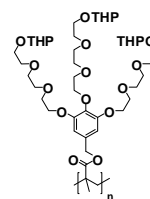
PPTS (65.2 mg, 0.26 mmol) was added to a solution of **5a** (0.43 g, 0.14 mmol) in MeOH (20 mL) and the mixture stirred for 10 h at 50 °C. Then MeOH was evaporated in vacuum at r.t. and the residue extracted with DCM. The DCM phase was washed with brine for three times. Removal of the solvent afforded **5b** (0.28 g, 88%) as colorless oil. ¹H NMR (CDCl₃): δ = 1.94 (s, 3H, CH₃), 3.57–3.70 (m, 96H, CH₂), 3.82



(m, 24H, CH₂), 4.14 (m, 24H, CH₂), 4.43 (s, 6H, CH₂), 5.05 (s, 2H, CH₂), 5.57 (s, 1H, CH₂), 6.12 (s, 1H, CH₂), 6.55 (s, 6H, CH), 6.59 (s, 2H, CH), ¹³C NMR (CDCl₃): δ = 18.50, 61.76, 61.80, 66.53, 68.84, 69.03, 69.54, 69.86, 70.53, 70.63, 70.68, 70.76, 70.81, 70.95, 72.49, 72.83, 72.94, 73.34, 107.12, 108.06, 126.05, 131.72, 134.09, 136.32, 137.68, 138.49, 152.66, 152.79, 167.31. HR-MS (MALDI): m/z calcd. for C₁₀₄H₁₇₄O₅₀ [M + Na]⁺ 2246.11; found 2247.093.

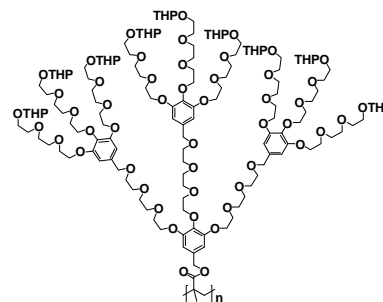
Poly(3,4,5-tris(2-(2-(2-(tetrahydro-2H-pyran-2-yloxy)ethoxy)ethoxy)ethoxy)enzyl methacrylate) (THP-PG1).

Route 1: According to general procedure H from **3a** (0.6 g), AIBN (3 mg) and DMF (0.4 mL), polymerization for 19 h yielded **THP-PG1** as colorless gel (0.40 g, 67%). ¹H NMR (CD₂Cl₂): δ = 0.88 (br, 2H, CH₃), 1.09 (br, 1H, CH₃), 1.50–1.54 (m, 12H, CH₂), 1.67–1.72 (m, 3H, CH₂), 1.77–1.79 (m, 3H, CH₂), 3.43–3.47 (m, 3H, CH₂), 3.50–3.63 (m, 21H, CH₂), 3.74–3.84 (m, 12H, CH₂), 4.06 (br, 6H, CH₂), 4.57–4.59 (m, 3H, CH), 4.80 (br, 2H, CH₂), 6.52 (br, 2H, CH). ¹³C NMR (CDCl₃): δ = 19.62, 22.91, 25.62, 30.72, 45.40, 53.59, 62.16, 62.22, 65.93, 66.74, 66.76, 68.94, 69.81, 70.62, 70.70, 70.76, 70.84, 72.42, 96.27, 98.94, 98.99, 100.91, 107.01, 138.04, 144.22, 152.77. **Route 2:** According to general procedure I from **3a** (0.6 g) and AIBN (3 mg), polymerization for 3 h yielded **THP-PG1** as colorless gel (0.42 g, 70%). The identical spectral data as in route 1 were obtained.



Poly(3,4,5-tris(2-(2-(2-(3,4,5-tris(2-(2-(2-(tetrahydro-2H-pyran-2-yloxy)ethoxy)ethoxy)ethoxy)benzyl)ethoxy)ethoxy)benzyl methacrylate) (THP-PG2).

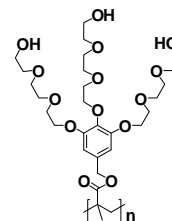
According to general procedure I from **5a** (0.19 g) and AIBN (1.0 mg), polymerization for 3 h yielded **THP-PG2** as colorless gel (0.12 g, 64%). ¹H NMR (CD₂Cl₂): δ = 1.49 (br, 36H, CH₂), 1.65 (br, 9H, CH₂), 1.77 (br, 9H, CH₂), 3.34–3.77 (m, 138H, CH₂), 4.06 (br, 24H, CH₂), 4.38 (br, 8H, CH₂), 4.56 (br, 9H, CH), 6.53 (br, 8H, CH).



¹³C NMR (CD₂Cl₂): δ = 19.66, 25.65, 29.82, 30.75, 62.05, 66.70, 68.89, 69.67, 69.84, 70.56, 70.61, 70.67, 70.84, 72.47, 73.14, 98.90, 106.56, 134.12, 137.62, 152.72. The signals of the polymer backbone were so broad that they disappeared in the baseline.

Poly(3,4,5-tris(2-(2-(2-hydroxyethoxy)ethoxy)ethoxy)benzylmethacrylate) [PG1(HT)].

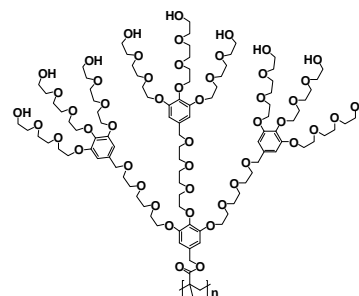
Route 1: According to general procedure **J** from **3b** (0.33 g), ACVA (2.3 mg) and water (0.25 mL), polymerization 3 h yielded **PG1(HT)** as colorless gel (0.26 g, 78%). ^1H NMR (D_2O): δ = 0.70–0.93 (m, 3H, CH_3), 1.96–1.99 (m, 2H, CH_2), 3.25–3.27 (m, 3H, OH), 3.48–3.74 (m, 30H, CH_2), 4.07 (br, 6H, CH_2), 4.80 (br, 2H, CH_2), 6.62 (br, 2H, CH).



The carbon signals were so broad that they disappeared in the baseline. Elemental analysis (%) calcd for $(\text{C}_{29}\text{H}_{48}\text{O}_{14})_n$ (620.69) $_n$: C, 56.12; H, 7.79. Found: C, 54.84; H, 7.80. **Route 2:** According to general procedure **K** from **THP-PG1** (0.40 g), AcOH (16 mL), THF (8 mL) and water (4 mL), was yielding **PG1(HT)** as colorless gel (0.25 g, 88%). The identical spectral data as in route 1 were obtained. Elemental analysis (%) calcd for $(\text{C}_{29}\text{H}_{48}\text{O}_{14})_n$ (620.69) $_n$: C, 56.12; H, 7.79. Found: C, 54.37; H, 7.78.

Poly(3,4,5-tris(2-(2-(2-(3,4,5-tris(2-(2-(2-hydroxyethoxy)ethoxy)ethoxy)benzyl methacrylate) [PG2(HT)].

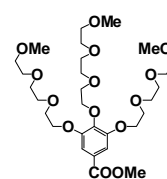
According to general procedure **K** from **THP-PG2** (0.34 g), AcOH (12 mL), THF (6 mL) and water (3 mL), was yielding **PG2(HT)** as colorless oil (0.20 g, 80%). ^1H NMR (D_2O): δ = 3.58–3.78 (m, 120H, CH_2), 4.06 (br, 24H, CH_2), 4.37 (br, 6H, CH_2), 6.62 (br, 8H, CH). The proton signals of backbone and carbon signals were so broad that they disappeared in the baseline. Elemental analysis (%) calcd for $(\text{C}_{104}\text{H}_{174}\text{O}_{50})_n$ (2224.49) $_n$: C, 56.15; H, 7.88. Found: C, 55.03; H, 7.93.



8.3.2 Compounds of Chapter 4.1

Methyl 3,4,5-tris(2-(2-(2-methoxyethoxy)ethoxy)ethoxy)benzoate (6a).

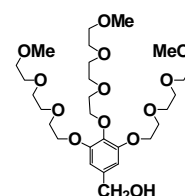
According to general procedure **B** from methyl gallate (12.04 g, 65.38 mmol), Me-TEG-Ts (83.23 g, 261.5 mmol), KI (8.37 g, 52.30 mmol) and potassium carbonate (K_2CO_3) (90.36 g, 653.8 mmol) in dry DMF, purification by column chromatography with DCM / MeOH (30:1, v/v) afforded **6a** as colorless oil (38.40 g, 94%). ^1H NMR (CDCl_3): δ = 3.36 (s, 9H, CH_3), 3.52–3.53 (m, 6H, CH_2), 3.60–3.65 (m, 12H, CH_2), 3.69–3.72 (m, 6H, CH_2), 3.78 (t,



2H, CH₂), 3.84–3.86 (m, 7H, CH₂ + CH₃), 4.18 (t, 4H, CH₂), 4.20 (t, 2H, CH₂), 7.27 (s, 2H, CH). ¹³C NMR (CDCl₃): δ = 52.32, 59.17, 68.96, 69.76, 70.67, 70.71, 70.83, 70.97, 72.07, 72.54, 76.95, 77.20, 77.46, 109.11, 125.09, 142.67, 152.43, 166.75. HR-MS (MALDI): m/z calcd. for C₂₉H₅₀O₁₄ [M + Na]⁺ 645.32; found 645.3094.

3,4,5-Tris(2-(2-(2-methoxyethoxy)ethoxy)ethoxy)benzyl alcohol (**6b**).

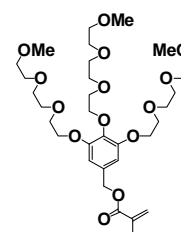
According to general procedure **C** from LAH (3.95 g, 104.1 mmol), **6a** (32.40 g, 52.03 mmol) in dry THF (300 mL), the mixture was stirred for 30 min, then warmed to r.t. and stirred for another 3 h, purification by column chromatography with DCM / MeOH (20:1, v/v) afforded **6b**



(28.70 g, 93%) as colorless oil. ¹H NMR (D₂O): δ = 3.33 (s, 6H, CH₃), 3.35 (s, 3H, CH₃), 3.53–3.59 (m, 6H, CH₂), 3.63–3.68 (m, 12H, CH₂), 3.71 (t, 2H, CH₂), 3.74 (t, 4H, CH₂), 3.82 (t, 2H, CH₂), 3.90 (t, 4H, CH₂), 4.17 (t, 2H, CH₂), 4.22 (t, 4H, CH₂), 4.55 (s, 2H, CH₂), 6.75 (s, 2H, CH). ¹³C NMR (D₂O): δ = 58.13, 63.79, 68.30, 69.33, 69.58, 69.60, 69.63, 69.75, 69.80, 69.92, 70.21, 71.12, 72.14, 106.45, 135.96, 137.29, 151.99. HR-MS (MALDI): m/z calcd. for C₂₈H₅₀O₁₃ [M + Na]⁺ 617.33; found 617.3150.

3,4,5-Tris(2-(2-(2-methoxyethoxy)ethoxy)ethoxy)benzyl methacrylate (**6c**).

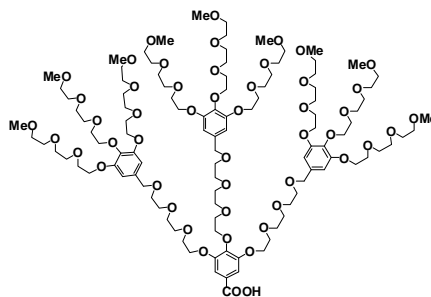
According to general procedure **D** from MAC (0.70 g, 6.72 mmol), **6b** (2.00 g, 3.36 mmol), TEA (1.70 g, 16.80 mmol), DMAP (0.10 g) and dry DCM, the mixture was stirred for 3 h at r.t., purification by column chromatography with DCM / MeOH (20:1, v/v) afforded **6c**



(2.00 g, 90%) as colorless oil. ¹H NMR (D₂O): δ = 1.88 (s, 3H, CH₃), 3.32 (s, 6H, CH₃), 3.34 (s, 3H, CH₃), 3.53–3.55 (m, 4H, CH₂), 3.56–3.58 (m, 2H, CH₂), 3.61–3.66 (m, 12H, CH₂), 3.67–3.69 (m, 2H, CH₂), 3.71–3.73 (m, 4H, CH₂), 3.81 (t, 2H, CH₂), 3.87 (t, 4H, CH₂), 4.16–4.18 (m, 6H, CH₂), 5.08 (s, 2H, CH₂), 5.69 (s, 1H, CH₂), 6.10 (s, 1H, CH₂), 6.75 (s, 2H, CH). ¹³C NMR (D₂O): δ = 17.53, 58.13, 66.78, 68.34, 69.27, 69.60, 69.66, 69.78, 69.98, 70.22, 71.13, 72.12, 107.35, 127.20, 132.41, 135.85, 136.69, 152.09, 169.18. HR-MS (MALDI): m/z calcd. for C₃₂H₅₄O₁₄ [M + Na]⁺ 685.35; found 685.3397.

3,4,5-Tris(2-(2-(2-(3,4,5-tris(2-(2-(2-methoxyethoxy)ethoxy)ethoxy)benzyl-oxy)ethoxy)ethoxy)ethoxy)benzoic acid (7a).

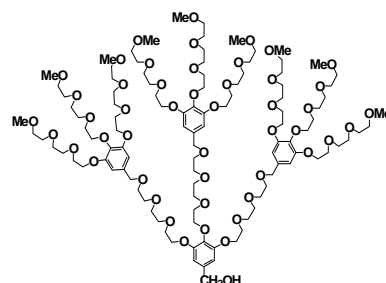
According to general procedure **E** from **2d** (5.30 g, 5.08 mmol) in dry THF (50 mL), **6b** (10.00 g, 16.76 mmol), KI (0.49 g, 3.05 mmol), 15-crown-5 (3.69 g, 16.76 mmol), and NaH (1.21 g, 50.29 mmol) in dry THF (100 mL), purification by column chromatography with DCM / MeOH (15:1, v/v)



afforded **7a** (5.20 g, 44%) as yellow oil. ^1H NMR (D_2O): δ = 3.31 (s, 18H, CH_3), 3.34 (s, 9H, CH_3), 3.54–3.69 (m, 96H, CH_2), 3.79–3.82 (m, 24H, CH_2), 4.10–4.12 (m, 24H, CH_2), 4.40 (s, 4H, CH_2), 4.43 (s, 2H, CH_2), 6.64 (s, 4H, CH), 6.68 (s, 2H, CH), 7.21 (s, 2H, CH). ^{13}C NMR (D_2O): δ = 58.16, 58.18, 68.25, 68.57, 69.07, 69.29, 69.61, 69.63, 69.68, 69.77, 69.81, 69.88, 69.97, 70.17, 70.31, 71.15, 72.17, 72.35, 72.65, 106.97, 107.01, 108.63, 125.61, 134.28, 134.36, 136.19, 141.36, 151.87, 151.97, 152.00, 169.11. HR-MS (MALDI): m/z calcd. for $\text{C}_{109}\text{H}_{186}\text{O}_{50}$ $[\text{M} + \text{Na}]^+$ 2319.20; found 2319.179.

3,4,5-Tris(2-(2-(2-(3,4,5-tris(2-(2-(2-methoxyethoxy)ethoxy)ethoxy)benzyl-oxy)ethoxy)ethoxy)ethoxy)benzyl alcohol (7b).

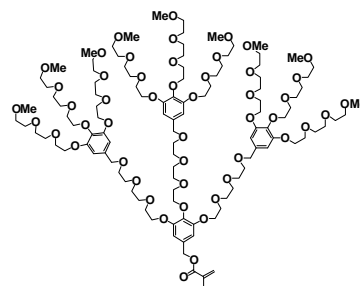
According to general procedure **F** from *N*-Methylmorpholine (0.65 g, 6.44 mmol), ethyl chloroformate (0.70 g, 6.44 mmol), **7a** (3.70 g, 1.61 mmol), dry THF (80 mL) and NaBH_4 (0.49 g, 12.88 mmol), the mixture was stirred for another 2 h after



addition of NaBH_4 , purification by column chromatography with DCM / MeOH (15:1, v/v) afforded **7b** (3 g, 82%) as colorless oil. ^1H NMR (CD_2Cl_2): δ = 3.33 (s, 27H, CH_3), 3.50–3.69 (m, 96H, CH_2), 3.76 (t, 8H, CH_2), 3.80–3.83 (m, 16H, CH_2), 4.10 (t, 8H, CH_2), 4.12–4.14 (m, 16H, CH_2), 4.44 (s, 6H, CH_2), 4.54 (s, 2H, CH_2), 6.60 (s, 6H, CH), 6.62 (s, 2H, CH). ^{13}C NMR (CD_2Cl_2): δ = 58.98, 65.20, 69.03, 69.89, 70.07, 70.14, 70.76, 70.77, 70.79, 70.90, 70.92, 70.97, 71.09, 72.27, 72.65, 73.41, 77.47, 106.24, 106.29, 107.04, 127.20, 134.44, 137.57, 137.81, 152.93, 152.99. HR-MS (MALDI): m/z calcd. for $\text{C}_{109}\text{H}_{188}\text{O}_{49}$ $[\text{M} + \text{Na}]^+$ 2305.23; found 2305.206.

3,4,5-Tris(2-(2-(2-(3,4,5-tris(2-(2-(2-methoxyethoxy)ethoxy)ethoxy)benzyl-oxy)ethoxy)ethoxy)benzyl methacrylate (**7c**).

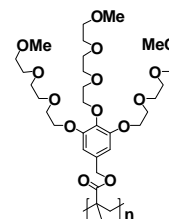
According to general procedure **D** from MAC (0.55 g, 5.26 mmol), **7b** (2.40 g, 1.05 mmol), TEA (0.53 g, 5.26 mmol), DMAP (0.1 g) and dry DCM (50 mL), the mixture was stirred for 5 h at r.t., purification by column chromatography with DCM / MeOH (20:1, v/v) afforded



7c (2.16 g, 88%) as colorless oil. ^1H NMR (CD_2Cl_2): δ = 1.99 (s, 3H, CH_3), 3.36 (s, 18H, CH_3), 3.37 (s, 9H, CH_3), 3.53–3.55 (m, 18H, CH_2), 3.62–73 (m, 78H, CH_2), 3.79 (t, 8H, CH_2), 3.86–3.87 (m, 16H, CH_2), 4.13–4.18 (m, 24H, CH_2), 4.47 (s, 6H, CH_2), 5.11 (s, 2H, CH_2), 5.63 (s, 1H, CH_2), 6.16 (s, 1H, CH_2), 6.63 (s, 6H, CH), 6.67 (s, 2H, CH). ^{13}C NMR (CD_2Cl_2): δ = 18.25, 58.74, 66.45, 68.82, 68.89, 69.66, 69.84, 70.55, 70.57, 70.67, 70.70, 70.87, 72.04, 72.43, 72.46, 73.19, 106.83, 107.49, 125.55, 134.18, 136.55, 137.63, 138.21, 152.71, 152.79, 167.08. HR-MS (MALDI): m/z calcd. for $\text{C}_{113}\text{H}_{192}\text{O}_{50}$ $[\text{M} + \text{Na}]^+$ 2373.25; found 2373.243.

Poly(3,4,5-tris(2-(2-(2-methoxyethoxy)ethoxy)ethoxy)benzylmethacrylate) [**PG1(MT)**].

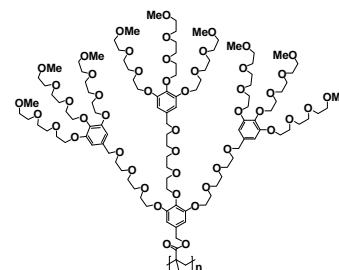
Route 1: According to general procedure **H** from **6c** (0.40 g, 0.60 mmol), AIBN (2.0 mg) and DMF (0.2 mL), polymerization for 7 h yielded **PG1(MT)** as colorless gel (0.22 g, 55%). ^1H NMR (CD_2Cl_2): δ = 0.86 – 1.09 (m, 3H, CH_3), 1.90 – 2.05 (m, 2H, CH_2), 3.29 – 3.31 (m, 9H, CH_3), 3.46 – 3.64 (m, 24H, CH_2), 3.74 (br, 6H, CH_2), 4.06 (br, 6H, CH_2), 4.81 (br, 2H, CH_2), 6.54 (br, 2H, CH). ^{13}C NMR (CD_2Cl_2): δ = 58.68, 68.91, 69.76, 70.50, 72.03, 72.50, 107.12, 130.87, 138.13, 152.83. The signals from the polymer backbone were so broad that they disappeared in the baseline. Elemental analysis (%) calcd for $(\text{C}_{32}\text{H}_{54}\text{O}_{14})_n$ (662.77) $_n$: C, 57.99; H, 8.21. Found: C, 57.27; H, 8.22.



Route 2: According to general procedure **J** from **6c** (0.50 g, 0.75 mmol), ACVA (3.6 mg) and pure water (1.11 mL), polymerization for 15 h yielded **PG1(MT)** as colorless gel (0.30 g, 60%). The identical spectral data as in route 1 were obtained. **Route 3:** According to general procedure **I** from **6c** (3.2 g, 4.8 mmol), AIBN (16 mg), polymerization for 4.5 h yielded **PG1(MT)** as colorless gel (2.38 g, 74%). The identical spectral data as in route 1 were obtained.

Poly(3,4,5-tris(2-(2-(2-(3,4,5-tris(2-(2-(2-methoxyethoxy)ethoxy)ethoxy)benzyloxy)ethoxy)ethoxy)benzyl methacrylate)[PG2(MT)].

Route 1: According to general procedure **J** from **7c** (0.40 g, 0.17 mmol), ACVA (2.8 mg) and pure water (0.2 mL), polymerization for 15 h yielded **PG2(MT)** as colorless gel (0.25 g, 63%). ^1H NMR (CD_2Cl_2): δ = 3.30 – 3.37 (m, 27H, CH_3), 3.46 – 3.66 (m, 96H, CH_2), 3.78 (br, 24H, CH_2), 4.08

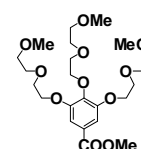


(br, 24H, CH_2), 4.40 (br, 6H, CH_2), 6.53 – 6.56 (br, 8H, CH). ^{13}C NMR (CD_2Cl_2): δ = 58.71, 68.84, 69.67, 69.79, 70.48, 70.61, 70.80, 72.00, 72.44, 73.09, 106.52, 134.14, 137.54, 152.70. The signals from the polymer backbone were so broad that they disappeared in the baseline. Elemental analysis (%) calcd for $(\text{C}_{113}\text{H}_{192}\text{O}_{50})_n$ (2350.73) $_n$: C, 57.74; H, 8.23. Found: C, 57.46; H, 8.25. **Route 2:** According to general procedure **I** from **7c** (0.4 g, 0.17 mmol) and AIBN (2 mg), polymerization for 14 h yielded **PG2(MT)** as colorless gel (0.26 g, 65%). The identical spectral data as in route 1 were obtained.

8.3.3 Compounds of Chapter 4.2

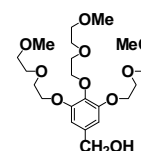
Methyl 3,4,5-tris(2-(2-methoxyethoxy)ethoxy)benzoate (8a).

According to general procedure **B**, from methyl gallate (8.4 g, 45.6 mmol), Me-DEG-Ts (50.0 g, 182.3 mmol), KI (5.8 g, 36.5 mmol), K_2CO_3 (63.0 g, 456.0 mmol) and DMF (200 mL), purification by column chromatography with hexane/ethyl acetate (1:5, v/v) afforded **8a** as a colorless oil (19.5 g, 87%). ^1H NMR (CD_2Cl_2): δ 3.32–3.35 (m, 9H, CH_3), 3.48–3.55 (m, 6H, CH_2), 3.62–3.69 (m, 6H, CH_2), 3.74–3.76 (m, 2H, CH_2), 3.82–3.86 (m, 7H, CH_2 + CH_3), 4.16–4.18 (m, 6H, CH_2), 7.28 (s, 2H, CH). ^{13}C NMR (CD_2Cl_2): δ 52.12, 58.75, 58.78, 68.93, 69.68, 70.47, 70.71, 70.75, 72.07, 72.11, 72.58, 108.65, 125.20, 142.46, 152.46, 166.54. HR-MS (MALDI): m/z calcd. for $\text{C}_{23}\text{H}_{38}\text{O}_{11}$ $[\text{M} + \text{Na}]^+$ 513.24; found 513.2315. Elemental analysis (%) calcd for $\text{C}_{23}\text{H}_{38}\text{O}_{11}$, 490.55: C, 56.32; H, 7.81. Found: C, 56.13; H, 7.85.



3,4,5-Tris(2-(2-methoxyethoxy)ethoxy)benzyl alcohol (8b).

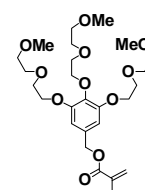
According to general procedure **C**, from LAH (0.95 g, 25.1 mmol), **8a** (8.2 g, 16.7 mmol), dry THF (100 mL), water (6 mL), 10% NaOH (15



mL), and water (20 mL), purification by column chromatography with DCM/MeOH (20:1, v/v) afforded **8b** as a colorless oil (7 g, 91%). ^1H NMR (CD_2Cl_2): δ 3.35 (s, 9H, CH_3), 3.52–3.55 (m, 6H, CH_2), 3.64–3.68 (m, 6H, CH_2), 3.75 (t, 2H, CH_2), 3.82 (t, 4H, CH_2), 4.10 (t, 2H, CH_2), 4.14 (t, 4H, CH_2), 4.56 (s, 2H, CH_2), 6.62 (s, 2H, CH). ^{13}C NMR (CD_2Cl_2): δ 58.76, 65.11, 68.82, 69.88, 70.42, 70.68, 72.08, 72.12, 72.44, 105.99, 137.13, 137.47, 152.77. HR-MS (MALDI): m/z calcd. for $\text{C}_{22}\text{H}_{38}\text{O}_{10}$ $[\text{M} + \text{Na}]^+$ 485.25; found 485.2363. Elemental analysis (%) calcd for $\text{C}_{22}\text{H}_{38}\text{O}_{10}$, 462.54: C, 57.13; H, 8.28. Found: C, 56.53; H, 8.31.

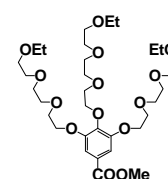
3,4,5-Tris(2-(2-methoxyethoxy)ethoxy)benzyl methacrylate (**8c**).

According to general procedure **D**, from MAC (0.90 g, 8.65 mmol), **8b** (2.00 g, 4.32 mmol), TEA (2.19 g, 21.60 mmol), DMAP (0.1 g) and dry DCM (50 mL), purification by column chromatography with DCM/MeOH (20:1, v/v) afforded **8c** as a colorless oil (2.10 g, 92%). ^1H NMR (CD_2Cl_2): δ 1.96 (s, 3H, CH_3), 3.35 (s, 9H, CH_3), 3.48–3.54 (m, 6H, CH_2), 3.64–3.68 (m, 6H, CH_2), 3.75 (t, 2H, CH_2), 3.83 (t, 4H, CH_2), 4.10–4.15 (m, 6H, CH_2), 5.08 (s, 2H, CH_2), 5.60 (s, 1H, CH_2), 6.13 (s, 1H, CH_2), 6.63 (s, 2H, CH). ^{13}C NMR (CD_2Cl_2): δ = 18.23, 58.76, 58.78, 66.46, 68.91, 69.78, 70.44, 70.69, 70.74, 72.08, 72.12, 72.46, 107.42, 125.53, 131.82, 136.57, 138.19, 152.79, 167.10. HR-MS (MALDI): m/z calcd. for $\text{C}_{26}\text{H}_{42}\text{O}_{11}$ $[\text{M} + \text{Na}]^+$ 553.27; found 553.2627. Elemental analysis (%) calcd for $\text{C}_{26}\text{H}_{42}\text{O}_{11}$, 530.61: C, 58.85; H, 7.98. Found: C, 58.26; H, 7.71.



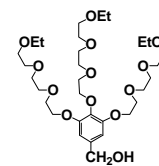
Methyl 3,4,5-Tris(2-(2-ethoxyethoxy)ethoxy)benzoate (**8d**).

According to general procedure **B**, from methyl gallate (8.86 g, 48.13 mmol), Et-TEG-Ts (64.00 g, 192.53 mmol), KI (6.16 g, 38.50 mmol), K_2CO_3 (66.52 g, 481.30 mmol) and dry DMF (250 mL), purification by column chromatography with hexane/ethyl acetate (1:5, v/v) afforded **8d** as a colorless oil (26.50 g, 83%). ^1H NMR (CD_2Cl_2): δ 1.18–1.19 (m, 9H, CH_3), 3.46–3.51 (m, 6H, CH_2), 3.53–3.71 (m, 24H, CH_2), 3.77 (t, 2H, CH_2), 3.85–3.87 (m, 7H, $\text{CH}_2 + \text{CH}_3$), 4.19–4.23 (m, 6H, CH_2), 7.30 (s, 2H, CH). ^{13}C NMR (CD_2Cl_2): δ 15.14, 52.12, 66.55, 68.93, 69.71, 69.96, 70.63, 70.68, 70.75, 70.78, 70.90, 72.56, 108.68, 125.20, 142.49, 152.47, 166.54. HR-MS (MALDI): m/z calcd. for $\text{C}_{32}\text{H}_{56}\text{O}_{14}$ $[\text{M} + \text{Na}]^+$ 687.37; found 687.3572. Elemental analysis (%) calcd for $\text{C}_{32}\text{H}_{56}\text{O}_{14}$, 664.79: C, 57.82; H, 8.49. Found: C, 57.35; H, 8.55.

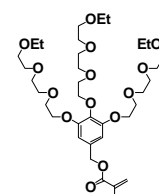


3,4,5-Tris(2-(2-(2-ethoxyethoxy)ethoxy)ethoxy)benzyl alcohol (8e).

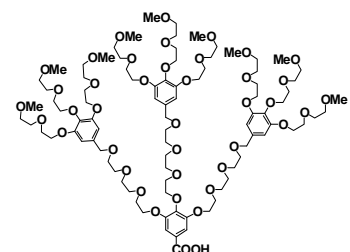
According to general procedure **C**, from LAH (1.28 g, 33.70 mmol), **8d** (11.20 g, 16.85 mmol), dry THF (150 mL), water (8 mL), 10% NaOH (20 mL) and water (30 mL), purification by column chromatography with DCM/MeOH (20:1, v/v) afforded **8e** as a colorless oil (9.9 g, 92%). ^1H NMR (CD_2Cl_2): δ 1.16–1.20 (m, 9H, CH_3), 3.47–3.70 (m, 30H, CH_2), 3.76 (t, 2H, CH_2), 3.83 (t, 4H, CH_2), 4.11 (t, 2H, CH_2), 4.16 (t, 4H, CH_2), 4.56 (s, 2H, CH_2), 6.63 (s, 2H, CH). ^{13}C NMR (CD_2Cl_2): δ 15.13, 65.13, 66.56, 68.86, 69.91, 69.96, 70.58, 70.70, 70.74, 70.86, 72.40, 106.15, 137.13, 137.59, 152.80. HR-MS (MALDI): m/z calcd. for $\text{C}_{31}\text{H}_{59}\text{O}_{13}$ $[\text{M} + \text{Na}]^+$ 659.37; found 659.3621. Elemental analysis (%) calcd for $\text{C}_{31}\text{H}_{56}\text{O}_{13}$, 636.78: C, 58.47; H, 8.86. Found: C, 58.22; H, 8.91.

**3,4,5-Tris(2-(2-(2-ethoxyethoxy)ethoxy)ethoxy)benzyl methacrylate (8f).**

According to general procedure **D**, from MAC (0.79 g, 7.54 mmol), **8e** (2.40 g, 3.77 mmol), TEA (1.91 g, 18.85 mmol), DMAP (0.15 g) and dry DCM (50 mL), purification by column chromatography with DCM/MeOH (20:1, v/v) afforded **8f** as a colorless oil (2.44 g, 92%). ^1H NMR (CD_2Cl_2): δ 1.16–1.19 (m, 9H, CH_3), 1.96 (s, 3H, CH_3), 3.47–3.70 (m, 30H, CH_2), 3.76 (t, 2H, CH_2), 3.84 (t, 4H, CH_2), 4.11–4.16 (m, 6H, CH_2), 5.08 (s, 2H, CH_2), 5.60 (s, 1H, CH_2), 6.13 (s, 1H, CH_2), 6.63 (s, 2H, CH). ^{13}C NMR (CD_2Cl_2): δ 15.15, 18.25, 66.47, 66.55, 68.89, 69.80, 69.97, 70.59, 70.68, 70.70, 70.77, 70.89, 72.46, 107.42, 125.54, 131.82, 136.56, 138.20, 152.79, 167.09. HR-MS (MALDI): m/z calcd. for $\text{C}_{35}\text{H}_{60}\text{O}_{14}$ $[\text{M} + \text{Na}]^+$ 727.40; found 727.3862. Elemental analysis (%) calcd for $\text{C}_{35}\text{H}_{60}\text{O}_{14}$, 704.85: C, 59.64; H, 8.58. Found: C, 59.87; H, 8.61.

**3,4,5-tris(2-(2-(2-(3,4,5-tris(2-(2-methoxyethoxy)ethoxy)benzyl-oxy)ethoxy)ethoxy)ethoxy)benzoic acid (9a).**

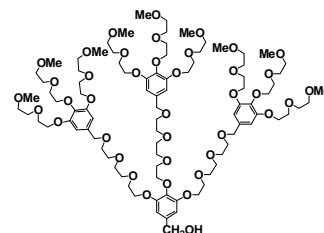
According to general procedure **E**, from **2g** (3.42 g, 3.28 mmol), dry THF (30 mL), **8b** (5.00 g, 10.81 mmol), KI (1.57 g, 9.84 mmol), 15-crown-5 (0.72 g, 3.28 mmol), NaH (0.78 g, 32.5 mmol) and dry THF (60 mL), purification by column chromatography with DCM/MeOH (15:1, v/v) afforded **9a** as a yellow oil (3.00 g, 48%). ^1H NMR (CD_2Cl_2): δ 3.35 (s, 27H, CH_3), 3.53–3.83 (m, 84H, CH_2), 4.09–4.17 (m, 24H, CH_2), 4.42 (s, 6H, CH_2), 6.58 (s, 6H, CH), 7.31 (s, 2H,



CH). ^{13}C NMR (CD_2Cl_2): δ 58.76, 68.79, 68.89, 69.69, 69.83, 70.40, 70.68, 70.74, 70.88, 72.07, 72.12, 72.40, 72.54, 73.19, 106.83, 109.00, 109.07, 125.11, 134.20, 137.59, 142.59, 152.40, 152.54, 152.69, 167.89. HR-MS (MALDI): m/z calcd. for $\text{C}_{91}\text{H}_{150}\text{O}_{41}$ $[\text{M} + \text{Na}]^+$ 1921.97; found 1921.9584. Elemental analysis (%) calcd for $\text{C}_{91}\text{H}_{150}\text{O}_{41}$, 1900.16: C57.52; H, 7.96. Found: C, 57.09; H, 7.83.

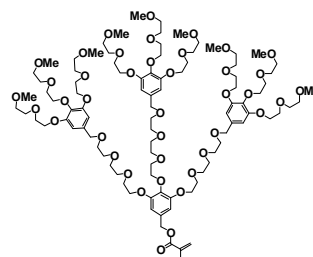
3,4,5-tris(2-(2-(2-(3,4,5-tris(2-(2-methoxyethoxy)ethoxy)benzyl-oxy)ethoxy)ethoxy)benzyl alcohol (9b).

According to general procedure **F**, from *N*-Methylmorpholine (0.45 g, 4.45 mmol), ethyl chloroformate (0.46 g, 4.2 mmol), **9a** (1.6 g, 0.84 mmol), dry THF (50 mL) and NaBH_4 (0.25 g, 6.61 mmol), purification by column chromatography with DCM/MeOH (10:1, v/v) afforded **9b** as a colorless oil (1.3 g, 82%). ^1H NMR (CD_2Cl_2): δ 3.30–3.34 (m, 27H, CH_3), 3.52–3.81 (m, 84H, CH_2), 4.08–4.13 (m, 24H, CH_2), 4.43 (s, 6H, CH_2), 4.53 (s, 2H, CH_2), 6.59 (s, 6H, CH), 6.61 (s, 2H, CH). ^{13}C NMR (CD_2Cl_2): δ 58.76, 58.78, 64.93, 68.82, 69.66, 69.82, 69.89, 70.43, 70.59, 70.68, 70.72, 70.85, 72.08, 72.13, 72.43, 73.18, 106.01, 106.79, 134.19, 137.61, 152.71, 152.75. HR-MS (MALDI): m/z calcd. for $\text{C}_{91}\text{H}_{152}\text{O}_{40}$ $[\text{M} + \text{Na}]^+$ 1907.99; found 1907.9714. Elemental analysis (%) calcd for $\text{C}_{91}\text{H}_{152}\text{O}_{40}$, 1886.18: C57.95; H, 8.12. Found: C, 57.68; H, 8.03.



3,4,5-tris(2-(2-(2-(3,4,5-tris(2-(2-methoxyethoxy)ethoxy)benzyl-oxy)ethoxy)ethoxy)benzyl methacrylate (9c).

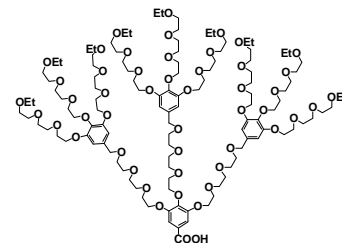
According to general procedure **D**, from MAC (0.33 g, 3.18 mmol), **9b** (1.2 g, 0.64 mmol), TEA (0.32 g, 3.18 mmol), DMAP (0.15 g) and dry DCM (40 mL), purification by column chromatography with ethyl acetate/MeOH (5:1, v/v) afforded **9c** as a colorless oil (1.05 g, 85%). ^1H NMR (CD_2Cl_2): δ 3.30–3.35 (m, 27H, CH_3), 3.49–3.83 (m, 84H, CH_2), 4.08–4.15 (m, 24H, CH_2), 4.43 (s, 6H, CH_2), 5.07 (s, 2H, CH_2), 5.59 (s, 1H, CH_2), 6.12 (s, 1H, CH_2), 6.59 (s, 6H, CH), 6.63 (s, 2H, CH). ^{13}C NMR (CD_2Cl_2): δ 18.51, 59.02, 59.04, 66.70, 69.00, 69.09, 69.15, 69.92, 70.08, 70.69, 70.85, 70.95, 70.98, 71.14, 72.34, 72.39, 72.69, 73.45, 106.90, 107.06, 107.64, 107.74, 125.80, 132.11, 134.43, 136.81, 137.89, 138.48, 152.98, 153.05, 153.11, 153.17, 167.32. HR-MS (MALDI): m/z calcd. for $\text{C}_{95}\text{H}_{156}\text{O}_{41}$ $[\text{M} + \text{Na}]^+$



1976.01; found 1976.005. Elemental analysis (%) calcd for $C_{95}H_{156}O_{41}$, 1954.25: C58.39; H, 8.05. Found: C, 58.12; H, 7.93.

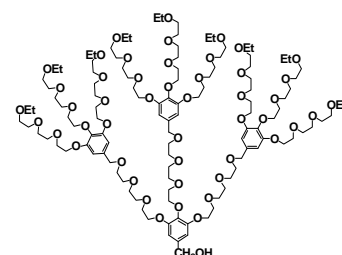
3,4,5-Tris(2-(2-(2-(3,4,5-tris(2-(2-(2-ethoxyethoxy)ethoxy)ethoxy)benzyl-oxy)ethoxy)ethoxy)benzoic acid (9d).

According to general procedure **E**, from **2g** (4.05 g, 3.88 mmol), dry THF (30 mL), **8e** (8.15 g, 12.80 mmol), KI (1.86 g, 11.60 mmol), 15-crown-5 (0.85 g, 3.88 mmol), NaH (0.92 g, 38.40 mmol) and dry THF (100 mL), purification by column chromatography with DCM/MeOH (15:1, v/v) afforded **9d** as a yellow oil (4.7 g, 50 %). 1H NMR (CD_2Cl_2): δ 1.16–1.19 (m, 27H, CH_3), 3.47–3.51 (m, 18H, CH_2), 3.55–3.70 (m, 96H, CH_2), 3.75–3.77 (m, 8H, CH_2), 3.82–3.84 (m, 16H, CH_2), 4.10 (t, 6H, CH_2), 4.13–4.18 (m, 16H, CH_2), 4.20 (t, 2H, CH_2), 4.42 (s, 6H, CH_2), 6.59 (s, 6H, CH), 7.31 (s, 2H, CH). ^{13}C NMR (CD_2Cl_2): δ 15.13, 66.56, 68.76, 68.86, 69.65, 69.69, 69.74, 69.83, 69.94, 70.54, 70.59, 70.66, 70.72, 70.83, 70.88, 71.07, 72.39, 72.52, 73.18, 106.82, 108.98, 125.97, 134.24, 137.55, 142.25, 152.33, 152.67, 167.71. HR-MS (MALDI): m/z calcd. for $C_{118}H_{204}O_{50}$ $[M + Na]^+$ 2444.34; found 2444.335. Elemental analysis (%) calcd for $C_{118}H_{204}O_{50}$, 2422.88: C, 58.50; H, 8.49. Found: C, 57.39; H, 8.27.



3,4,5-Tris(2-(2-(2-(3,4,5-tris(2-(2-(2-ethoxyethoxy)ethoxy)ethoxy)benzyl-oxy)ethoxy)ethoxy)benzyl alcohol (9e).

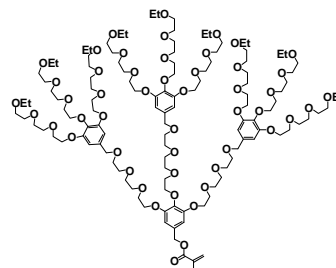
According to general procedure **F**, from *N*-Methylmorpholine (0.31 g, 3.06 mmol), ethyl chloroformate (0.34 g, 3.13 mmol), **9d** (1.50 g, 0.62 mmol), dry THF (30 mL) and $NaBH_4$ (0.19 g, 4.96 mmol), purification by column chromatography with DCM/MeOH (10:1, v/v) afforded **9e** as a colorless oil (1.2 g, 81%). 1H NMR (CD_2Cl_2): δ 1.16–1.19 (m, 27H, CH_3), 3.46–3.70 (m, 114H, CH_2), 3.76 (t, 8H, CH_2), 3.82–3.83 (m, 16H, CH_2), 4.09–4.14 (m, 24H, CH_2), 4.44 (s, 6H, CH_2), 4.54 (s, 2H, CH_2), 6.59 (s, 6H, CH), 6.61 (s, 2H, CH). ^{13}C NMR (CD_2Cl_2): δ 15.15, 64.88, 66.55, 68.79, 69.65, 69.83, 69.89, 69.96, 70.57, 70.67, 70.70, 70.75, 70.76, 70.86, 72.42, 73.18, 105.99, 106.79, 134.19, 137.41, 137.60, 152.71, 152.73. HR-MS (MALDI): m/z calcd. for $C_{118}H_{206}O_{49}$ $[M + Na]^+$



2430.36; found 2430.355. Elemental analysis (%) calcd for $C_{118}H_{206}O_{49}$, 2408.90: C, 58.84; H, 8.62. Found: C, 58.28; H, 8.50.

3,4,5-Tris(2-(2-(2-(3,4,5-tris(2-(2-(2-ethoxyethoxy)ethoxy)ethoxy)benzyl-oxy)ethoxy)ethoxy)benzylmethacrylate (9f).

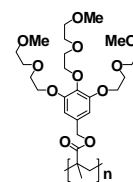
According to general procedure **D**, from MAC (0.22 g, 2.08 mmol), **9e** (1.00 g, 0.42 mmol), TEA (0.21 g, 2.08 mmol), DMAP (0.15 g) and dry DCM (40 mL), purification by column chromatography with ethyl acetate/MeOH (5:1, v/v) afforded **9f** as a colorless oil (0.85 g, 83%). 1H NMR



(CD_2Cl_2): δ 1.17–1.19 (m, 27H, CH_3), 1.95 (s, 3H, CH_3), 3.46–3.70 (m, 114H, CH_2), 3.76 (t, 8H, CH_2), 3.83 (t, 16H, CH_2), 4.09–4.15 (m, 24H, CH_2), 4.43 (s, 6H, CH_2), 5.07 (s, 2H, CH_2), 5.59 (s, 1H, CH_2), 6.12 (s, 1H, CH_2), 6.59 (s, 6H, CH), 6.64 (s, 2H, CH). ^{13}C NMR (CD_2Cl_2): δ 15.15, 18.26, 66.45, 66.54, 68.81, 68.87, 69.65, 69.81, 69.84, 69.97, 70.58, 70.68, 70.70, 70.75, 70.76, 70.87, 72.43, 73.20, 106.81, 107.48, 125.57, 131.86, 134.17, 136.54, 137.63, 138.20, 152.72, 152.78, 167.07. HR-MS (MALDI): m/z calcd. for $C_{122}H_{210}O_{50}$ $[M + Na]^+$ 2498.39; found 2498.382. Elemental analysis (%) calcd for $C_{122}H_{210}O_{50}$, 2476.97: C, 59.16; H, 8.55. Found: C, 58.34; H, 8.35.

Poly(3,4,5-Tris(2-(2-methoxyethoxy)ethoxy)benzylmethacrylate)[PG1(MD)].

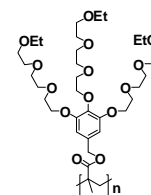
According to general procedure **H** from **8c** (0.50 g, 0.94 mmol), AIBN (2.5 mg) and DMF (0.4 mL), polymerization for 4 h yielded **PG1(MD)** as colorless gel (0.14 g, 28%). 1H NMR (CD_2Cl_2): δ 0.83–1.06 (m, 3H, CH_3), 1.90 (br, 2H, CH_2), 3.29–3.32 (m, 9H, CH_3), 3.47–3.49 (m, 6H, CH_2), 3.62



(br, 6H, CH_2), 3.74 (br, 6H, CH_2), 4.06 (br, 6H, CH_2), 4.81 (br, 2H, CH_2), 6.55 (br, 2H, CH). ^{13}C NMR (CD_2Cl_2): δ 58.72, 67.03, 68.84, 69.74, 70.41, 70.66, 70.80, 72.05, 72.11, 72.40, 72.48, 72.92, 107.16, 130.86, 130.96, 138.04, 152.77. The signals from the polymer backbone were so broad that they disappeared in the baseline. Elemental analysis (%) calcd for $(C_{26}H_{42}O_{11})_n$ (530.61) $_n$: C, 58.85; H, 7.98. Found: C, 62.74; H, 7.59.

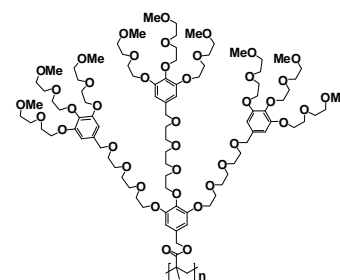
Poly(3,4,5-Tris(2-(2-(2-ethoxyethoxy)ethoxy)ethoxy)benzylmethacrylate) [PG1(ET)].

According to general procedure I from **8f** (0.50 g, 0.71 mmol) and AIBN (2.5 mg), polymerization for 3 h yielded **PG1(ET)** as colorless gel (0.34 g, 68%). ^1H NMR (CD_2Cl_2): δ 0.86 (br, 2H, CH_3), 1.13–1.18 (m, 10H, CH_3 + CH_3), 3.43–3.64 (m, 30H, CH_3), 3.74 (br, 6H, CH_2), 4.06 (br, 6H, CH_2), 4.80 (br, 2H, CH_2), 6.53 (br, 2H, CH). ^{13}C NMR (CD_2Cl_2): δ 15.22, 45.24, 66.49, 68.83, 69.75, 69.95, 70.55, 70.62, 70.70, 70.80, 72.48, 106.94, 130.83, 137.97, 152.76. The signals from the polymer backbone were so broad that they disappeared in the baseline. Elemental analysis (%) calcd for $(\text{C}_{35}\text{H}_{60}\text{O}_{14})_n$ (704.85) $_n$: C, 59.64; H, 8.58. Found: C, 58.88; H, 8.55.



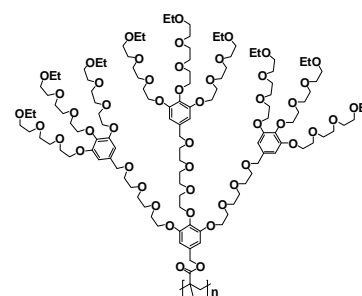
Poly(3,4,5-tris(2-(2-(2-(3,4,5-tris(2-(2-methoxyethoxy)ethoxy)benzyl-oxy)ethoxy)ethoxy)benzyl methacrylate) [PG2(MD)].

According to general procedure I from **9c** (0.49 g, 0.25 mmol) and AIBN (2.5 mg), polymerization for 24 h yielded **PG2(MD)** as colorless gel (0.3 g, 61%). ^1H NMR (CD_2Cl_2): δ 3.27–3.32 (m, 27H, CH_3), 3.47–3.74 (m, 84H, CH_2), 4.04 (br, 24H, CH_2), 4.35 (br, 6H, CH_2), 6.52 (br, 8H, CH). ^{13}C NMR (CD_2Cl_2): δ 58.72, 68.83, 69.65, 69.78, 70.38, 70.56, 70.65, 72.04, 72.09, 72.44, 73.08, 106.59, 134.15, 137.58, 152.70. The signals from the polymer backbone were so broad that they disappeared in the baseline. Elemental analysis (%) calcd for $(\text{C}_{95}\text{H}_{156}\text{O}_{41})_n$ (1948.21) $_n$: C, 58.57; H, 7.76. Found: C, 57.58; H, 8.01.



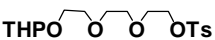
Poly(3,4,5-Tris(2-(2-(2-(3,4,5-tris(2-(2-(2-ethoxyethoxy)ethoxy)ethoxy)benzyl-oxy)ethoxy)ethoxy)benzyl methacrylate) [PG2(ET)].

According to general procedure I from **9f** (0.76 g, 0.31 mmol) and AIBN (3.8 mg), polymerization for 24 h yielded **PG2(ET)** as colorless gel (0.47 g, 62%). ^1H NMR (CD_2Cl_2): δ 1.12–1.13 (m, 27H, CH_3), 3.43–3.75 (m, 138H, CH_2), 4.05 (br, 24H, CH_2), 4.37 (br, 6H, CH_2), 6.52 (br, 8H, CH). ^{13}C NMR (CD_2Cl_2): δ 15.23, 66.47, 68.87, 69.68, 69.81, 69.95, 70.54, 70.63, 70.70, 70.82, 72.45, 73.11, 106.56, 134.13, 137.63, 152.71. The signals from the polymer backbone were so broad that they disappeared in the



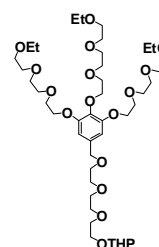
baseline. Elemental analysis (%) calcd for $(C_{122}H_{210}O_{50})_n$ (2476.97)_n: C, 59.16; H, 8.55. Found: C, 58.45; H, 8.43.

2-(2-(2-(Tetrahydro-2H-pyran-2-yloxy)ethoxy)ethoxy)ethyl 4-methyl benzene sulfonate (10).

Pyridinium toluenesulfonate (PPTS) (5.1 g, 20.4 mmol) was added  to a mixture of **1b** (31.0 g, 101.9 mmol), 3,4-dihydro-2H-pyran (DHP) (10.3 g, 122.2 mmol) in dry DCM (mL) at -5 °C, the mixture was stirred for 30 min, then warmed to r.t. and stirred over night. After washing with brine, the organic phase was dried over MgSO₄. Purification by column chromatography with hexane / ethyl acetate (2:1 then 1:1, v/v) afforded **10** (39.1 g, 98 %) as colorless oil. ¹H NMR (CD₂Cl₂): δ = 1.51–1.52 (m, 4H, CH₂), 1.68–1.71 (m, 1H, CH₂), 1.79–1.80 (m, 1H, CH₂), 2.45 (s, 3H, CH₃), 3.45–3.60 (m, 8H, CH₂), 3.66 (t, 2H, CH₂), 3.78–3.85 (m, 2H, CH₂), 4.13 (t, 2H, CH₂), 4.58 (t, 1H, CH), 7.39 (d, 2H, CH), 7.80 (d, 2H, CH). ¹³C NMR (CD₂Cl₂): δ = 19.73, 21.51, 25.63, 30.77, 62.26, 66.71, 68.72, 69.65, 70.57, 70.66, 70.80, 99.06, 128.01, 130.01, 133.07, 145.22. HR-MS (ESI): *m/z* calcd. for C₁₈H₂₈O₇S [M + Na]⁺ 411.16; found 411.1454.

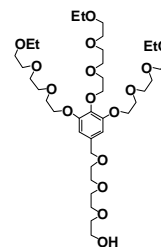
2-(2-(2-(2-(3,4,5-Tris(2-(2-(2ethoxyethoxy)ethoxy)ethoxy)benzyloxy)ethoxy)ethoxy) tetrahydro-2H-pyran (11a).

According to general procedure **E** from **8e** (21.6 g, 55.6 mmol) in dry THF (50 mL), compound **10** (29.5 g, 46.3 mmol), KI (1.5 g, 9.3 mmol), 15-crown-5 (10.2 g, 46.3 mmol), NaH (4.4 g, 185.3 mmol), and dry THF (180 mL), purification by column chromatography with hexane/ethyl acetate (1:3, v/v) then DCM/MeOH (30:1, v/v) afforded **11a** (38.0 g, 96%) as a yellow oil. ¹H NMR (CD₂Cl₂): δ = 1.17–1.19 (m, 9H, CH₃), 1.51–1.56 (m, 4H, CH₂), 1.69–1.71 (m, 1H, CH₂), 1.80–1.81 (m, 1H, CH₂), 3.46–3.70 (m, 42H, CH₂), 3.76 (t, 2H, CH₂), 3.80–3.85 (m, 6H, CH₂), 4.10 (t, 2H, CH₂), 4.14–4.16 (m, 4H, CH₂), 4.44 (s, 2H, CH₂), 4.59 (t, 1H, CH), 6.60 (s, 2H, CH). ¹³C NMR (CD₂Cl₂): δ = 15.15, 19.73, 25.64, 30.77, 62.27, 66.54, 66.74, 68.79, 69.65, 69.84, 69.97, 70.55, 70.58, 70.65, 70.70, 70.75, 70.77, 70.88, 72.42, 73.21, 99.07, 106.82, 134.18, 137.61, 152.71. HR-MS (MALDI): *m/z* calcd. for C₄₂H₇₆O₁₇ [M + Na]⁺ 875.51; found 875.4970.



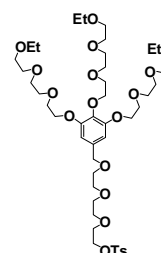
2-(2-(2-(3,4,5-Tris(2-(2-(2-ethoxyethoxy)ethoxy)ethoxy)benzyloxy)ethoxy)ethoxy)ethanol (11b).

According to general procedure **G** from PTSA (8.0 g, 42.2 mmol), **11a** (36.0 g, 42.2 mmol), and MeOH (180 mL), purification by column chromatography with DCM / MeOH (20:1, v/v) yielded **11b** (29.5 g, 91%) as a colorless oil. ^1H NMR (CD_2Cl_2): δ = 1.16–1.19 (m, 9H, CH_3), 2.59 (s, 1H, OH), 3.49–3.70 (m, 42H, CH_2), 3.75 (t, 2H, CH_2), 3.83 (t, 4H, CH_2), 4.10 (t, 2H, CH_2), 4.15 (t, 4H, CH_2), 4.44 (s, 2H, CH_2), 6.60 (s, 2H, CH). ^{13}C NMR (CD_2Cl_2): δ = 15.15, 61.71, 66.54, 68.79, 69.58, 69.84, 69.96, 70.45, 70.53, 70.57, 70.68, 70.70, 70.76, 70.87, 72.42, 72.64, 73.18, 106.83, 134.11, 137.62, 152.71. HR-MS (MALDI): m/z calcd. for $\text{C}_{37}\text{H}_{68}\text{O}_{16}$ $[\text{M} + \text{Na}]^+$ 791.45; found 791.4415.



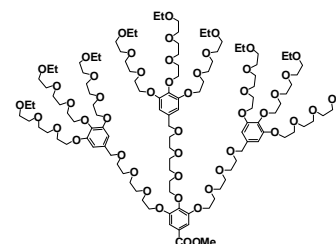
2-(2-(2-(3,4,5-Tris(2-(2-(2-ethoxyethoxy)ethoxy)ethoxy)benzyloxy)ethoxy)ethoxy)ethyl 4-methylbenzenesulfonate (11c).

According to general procedure **A** from TsCl (13.9 g, 72.8 mol) in THF (40 mL), NaOH (4.4 g, 109.2 mmol) in aqueous solution (60 mL) and **11b** (28.0 g, 36.4 mol) in THF (100 mL), purification by column chromatography with DCM / MeOH (30:1, v/v) afforded **11c** (27.9 g, 83%) as a colorless oil. ^1H NMR (CD_2Cl_2): δ = 1.16–1.19 (m, 9H, CH_3), 2.44 (s, 3H, CH_3), 3.46–3.70 (m, 40H, CH_2), 3.76 (t, 2H, CH_2), 3.83 (t, 4H, CH_2), 4.09–4.15 (m, 8H, CH_2), 4.43 (s, 2H, CH_2), 6.59 (s, 2H, CH), 7.38 (d, 2H, CH), 7.79 (d, 2H, CH). ^{13}C NMR (CD_2Cl_2): δ = 15.16, 21.51, 66.54, 68.72, 68.80, 69.63, 69.83, 69.97, 70.55, 70.58, 70.68, 70.70, 70.75, 70.77, 70.81, 70.87, 72.43, 73.19, 106.82, 128.00, 130.02, 133.06, 134.16, 137.63, 145.22, 152.72. HR-MS (MALDI): m/z calcd. for $\text{C}_{44}\text{H}_{74}\text{O}_{18}\text{S}$ $[\text{M} + \text{Na}]^+$ 945.46; found 945.4483.



Methyl-3,4,5-tris(2-(2-(2-(3,4,5-tris(2-(2-(2-ethoxyethoxy)ethoxy)ethoxy)benzyloxy)ethoxy)ethoxy)ethoxy)benzoate (12).

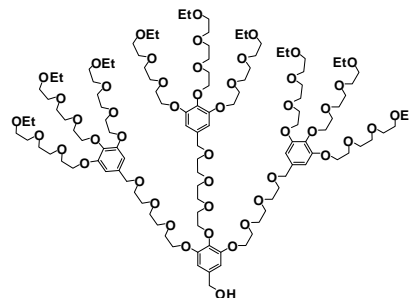
According to general procedure **B** from **11c** (25.6 g, 27.7 mmol), methyl gallate (1.55 g, 8.4 mmol), KI (1.1 g, 6.7 mmol), K_2CO_3 (11.6 g, 84.0 mmol) and dry DMF (160 mL), purification by column chromatography with DCM/MeOH (20:1, v/v) afforded **12** (18.8 g, 92%) as a slight yellow oil. ^1H NMR (CD_2Cl_2): δ = 1.16–1.19 (m, 27H, CH_3), 3.46–3.77 (m, 122H, CH_2), 3.82–3.86 (m, 19H, $\text{CH}_2 + \text{CH}_3$),



4.09–4.20 (m, 24H, CH₂), 4.43 (s, 6H, CH₂), 6.59 (s, 6H, CH), 7.30 (s, 2H, CH). ¹³C NMR (CD₂Cl₂): δ = 15.16, 66.54, 68.81, 68.92, 69.65, 69.73, 69.84, 69.97, 70.58, 70.63, 70.68, 70.71, 70.77, 70.87, 72.43, 72.56, 73.20, 106.80, 108.73, 125.22, 134.17, 137.63, 142.49, 152.47, 152.72, 166.49. HR-MS (MALDI): *m/z* calcd. for C₁₁₉H₂₀₆O₅₀ [M + Na]⁺ 2458.36; found 2458.340.

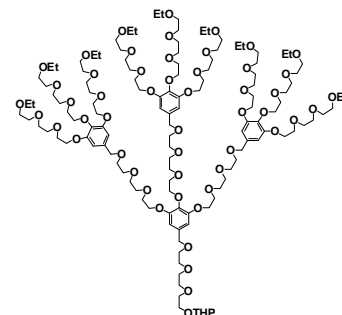
(3,4,5-Tris(2-(2-(2-(3,4,5-tris(2-(2-(2-ethoxyethoxy)ethoxy)ethoxy)benzyloxy)ethoxy)ethoxy)ethoxy)phenyl)methanol (9e).

According to general procedure **C** from LAH (0.38 g, 10.0 mmol), **12** (12.2 g, 5.0 mmol) and dry THF (120 mL), purification by column chromatography with DCM/MeOH (15:1, v/v) yielded **9e** (10.6 g, 88%) as a colorless oil. ¹H and ¹³C NMR spectra are the same as previous one. HR-MS (MALDI): *m/z* calcd. for C₁₁₈H₂₀₆O₄₉ [M + Na]⁺ 2430.36; found 2430.346.



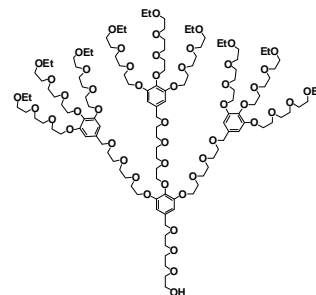
2-(2-(2-(2-(3,4,5-Tris(2-(2-(2-(3,4,5-tris(2-(2-(2-ethoxyethoxy)ethoxy)ethoxy)benzyloxy)ethoxy)ethoxy)benzyloxy)ethoxy)ethoxy)tetrahydro-2H-pyran (13a).

According to general procedure **E** from **9e** (7.06 g, 2.93 mmol) in THF (70 mL), KI (0.28 g, 1.76 mmol), 15-crown-5 (0.65 g, 2.93 mmol), NaH (0.35 g, 14.65 mmol), and **10** (1.59 g, 4.1 mmol) in THF (10 mL), purification by column chromatography with DCM/MeOH (20:1, v/v) afforded **13a** (7.26 g, 94%) as a colorless oil. ¹H NMR (CD₂Cl₂): δ = 1.15–1.19 (m, 27H, CH₃), 1.50–1.56 (m, 4H, CH₂), 1.66–1.71 (m, 1H, CH₂^a), 1.79–1.81 (m, 1H, CH₂^b), 3.46–3.84 (m, 152H, CH₂), 4.09–4.15 (m, 24H, CH₂), 4.43 (s, 8H, CH₂), 4.58–4.59 (m, 1H, CH), 6.59–6.60 (m, 8H, CH). ¹³C NMR (CD₂Cl₂): δ = 15.17, 19.73, 25.64, 30.77, 62.24, 66.53, 66.74, 68.81, 69.66, 69.84, 69.97, 70.52, 70.58, 70.65, 70.71, 70.75, 70.77, 70.87, 72.43, 73.20, 99.05, 106.79, 134.17, 134.22, 137.63, 152.72. HR-MS (MALDI): *m/z* calcd. for C₁₂₉H₂₂₆O₅₃ [M + Na]⁺ 2646.50; found 2646.481.



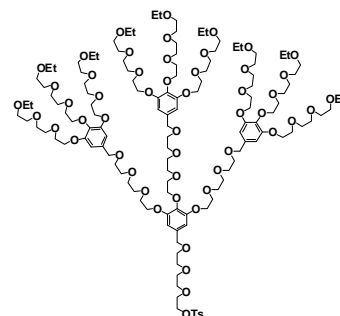
2-(2-(2-(3,4,5-Tris(2-(2-(2-(3,4,5-tris(2-(2-(2-ethoxyethoxy)ethoxy)ethoxy)benzyloxy)ethoxy)ethoxy)ethoxy)benzyloxy)ethoxy)ethoxy)ethanol (13b).

According to general procedure **G** from **13a** (7.1 g, 2.7 mmol), PTSA (0.51 g, 2.7 mmol) and MeOH (50 mL), purification by column chromatography with DCM/MeOH (15:1, v/v) yielded **13b** (6.09 g, 89%) as a colorless oil. ^1H NMR (CD_2Cl_2): δ = 1.16–1.19 (m, 27H, CH_3), 3.48–3.70 (m, 126H, CH_2), 3.76 (t, 8H, CH_2), 3.83 (t, 16H, CH_2), 4.09–4.14 (m, 24H, CH_2), 4.43 (s, 8H, CH_2), 6.59–6.61 (m, 8H, CH). ^{13}C NMR (CD_2Cl_2): δ = 15.13, 61.74, 66.52, 68.85, 68.90, 69.68, 69.86, 69.96, 70.59, 70.69, 70.71, 70.75, 70.77, 70.88, 72.44, 73.19, 106.96, 134.19, 152.74. HR-MS (MALDI): m/z calcd. for $\text{C}_{124}\text{H}_{218}\text{O}_{52}$ $[\text{M} + \text{Na}]^+$ 2562.44; found 2562.438.



2-(2-(2-(3,4,5-Tris(2-(2-(2-(3,4,5-tris(2-(2-(2-ethoxyethoxy)ethoxy)ethoxy)benzyloxy)ethoxy)ethoxy)benzyloxy)ethoxy)ethoxy)ethyl 4-methyl benzenesulfonate (13c).

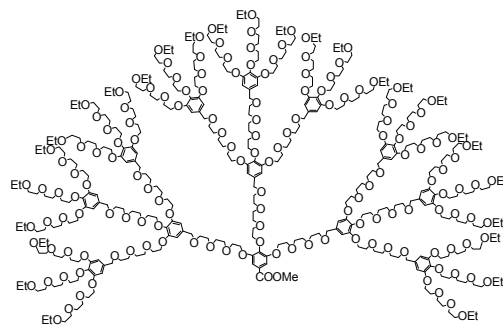
According to general procedure **A** from **13b** (5.44 g, 2.14 mmol) in THF (20 mL), NaOH (0.51 g, 12.85 mmol) in H_2O (10 mL), and TsCl (1.63 g, 8.56 mmol) in THF (5 mL), purification by column chromatography with DCM/MeOH (20:1, v/v) afforded **13c** (4.74 g, 82%) as a colorless oil. ^1H NMR (CD_2Cl_2): δ = 1.16–1.17 (m, 27H, CH_3), 2.44 (s, 3H, CH_3), 3.47–3.83 (m, 148H, CH_2), 4.10–4.14 (m, 26H, CH_2), 4.43 (s, 8H, CH_2), 6.59 (s, 8H, CH), 7.38 (s, 2H, CH), 7.77 (s, 2H, CH). ^{13}C NMR (CD_2Cl_2): δ = 15.16, 21.51, 66.54, 68.80, 69.02, 69.64, 69.84, 69.96, 70.57, 70.68, 70.70, 70.75, 70.86, 72.43, 73.19, 106.78, 127.99, 130.02, 133.05, 134.17, 137.60, 145.22, 152.71. HR-MS (MALDI): m/z calcd. for $\text{C}_{131}\text{H}_{224}\text{O}_{54}\text{S}$ $[\text{M} + \text{Na}]^+$ 2716.45; found 2716.440.



Methyl 3,4,5-tris(2-(2-(2-(3,4,5-tris(2-(2-(2-(3,4,5-tris(2-(2-(2-ethoxyethoxy)ethoxy)ethoxy)benzyloxy)ethoxy)ethoxy)benzyloxy)ethoxy)ethoxy)ethoxy)benzoate (14a).

A mixture of **13c** (3.5 g, 1.3 mmol), methyl gallate (66.4 mg, 0.36 mmol), KI (57.6 mg, 0.36 mmol), and potassium carbonate (Cs_2CO_3) (1.17 g, 3.6 mmol) in dry DMF (30 mL) was stirred at 80 °C for 48 h. After removal of DMF in vacuo, the residue was

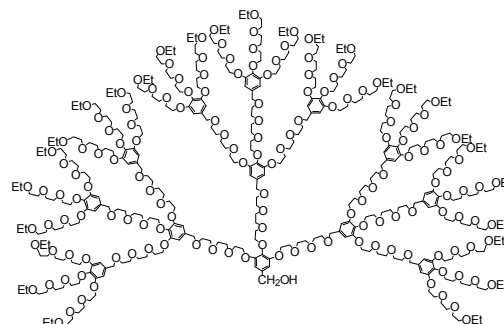
dissolved in DCM and washed sequentially with NaHCO_3 and brine. After drying over MgSO_4 , first purification by column chromatography with DCM/MeOH (10:1, v/v), followed by purification by HPLC, afforded **14a** (0.85 g, 30 %) as a slight yellow oil. ^1H NMR



(CD_2Cl_2): δ = 1.19–1.22 (m, 81H, CH_3), 3.52–3.89 (m, 447H, CH_2 + CH_3), 4.14 (t, 24H, CH_2), 4.18 (t, 48H, CH_2), 4.22–4.25 (m, 6H, CH_2), 4.47 (s, 24H, CH_2), 6.63 (s, 24H, CH), 7.35 (s, 2H, CH). ^{13}C NMR (CD_2Cl_2): δ = 15.16, 52.14, 66.54, 68.80, 69.65, 69.72, 69.84, 69.97, 70.57, 70.70, 70.76, 70.87, 72.43, 73.19, 106.78, 108.77, 134.17, 137.61, 152.45, 152.71. Some signals seem to be superimposed by others. HR-MS (MALDI): m/z calcd. for $\text{C}_{380}\text{H}_{656}\text{O}_{158}$ $[\text{M} + \text{Na}]^+$ 7771.33; found 7775.65. Elemental analysis (%) calcd for $\text{C}_{380}\text{H}_{656}\text{O}_{158}$, 7753.27: C, 58.87; H, 8.53. Found: C, 58.62; H, 8.50.

(3,4,5-Tris(2-(2-(2-(3,4,5-tris(2-(2-(2-(3,4,5-tris(2-(2-(2ethoxyethoxy)ethoxy)ethoxy)benzyloxy)ethoxy)ethoxy)ethoxy)benzyloxy)ethoxy)ethoxy)phenyl)methanol (14b).

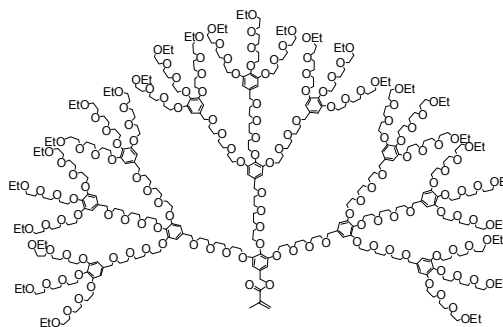
According to general procedure **C** from **14a** (0.8 g, 0.1 mmol), LAH (20 mg, 0.52 mmol) and THF (20 mL), purification by column chromatography with DCM/MeOH (10:1, v/v) afforded **14b** (0.62 g, 78%) as a colorless oil.



^1H NMR (CD_2Cl_2): δ = 1.20–1.22 (m, 81H, CH_3), 3.50–3.74 (m, 366H, CH_2), 3.79 (t, 26H, CH_2), 3.86 (t, 52H, CH_2), 4.14 (t, 26H, CH_2), 4.18 (t, 52H, CH_2), 4.47 (s, 24H, CH_2), 4.57(d, 2H, CH_2), 6.63–6.65 (m, 26H, CH). ^{13}C NMR (CD_2Cl_2): δ = 15.16, 64.79, 66.54, 68.80, 69.64, 69.84, 69.97, 70.57, 70.68, 70.69, 70.76, 70.87, 72.43, 73.19, 105.95, 106.78, 134.17, 137.61, 152.71. HR-MS (MALDI): m/z calcd. for $\text{C}_{379}\text{H}_{656}\text{O}_{157}$ $[\text{M} + \text{Na}]^+$ 7743.33; found 7748.20. Elemental analysis (%) calcd for $\text{C}_{379}\text{H}_{656}\text{O}_{157}$, 7725.26: C, 58.93; H, 8.56. Found: C, 59.06; H, 8.83.

3,4,5-Tris(2-(2-(2-(3,4,5-tris(2-(2-(2-(3,4,5-tris(2-(2-(2-ethoxyethoxy)ethoxy)ethoxy)benzyloxy)ethoxy)ethoxy)ethoxy)benzyloxy)ethoxy)ethoxy)benzyl methacrylate (14c).

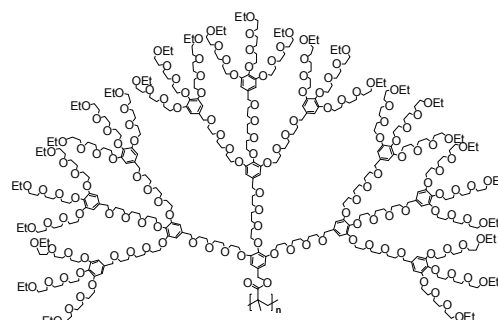
According to general procedure **D** from MAC (81.2 mg, 0.78 mmol), **14b** (0.6 g, 0.078 mmol), triethyl amine (79 mg, 0.78 mmol), DMAP (0.1 g) in dry DCM (20 mL), the mixture was stirred for another 5 h at r.t., purification with column chromatography with DCM/MeOH



(15:1 then 10:1, v/v) afforded **14c** (0.52 g, 86%) as a colorless oil. ^1H NMR (CD_2Cl_2): δ = 1.20–1.22 (m, 81H, CH_3), 1.98 (s, 3H, CH_3), 3.50–3.74 (m, 366H, CH_2), 3.79 (t, 26H, CH_2), 3.87 (t, 52H, CH_2), 4.14 (t, 26H, CH_2), 4.18 (t, 52H, CH_2), 4.47 (s, 24H, CH_2), 5.11(s, 2H, CH_2), 5.62 (s, 1H, CH_2^{a}), 6.15 (s, 1H, CH_2^{b}), 6.63-6.65 (m, 26H, CH). ^{13}C NMR (CD_2Cl_2): δ = 15.42, 18.54, 66.80, 69.06, 69.91, 70.10, 70.23, 70.83, 70.95, 71.02, 71.12, 72.69, 73.46, 107.03, 107.78, 125.85, 134.44, 137.87, 152.97. Some signals seem to be superimposed by others. HR-MS (MALDI): m/z calcd. for $\text{C}_{383}\text{H}_{660}\text{O}_{158}$ $[\text{M} + \text{Na}]^+$ 7811.36; found 7816.05. Elemental analysis (%) calcd for $\text{C}_{383}\text{H}_{660}\text{O}_{158}$, 7793.33: C, 59.03; H, 8.54. Found: C, 58.44; H, 8.48.

Poly(3,4,5-Tris(2-(2-(2-(3,4,5-tris(2-(2-(2-(3,4,5-tris(2-(2-(2-ethoxyethoxy)ethoxy)ethoxy)benzyloxy)ethoxy)ethoxy)ethoxy)benzyloxy)ethoxy)ethoxy)ethoxy)benzyl methacrylate) [PG3(ET)].

According to general procedure I from **14c** (0.3 g, 0.038 mmol) and AIBN (1.5 mg), polymerization was carried out first at 65 °C for 12 h, then at 80 °C for another 6 h. After purification **PG3(ET)** was yielded (0.15 g,



50%) as a high viscous oil. ^1H NMR (CD_2Cl_2): δ = 1.19 (b, 81H, CH_3), 3.50–3.84 (m, 444H, CH_2), 4.12–4.15 (m, 78H, CH_2), 4.44 (b, 24H, CH_2), 6.60 (m, 26H, CH). ^{13}C NMR (CD_2Cl_2): δ = 15.45, 66.77, 69.08, 69.91, 70.09, 70.22, 70.82, 70.93, 70.99, 71.11, 72.69, 73.42, 106.98, 134.42, 137.86, 152.97. Elemental analysis (%) calcd for $(\text{C}_{383}\text{H}_{660}\text{O}_{158})_n$, (7793.33) $_n$: C, 59.03; H, 8.54. Found: C, 58.42; H, 8.43.

8.3.4 Compounds of Chapter 4.3

General procedure for synthesis of G1 benzyl chloride (L). SOCl_2 (6.45 mmol) in DCM (5 mL) was added dropwise into the solution of benzyl alcohol (1.29 mmol) and DMAP (2.57 mmol) in DCM (20 mL). The mixture was stirred at r.t. for 4 h. After being successively washed with saturated NaHCO_3 and brine, the organic phase was dried over MgSO_4 . Purification by column chromatography with DCM/MeOH (20:1 then 10:1, v/v) afforded the product as colorless oil.

General procedure for synthesis of G2 benzyl chloride (M). SOCl_2 (5.80 mmol) in DCM (4 mL) was added dropwise into the solution of benzyl alcohol (0.29 mmol) and DMAP (1.74 mmol) in DCM (20 mL). The mixture was stirred at r.t. for 4 h. After being successively washed with saturated NaHCO_3 and brine, the organic phase was dried over MgSO_4 . Purification by column chromatography with DCM/MeOH (20:1 then 10:1, v/v) afforded the product as colorless oil.

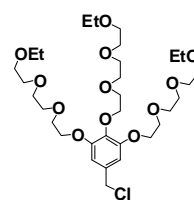
General procedure for synthesis of G1 dendrimer (N). A mixture of THPE (0.20 mmol), benzyl chloride (0.65 mmol), KI (0.13 mmol), and potassium carbonate (2.00 mmol) in dry DMF (30 mL) was stirred at 80 °C over 24 h. After removal of DMF *in vacuo*, the residue was dissolved in DCM and washed sequentially with saturated NaHCO_3 and brine. After drying over MgSO_4 , purification by column chromatography with DCM/MeOH (20:1, v/v) afforded dendrimer G1 as a colorless oil.

General procedure for synthesis of G2 dendrimer (O). A mixture of THPE (0.097 mmol), benzyl chloride (0.43 mmol), KI (0.32 mmol) and cesium carbonate (1.94 mmol) in dry DMF (30 mL) was stirred at 80 °C over 48 h. After removal of DMF *in vacuo*, the residue was dissolved in DCM and washed sequentially with saturated NaHCO_3 and brine. After drying over MgSO_4 , purification by column chromatography with DCM/MeOH (10:1, v/v) afforded dendrimer G2 as a colorless oil.

3,4,5-Tris(2-(2-(2-ethoxyethoxy)ethoxy)ethoxy)benzyl chloride (15).

According to general procedure L from SOCl_2 (0.77 g, 6.45 mmol), DCM (5 mL), **8e** (0.82 g, 1.29 mmol), DMAP (0.31 g, 2.57 mmol) and DCM (20 mL), **15** was yielded as colorless oil (0.71 g, 84%).

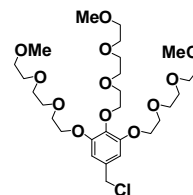
^1H NMR (CD_2Cl_2): δ 1.16–1.19 (m, 9H, CH_3), 3.47–3.69 (m, 30H, CH_2), 3.76 (t, 2H, CH_2), 3.84 (t, 4H, CH_2), 4.12 (t, 2H, CH_2), 4.16 (t, 4H, CH_2), 4.54 (s,



2H, CH₂), 6.66 (s, 2H, CH). ¹³C NMR (CD₂Cl₂): δ 15.40, 47.17, 66.80, 69.20, 70.05, 70.22, 70.84, 70.94, 71.03, 71.15, 72.73, 108.30, 133.26, 138.76, 153.08. HR-MS (MALDI): m/z calcd. for C₃₁H₅₅O₁₂Cl [M + Na]⁺ 677.34; found 677.3285. Elemental analysis (%) calcd for C₃₁H₅₅O₁₂Cl, 655.22: C, 56.83; H, 8.46. Found: C, 56.82; H, 8.39.

3,4,5-Tris(2-(2-(2-methoxyethoxy)ethoxy)ethoxy)benzyl chloride (16).

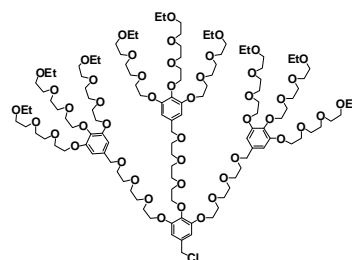
According to general procedure L from SOCl₂ (2.00 g, 16.81 mmol), DCM (5 mL), **6b** (2.00 g, 3.36 mmol), DMAP (0.8 g, 6.55 mmol) and DCM (40 mL), **16** was yielded as a colorless oil (1.70 g, 82%).



¹H NMR (CD₂Cl₂): δ 3.33 (s, 9H, CH₃), 3.49–3.51 (m, 6H, CH₂), 3.59–3.70 (m, 18H, CH₂), 3.76 (t, 2H, CH₂), 3.84 (t, 4H, CH₂), 4.12 (t, 2H, CH₂), 4.16 (t, 4H, CH₂), 4.53 (s, 2H, CH₂), 6.65 (s, 2H, CH). ¹³C NMR (CD₂Cl₂): δ 46.91, 58.74, 68.96, 69.80, 70.54, 70.56, 70.59, 70.68, 70.90, 72.05, 72.48, 108.05, 133.00, 138.52, 152.83. HR-MS (MALDI): m/z calcd. for C₂₈H₄₉O₁₂Cl [M + Na]⁺ 635.29; found 635.2816. Elemental analysis (%) calcd for C₂₈H₄₉O₁₂Cl, 613.14: C, 54.85; H, 8.05. Found: C, 54.56; H, 7.91.

3,4,5-Tris(2-(2-(2-(3,4,5-tris(2-(2-(2-ethoxyethoxy)ethoxy)ethoxy)benzyl-oxy)ethoxy)ethoxy)benzyl chloride (17).

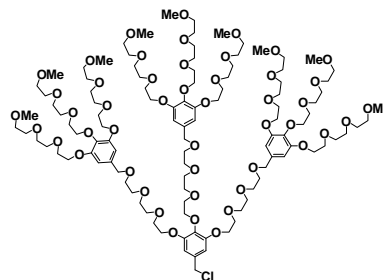
According to general procedure M from SOCl₂ (0.69 g, 5.80 mmol), DCM (4 mL), **9e** (0.70 g, 0.29 mmol), DMAP (0.21 g, 1.74 mmol) and DCM (20 mL), **17** was yielded as a colorless oil (0.51 g, 72%).



¹H NMR (CD₂Cl₂): δ 1.19–1.23 (m, 27H, CH₃), 3.48–3.74 (m, 114H, CH₂), 3.79 (t, 8H, CH₂), 3.85–3.88 (m, 16H, CH₂), 4.12–4.18 (m, 24H, CH₂), 4.47 (s, 6H, CH₂), 4.56 (s, 2H, CH₂), 6.63 (s, 6H, CH), 6.69 (s, 2H, CH). ¹³C NMR (CD₂Cl₂): δ 15.15, 46.90, 66.54, 68.82, 68.90, 68.93, 69.66, 69.79, 69.84, 69.97, 70.58, 70.68, 70.70, 70.76, 70.77, 70.88, 72.43, 73.20, 106.83, 107.90, 134.18, 137.62, 152.72, 152.82, 152.83. HR-MS (MALDI): m/z calcd. for C₁₁₈H₂₀₅O₄₈Cl [M + Na]⁺ 2448.33; found 2448.312. Elemental analysis (%) calcd for C₁₁₈H₂₀₅O₄₈Cl, 2427.34: C, 58.39; H, 8.51. Found: C, 58.29; H, 8.38.

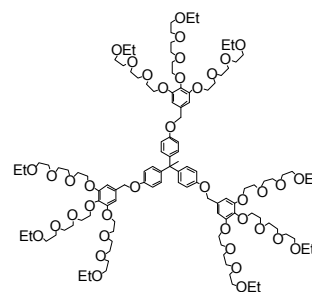
3,4,5-Tris(2-(2-(2-(3,4,5-tris(2-(2-(2-methoxyethoxy)ethoxy)ethoxy)benzyl-oxy)ethoxy)ethoxy)benzyl chloride (18).

According to general procedure **M** from SOCl_2 (1.53 g, 12.88 mmol), DCM (5 mL), **7b** (1.47 g, 0.64 mmol), DMAP (0.47 g, 3.86 mmol) and DCM (30 mL), **18** was yielded as a colorless oil (1.10 g, 74%). ^1H NMR (CD_2Cl_2): δ 3.33–3.34 (m, 27H, CH_3), 3.49–3.52 (m, 18H, CH_2), 3.58–3.69 (m, 78H, CH_2), 3.75 (t, 8H, CH_2), 3.82–3.83 (m, 16H, CH_2), 4.10 (t, 8H, CH_2), 4.13–4.16 (m, 16H, CH_2), 4.44 (s, 6H, CH_2), 4.53 (s, 2H, CH_2), 6.59 (s, 6H, CH), 6.65 (s, 2H, CH). ^{13}C NMR (CD_2Cl_2): δ 47.16, 59.00, 69.06, 69.17, 69.91, 70.06, 70.09, 70.79, 70.81, 70.93, 70.95, 71.12, 72.30, 72.68, 73.45, 107.05, 108.33, 134.43, 137.87, 138.73, 152.97, 153.06. HR-MS (MALDI): m/z calcd. for $\text{C}_{109}\text{H}_{187}\text{O}_{48}\text{Cl}$ $[\text{M} + \text{Na}]^+$ 2322.19; found 2322.174. Elemental analysis (%) calcd for $\text{C}_{109}\text{H}_{187}\text{O}_{48}\text{Cl}$, 2301.10: C, 56.89; H, 8.19. Found: C, 55.91; H, 8.01.



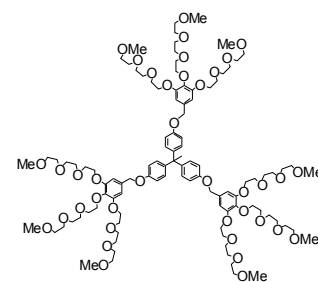
5,5',5''-(4,4',4''-(ethane-1,1,1-triyl)tris(benzene-4,1-diyl))tris(oxy)tris(methylene)tris(1,2,3-tris(2-(2-(2-ethoxyethoxy)ethoxy)ethoxy)benzene)(Et-G1).

According to general procedure **N** from 1, 1, 1-Tris(4-hydroxy-phenyl)ethane (85.8 mg, 0.28 mmol), **15** (0.6 g, 0.92 mmol), KI (28.8 mg, 0.18 mmol), K_2CO_3 (387.0 mg, 2.80 mmol) and dry DMF (40 mL), **Et-G1** was yielded as a colorless oil (0.53 g, 88%). ^1H NMR (CD_2Cl_2): δ 1.16–1.20 (m, 27H, CH_3), 2.08–2.11 (m, 3H, CH_3), 3.46–3.68 (m, 90H, CH_2), 3.76–3.77 (m, 6H, CH_2), 3.83–3.84 (m, 12H, CH_2), 4.12–4.16 (m, 18H, CH_2), 4.93 (s, 4H, CH_2), 4.96 (s, 2H, CH_2), 6.66–6.74 (m, 6H, CH), 6.84–6.88 (m, 6H, CH), 6.99–7.03 (m, 6H, CH). ^{13}C NMR (CD_2Cl_2): δ 15.15, 30.71, 50.70, 50.78, 66.55, 68.85, 68.91, 69.79, 69.83, 69.97, 70.13, 70.20, 70.59, 70.69, 70.75, 70.77, 70.85, 70.89, 72.47, 106.81, 106.95, 114.02, 114.21, 114.66, 129.73, 132.77, 132.84, 137.93, 138.05, 142.21, 142.36, 152.83, 152.88, 156.83, 157.01. HR-MS (MALDI): m/z calcd. for $\text{C}_{113}\text{H}_{180}\text{O}_{39}$ $[\text{M} + \text{Na}]^+$ 2184.21; found 2184.206. Elemental analysis (%) calcd for $\text{C}_{113}\text{H}_{180}\text{O}_{39}$, 2162.64: C, 62.76; H, 8.39. Found: C, 62.75; H, 8.21.



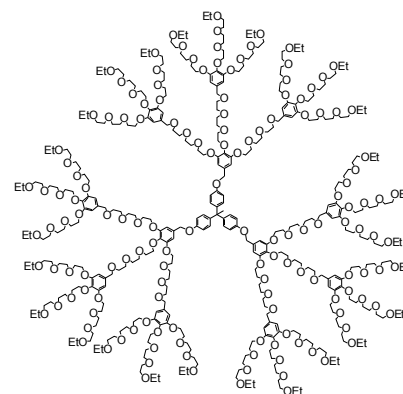
5,5',5''-(4,4',4''-(ethane-1,1,1-triyl)tris(benzene-4,1-diyl))tris(oxy)tris(methylene) tris(1,2,3-tris(2-(2-(2methoxyethoxy)ethoxy)ethoxy)ethoxy)benzene)(Me-G1).

According to general procedure **N** from 1, 1, 1-Tris(4-hydroxy-phenyl)ethane (60.6 mg, 0.20 mmol), **16** (0.40 g, 0.65 mmol), KI (20.8 mg, 0.13 mmol), and K₂CO₃ (276.4 mg, 2.00 mmol) in dry DMF (30 mL), **Me-G1** was yielded as a colorless oil (0.36 g, 90%). ¹H NMR (CD₂Cl₂): δ 2.08–2.17 (m, 3H, CH₃), 3.33–3.34 (m, 27H, CH₃), 3.49–3.69 (m, 72H, CH₂), 3.76–3.78 (m, 6H, CH₂), 3.81–3.85 (m, 12H, CH₂), 4.12–4.17 (m, 18H, CH₂), 4.93 (s, 4H, CH₂), 4.96 (s, 2H, CH₂), 6.66–6.70 (m, 6H, CH), 6.84–6.88 (m, 6H, CH), 6.99–7.03 (m, 6H, CH). ¹³C NMR (CD₂Cl₂): δ 30.58, 50.70, 50.78, 58.74, 68.85, 68.91, 69.79, 69.82, 70.13, 70.20, 70.52, 70.55, 70.68, 70.85, 70.88, 72.04, 72.44, 72.47, 106.81, 106.95, 114.03, 114.20, 114.64, 129.72, 132.78, 132.85, 137.91, 138.03, 142.21, 142.35, 152.83, 152.87, 156.83, 157.01. HR-MS (MALDI): m/z calcd. for C₁₀₄H₁₆₂O₃₉ [M + Na]⁺ 2058.07; found 2058.063. Elemental analysis (%) calcd for C₁₀₄H₁₆₂O₃₉, 2036.40: C, 61.34; H, 8.02. Found: C, 61.07; H, 7.87.



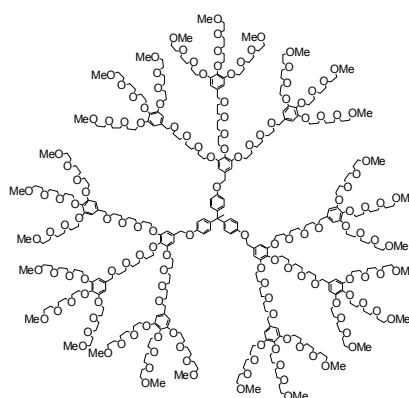
Et-G2.


According to general procedure **O** from 1, 1, 1-Tris(4-hydroxy-phenyl)ethane (5.5 mg, 0.018 mmol), **17** (200.0 g, 0.082 mmol), KI (9.6 mg, 0.06 mmol), Cs₂CO₃ (117.3 mg, 0.36 mmol) and dry DMF (20 mL), **Et-G2** was yielded as a colorless oil (0.10 g, 74%). ¹H NMR (CD₂Cl₂): δ 1.18–1.23 (m, 81H, CH₃), 2.14 (s, 3H, CH₃), 3.45–3.88 (m, 414H, CH₂), 4.12–4.19 (m, 72H, CH₂), 4.47 (s, 18H, CH₂), 4.95 (s, 6H, CH₂), 6.63 (s, 18H, CH), 6.73 (s, 6H, CH), 6.93 (d, 6H, CH), 7.06 (d, 6H, CH). ¹³C NMR (CD₂Cl₂): δ 4.60, 15.01, 60.57, 66.39, 68.71, 69.53, 69.71, 69.82, 70.09, 70.54, 70.56, 70.61, 70.63, 70.74, 72.30, 72.37, 73.04, 106.72, 106.88, 107.13, 129.61, 132.57, 134.05, 137.00, 137.55, 142.08, 152.59, 152.74, 156.90. HR-MS (MALDI): m/z calcd. for C₃₇₄H₆₃₀O₁₄₇ [M + Na]⁺ 7497.18; found 7506.85. Elemental analysis (%) calcd for C₃₇₄H₆₃₀O₁₄₇, 7479.00: C, 60.06; H, 8.49. Found: C, 59.59; H, 8.24.




Me-G2.

According to general procedure **O** from **1**, **1**, **1**-Tris(4-hydroxy-phenyl)ethane (29.7 mg, 0.097 mmol), **18** (1.00 g, 0.43 mmol), KI (51.2 mg, 0.32 mmol), Cs₂CO₃ (632.1 mg, 1.94 mmol) and dry DMF (30 mL), **Me-G2** was yielded as a colorless oil (0.5 g, 73%). ¹H NMR (CD₂Cl₂): δ 2.14 (s, 3H, CH₃), 3.36–3.37 (m, 81H, CH₃), 3.53–3.87 (m, 360H, CH₂), 4.12–4.19 (m, 72H, CH₂), 4.46 (s, 18H, CH₂), 4.95 (s, 6H, CH₂), 6.62 (s, 18H, CH), 6.73 (s, 6H, CH), 6.93 (d, 6H, CH), 7.06 (d, 6H, CH). ¹³C NMR (CD₂Cl₂): δ 58.59, 68.70, 68.79, 69.53, 69.70, 70.09, 70.38, 70.40, 70.42, 70.53, 70.55, 70.72, 71.90, 72.28, 72.37, 73.04, 106.72, 106.88, 113.84, 129.62, 132.58, 134.05, 137.53, 137.95, 142.08, 152.58, 152.73, 156.94. HR-MS (MALDI): *m/z* calcd. for C₃₄₇H₅₇₆O₁₄₇ [M + Na]⁺ 7118.76; found 7125.62. Elemental analysis (%) calcd for C₃₄₇H₅₇₆O₁₄₇, 7100.28: C, 58.70; H, 8.18. Found: C, 58.44; H, 8.06.

**8.3.5 Compounds of Chapter 4.4****8-hydroxyoctyl 4-methylbenzenesulfonate (19b).**

According to general procedure **A** from TsCl (4.35 g, 22.8 mmol) in  THF (20 mL), NaOH (1.37 g, 34.2 mmol) aqueous solution (20 mL), octamethylene glycol (10 g, 68.5 mmol) in THF (60 mL). Purification by column chromatography with hexane/ethyl acetate (first 3:1, then 2:1) afforded **19b** as a colourless oil. (3.87 g, 56%). ¹H NMR (CDCl₃): δ = 1.23–1.28 (m, 8H, CH₂), 1.50–1.53 (m, 2H, CH₂), 1.60–1.63 (m, 2H, CH₂), 2.43 (s, 3H, CH₃), 3.61 (t, 2H, CH₂), 4.00 (t, 2H, CH₂), 7.32 (d, 2H, CH), 7.76 (d, 2H, CH). ¹³C NMR (CDCl₃): δ = 21.78, 25.39, 25.68, 28.92, 28.98, 29.25, 32.62, 63.12, 70.82, 128.02, 129.97, 133.33, 144.83. HR-MS (ESI): *m/z* calcd. for C₁₅H₂₄O₄S [M + Na]⁺ 323.14; found 323.1287.

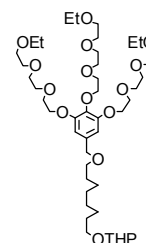
8-(tetrahydro-2H-pyran-2-yloxy)octyl 4-methylbenzenesulfonate (19c).

Pyridinium toluenesulfonate (PPTS) (0.65 g, 2.58 mmol) was added  to a mixture of **19b** (3.87 g, 12.88 mmol), 3,4-dihydro-2H-pyran (DHP) (1.30 g, 15.46 mmol) in dry DCM (40 mL) at -5 °C, the mixture was stirred for 30 min, then warmed to r.t. and stirred for another 4 h. After washing with brine, the organic phase was

dried over MgSO_4 . Purification by column chromatography with hexane / ethyl acetate (6:1, v/v) afforded **19c** (4.25 g, 86 %) as a colourless oil. ^1H NMR (CD_2Cl_2): δ = 1.22–1.28 (m, 8H, CH_2), 1.52–1.62 (m, 8H, $\text{CH}_2 + \text{CH}_2^{\text{a}} + \text{CH}_2^{\text{m}}$), 1.67–1.71 (m, 1H, CH_2^{b}), 1.80–1.81 (m, 1H, CH_2^{n}), 2.43 (s, 3H, CH_3), 3.32–3.37 (m, 1H, CH_2^{a}), 3.47–3.49 (m, 1H, CH_2^{b}), 3.67–3.72 (m, 1H, CH_2^{x}), 3.82–3.86 (m, 1H, CH_2^{y}), 3.40 (t, 2H, CH_2), 4.54–4.55 (m, 1H, CH), 7.32 (d, 2H, CH), 7.76 (d, 2H, CH). ^{13}C NMR (CDCl_3): δ = 19.88, 21.78, 25.42, 25.64, 26.23, 28.93, 28.99, 29.35, 29.82, 30.93, 62.55, 67.73, 70.81, 99.05, 128.02, 129.95, 133.37, 144.78. HR-MS (ESI): m/z calcd. for $\text{C}_{20}\text{H}_{32}\text{O}_5\text{S}$ $[\text{M} + \text{Na}]^+$ 407.20; found 407.1871.

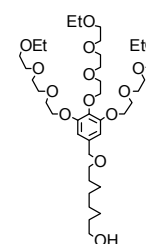
2-(8-(3,4,5-tris(2-(2-(2-ethoxyethoxy)ethoxy)ethoxy)benzyloxy)octyloxy)tetrahydro-2H-pyran (20a).

According to general procedure **E** from **19c** (2.75 g, 7.15 mmol) in dry THF (8 mL), **8e** (3.50 g, 5.50 mmol), KI (0.18 g, 1.10 mmol), 15-crown-5 (1.21 g, 5.50 mmol) and NaH (0.66 g, 27.48 mmol) in dry THF (25 mL), purification by column chromatography with DCM/MeOH (30:1, v/v) afforded **20a** as a colorless oil (4.5 g, 96 %). ^1H NMR (CD_2Cl_2): δ = 1.17–1.19 (m, 9H, CH_3), 1.33 (br, 8H, CH_2), 1.50–1.80 (m, 10H, CH_2), 3.32–3.70 (m, 35H, $\text{CH}_2 + \text{CH}_2^{\text{a}}$), 3.76 (t, 2H, CH_2), 3.80–3.85 (m, 5H, $\text{CH}_2 + \text{CH}_2^{\text{b}}$), 4.09–4.16 (m, 6H, CH_2), 4.38 (s, 2H, CH_2), 4.53–4.54 (m, 1H, CH), 6.58 (s, 2H, CH). ^{13}C NMR (CDCl_3): δ = 15.15, 19.83, 25.74, 26.35, 29.60, 29.62, 29.92, 30.96, 62.19, 66.54, 67.56, 68.79, 69.85, 69.97, 70.57, 70.60, 70.68, 70.70, 70.74, 70.77, 70.88, 72.42, 72.80, 98.87, 106.66, 134.72, 137.50, 152.67. HR-MS (MALDI): m/z calcd. for $\text{C}_{44}\text{H}_{80}\text{O}_{15}$ $[\text{M} + \text{Na}]^+$ 871.55; found 871.5399.



8-(3,4,5-tris(2-(2-(2-ethoxyethoxy)ethoxy)ethoxy)benzyloxy)octan-1-ol (20b).

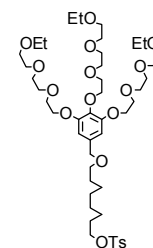
According to general procedure **G** from PTSA (0.83 g, 4.36 mmol), **20a** (3.7 g, 4.36 mmol) and MeOH (40 mL), purification by column chromatography with DCM/MeOH (20:1, v/v) afforded **20b** as a colorless oil (3.0 g, 90%). ^1H NMR (CD_2Cl_2): δ = 1.16–1.19 (m, 9H, CH_3), 1.32 (br, 8H, CH_2), 1.52–1.60 (m, 4H, CH_2), 3.42–3.70 (m, 34H, CH_2), 3.76 (t, 2H, CH_2), 3.84 (t, 4H, CH_2), 4.10 (t, 2H, CH_2), 4.14 (t, 4H, CH_2), 4.38 (s, 2H, CH_2), 6.58 (s, 2H, CH). ^{13}C NMR (CDCl_3): δ = 15.14, 25.85, 26.31, 29.54, 29.88, 32.99, 62.79,



66.55, 68.78, 69.85, 69.96, 70.49, 70.57, 70.68, 70.70, 70.76, 70.87, 72.42, 72.78, 106.67, 134.73, 137.49, 152.67. HR-MS (MALDI): m/z calcd. for $C_{39}H_{72}O_{14}$ $[M + Na]^+$ 787.49; found 787.4815.

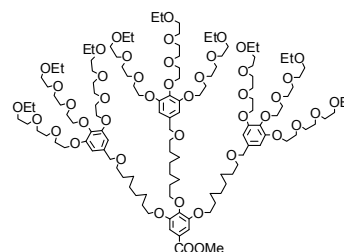
8-(3,4,5-tris(2-(2-(2-ethoxyethoxy)ethoxy)ethoxy)benzyloxy)octyl 4-methyl benzenesulfonate (20c).

TsCl (1.43 g, 7.48 mmol) was added to a solution of **20b** (2.86 g, 3.74 mmol), triethyl amine (1.89 g, 18.70 mmol), DMAP (0.10 g) in dry DCM (35 mL) at $-5\text{ }^{\circ}\text{C}$. The mixture was stirred for another 3 h at room temperature. It was then washed with brine and the organic phase dried over $MgSO_4$. After filtration, the solvent was evaporated *in vacuo* at room temperature. Purification with column chromatography with DCM/MeOH (30:1, v/v) afforded **20c** (3.05 g, 89%) as a colorless oil. 1H NMR (CD_2Cl_2): δ = 1.16–1.19 (m, 9H, CH_3), 1.24–1.29 (m, 8H, CH_2), 1.53–1.62 (m, 4H, CH_2), 2.44 (s, 3H, CH_3), 3.41–3.70 (m, 32H, CH_2), 3.76 (t, 2H, CH_2), 3.84 (t, 4H, CH_2), 3.99 (t, 2H, CH_2), 4.10 (t, 2H, CH_2), 4.14 (t, 4H, CH_2), 4.37 (s, 2H, CH_2), 6.58 (s, 2H, CH), 7.38 (d, 2H, CH), 7.77 (d, 2H, CH). ^{13}C NMR ($CDCl_3$): δ = 15.15, 21.49, 25.40, 26.23, 28.89, 28.99, 29.38, 29.86, 66.55, 68.79, 69.84, 69.97, 70.52, 70.57, 70.68, 70.70, 70.76, 70.87, 70.97, 72.42, 72.82, 106.69, 127.91, 129.97, 133.32, 134.68, 137.51, 145.02, 152.67. HR-MS (MALDI): m/z calcd. for $C_{46}H_{78}O_{16}S$ $[M + Na]^+$ 941.50; found 941.4918.



methyl 3,4,5-tris(8-(3,4,5-tris(2-(2-(2-ethoxyethoxy)ethoxy)ethoxy)benzyloxy)octyloxy)benzoate (21a).

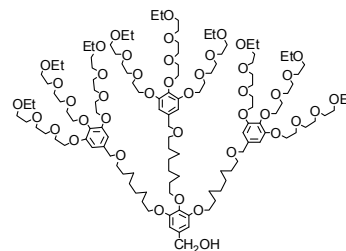
According to general procedure **B** from **20c** (3.6 g, 3.92 mmol), methyl gallate (0.22 g, 1.19 mmol), KI (0.15 g, 0.95 mmol), and potassium carbonate (K_2CO_3) (1.64 g, 11.87 mmol) in dry DMF (20 mL), purification by column chromatography with DCM/MeOH (30:1 then 20:1, v/v) afforded **21a** (2.4 g, 83%) as a slight yellow oil. 1H NMR (CD_2Cl_2): δ = 1.16–1.19 (m, 27H, CH_3), 1.35–1.37 (m, 18H, CH_2), 1.47–1.61 (m, 12H, CH_2), 1.71–1.83 (m, 6H, CH_2), 3.43–3.77 (m, 102H, CH_2), 3.83–3.86 (m, 15H, $CH_2 + CH_3$), 3.99–4.02 (m, 6H, CH_2), 4.09–4.14 (m, 18H, CH_2), 4.38 (s, 6H, CH_2), 6.58 (s, 6H, CH), 7.24 (s, 2H, CH). ^{13}C NMR (CD_2Cl_2): δ = 15.40, 26.40, 26.62, 26.68, 29.70, 29.75, 29.91, 29.99,



30.20, 30.69, 52.31, 66.79, 69.05, 69.49, 70.10, 70.22, 70.83, 70.89, 70.94, 70.95, 71.00, 71.02, 71.13, 72.67, 73.08, 73.74, 106.91, 108.06, 125.19, 134.96, 137.75, 142.52, 152.93, 153.22, 167.03. HR-MS (MALDI): m/z calcd. for $C_{125}H_{218}O_{44}$ $[M + Na]^+$ 2446.48; found 2446.472.

(3,4,5-tris(8-(3,4,5-tris(2-(2-(2-ethoxyethoxy)ethoxy)ethoxy)benzyloxy)octyloxy)phenyl)methanol (21b).

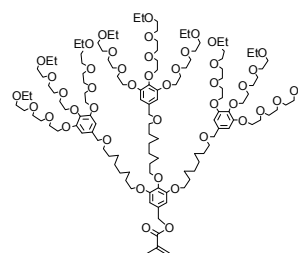
According to general procedure **C** from LAH (66.67 mg, 1.76 mmol), **21a** (2.13 g, 0.88 mmol) and dry THF (30 mL), the mixture was stirred for 2 h after warmed to r.t., purification by column chromatography with DCM/MeOH (15:1, v/v) afforded **21b** (2 g, 95%) as a colorless oil. 1H



NMR (CD_2Cl_2): δ = 1.16–1.19 (m, 27H, CH_3), 1.36 (br, 18H, CH_2), 1.47–1.60 (m, 12H, CH_2), 1.70–1.79 (m, 6H, CH_2), 3.43–3.69 (m, 96H, CH_2), 3.75–3.83 (m, 18H, CH_2), 3.90 (t, 2H, CH_2), 3.95 (t, 4H, CH_2), 4.09–4.14 (m, 18H, CH_2), 4.38 (s, 6H, CH_2), 4.55 (s, 2H, CH_2), 6.56 and 6.58 (2s, 8H, CH). ^{13}C NMR (CD_2Cl_2): δ = 15.15, 26.14, 26.24, 26.36, 26.42, 29.48, 29.54, 29.61, 29.68, 29.73, 29.92, 29.98, 30.42, 65.17, 66.55, 68.79, 69.05, 69.84, 69.96, 70.57, 70.60, 70.68, 70.70, 70.76, 70.87, 72.42, 72.81, 73.34, 105.05, 106.65, 134.72, 136.87, 137.18, 137.49, 152.67, 153.26. HR-MS (MALDI): m/z calcd. for $C_{124}H_{218}O_{43}$ $[M + Na]^+$ 2418.49; found 2418.473.

3,4,5-tris(8-(3,4,5-tris(2-(2-(2-ethoxyethoxy)ethoxy)ethoxy)benzyloxy)octyloxy)benzyl methacrylate (21c).

According to general procedure **D** from MAC (0.33 g, 3.13 mmol), **21b** (1.50 g, 0.63 mmol), triethyl amine (0.32 g, 3.13 mmol), DMAP (0.10 g) and dry DCM (30 mL), the mixture was stirred for another 3 h at r.t., purification with column chromatography with DCM/MeOH (30:1, v/v) afforded **21c** (1.3



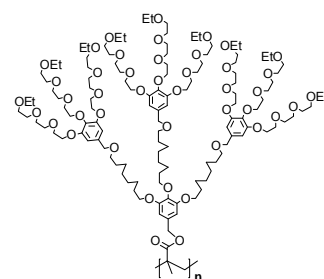
g, 84%) as a colorless oil. 1H NMR (CD_2Cl_2): δ = 1.16–1.19 (m, 27H, CH_3), 1.36–1.52 (m, 24H, CH_2), 1.59–1.81 (m, 12H, CH_2), 2.16 (br, 3H, CH_3), 3.43–3.84 (m, 114H, CH_2), 3.90–3.97 (m, 6H, CH_2), 4.09–4.16 (m, 18H, CH_2), 4.38 (s, 6H, CH_2), 5.07 (s, 2H, CH_2), 5.59 (s, 1H, CH_2^a), 6.12 (s, 1H, CH_2^b), 6.55–6.58 (m, 8H, CH). ^{13}C NMR (CD_2Cl_2): δ = 15.15, 18.25, 26.18, 26.25, 26.38, 26.43, 29.52, 29.65, 29.70, 29.76, 29.95, 29.99, 30.45, 66.54, 66.68, 68.80, 69.12, 69.85, 69.97, 70.75, 70.62, 70.68,

70.76, 70.88, 70.94, 72.42, 72.82, 73.39, 106.50, 106.66, 125.45, 131.43, 134.70, 136.62, 137.51, 137.94, 152.67, 153.26, 167.11. HR-MS (MALDI): m/z calcd. for $C_{128}H_{222}O_{44}$ $[M + Na]^+$ 2486.51; found 2486.497. Elemental analysis (%) calcd for $C_{128}H_{222}O_{44}$, 2465.14: C, 62.37; H, 9.08. Found: C, 62.08; H, 8.97.

Poly(3,4,5-tris(8-(3,4,5-tris(2-(2-(2-ethoxyethoxy)ethoxy)ethoxy)benzyloxy)octyloxy)benzyl methacrylate) [PG2(ETalkyl)]).

According to general procedure I, from monomer **21c** (0.4 g, 0.16 mmol) and AIBN (2 mg), polymerization for 14 h at 60 °C yielded the polymer which couldn't dissolve well in DCM.

According to general procedure I, from monomer **21c** (0.2 g, 0.08 mmol) and AIBN (1 mg), polymerization for 3 h at 60 °C yielded the polymer as a gel with little turbid (90.00 mg, 45%). 1H NMR (CD_2Cl_2): δ = 1.13–1.14 (m, 30H, CH_3), 1.34 (br, 24H, CH_2), 1.59 and 1.69 (2br, 12H, CH_2), 1.97 (br, 2H, CH_2), 3.42–3.75 (m, 120H, CH_2), 4.05 (br, 18H, CH_2), 4.32



(br, 6H, CH_2), 6.51 (br, 8H, CH). ^{13}C NMR (CD_2Cl_2): δ = 15.23, 26.75, 30.19, 66.48, 68.85, 69.82, 69.96, 70.55, 70.65, 70.68, 70.71, 70.83, 70.93, 72.45, 72.83, 106.39, 134.58, 137.54, 152.69. The signals from the polymer backbone were so broad that they disappeared in the baseline. Elemental analysis (%) calcd for $(C_{128}H_{222}O_{44})_n$, (2465.14) $_n$: C, 62.37; H, 9.08. Found: C, 61.33; H, 8.93.

8.3.6 Compounds of Chapter 5.1

General procedure for saponification of methyl ester by $LiOH \cdot H_2O$ (P). $LiOH \cdot H_2O$ was added into a solution of methyl ester in methanol and water at -5 °C with stirring, and then the reaction temperature was allowed to rise to room temperature. After stirred for 6 h, the solvents were evaporated *in vacuo* at room temperature, and the residue was dissolved with DCM. The pH value of the solution was adjusted carefully to around 5~6 with 10% $KHSO_4$ aqueous solution. The organic phase was washed with brine. All aqueous phase was extracted with DCM three times. The combined organic phase was dried over $MgSO_4$. After filtration, the solvent was evaporated *in*

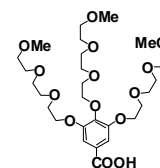
vacuo. Purification by column chromatography with DCM/MeOH (15:1 then 10:1, v/v) afforded the corresponding acid.

General procedure for Pfp active ester (Q). DCC (18.73 mmol) was added into a solution of acid and pentafluoro-phenol in DCM at -15°C , and the mixture was stirred at room temperature over night. After the solid was filtered off, purification by column chromatography with DCM/MeOH (30:1, v/v) afforded the corresponding active ester.

General procedure for amide coupling (R): The amine and DiPEA in dry DCM was added into a solution of active ester in dry DCM at -15°C . After stirring over night, the mixture was washed successively with NaHCO_3 and brine, and all aqueous phases were extracted with DCM three times. The combined organic phases were dried over MgSO_4 . After filtration, the solvent was evaporated *in vacuo*. Purification with column chromatography afforded the product.

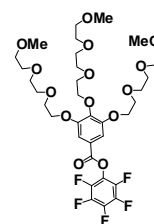
3,4,5-tris(2-(2-(2-methoxyethoxy)ethoxy)ethoxy)benzoic acid (**22a**).

According to general procedure **P** from $\text{LiOH}\cdot\text{H}_2\text{O}$ (6.06 g, 144.53 mmol) and compound **6a** (9.0 g, 14.45 mmol) in MeOH (60 mL) and H_2O (12 mL), **22a** was yielded as colorless oil (8.0 g, 91%). ^1H NMR (CD_2Cl_2): δ = 3.34 (s, 9H, CH_3), 3.50–3.71 (m, 24H, CH_2), 3.78 (t, 2H, CH_2), 3.86 (t, 4H, CH_2), 4.19–4.24 (m, 6H, CH_2), 7.35 (s, 2H, CH). ^{13}C NMR (CD_2Cl_2): δ = 58.74, 68.90, 69.72, 70.49, 70.52, 70.58, 70.65, 70.71, 70.85, 72.02, 72.55, 109.18, 124.93, 142.78, 152.40, 169.88. HR-MS (MALDI): m/z calcd. for $\text{C}_{28}\text{H}_{48}\text{O}_{14}$ $[\text{M} + \text{Na}]^+$ 631.30; found 631.2940.



3,4,5-tris(2-(2-(2-methoxyethoxy)ethoxy)ethoxy)benzoic pentafluoro-phenol ester (**22b**).

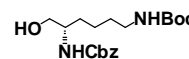
According to general procedure **Q** from DCC (3.86 g, 18.73 mmol), **22a** (7.6 g, 12.49 mmol) and pentafluoro-phenol (2.76 g, 14.98 mmol) in DCM (40 mL), **22b** was yielded as a colorless oil (8.7 g, 90 %). ^1H NMR (CD_2Cl_2): δ = 3.32 and 3.34 (2s, 9H, CH_3), 3.48–3.71 (m, 24H, CH_2), 3.80 (t, 2H, CH_2), 3.88 (t, 4H, CH_2), 4.24 (t, 4H, CH_2), 4.29 (t, 2H, CH_2), 7.47 (s, 2H, CH). ^{13}C NMR (CD_2Cl_2): δ = 58.70, 69.18, 69.67, 70.53, 70.55, 70.60, 70.67, 70.78, 70.92, 71.98, 72.03, 72.08, 72.09, 72.75, 110.01, 121.35, 137.12, 139.11,



140.61, 142.59, 144.35, 152.80, 162.30. HR-MS (MALDI): m/z calcd. for $C_{34}H_{47}F_5O_{14}$ $[M + Na]^+$ 797.29; found 797.2792.

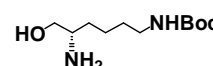
Compound 23b.

$LiBH_4$ (1.66 g, 76 mmol) was added to a solution of **23a** (15 g, 38 mmol) in dry THF (150 mL) at $-10\text{ }^\circ\text{C}$. The mixture was stirred for 2 h followed by over night at room temperature. The reaction was quenched by successive dropwise addition of ethyl acetate and water. After evaporation of the solvents *in vacuo* at room temperature, the residue was dissolved in DCM and washed with brine. The organic phase was collected and dried over $MgSO_4$. Purification by column chromatography with DCM/MeOH (20:1, v/v) afforded **23b** as white powder (13.0 g, 93 %). 1H NMR (CD_2Cl_2): δ = 1.34–1.57 (m, 15H, $CH_3 + CH_2$), 3.08–3.09 (m, 2H, CH_2), 3.56–3.62 (m, 2H, CH_2), 4.75 (br, 1H, CH), 5.08 (s, 2H, CH_2), 5.24 (br, 1H, NH), 7.32–7.36 (m, 5H, CH). ^{13}C NMR ($CDCl_3$): δ = 22.79, 28.27, 29.93, 30.05, 30.70, 39.89, 52.50, 64.96, 66.64, 78.98, 128.04, 128.11, 128.57, 137.04, 156.37. HR-MS (ESI): m/z calcd. for $C_{19}H_{30}N_2O_5$ $[M + Na]^+$ 389.22; found 389.2048.



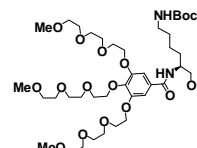
(S)-tert-butyl 5-amino-6-hydroxyhexylcarbamate (23c).

Pd/C (1.3 g, 10% by weight) was added to a solution of **23b** (12.58 g, 34.3 mmol) in ethanol/ethyl acetate (200 mL, 1/1) in a hydrogenation flask. The mixture was hydrogenated under 3 bar of H_2 at r.t. over night. After filtration, the solvent was evaporated. Further purification of the residue by column chromatography with DCM/MeOH (10:1, v/v) then MeOH afforded **23c** as white solid (13.0 g, 93 %). 1H NMR ($CDCl_3$): δ = 1.30–1.46 (m, 15H, $CH_3 + CH_2$), 2.47 (s, 3H, $NH_2 + NH$), 2.82 (s, 1H, CH), 3.10 (s, 2H, CH_2), 3.29 (t, 1H, CH_2^a), 3.56 (d, 1H, CH_2^b), 4.65 (br, 1H, OH). ^{13}C NMR ($CDCl_3$): δ = 23.26, 28.57, 30.27, 33.76, 40.36, 52.9, 66.42, 79.29, 156.27. HR-MS (ESI): m/z calcd. for $C_{11}H_{24}N_2O_3$ $[M + H]^+$ 233.18; found 233.1857.



(S)-tert-butyl 6-hydroxy-5-(3,4,5-tris(2-(2-(2-methoxyethoxy)ethoxy)ethoxy)benzamido)hexylcarbamate (24a).

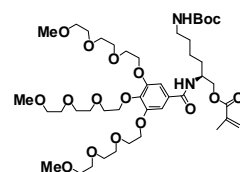
According to general procedure **R** from **22b** (4.2 g, 5.42 mmol) in DCM (10 mL), **23c** (1.51 g, 6.5 mmol) and DiPEA (3.5 g, 27.1



mmol) in DCM (40 mL), purification with column chromatography using DCM/MeOH (15:1, v/v) afforded **24a** as a colorless oil (3.7 g, 83%). ^1H NMR (CD_2Cl_2): δ = 1.39 (br, 11H, $\text{CH}_3 + \text{CH}_2$), 1.49–1.67 (m, 4H, CH_2), 3.05–3.13 (m, 2H, CH_2), 3.20 (br, 1H, CH_2^{a}), 3.31–3.34 (m, 9H, CH_3), 3.48–3.68 (m, 25H, $\text{CH}_2 + \text{CH}_2^{\text{b}}$), 3.75–3.84 (m, 6H, CH_2), 4.05 (br, 1H, CH), 4.16–4.21 (m, 6H, CH_2), 4.78 (br, 1H, NH), 6.72 (d, 1H, NH), 7.12 (s, 2H, CH). ^{13}C NMR (CD_2Cl_2): δ = 23.23, 28.25, 30.14, 30.67, 40.05, 52.33, 58.72, 58.74, 64.90, 69.21, 69.87, 70.42, 70.52, 70.60, 70.69, 70.74, 72.01, 72.05, 72.52, 78.83, 107.17, 130.03, 141.39, 152.60, 156.25, 167.35. HR-MS (MALDI): m/z calcd. for $\text{C}_{39}\text{H}_{70}\text{N}_2\text{O}_{16}$ $[\text{M} + \text{Na}]^+$ 845.47; found 845.4603.

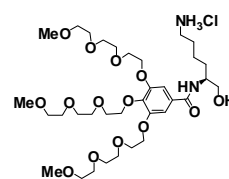
(S)-6-(tert-butoxycarbonylamino)-2-(3,4,5-tris(2-(2-methoxyethoxy)ethoxy)benzamido)hexyl methacrylate (24b).

According to general procedure **D** from **24a** (0.72 g, 0.875 mmol), TEA (0.442 g, 4.374 mmol), DMAP (0.1 g), MAC (0.274 g, 2.62 mmol) and DCM (30 mL), purification with column chromatography using DCM/MeOH (20:1, v/v) afforded **24b** as a colorless oil (0.65 g, 83%). ^1H NMR (CD_2Cl_2): δ = 1.39–1.66 (m, 15H, $\text{CH}_3 + \text{CH}_2$), 1.93 (s, 3H, CH_3), 3.08 (s, 2H, CH_2), 3.32–3.34 (m, 9H, CH_3), 3.49–3.69 (m, 24H, CH_2), 3.75–3.85 (m, 6H, CH_2), 4.17–4.26 (m, 8H, $\text{CH}_2 + \text{CH} + \text{CH}_2^{\text{a}}$), 4.36 (br, 1H, CH_2^{b}), 4.69 (br, 1H, NH), 5.58 (s, 1H, CH_2^{a}), 6.10 (s, 1H, CH_2^{b}), 6.34 (d, 1H, NH), 7.03 (s, 2H, CH). ^{13}C NMR (CD_2Cl_2): δ = 18.22, 23.24, 28.24, 30.02, 31.40, 40.34, 49.24, 58.72, 66.28, 69.13, 69.79, 70.50, 70.61, 70.65, 70.69, 70.83, 72.03, 72.05, 72.53, 78.71, 106.74, 125.83, 130.06, 136.35, 141.31, 152.65, 155.97, 166.67, 167.56. HR-MS (MALDI): m/z calcd. for $\text{C}_{43}\text{H}_{74}\text{N}_2\text{O}_{17}$ $[\text{M} + \text{Na}]^+$ 913.5; found 913.4896. Elemental analysis (%) calcd for $\text{C}_{43}\text{H}_{74}\text{N}_2\text{O}_{17}$, 891.05: C, 57.96; H, 8.37; N, 3.14. Found: C, 57.79; H, 8.17; N, 3.00.



(S)-N-(6-amino-1-hydroxyhexan-2-yl)-3,4,5-tris(2-(2-methoxyethoxy)ethoxy)benzamide (24c).

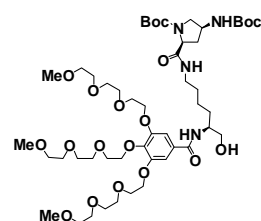
25% HCl (5.39 g, 36.94 mmol) was added to a solution of **24a** (1.52 g, 1.85 mmol) in THF (15 mL) at 0 °C. The mixture was stirred for another 10 h. After evaporation of the solvent and HCl, the residue was dissolved in water and washed with DCM. The aqueous phase was collected and **24c** was obtained as a high viscous colorless oil (1.28 g, 91%)



after evaporation of water. ^1H NMR (D_2O): δ = 1.31–1.34 (m, 2H, CH_2), 1.44–1.60 (m, 4H, CH_2), 2.86 (t, 2H, CH_2), 3.21–3.23 (m, 9H, CH_3), 3.44–3.64 (m, 26H, CH_2), 3.72 (br, 2H, CH_2), 3.81 (br, 4H, CH_2), 3.98–3.99 (m, 1H, CH), 4.15 (br, 6H, CH_2), 7.03 (s, 2H, CH). ^{13}C NMR (D_2O): δ = 22.44, 26.59, 29.77, 39.42, 51.89, 58.13, 58.15, 63.65, 68.56, 69.33, 69.56, 69.59, 69.66, 69.75, 69.79, 69.96, 70.33, 71.11, 72.21, 106.81, 129.95, 139.92, 151.99, 169.98. HR-MS (ESI): m/z calcd. for $\text{C}_{34}\text{H}_{62}\text{N}_2\text{O}_{14}$ $[\text{M} + \text{Na}]^+$ 745.42; found 745.4054.

(2S,4S)-tert-butyl 4-(tert-butoxycarbonylamino)-2-((S)-6-hydroxy-5-(3,4,5-tris(2-(2-methoxyethoxy)ethoxy)ethoxy)benzamido)hexylcarbamoyl)pyrrolidine-1-carboxylate (26a).

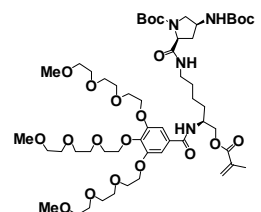
According to general procedure **R**, from **23c** (0.68 g, 0.9 mmol) and DiPEA (1.16 g, 9 mmol) in DCM (3 mL), compound **25** (0.67 g, 1.34 mmol) in DCM (25 mL), purification with column chromatography using DCM/MeOH (15:1, v/v) afforded **26a** as a white solid (0.79 g, 85%). ^1H NMR (CD_2Cl_2): δ = 1.39 (br, 20H,



$\text{CH}_3 + \text{CH}_2$), 1.57–1.65 (m, 4H, CH_2), 2.14 (br, 2H, CH_2), 3.12 (br, 1H, CH_2^a), 3.25 (br, 2H, $\text{CH}_2^b + \text{CH}_2^m$), 3.32 and 3.34 (2s, 9H, CH_3), 3.48–3.69 (m, 27H, $\text{CH}_2 + \text{CH}_2^n$), 3.75–3.84 (m, 6H, CH_2), 4.06 (br, 1H, CH), 4.16–4.22 (m, 7H, $\text{CH}_2 + \text{CH}$), 4.29 (br, 1H, CH), 6.52 (br, 1H, NH), 6.75 (br, 1H, NH), 7.13 (s, 2H, CH), 7.25 (br, 1H, NH). ^{13}C NMR (D_2O): δ = 23.23, 28.20, 28.29, 29.11, 30.55, 39.12, 50.25, 55.38, 58.72, 59.68, 65.17, 69.21, 69.86, 70.40, 70.51, 70.59, 70.67, 70.73, 72.01, 72.03, 72.51, 78.97, 80.27, 80.71, 107.27, 141.38, 152.57, 155.35, 167.42, 170.46, 172.68. HR-MS (MALDI): m/z calcd. for $\text{C}_{49}\text{H}_{86}\text{N}_4\text{O}_{19}$ $[\text{M} + \text{Na}]^+$ 1057.59; found 1057.576.

(2S,4S)-tert-butyl 4-(tert-butoxycarbonylamino)-2-((S)-6-(methacryloyloxy)-5-(3,4,5-tris(2-(2-(2-methoxyethoxy)ethoxy)ethoxy)benzamido)hexylcarbamoyl)pyrrolidine-1-carboxylate (26b).

According to general procedure **D**, from **26a** (0.88 g, 0.85 mmol), TEA (0.43 g, 4.25 mmol), DMAP (0.1 g), MAC (0.355 g, 3.40 mmol) and DCM (30 mL), purification with column chromatography using DCM/MeOH (20:1, v/v) afforded **26b** as a

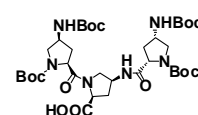


white solid (0.8 g, 85%). ^1H NMR (CD_2Cl_2): δ = 1.42 (br, 20H, $\text{CH}_3 + \text{CH}_2$), 1.57–1.65 (m, 4H, CH_2), 1.92 (s, 3H, CH_3), 2.14 (br, 2H, CH_2), 3.25 (br, 2H, CH_2), 3.32 and 3.34

(2s, 9H, CH₃), 3.49–3.69 (m, 27H, CH₂ + CH₂ⁿ), 3.75–3.85 (m, 6H, CH₂), 4.16–4.27 (m, 10H, CH₂ + CH), 4.36 (br, 1H, CH), 5.58 (s, 1H, CH₂^a), 6.10 (s, 1H, CH₂^b), 6.48 (br, 1H, NH), 6.55 (br, 1H, NH), 7.05 (s, 2H, CH), 7.23 (br, 1H, NH). ¹³C NMR (CD₂Cl₂): δ = 18.22, 23.09, 28.20, 28.30, 29.03, 31.11, 32.79, 39.20, 49.22, 50.25, 53.16, 55.39, 58.72, 59.66, 66.24, 69.08, 69.78, 70.49, 70.51, 70.60, 70.64, 70.68, 70.83, 72.02, 72.04, 72.53, 78.91, 80.63, 106.76, 125.84, 130.03, 136.34, 141.25, 152.61, 155.34, 155.91, 166.68, 167.55, 172.52. HR-MS (MALDI): *m/z* calcd. for C₅₃H₉₀N₄O₂₀ [M + Na]⁺ 1125.61; found 1125.609. Elemental analysis (%) calcd for C₅₃H₉₀N₄O₂₀, 1103.31: C, 57.70; H, 8.22; N, 5.08. Found: C, 56.79; H, 8.04; N, 4.99.

2S,4S)-1-[(2S,4S)-1-(tert-Butoxycarbonyl)-4-(tert-butoxycarbonylamino)pyrrolidine-2-carbonyl]-4-[(2S,4S)-1-(tert-butoxycarbonyl)-4-(tert-butoxy-carbonylamino)pyrrolidine-2-carbonylamino]-proline acid (27b).

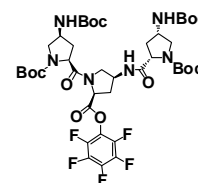
According to general procedure **P** from LiOH·H₂O (1.44 g, 34.32 mmol) and compound **27a** (3.3 g, 4.29 mmol) in MeOH (80 mL) and H₂O (8 mL), **27b** was yielded as a white foam (2.75 g, 85%). ¹H NMR



(CD₂Cl₂): δ = 1.24–1.43 (m, 36H, CH₃), 1.85–2.43 (m, 6H, CH₂), 3.40–3.73 (m, 5H, CH₂ + CH₂^a), 3.98–4.68 (m, 7H, CH + CH₂^b). Only the signal from Boc can be detected in ¹³C NMR spectrum. HR-MS (ESI): *m/z* calcd. for C₃₅H₅₈N₆O₁₂ [M + Na]⁺ 777.41; found 777.4004.

(2S,4S)-1-[(2S,4S)-1-(tert-Butoxycarbonyl)-4-(tert-butoxycarbonylamino) pyrrolidine-2-carbonyl]-4-[(2S,4S)-1-(tert-butoxycarbonyl)-4-(tert-butoxy-carbonylamino)pyrrolidine-2-carbonylamino]-proline pentafluoro-phenol ester (27c).

According to general procedure **Q** from DCC (1.17 g, 5.68 mmol), **27b** (1.95 g, 2.58 mmol) and pentafluoro-phenol (0.95 g, 5.17 mmol) in DCM (40 mL), purification by column chromatography with DCM/MeOH (30:1, v/v) afforded **27c** as white foam (1.9 g, 80 %). ¹H

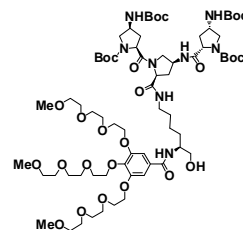


NMR (CD₂Cl₂): δ = 1.08–1.44 (m, 36H, CH₃), 1.67–2.20 (m, 5H, CH₂ + CH₂^a), 2.39–2.47 (m, 1H, CH₂^b), 3.29–3.61 (m, 5H, CH₂ + CH₂^m), 4.18–4.37 (m, 4H, CH + CH₂ⁿ), 4.44–4.84 (m, 3H, CH), 6.14–6.33 (m, 2H, NH), 7.82 (2br, 1H, NH). ¹³C NMR (CD₂Cl₂): δ = 25.13, 25.77, 28.07, 28.22, 31.20, 32.44, 33.99, 34.14, 34.27, 35.10, 35.96, 36.37, 49.14, 49.33, 49.40, 50.32, 52.19, 52.34, 54.38, 54.94, 55.17, 56.61, 56.69, 57.57, 57.66, 59.53, 78.82, 79.12, 80.23, 81.01, 137.01, 139.01, 140.24,

142.27, 153.18, 154.41, 155.35, 156.24, 168.35, 172.69, 172.91, 173.03. HR-MS (ESI): m/z calcd. for $C_{41}H_{57}F_5N_6O_{12}$ $[M + Na]^+$ 943.40; found 943.3859.

Compound 28a.

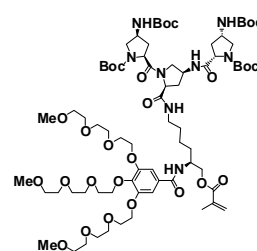
According to general procedure **R**, from **23c** (0.726 g, 0.956 mmol) and DiPEA (1.123 g, 8.69 mmol) in DCM (3 mL), compound **27c** (0.8 g, 0.869 mmol) in DCM (25 mL), purification with column chromatography using DCM/MeOH (20:1 then 15:1, v/v) afforded **28a** as a colorless foam (1.1 g, 87%). 1H NMR



(CD_2Cl_2): δ = 1.27–1.49 (m, 38H, $CH_3 + CH_2$), 1.59 and 1.73 (2br, 4H, CH_2), 2.11–2.38 (m, 7H, $CH_2 + OH$), 3.03–3.07 (m, 1H, CH_2^a), 3.32–3.34 (m, 10H, $CH_3 + CH_2^b$), 3.44–3.84 (m, 37H, $CH_2 + CH_2^m$), 3.94–4.39 (m, 12H, $CH + CH_2^n$), 4.63 and 4.72 (2br, 2H, CH), 6.23–6.31 (m, 2H, NH), 7.01–7.47 (m, 4H, $CH + NH$), 8.51–8.60 (2br, 1H, NH). ^{13}C NMR (CD_2Cl_2): δ = 17.14, 18.38, 23.23, 28.21, 28.30, 28.92, 35.28, 35.53, 37.41, 42.06, 49.07, 49.19, 50.07, 50.29, 52.17, 53.16, 56.69, 58.72, 58.74, 59.99, 60.29, 69.13, 69.83, 70.42, 70.49, 70.59, 70.64, 70.73, 72.00, 72.49, 79.00, 80.12, 107.15, 129.96, 141.15, 152.50, 153.11, 154.28, 155.19, 155.38, 166.99, 172.14. HR-MS (MALDI): m/z calcd. for $C_{69}H_{118}N_8O_{25}$ $[M + Na]^+$ 1481.82; found 1481.807.

Compound 28b.

According to general procedure **D**, from **28a** (1 g, 0.685 mmol), TEA (0.346 g, 3.425 mmol), DMAP (0.1 g), MAC (0.286 g, 2.74 mmol) and DCM (30 mL), purification with column chromatography using DCM/MeOH (15:1, v/v) afforded **28b** as a colorless foam (0.94 g, 90%). 1H NMR (CD_2Cl_2): δ = 1.36–1.40



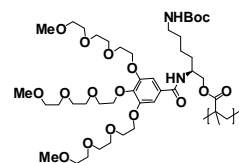
(m, 38H, $CH_3 + CH_2$), 1.58 and 1.73 (2br, 5H, $CH_2 + CH_2^a$), 2.02 (d, 1H, CH_2^b), 2.14 (s, 3H, CH_3), 2.30 and 2.40 (2br, 4H, CH_2), 3.32–3.33 (m, 11H, $CH_3 + CH_2$), 3.42–3.85 (m, 35H, $CH_2 + CH_2^m$), 4.15–4.38 (m, 14H, $CH + CH_2^n$), 4.70 (br, 2H, CH), 5.58 (s, 1H, CH_2^p), 6.10 (s, 1H, CH_2^q), 6.24–6.38 (m, 2H, NH), 6.52–6.71 (m, 1H, NH), 7.05 and 7.06 (2s, 2H, CH), 7.14–7.36 (m, 1H, NH), 8.41–8.68 (m, 1H, NH). ^{13}C NMR (CD_2Cl_2): δ = 18.22, 23.00, 23.35, 28.30, 28.84, 31.09, 35.54, 37.30, 39.36, 39.64, 49.07, 49.23, 49.39, 50.03, 50.28, 53.16, 56.63, 58.72, 60.28, 66.30, 69.09, 69.80, 70.47, 70.51, 70.59, 70.62, 70.66, 70.82, 72.02, 72.03, 72.53, 79.01, 80.07, 86.94,

106.83, 125.97, 129.83, 136.31, 141.31, 152.60, 153.13, 154.27, 154.81, 155.19, 166.68, 167.62, 172.06. HR-MS (MALDI): m/z calcd. for $C_{73}H_{122}N_8O_{26}$ $[M + Na]^+$ 1549.85; found 1549.837. Elemental analysis (%) calcd for $C_{73}H_{122}N_8O_{26}$, 1527.80: C, 57.39; H, 8.05; N, 7.33. Found: C, 56.55; H, 8.12; N, 7.23.

PG2(0).

According to general procedure **I** from monomer **24b** (0.4 g, 0.449 mmol) and AIBN (2 mg), polymerization for 17 h at 60 °C yielded

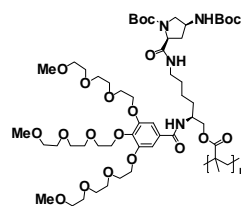
PG2(0) as a colorless solid (0.26 g, 65 %). 1H NMR (CD_2Cl_2): δ = 0.92–1.88 (m, 20H, $CH_3 + CH_2$), 2.92–3.67 (m, 41H, $CH_3 + CH_2$), 4.03–4.15 (m, 9H, $CH_2 + CH$), 5.98 (br, 1H, NH), 7.08 (br, 2H, CH), 7.84 (br, 1H, NH). Elemental analysis (%) calcd for $(C_{43}H_{74}N_2O_{17})_n$ (891.05) $_n$: C, 57.96; H, 8.37; N, 3.14. Found: C, 57.15; H, 8.44; N, 3.10.



PG2(1).

According to general procedure **H**, from **26b** (0.5 g, 0.453 mmol), AIBN (2.5 mg), DMF (0.2 mL), polymerization for 16 h at 80 °C yielded **PG2(1)** as a colorless solid (0.3 g, 60 %).

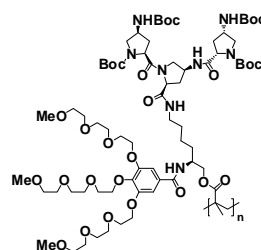
1H NMR (CD_2Cl_2): δ = 0.81–2.25 (m, 31H, $CH_3 + CH_2$), 3.02–4.03 (m, 54H, $CH_3 + CH_2 + CH$), 6.56 (br, 1H, NH), 7.08 (br, 2H, CH), 7.52 (br, 1H, NH). 7.85 (br, 1H, NH). Elemental analysis (%) calcd for $(C_{53}H_{90}N_4O_{20})_n$ (1103.31) $_n$: C, 57.70; H, 8.22; N, 5.08. Found: C, 56.66; H, 8.26; N, 5.00.



PG2(2).

According to general procedure **A**, from **28b** (0.5 g, 0.327 mmol), AIBN (2.5 mg), DMF (0.2 mL), polymerization for 18 h at 60 °C yielded **PG2(2)** as a white solid (0.2 g, 40 %).

1H NMR (CD_2Cl_2): δ = 0.85–2.34 (m, 53H, $CH_3 + CH_2$), 3.03–4.31 (m, 62H, $CH_3 + CH_2 + CH$), 6.51 (br, 2H, NH), 7.09 (br, 2H, CH), 8.06 (br, 3H, NH). Elemental analysis (%) calcd for $(C_{73}H_{122}N_8O_{26})_n$ (1527.80) $_n$: C, 57.39; H, 8.05; N, 7.33. Found: C, 56.48; H, 8.19; N, 7.14.



Preparation of films with the “breath figure” technique.

The films were prepared in a chamber by casting 20 μL of a chloroform solution of the polymer (5 mg/mL or 10 mg/mL) onto freshly cleaved mica via a microsyringe under a flow of moist nitrogen (60% or 70% RH at room temperature). The moist nitrogen was generated by flowing nitrogen through a two-necked flask filled with water. The films were obtained after evaporation of chloroform and water.

9. Reference

- [1] Boas, U.; Christensen, J. B.; Heegaard, P. M. H. *J. Mater. Chem.* **2006**, *16*, 3785–3798.
- [2] Buhleier, E.; Wehner, W.; Vögtle, F. *Synthesis* **1978**, 155–158.
- [3] Tomalia, D. A.; Baker, H.; Dewald, J.; Hall, M.; Kallos, G.; Martin, S.; Roeck, J.; Ryder, J.; Smith, P. *Polymer Journal* **1985**, *17*, 117–132.
- [4] Tomalia, D. A.; Fréchet, J. M. J. *J. Polym. Sci., Part A: Polym. Chem.* **2002**, *40*, 2719–2728.
- [5] Newkome, G. R.; Yao, Z.; Baker, G. R.; Gupta, V. K. *J. Org. Chem.* **1985**, *50*, 2003–2004.
- [6] Wörner, C.; Mülhaupt, R. *Angew. Chem., Int. Ed.* **1993**, *32*, 1306–1308.
- [7] Brabander-van den Berg, E. M. M.; Meijer, E. W. *Angew. Chem., Int. Ed.* **1993**, *32*, 1308–1310.
- [8] Helms, B.; Meijer, E. W. *Science* **2006**, *313*, 929–930.
- [9] Medina, S. H.; El-Sayed, M. E. H. *Chem. Rev.* **2009**, *109*, 3141–3157.
- [10] Svenson, S. *Eur. J. Pharm. Biopharm.* **2009**, *71*, 445–462.
- [11] Li, J.; Liu, D. *J. Mater. Chem.* **2009**, *19*, 7584–7591.
- [12] Hwang, S.; Moorefield, C. N.; Newkome, G. R. *Chem. Soc. Rev.* **2008**, *37*, 2543–2557.
- [13] Astruc, D.; Ornelas, C.; Ruiz, A. J. *Acc. Chem. Res.* **2008**, *41*, 841–856.
- [14] Peng, X.; Pan, Q.; Rempel, G. L. *Chem. Soc. Rev.* **2008**, *37*, 1619–1628.
- [15] Tomalia, D. A.; Kirchhoff, P. M. Rod-shaped dendrimers. 694 Midland, MI, USA: The Dow Chemical Company; **1987**. US Patent 4,694,064.
- [16] Tomalia, D. A.; Naylor, A. M.; Goddard III, W. A. *Angew. Chem., Int. Ed.* **1990**, *29*, 138–175;
- [17] Yin, R.; Zhu, Y.; Tomalia, D. A.; Ibuki, H. *J. Am. Chem. Soc.* **1998**, *120*, 2678–2679.
- [18] Percec, V.; Heck, J. *J. Polym. Sci., Part A, Polym. Chem.* **1991**, *29*, 591–597.
- [19] Schlüter, A. D. *Top. Curr. Chem.* **1998**, *197*, 165–191.
- [20] Hawker, C. J.; Fréchet, J. M. J. *Polymer* **1992**, *33*, 1507–1511.
- [21] Schlüter, A. D.; Rabe, J. P. *Angew. Chem., Int. Ed.* **2000**, *39*, 864–883.
- [22] Zhang, A.; Shu, L.; Bo, Z.; Schlüter, A. D. *Macromol. Chem. Phys.* **2003**, *204*, 328–339.

- [23] Zhang, A. *Prog. Chem.* **2005**, *17*, 157–171.
- [24] Frauenrath, H. *Prog. Polym. Sci.* **2005**, *30*, 325–384.
- [25] Schlüter, A. D. *Top. Curr. Chem.* **2005**, *245*, 151–191.
- [26] Guo, Y.; Beek, J. D.; Zhang, B.; Colussi, M.; Walde, P.; Ding, Y.; Kröger, M.; Schmidt, M.; Zhang, A.; Halperin, Schlüter, A. D. *J. Am. Chem. Soc.* **2009**, *131*, 11841–11845.
- [27] Zhang, A.; Zhang, B.; Wächtersbach, E.; Schmidt, M.; Schlüter, A. D. *Chem. Eur. J.* **2003**, *9*, 6083–6092.
- [28] Zhang, A.; Okrasa, L.; Pakula, T.; Schlüter, A. D. *J. Am. Chem. Soc.* **2004**, *126*, 6658–6666.
- [29] Sonar, P.; Benmansour, H.; Geiger, Thomas.; Schlüter, A. D. *Polymer* **2007**, *48*, 4996–5004.
- [30] Zhang, A.; Roper, F. R.; Zanuy, D.; Alemán, K.; Meijer, E. W.; Schlüter, A. D. *Chem. Eur. J.* **2008**, *14*, 6924–6934.
- [31] Zhu, B.; Han, Y.; Sun, M.; Bo, Z. *Macromolecules* **2007**, *40*, 4494–4500.
- [32] Balagurusamy, V. S. K.; Ungar, G.; Percec, V.; Johansson, G. *J. Am. Chem. Soc.* **1997**, *119*, 1539–1555.
- [33] Rudick, J. G.; Percec, V. *Acc. Chem. Res.* **2008**, *41*, 1641–1652.
- [34] Xiong, X.; Chen, Y.; Feng, S.; Wang, W. *Macromolecules* **2007**, *40*, 9084–9093.
- [35] Hawker, C. J.; Fréchet, J. M. J. *Polymer* **1992**, *33*, 1507–1511.
- [36] Wooley, K. L.; Hawker, C. J.; Fréchet, J. M. J. *J. Am. Chem. Soc.* **1991**, *113*, 4252–4261.
- [37] Lee, C. C.; Fréchet, J. M. J. *Macromolecules* **2006**, *39*, 476–481.
- [38] Kamikawa, Y.; Kato, T.; Onouchi, H.; Kashiwagi, D.; Maeda, K.; Yashima, E. *J. Polym. Sci., Part A: Polym. Chem.* **2004**, *42*, 4580–4586.
- [39] Leung, K. C. F.; Mendes, P. M.; Magonov, S. N.; Northrop, B. H.; Kim, S.; Patel, K.; Flood, A. H.; Tseng, H. R.; Stoddart, J. F. *J. Am. Chem. Soc.* **2006**, *128*, 10707–10715.
- [40] Xie, D.; Jiang, M.; Zhang, G.; Chen, D. *Chem. Eur. J.* **2007**, *13*, 3346–3353.
- [41] Cheng, Z.; Ren, B.; Shan, H.; Liu, X.; Tong, Z. *Macromolecules* **2008**, *41*, 2656–2662.
- [42] Gössl, I.; Shu, L.; Schlüter, A. D. Rabe, J. P. *J. Am. Chem. Soc.* **2002**, *124*, 6860–6865.

- [43] Böttcher, C.; Schade, B.; Ecker, C.; Rabe, J. P.; Shu, L.; Schlüter, A. D. *Chem. Eur. J.* **2005**, *11*, 2923–2928.
- [44] Canilho, N.; Kasëmi, E.; Schlüter, A. D.; Mezzenga, R. *Macromolecules* **2007**, *40*, 2822–2830.
- [45] Al-Hellani, R.; Barner, J.; Rabe, J. P.; Schlüter, A. D. *Chem. Eur. J.* **2006**, *12*, 6542–6551.
- [46] Liang, C. O.; Helms, B.; Hawker, C. J.; Fréchet, J. M. J. *Chem. Commun.* **2003**, 2524–2525.
- [47] Zhang, Y.; Chen, Y.; Niu, H.; Gao, M. *Small* **2006**, *2*, 1314–1319.
- [48] Cheng, C.; Huang, Y.; Tang, R.; Chen, E.; Xi, F. *Macromolecules* **2005**, *38*, 3044–3047.
- [49] Lee, C. C.; Yoshida, M.; Fréchet, J. M. J.; Dy, E. E.; Szoka, F. C. *Bioconjugate Chem.* **2005**, *16*, 535–541.
- [50] Ossenbach, A.; Rüegger, H.; Zhang, A.; Fischer, K.; Schlüter, A. D. Schmidt, M. *Macromolecules* **2009**, *42*, 8781–8793.
- [51] Cheng, C.; Schmidt, M.; Zhang, A.; Schlüter, A. D. *Macromolecules* **2007**, *40*, 220–227.
- [52] Lee, C. C.; Grayson, S. M.; Fréchet, J. M. J. *J. Polym. Sci., Part A: Polym. Chem.* **2004**, *42*, 3563–3578.
- [53] Durme, K. V.; Verbrugghe, S.; Prez, F. E. D.; Mele, B. V. *Macromolecules* **2004**, *37*, 1054–1061.
- [54] Durme, K. V.; Assche, G. V.; Aseyev, V.; Raula, J.; Tenhu, H.; Mele, B. V. *Macromolecules* **2007**, *40*, 3765–3772.
- [55] Langer, R.; Tirrell, D. A. *Nature* **2004**, *428*, 487–492.
- [56] Alarcón, C. H.; Pennadam, S.; Alexander, C. *Chem. Soc. Rev.* **2005**, *34*, 276–285.
- [57] Schmaljohann, D. *Adv. Drug Delivery Rev.* **2006**, *58*, 1655–1670.
- [58] Stenzel, M. H. *Chem. Commun.* **2008**, 3486–3503.
- [59] Nath, N.; Chilkoti, A. *Adv. Mater.* **2002**, *14*, 1243–1247.
- [60] Hatakeyama, H.; Kikuchi, A.; Yamato, M.; Okano, T. *Biomaterials* **2007**, *28*, 3632–3643.
- [61] Kikuchi, A.; Okano, T. *Prog. Polym. Sci.* **2002**, *27*, 1165–1193.
- [62] Wischerhoff, E.; Uhlig, K.; Lankenau, A.; Börner, H. G.; Laschewsky, A.; Duschl, C.; Lutz, J. F. *Angew. Chem., Int. Ed.* **2008**, *47*, 5666–5668.

- [63] Li, D.; He, Q.; Cui, Y.; Wang, K.; Zhang, X.; Li, J. *Chem. Eur. J.* **2007**, *13*, 2224–2229.
- [64] Raula, J.; Shan, J.; Nuopponen, M.; Niskanen, A.; Jiang, H.; Kauppinen, E. I.; Tenhu, H. *Langmuir* **2003**, *19*, 3499–3504.
- [65] Zhu, M.; Wang, L.; Exarhos, G. J.; Li, A. D. Q. *J. Am. Chem. Soc.* **2004**, *126*, 2656–2657.
- [66] Shen, Y.; kuang, M.; Shen, Z.; Nieberle, J.; Duan, H.; Frey, H. *Angew. Chem., Int. Ed.* **2008**, *47*, 2227–2230.
- [67] Osada, Y.; Kishi, R.; Hasebe, M. *J. Polym. Sci., Part C: Polym. Lett.* **1987**, *25*, 481–485.
- [68] Shinohara, S.; Tajima, N.; Yanagisawa, K. *J. Intell. Mater. Syst. Struct.* **1996**, *7*, 254–259.
- [69] Li, C.; Gunari, N.; Fischer, K.; Janshoff, A.; Schmidt, M. *Angew. Chem., Int. Ed.* **2004**, *43*, 1101–1104.
- [70] Liu, Z.; Calvent, P. *Adv. Mater.* **2000**, *12*, 288–291.
- [71] Bergbreiter, D. E.; *Chem. Rev.* **2002**, *102*, 3345–3384.
- [72] Schild, H. G. *Prog. Polym. Sci.* **1992**, *17*, 163–249.
- [73] Van Durme, K.; VanAssche, G.; Van Mele, B. *Macromolecules* **2004**, *37*, 9596–9605.
- [74] Cheng, H.; Shen, L.; Wu, C. *Macromolecules* **2006**, *39*, 2325–2329.
- [75] Zhang, X.; Li, J.; Li, W.; Zhang, A. *Biomacromolecules* **2007**, *8*, 3557–3567.
- [76] Lin, H.; Cheng, Y. *Macromolecules* **2001**, *34*, 3710–3715.
- [77] Plummer, R.; Hill, D. J. T.; Whittaker, A. K. *Macromolecules* **2006**, *39*, 8379–8388.
- [78] Xu, X.; Smith, A. E.; Kirkland, S. E.; McCormick, C. L. *Macromolecules* **2008**, *41*, 8429–8435.
- [79] Pong, F. Y.; Lee, M.; Bell, J. R.; Flynn, N. T. *Langmuir* **2006**, *22*, 3851–3857.
- [80] You, Y.; Hong, C.; Pan, C.; Wang, P. *Adv. Mater.* **2004**, *16*, 1953–1957.
- [81] Lutz, J. F.; Akdemir, Ö.; Hoth, A. *J. Am. Chem. Soc.* **2006**, *128*, 13046–13047.
- [82] Saeki, S.; Kuwahara, N.; Nakata, M.; Kaneko, M. *Polymer* **1976**, *17*, 685–689.
- [83] Allcock, H. R.; Dudley, G. K. *Macromolecules* **1996**, *29*, 1313–1319.
- [84] Han, S.; Hagiwara, M.; Ishizone, T. *Macromolecules* **2003**, *36*, 8312–8319.
- [85] Ishizone, T.; Seki, A.; Hagiwara, M.; Han, S.; Yokoyama, H.; Oyaane, A.; Deffieux, A.; Carlotti, S. *Macromolecules* **2008**, *41*, 2963–2967.

- [86] Hua, F.; Jiang, X.; Li, D.; Zhao, B. *J. Polym. Sci., Part A: Polym. Chem.* **2006**, *44*, 2454–2467.
- [87] Jiang, X.; Zhao, B. *J. Polym. Sci., Part A: Polym. Chem.* **2007**, *45*, 3707–3721.
- [88] Lutz, J. F.; Hoth, A. *Macromolecules* **2006**, *39*, 893–896.
- [89] Kimura, M.; Kato, M.; Muto, T.; Hanabusa, K.; Shirai, H. *Macromolecules* **2000**, *33*, 1117–1119.
- [90] Haba, Y.; Harada, A.; Takagishi, T.; Kono, K. *J. Am. Chem. Soc.* **2004**, *126*, 12760–12781.
- [91] You, Y.; Hong, C.; Pan, C.; Wang, P. *Adv. Mater.* **2004**, *16*, 1953–1957.
- [92] Chang, D. W.; Dai, L. *J. Mater. Chem.* **2007**, *17*, 364–371.
- [93] Aathimanikandan, S. V.; Savariar, E. N.; Thayumanavan, S. *J. Am. Chem. Soc.* **2005**, *127*, 14922–14929.
- [94] Parrott, M. C.; Marchington, E. B.; Valliant, J. F.; Adronov, A. *J. Am. Chem. Soc.* **2005**, *127*, 12081–12089.
- [95] Haba, Y.; Kojima, C.; Harada, A.; Kono, K. *Macromolecules* **2006**, *39*, 7451–7453.
- [96] Haba, Y.; Kojima, C.; Harada, A.; Kono, K. *Angew. Chem., Int. Ed.* **2007**, *46*, 234–237.
- [97] Roberts, J.; Bhalgat, M.; Zera, R. *J. Biomed. Mater. Res.* **1996**, *30*, 53–65.
- [98] Jevprasesphant, R.; Penny, J.; Jalal, R.; Attwood, D.; McKeown, N.; D'Emanuele, A. *Int. J. Pharm.* **2003**, *252*, 263–266.
- [99] Jia, Z.; Chen, H.; Zhu, X.; Yan, D. *J. Am. Chem. Soc.* **2006**, *128*, 8144–8145.
- [100] Wu, C.; Zhou, S. *Macromolecules* **1995**, *28*, 5388–5390.
- [101] Wu, C.; Zhou, S. *Macromolecules* **1995**, *28*, 8381–8387.
- [102] Wu, C.; Zhou, S. *Phys. Rev. Lett.* **1996**, *77*, 3053–3055.
- [103] Wang, X.; Qiu, X.; Wu, C. *Macromolecules* **1998**, *31*, 2972–2976.
- [104] Skrabania, K.; Li, W.; Laschewsky, A. *Macromol. Chem. Phys.* **2008**, *209*, 1389–1403.
- [105] Keerl, M.; Smirnovas, V.; Winter, R.; Richtering, W. *Angew. Chem., Int. Ed.* **2008**, *47*, 338–341.
- [106] Shibayama, M.; Mizutani, S.; Nomura, S. *Macromolecules* **1996**, *29*, 2019–2024.
- [107] Luo, S.; Xu, J.; Zhu, Z.; Wu, C.; Liu, S. *J. Phys. Chem. B* **2006**, *110*, 9132–9139.

- [108] Halperin, A.; Tirrell, M.; Lodge, T. P. *Adv. Polym. Sci.* **1992**, *100*, 31–71.
- [109] Turner, K.; Zhu, P. W.; Napper, D. H. *Colloid Polym. Sci.* **1996**, *274*, 622–627.
- [110] Ono, Y.; Shikata, T. *J. Am. Chem. Soc.* **2006**, *128*, 10030–10031.
- [111] Ono, Y.; Shikata, T. *J. Phys. Chem. B*, **2007**, *111*, 1511–1513.
- [112] Junk, M. J. N.; Jonas, U.; Hinderberger, D. *Small* **2008**, *4*, 1485–1493.
- [113] Chen, D.; Jiang, M. *Acc. Chem. Res.* **2005**, *38*, 494–502.
- [114] Zhang, L. F.; Eisenberg, A. *Science* **1995**, *268*, 1728–1731.
- [115] Zhu, J.; Hayward, R. C. *J. Am. Chem. Soc.* **2008**, *130*, 7496–7502.
- [116] Harada, A.; Kataoka, K. *Prog. Polym. Sci.* **2006**, *31*, 949–982.
- [117] Wang, Y.; Xu, H.; Zhang, X. *Adv. Mater.* **2009**, *21*, 2849–2864.
- [118] Förster, S.; Antonietti, M. *Adv. Mater.* **1998**, *10*, 195–217.
- [119] K. Kataoka, A. Harada, Y. Nagasaki, *Adv. Drug Delivery Rev.* **2001**, *47*, 113–131.
- [120] Velichkova, R. S.; Christova, D. C. *Prog. Polym. Sci.* **1995**, *20*, 819–887.
- [121] Ge, Z.; Liu, S. *Macromol. Rapid Commun.* **2009**, *30*, 1523–1532.
- [122] Soo, P. L.; Eisenberg, A. *J. Polym. Sci., Part B: Polym. Phys.* **2004**, *42*, 923–938.
- [123] Förster, S.; Antonietti, M. *Adv. Mater.* **1998**, *10*, 195–217.
- [124] Burke, S.; Eisenberg, A. *High Perform. Polym.* **2000**, *12*, 535–542.
- [125] Rosen, B. M.; Wilson, C. J.; Wilson, D. A.; Peterca, M.; Imam, M. R. Percec, V. *Chem. Rev.* **2009**, *109*, 6275–6540.
- [126] Smith, D. K.; Hirst, A. R.; Love, C. S.; Hardy, J. G.; Brignell, S. V.; Huang, B. *Prog. Polym. Sci.* **2005**, *30*, 220–293.
- [127] Cheng, C.; Jiao, T.; Tang, R.; Chen, E.; Liu, M.; Xi, F. *Macromolecules* **2006**, *39*, 6327–6330.
- [128] Yi, Z.; Liu, X.; Jiao, Q.; Chen, E.; Chen, Y.; Fu, X. *J. Polym. Sci., Part A: Polym. Chem.* **2008**, *46*, 4205–4217.
- [129] Cheng, C.; Schlüter, A. D.; Zhang, A. *Israel J. Chem.* **2009**, *49*, 49–53.
- [130] Li, B. S.; Cheuk, K. K. L.; Yang, D.; Lam, J. W. Y.; Wan, L. J.; Bai, C.; Tang, B. *Z. Macromolecules* **2003**, *36*, 5447–5450.
- [131] Kale, T. S.; Klaikherd, A.; Popere, B.; Thayumanavan, S. *Langmuir* **2009**, *25*, 9660–9670.
- [132] Cheng, G.; Böker, A.; Zhang, M.; Krausch, G.; Müller, A. H. E. *Macromolecules* **2001**, *34*, 6883–6888.

- [133] Bo, Z.; Rabe, J. P.; Schlüter, A. D. *Angew. Chem., Int. Ed.* **1999**, *38*, 2370–2372.
- [134] Bo, Z.; Zhang, C.; Severin, N.; Rabe, J. P. Schlüter, A. D. *Macromolecules* **2000**, *33*, 2688–2694.
- [135] Xiao, X.; Wu, Y.; Sun, M.; Zhou, J.; Bo, Z.; Li, L.; Chan, C. *J. Polym. Sci., Part A: Polym. Chem.* **2008**, *46*, 574–584.
- [136] Holland, B. T.; Blanford, C. F.; Stein, A. *Science* **1998**, *281*, 538–540.
- [137] Yan, H.; Blanford, C. F.; Holland, B. T.; Parent, M.; Smyrl, W. H.; Stein, A. *Adv. Mater.* **1999**, *11*, 1003–1006.
- [138] Velev, O. D.; Jede, T. A.; Lobo, R. F. Lenhoff, A. M. *Nature* **1997**, *389*, 447–448.
- [139] Kresge, C. T.; Leonowicz, M. E.; Roth, W. J.; Vartuli, J. C.; Beck, J. S. *Nature* **1992**, *359*, 710–712.
- [140] Monnier, A.; Schüth, F.; Huo, Q.; Kumar, D.; Margolese, D.; Maxwell, R. S.; Stucky, G. D.; Krishnamurty, M.; Petroff, P.; Firouzi, A.; Janicke, M.; Chmelka, B. F. *Science* **1993**, *261*, 1299–1303.
- [141] Park, M.; Harrison, C.; Chaikin, P. M.; Register, R. A.; Adamson, D. H. *Science* **1997**, *276*, 1401–1404.
- [142] Li, Z.; Zhao, W.; Liu, Y.; Rafailovich, M. H.; Sokolov, J.; Khougaz, K.; Eisenberg, A.; Lennox, R. B. Krausch, G. *J. Am. Chem. Soc.* **1996**, *118*, 10892–10893.
- [143] Heiko, U.; Bunz, F. *Adv. Mater.* **2006**, *18*, 973–989.
- [144] Stenzel, M. H.; Kowollik, C. B.; Davis, T. P. *J. Polym. Sci., Part A: Polym. Chem.* **2006**, *44*, 2363–2375.
- [145] Aitken, J. *Nature* **1911**, *86*, 516–517.
- [146] Rayleigh, L. *Nature* **1911**, *86*, 416–417.
- [147] Rayleigh, L. *Nature* **1912**, *90*, 436–438.
- [148] Knobler, C. M. Beysens, D. *Europhys. Lett.* **1988**, *6*, 707–712.
- [149] Widawski, G.; Rawiso, M.; Francois, B. *Nature* **1994**, *369*, 387–389.
- [150] Srinivasarao, M.; Collings, D.; Philips, A.; Patel, S. *Science* **2001**, *292*, 79–83.
- [151] Maruyama, N.; Koito, T.; Nishida, J.; Sawadaishi, T.; Cieren, X.; Ijro, K.; Karthaus, O.; Shimomura, M. *Thin Solid Films* **1998**, *327*, 854–856.
- [152] Connal, L. A.; Vestberg, R.; Hawker, C. J.; Qiao, G. G. *Adv. Funct. Mater.* **2008**, *18*, 3706–3714.

- [153] Lord, H. T.; Quinn, J. F.; Angus, S. D.; Whittaker, M. R.; Stenzel, M. H.; Davis, T. P. *J. Mater. Chem.* **2003**, *13*, 2819–2824.
- [154] Cheng, C.; Tian, Y.; Shi, Q.; Tang, R.; Xi, F. *Langmuir* **2005**, *21*, 6576–6581.
- [155] Song, L.; Bly, R. K.; Wilson, J. N.; Bakbak, S.; Park, J. O.; Srinivasarao, M.; Bunz, U. H. F. *Adv. Mater.* **2004**, *16*, 115–118.
- [156] Wong, K. H.; Davis, T. P.; Barner-Kowollik, C.; Stenzel, M. H. *Polymer* **2007**, *48*, 4950–4965.
- [157] Beattie, D.; Wong, K. H.; Williams, C.; Poole-Warren, L. A.; Davis, T. P.; Barner-Kowollik, C.; Stenzel, M. H. *Biomacromolecules* **2006**, *7*, 1072–1082.
- [158] Muñoz-Bonilla, A.; Ibarboure, E.; Papon, E.; Rodriguez-Hernandez, J. *Langmuir*, **2009**, *25*, 6493–6499.
- [159] Li, L.; Chen, C.; Li, J.; Zhang, A.; Liu, X.; Xu, B.; Gao, S.; Jin, G.; Ma, Z. *J. Mater. Chem.* **2009**, *19*, 2789–2796.
- [160] Liu, C.; Gao, C.; Yan, D. *Angew. Chem., Int. Ed.* **2007**, *46*, 4128–4131.
- [161] Nygard, A.; Davis, T. P.; Barner-Kowollik, C.; Stenzel, M. H. *Aust. J. Chem.* **2005**, *58*, 595v599.
- [162] Kojima, C.; Kono, K.; Maruyama, K.; Takagishi, T. *Bioconjug. Chem.* **2000**, *11*, 910–917.
- [163] Jevprasesphant, R.; Penny, J.; Jalal, R.; Attwood, D.; Mckeown, N. B.; Emanuele, A. D. *Int. J. Pharm.* **2003**, *252*, 263–266.
- [164] Kono, K.; Kojima, C.; Hayashi, N.; Nishisaka, E.; Kiura, K.; Watarai, S.; Harada, A. *Biomaterials* **2008**, *29*, 1664–1675.
- [165] Dhanikula, R. S.; Hildgen, P. *Bioconjug. Chem.* **2006**, *17*, 29–41.
- [166] Dhanikula, R. S.; Hildgen, P. *Biomaterials* **2007**, *28*, 3140–3152.
- [167] Baars, M. W. P. L.; Kleppinger, R.; Koch, M. H. J.; Yeu, S.; Meijer, E. W. *Angew. Chem., Int. Ed.* **2000**, *39*, 1285–1288.
- [168] Lutz, J. F. *J. Polym. Sci., Part A: Polym. Chem.* **2008**, *46*, 3459–3470.
- [169] Kato, T. *Science* **2002**, *295*, 2414–2418.
- [170] Kishimoto, K.; Yoshio, M.; Mukai, T.; Yoshizawa, M.; Ohno, H.; Kato, T. *J. Am. Chem. Soc.* **2003**, *125*, 3196–3197.
- [171] Kishimoto, K.; Suzawa, T.; Yokota, T.; Mukai, T.; Ohno, H.; Kato, T. *J. Am. Chem. Soc.* **2005**, *127*, 15618–15623.
- [172] Li, J.; Kamata, K.; Komura, M.; Yamada, T.; Yoshida, H.; Iyoda, T. *Macromolecules* **2007**, *40*, 8125–8128.

- [173] Cho, B. K.; Jain, A.; Gruner, S. M.; Wiesner, U. *Science* **2004**, *305*, 1598–1601.
- [174] Newkome, G. R.; Kotta, K. K.; Mishra, A.; Moorefield, C. N. *Macromolecules* **2004**, *37*, 8262–8268.
- [175] Tang, D.; Wu, D.; Luo, Q.; Hu, W.; Wang, F.; Liu, S.; Liu, X.; Fan, Q. *Chem. Eur. J.* **2009**, *15*, 10352–10355.
- [176] Allcock, H. R.; O'Connor, S. J. M.; Olmeijer, D. L.; Napierala, M. E.; Cameron, C. G. *Macromolecules* **1996**, *29*, 7544–7552.
- [177] Hawker, C. J.; Chu, F.; Pomery, P. J.; Hill, D. J. T. *Macromolecules* **1996**, *29*, 3831–3838.
- [178] Baars, M. W. P. L.; Kleppinger, R.; Koch, M. H. J.; Yeu, S.; Meijer, E. W. *Angew. Chem., Int. Ed.* **2000**, *39*, 1285–1288.
- [179] Jeppesen, J. O.; Perkins, J.; Becher, J.; Stoddart, J. F. *Org. Lett.* **2000**, *2*, 3547–3550.
- [180] Meunier, S. J.; Wu, Q.; Wang, S. N.; Roy, R. *Can. J. Chem.* **1997**, *75*, 1472–1482.
- [181] Chen, C. T.; Pawar, V. D.; Munot, Y. S.; Chen, C. C.; Hus, C. J. *Chem. Commun.* **2005**, 2483–2485.
- [182] Müller, S.; Schlüter, A. D. *Chem. Eur. J.* **2005**, *11*, 5589–5610.
- [183] Sashiwa, H.; Shigemasa, Y.; Roy, R. *Macromolecules* **2001**, *34*, 3905–3909.
- [184] Dhanikula, R. S.; Hildgen, P. *Bioconjug. Chem.* **2006**, *17*, 29–41.
- [185] Dhanikula, R. S.; Hildgen, P. *Biomaterials* **2007**, *28*, 3140–3152.
- [186] Quchi, M.; Inoue, Y.; Liu, Y.; Nagamune, S.; Nakamura, S.; Wada, K.; Hakushi, T. *Bull. Chem. Soc. Jpn.* **1990**, *63*, 1260–1262.
- [187] Sato, T.; Otera, J.; Nozaki, H. *J. Org. Chem.* **1990**, *55*, 4770–4772.
- [188] Bouzide, A.; Leberre, N.; Sauvé, G. *Tetrahedron Letters* **2001**, *42*, 8781–8783.
- [189] Peng, X. Lu, H.; Han, T.; Chen, C. *Org. Lett.* **2007**, *9*, 895–898.
- [190] Aspinall, H. C.; Greeves, N.; Lee, W.; Mclver, E. G.; Smith, P. M. *Tetrahedron Letters* **1997**, *38*, 4679–4682.
- [191] Kokotos, G. *Synthesis* **1990**, 299–301.
- [192] Loukas, V.; Noulas, C.; Kokotos, G. *J. Peptide Sci.* **2003**, *9*, 312–319.
- [193] Ito, K.; Tomi, Y.; Kawaguchi, S. *Macromolecules* **1992**, *25*, 1534–1538.
- [194] Percec, V.; Ahn, C. H.; Barboiu, B. *J. Am. Chem. Soc.* **1997**, *119*, 12978–12979.

- [195] Tasaki, K. *J. Am. Chem. Soc.* **1996**, *118*, 8459–8469.
- [196] Xia, Y.; Yin, X.; Burke, N. A. D.; Stover, H. D. H. *Macromolecules* **2005**, *38*, 5937–5943.
- [197] Jenekhe, S. A.; Chen, X. L. *Science* **1998**, *279*, 1903–1907.
- [198] Viswanadhan, V. N.; Ghose, A. K.; Revankar, G. R.; Robins, R. K. *J. Chem. Inf. Comput. Sci.* **1989**, *29*, 163–172.
- [199] Canilho, N.; Kasemi, E.; Mezzenga, R.; Schlüter, A. D. *J. Am. Chem. Soc.* **2006**, *128*, 13998–13999.
- [200] Kasemi, E.; Schlüter, A. D. *N. J. Chem.* **2007**, *31*, 1313–1320.
- [201] Zhang, Y.; Furyk, S.; Bergbreiter, D. E.; Cremer, P. S. *J. Am. Chem. Soc.* **2005**, *127*, 14505–14510.
- [202] Park, T. G.; Hoffman, A. S. *Macromolecules* **1993**, *26*, 5045–5048.
- [203] Durme, K. V.; Rahier, H.; Mele, B. V. *Macromolecules* **2005**, *38*, 10155–10163.
- [204] Lee, S. B.; Song, S. C.; Jin, J. I.; Sohn, Y. S. *Macromolecules* **1999**, *32*, 7820–7827.
- [205] Bolisetty, S.; Schneider, C.; Polzer, F.; Ballauff, M.; Li, W.; Zhang, A.; Schlüter, A. D. *Macromolecules* **2009**, *42*, 7122–7128.
- [206] Chen, H.; Zhang, Q.; Li, J.; Ding, Y.; Zhang, G.; Wu, C. *Macromolecules* **2005**, *38*, 8045–8050.
- [207] Aseyev, V.; Hietala, S.; Laukkanen, A.; Nuopponen, M.; Confortini, O.; Prez, F. E. D.; Tenhu, H. *Polymer* **2005**, *46*, 7118–7131.
- [208] Jeppesen, J. O.; Perkins, J.; Becher, J.; Stoddart, J. F. *Org. Lett.* **2000**, *2*, 3547–3550.
- [209] Zhang, A.; Schlüter, A. D. *Chem. Asian J.* **2007**, *2*, 1540–1548.
- [210] Zhang, W.; Shiotsuki, M.; Masuda, T. *Macromol. Rapid Commun.* **2007**, *28*, 1115–1121.

10. Appendix

Symbols and Abbreviations

AFM	atomic force microscopy
ATRP	atom transfer radical polymerization
BDE	1,4-Butanediol diglycidyl ether
BF	breath figure
Boc	<i>tert</i> -butyloxycarbonyl
Cbz	benzyloxycarbonyl
CD	circular dichroism
CdS	cadmium sulfide
CHCl ₃	chloroform
CS ₂	carbon disulfide
CWEPR	continuous wave electron paramagnetic resonance
DCC	<i>N,N'</i> -dicyclohexylcarbodiimide
DCM	dichloromethane
DEG	diethylene glycol
D _h	hydrodynamic diameter
DHP	3,4-dihydro-2 <i>H</i> -pyran
DLS	dynamic light scattering
DMAP	<i>N,N'</i> -dimethylaminopyridine
DMF	dimethylformamide
DP _n	number-average degree of polymerization
DSC	differential scanning calorimetry
3D	three dimensional
ESI	electron spray ionisation (MS)
FTIR	fourier-transform infrared spectroscopy
g	gram
G1	first generation
G2	second generation
G3	third generation
G4	fourth generation
G5	fifth generation
GPC	gel permeation chromatography

h	hour
HOPG	highly oriented pyrolytic graphite
HR-MS	high Resolution Mass Spectrometry
H ₂ S	hydrogen sulfide
Hz	hertz (sec ⁻¹ or cycles per second)
IBAM	<i>iso</i> -butylamide
LAH	lithium aluminium anhydride
LB	langmuir Blodgett
LCST	lower critical solution temperature (the LCST in this thesis is referred to the apparent value)
MAC	methacryloyl chloride
MALDI-TOF	matrix assisted laser desorption ionization - time of flight (MS)
MeOH	methanol
MHz	megahertz = 10 ⁶ Hz
mL	milliliter
mmol	millimol
min	minute
M _n	number average molar mass
M _w	weight average molar mass
m/z	mass to charge ratio in mass spectrometry
MTDSC	modulated temperature differential scanning calorimetry
nm	nanometer
NMRP	nitroxide mediate radical polymerization
NMR	nuclear magnetic resonance
OEG	oligoethylene glycol
OM	optical microscopy
OR	optical rotation
PAMAM	poly(amidoamine)
PEG	poly(ethylene glycol)
PEO	poly(ethylene oxide)
PBF	poly(binaphthyl- <i>alt</i> -fluorene)
PBS	phosphate buffer solution
PDI	polydispersity index
PF	polyfluorene

PG1	first generation dendronized polymer
PG2	second generation dendronized polymer
PG3	third generation dendronized polymer
PG4	fourth generation dendronized polymer
PNiPAM	poly(N-vinylcaprolactam)
PPI	poly(propylenimine)
ppm	parts per million (NMR)
PPTS	pyridinium toluenesulfonate
PS	poly(styrene)
PTSA	p-toluenesulfonic acid
RAFT	reversible addition fragmentation chain transfer
R_h	hydrodynamic radius
r.t.	room temperature
s	singlet (NMR)
SEM	scanning electron microscopy
t	triplet (NMR)
TEA	triethylamine
TEG	triethylene glycol
TEM	transmission electron microscopy
T_g	glass transition temperature
THF	tetrahydrofuran
THP	tetrahydropyranyl
THPE	1,1,1-tris(4-hydroxyphenyl)ethane
TLC	thin layer chromatography
TMP	trimethylolpropane
TME	trimethylolethane
TsCl	4-toluenesulfonyl chloride
UV	ultraviolet
wt%	weight percent
δ	chemical shift downfield from TMS, given as ppm
μm	micrometer
μg	microgram
λ	wave length

List of Publications

- 1) Wen Li, Dalin Wu, A. Dieter Schlüter, Afang Zhang. "Synthesis of an Oligo(Ethylene Glycol)-Based Third Generation Thermoresponsive Dendronized Polymer", *J. Polym. Sci., Part A: Polym. Chem.* **2009**, *47*, 6630–6640.
- 2) Sreenath Bolisetty, Christian Schneider, Frank Polzer, Matthias Ballauff, Wen Li, Afang Zhang, A. Dieter Schlüter. "Formation of Stable Mesoglobules by a Thermoresponsive Dendronized Polymer", *Macromolecules* **2009**, *42*, 7122–7128.
- 3) Wen Li, Afang Zhang, Yong Chen, Kirill Feldman, Hua Wu, A. Dieter Schlüter. "Low Toxic, Thermoresponsive Dendrimers Based on Oligoethylene Glycols with Sharp and Fully Reversible Phase Transitions", *Chem. Commun.* **2008**, 5948–5950.
- 4) Wen Li, Afang Zhang, A. Dieter Schlüter. "Thermoresponsive Dendronized Polymers with Tunable Lower Critical Solution Temperatures", *Chem. Commun.*, **2008**, 5523–5525.
- 5) Wen Li, Afang Zhang, Kirill Feldman, Peter Walde, A. Dieter Schlüter. "Thermoresponsive Dendronized Polymers", *Macromolecules* **2008**, *41*, 3659–3667.
- 6) Wen Li, Afang Zhang, A. Dieter Schlüter. "Efficient Synthesis of First- and Second-Generation, Water-Soluble Dendronized Polymers", *Macromolecules* **2008**, *41*, 43–49.

Manuscript in Preparation

- 1) Wen Li, A. Dieter Schlüter, Afang Zhang. "Ordered Porous Films from Amphiphilic Dendronized Homo-Polymers".
- 2) Matthias J. N. Junk,[#] Wen Li,[#] A. Dieter Schlüter, Gerhard Wegner, Hans W. Spiess, Afang Zhang, Dariush Hinderberger. "EPR Spectroscopy Reveals Local Nanoscopic Heterogeneities During the Thermal Collapse of Thermoresponsive Dendronized Polymers".

[#] These authors contributed equally to this work.

Poster Presentations

- 1) Wen Li, Afang Zhang, A. Dieter Schlüter. "Water-Soluble Dendronized Polymers", International Dendrimer Symposium 6 (IDS 6), Stockholm, Sweden, 14-18 June, 2009.
- 2) Wen Li, Afang Zhang, A. Dieter Schlüter. "Thermoresponsive Dendronized Polymers and Dendrimers", Frontiers in Polymer Science Symposium, Mainz, Germany, 07-09 June, 2009.
- 3) Wen Li, Afang Zhang, A. Dieter Schlüter. "Thermoresponsive Dendronized Polymers and Dendrimers", 3rd graduate symposium of the Materials Research Center (MRC), Zürich, Switzerland, 14 May, 2008.
- 4) Wen Li, Afang Zhang, A. Dieter Schlüter. "Thermoresponsive Dendronized Polymers and Dendrimers", Industry Day, Zürich, Switzerland, 08 May, 2008.
- 5) Wen Li, Afang Zhang, A. Dieter Schlüter. "Thermoresponsive Dendronized Polymers and Dendrimers", International Dendrimer Symposium 5 (IDS 5), Toulouse, France, 28 August ~ 01 September, 2007.
